The University Of Sheffield.

Role of macrophages metabolic reprogramming and mitochondrial fission against *Streptococcus pneumoniae*

By:

MD MOHASIN

Supervisors:

Professor David Dockrell

Dr. Helen Marriott

A dissertation submitted in partial fulfilment of the requirements for the degree of Doctor of Philosophy

The University of Sheffield
Faculty of Medicine, Dentistry and Health
Department of Infection, Immunity and Cardiovascular Disease

March 2018

Acknowledgements

I am grateful to almighty Allah for giving me this opportunity and keeping me healthy and sound over the period of my PhD tenure. The completion of my PhD thesis would not have been possible without the help and advice of a number of individuals.

Firstly, I would like to thank my supervisor, Professor David Dockrell, for giving me placement in his lab to complete a PhD. As a foreign and non-native English student I got enormous support from David and his lab members. He always encourages and inspired me and often gave me the necessary push to get over barriers for the success of my PhD. I enjoyed his supervision and I have gained key technical and soft skills as a scientist and researcher and will always be grateful for the experience.

I also thank Dr Helen Marriott as my secondary supervisors. She was very helpful during my PhD and showed and explained related techniques and methods that were quite useful for my project. She was always available to offer advice in any technical problems.

I would also grateful to the technical team particularly to Dr. Colin Gray for his kind help in confocal microscopy. I would also like to thank to Katie Cooke, Jon Finner, Jon Kilby and Jess for their endless work in category 2 and macrophage tissue culture laboratories. Their endless help always cheer me up on days. I would also thank Dr. De Vos Kurt for sharing his mitochondrial morphology analysis matrix using through the Imagej software. I would also want to thank the SiTran Seahorse technical team particularly Dr Scott Allen and Phillippa Carling. I also extend my gratitude towards flow cytometry technical team.

I am also grateful to all blood donors and COPD volunteers for their generous consent to carry out this study with their valuable cells. I would also like to thank Dr Christopher Jill for his technical support to use transmission electron microscopy in MBB department.

I must also acknowledge the endless support of David Dockrell's Sheffield research team and department of Infection, Immunity and Cardiovascular Disease technical team, particularly Paul Collini, Martin Bewley, Emily Fisk, Lucy Morris, Paul Morris and Joby Cole. When I had any research or technical question I often asked to Paul Collini and his explanation all time help me and I am really pleased to him. I would also want to give many thanks to Emily Fisk for her generous support and help during my lab experiment and thesis write up period. Emily kindly checked the initial draft of this thesis. I am really grateful to her. I am really lucky that I got lots of friends and colleagues around me who always cheer me up. Thank you Shakira, Lucy, Jake Mills, Jehan, Rahaf for your support.

I further thank to Professor Ian Sabroe for his suggestion as a personal tutor. I also offer thank to Dr. Lynne Prince and Dr. Heather Wilson who carefully read and discussed my literature review and transfer report which were the foundation of this thesis.

I would also like to thank my sponsor, the Commonwealth Scholarship Commission for funding my studentship. I would extend my acknowledgement to department of Biochemistry and Molecular Biology, University of Dhaka, Bangladesh to allow me to pursue study in the UK with a study leave.

I am really grateful to my parents and family for their enormous support. During this research, I lost my beloved father Mohammed Asad Mia who gave me enormous support, love and mental strength which brought me at this stage. I thank my mother and sisters who did plenty for my career.

I would like to thank my beloved wife Rahena Yasmin, my daughter Sameeha and little boy Sameed for two years accompanying me in Sheffield. I recognised their sacrifice particularly Rahena left her job, parents and gave invaluable time during this study. I am really grateful to her.

Abbreviations

A

AIM2 –Absent in melanoma-2

AKT –Protein kinase B

AM –Alveolar macrophage

AMP –Adenosine monophosphate

ANOVA –Analysis of variance

ANT –Adenine nucleotide translocase

AP-1 –Activator protein 1

Apaf-1 –Apoptotic protease activating factor 1

ATP –Adenosine triphosphate

B

BAL –Bronchoalveolar lavage

BCL-2 –B-Cell Lymphoma-2

BMDM –Bone marrow-derived macrophages

C

CAP –Community-acquired pneumonia

CARKL –Carbohydrate kinase like protein

CDCs –Cholesterol dependent cytolysins

CDK –Cyclin-dependent kinase

CFU –Colony forming unit

CoA –Coenzyme A

COPD –Chronic obstructive pulmonary disease

CpG –cytosine-phosphate-guanosine

CPS –Capsular polysaccharide

CR –Complement receptor

CXCL –Chemokine-CXC-ligand

D

DC –Dendritic cell

DAMPs –Danger-associated molecular patterns

2-DG –2-deoxy-D-glucose

DMSO –Dimethyl sulphoxide

DNA –Deoxy-nucleic acid

Drp1 –Dynamin related protein 1

E

ECAR –Extracellular acidification rate

ECSIT –Evolutionarily conserved signalling intermediate in Toll pathways

ER –Endoplasmic reticulum

ETC –Electron transport chain

EM –Electron microscopy

F

FACS –Fluorescence activated cell sorting

FADH2 –Flavin adenine dinucleotide (reduced form)

FSC –Forward scatter

Fis1 – Mitochondrial fission protein 1

G

G-CSF –Granulocyte colony-stimulating factor

GLUT1 –Glucose transporter chanel-1

GM-CSF –Granulocyte-macrophage colony-stimulating factor

gp120 –Glycoprotein 120

GRO-α –Growth related oncogene alpha

GTPase –Guanosine triphosphatase

H

HAART –Highly active anti-retroviral therapy

HAT –Histone acetyl transferase

HDAC2 –Histone deacetylase 2

HIF-1α –Hypoxia inducible factor-1 alpha

HIV –Human immunodeficiency virus

I

iC3b –Inactivated form of complement C3b

ICAM –Intracellular adhesion molecule

IFNγ –Interferon gamma

IL-4/13 –Interleukin-4 or 13

IMM –Inner mitochondrial membrane

iNOS –Inducible nitric oxide synthase

IPD –Invasive pneumococcal disease

IRF3 –interferon regulatory factor 3

L

LAMP1 –Lysosome-associated membrane protein 1

LC3B –Microtubule-associated protein 1- light chain 3

LLO –Listeriolysin O

LMP –Lysosomal membrane permeablisation

LPS –Lipopolysaccharide

LTA –Leipoteichoic acid

M

MAPK –Mitogen activated protein kinase

MARCO –Macrophage receptor with collagenous structure

Mcl-1 –Myeloid cell leukemia factor 1

MCP-1 –Monocyte chemoattractant protein 1

M-CSF –Macrophage colony-stimulating factor

MDM –Monocyte derived macrophages

Mdivi-1 –Mitotic division inhibitor 1

Mff –Mitochondrial fission factor

Mfn1/2 –Mitofusin 1 or 2

MiD49/51 –Mitochondrial dynamics protein (molecular weight 49 or 51 kDa)

MMP –Matrix metalloproteinase

MOMP –Mitochondrial outer membrane permeabilisation

mROS –Mitochondrial reactive oxygen species

MTP18 –Mitochondrial protein 18 kDa

MyD88 –Myeloid differentiation factor 88

N

NAD –Nicotinamide adenine dinucleotide

NADPH –Nicotinamide adenine dinucleotide phosphate

Nan A/B –Neuraminidase A/B

NF-κB -Nuclear factor kappa B

NLR – Nucleotide-binding oligomerization domain (NOD)-like receptor

NLRP3 –Nucleotide oligomerization domain like receptor P3

NMR –Nuclear magnetic resonance

NO –Nitric oxide

NOD2 –nucleotide-binding oligomerisation domain containing protein 2

NOS2 –Nitric oxide synthase 2

Nrf2 –Nuclear factor erythroid-2-related factor 2

O

OCR –Oxygen consumption rate

OPA1 –Optic atrophy protein 1

OXPHOS –Oxidative phosphorylation

P

PAMPs –Pathogen-associated molecular patterns

PFK1 –Phospho-fructo kinase 1

PGC-1β –Peroxisome proliferator-activated receptor (PPAR) γ-coactivator-1β

PI-3K –Phosphoinositide-3-kinase

PINK1 –PTEN-induced putative kinase 1

PLY –Pneumolysin

PPP –Pentose phosphate pathway

PPRs –Pattern recognition receptors

PsaA –Pneumococcal surface antigen A

R

ROS –Reactive oxygen species

RNA –Ribonucleic acid

RNS –Reactive nitrogen species

S

SOD –Superoxide dismutase

SRs –Scavenger receptors

STAT1 –Signal transducer and activator of transcription 1

STING –Stimulator interferon genes

T

TCA –Tricarboxylic acid

TEM –Transmission electron microscopy

TGF-β –Transforming growth factor beta

TIM –Translocase of inner membrane

TLRs –Toll-like receptors

TOM20 –Translocase of outer membrane protein 20

TNFα –Tumour necrosis factor alpha

TPSO –Translocator protein

TRAF6 –Tumour necrosis factor receptor-associated factor 6

U

UCP –Uncoupling protein

uPFK1 –Ubiquitous phospho-fructo kinase 1

V

VDAC –Voltage dependent anion channel

X

XF24 –Extracellular Flux Analyser (24 plate format)

XFAM –Extracellular flux assay medium

Abstract

Rationale & Hypothesis: Pneumonia is a leading cause of infection-related death and *Streptococcus pneumoniae,* the commonest cause, accounts for approximately one million deaths in children each year. Macrophages are key effectors of innate immune responses but the precise microbicidal mechanisms used to control *S. pneumoniae* are incompletely characterised. West et al. reported that TLR1/2/4 agonists augment intracellular bacterial killing through inducing mitochondrial reactive oxygen species (mROS). Recently, the Dockrell group has demonstrated that in addition macrophages use mROS as a component of the microbicidal response and mROS are important effectors of microbicidal responses in an apoptotic programme that contributes to intracellular bacteria killing when other canonical mechanisms are exhausted. I hypothesized that mitochondrial homeostasis would be altered in response to intracellular bacteria as an important element of the microbicidal response to *S. pneumoniae.*

Methodology: Mouse bone marrow cells and human monocytes were differentiated into macrophages. Macrophages metabolic profiles, mROS generation, bacterial killing and mitochondrial fission/mitophagy were evaluated by XF24 flux analyser, flow-cytometry, gentamicin protection assay and Confocal/Electron microscopy/Immunoblotting, respectively.

Findings: Measures of respiration during bacterial infection have been less studied than the use of microbial components such as LPS. Methods were optimised to study metabolic profiles in macrophages challenged with *S. pneumoniae*. The macrophage's bioenergetic profile demonstrated that *S. pneumoniae* significantly decreased mitochondrial respiration capacity and ATP-linked respiration but increased proton leakage, glycolytic respiration and mROS production. The HIV protein gp120 reduced ATP-linked oxygen consumption rate (OCR) and proton leakage while chronic obstructive pulmonary disease (COPD) reduced maximum respiration capacity, respiration reserve and ATP-linked OCR but increased proton leak. mROS were produced in close proximity to bacteria and to phagolysosomes as well as to nitric oxide production. Mitochondrial maximum respiration capacity was reduced following bacterial infection but this reduction was reversed by inhibiting mROS production. *S. pneumoniae* significantly increased mitochondrial fission resulting in reduced mitochondrial network complexity 12 hours after bacterial-challenge, before apoptosis

induction. Fission was induced via a Drp1-independent non-canonical pathway. Fragmented mitochondria were co-localised or adjacent to an E3 ubiquitin ligase Parkin, phagolysosomes and intracellular bacteria but LC3B was not recruited and electron microscopy failed to identify evidence of mitophagy. mROS co-localized with mitochondria that had undergone fission. Fission was reversed by the PI-3 kinase inhibitor 3-methyladenine (3MA) but was not altered by the Drp1 inhibitor Mdivi-1. Inhibiting mitochondrial fission with 3MA decreased mROS production, apoptosis and intracellular bacterial killing.

Conclusions: Mitochondrial fission occurs prior to apoptosis induction and enhances mROS production. Targeting mitochondrial homeostasis and fission represents potential cellular targets with which to modulate host innate immune responses against intracellular pathogens.

Publications from this thesis

1. HIV gp120 in lungs of ART-treated individuals impairs alveolar macrophage responses to pneumococci. Collini PJ, Bewley MA, **Mohasin M**, Marriott HM, Miller RF, Geretti AM, Beloukas A, Papadimitropoulos A, Read RC, Noursadeghi M, Dockrell DH. Am J Respir Crit Care Med. 2018 Jan 24. doi: 10.1164/rccm.201708-1755OC. [Epub ahead of print]

2. Impaired mitochondrial microbicidal responses in Chronic Obstructive Pulmonary Disease macrophages. Bewley MA, Preston JA, **Mohasin M**, Marriott HM, Budd RC, Swales J, Collini P, Greaves DR, Craig RW, Brightling CE, Donnelly LE, Barnes PJ, Singh D, Shapiro SD, Whyte MKB, Dockrell DH. Am J Respir Crit Care Med. 2017 Oct 1;196 (7):845-855. doi: 10.1164/rccm.201608-1714OC.

3. Alveolar macrophages utilize apoptosis-associated killing to clear bacteria when initial macrophage killing mechanisms are exhausted. Preston JA, Bewley MA, Houghton AM, Marriott HM, **Mohasin M**, Jubrail J, Morris L, Stephenson YL, Cross S, Greaves DR, Craig RW, Rooijen NV, Bingle CD, Read RC, Mitchell TJ, Whyte MKB, Shapiro SD and Dockrell DH. Revision in the Am J Respir Crit Care Med.

4. Macrophages utilize mitochondrial fission to enhance mROS production during responses to *S. pneumoniae.* **Mohasin M**, Marriott HM, Dockrell DH. Expected publication.

Published abstracts

1. Mitochondrial fission is associated with mROS-dependent microbicidal responses to *S. pneumoniae* in macrophages. **Mohasin M**, Marriott HM, Dockrell DH. British Society for Immunology annual congress, 4-7th December, 2017, Brighton, UK. (**Oral presentation).**

2. Alteration in mitochondrial homeostasis during responses to *Streptococcus pneumoniae* in macrophages. **Mohasin M**, Bewley MA, Collini PJ, Marriott HM, Dockrell DH. Symposium on Drugs Don't Work, September 19-20, 2017, Florey Institute, University of Sheffield, UK. (**Poster presentation**).

3. Alteration in mitochondrial homeostasis during responses to *Streptococcus pneumoniae* in macrophages. **Mohasin M**, Bewley MA, Collini PJ, Marriott HM, Dockrell DH. 13th Annual School Research Meeting, June 15-16, 2017. Medical School, University of Sheffield, UK. (**Poster presentation**).
4. Alteration in mitochondrial function influencing antimicrobial responses to *Streptococcus pneumoniae* in macrophages during COPD. **Mohasin M**, Bewley MA, Collini PJ, Marriott HM, Dockrell DH. British Society for Immunology annual congress, 6-9th December, 2016 ACC Liverpool, UK. (**Poster presentation).**

5. Alteration in mitochondrial function influencing antimicrobial responses to *Streptococcus pneumoniae* in macrophages during COPD. **Mohasin M**, Bewley MA, Marriott HM, Dockrell DH. 12th Annual School Research Meeting, June 15-16, 2016. Medical School, University of Sheffield, UK. (**Poster presentation).**

6. Pneumococcal infection exacerbates chronic obstructive pulmonary disease through changing metabolic status and phenotype of macrophages. **Mohasin M**, Bewley MA, Marriott HM, Dockrell DH. 11th Annual School Research Meeting, June 15-16, 2016. Medical School, University of Sheffield, UK. (**Poster presentation).**

Contents

List of figures

List of Table

Chapter 1. Introduction

1.1. General Introduction

Streptococcus pneumoniae (the pneumococcus) is a Gram-positive bacterium, and was formerly known as *Diplococcus pneumoniae.* The pneumococcus mostly lives asymptomatically in the nasopharynx of humans (i.e. upper respiratory tract), as part of the commensal flora. It can, however, cause infection and disease (e.g. pneumonia) when it spreads from the nasopharynx to small airways, or to the sinuses or middle ears (e.g. middle ear infection/otitis media). Moreover, pneumococcus may also penetrate through the respiratory epithelium into the blood circulation, resulting in local infection or bacteraemia and in some cases it may also cross the blood-brain barrier to the meninges, resulting the bacterial meningitis (Garcia-Suarez et al., 2007, Calbo and Garau, 2010). Pneumococcal invasion at sterile sites, such as blood, cerebrospinal fluid, or pleural space, is collectively defined as invasive pneumococcal disease (IPD) (Dockrell et al., 2012a).

Recent epidemiological studies also suggested that pneumococci causes a high rate of mortality and morbidity globally (Song et al., 2013). For example, pneumococci is responsible for approximately 1.6 million deaths annually (Lynch and Zhanel, 2009). In addition to causing pneumonia in older people, pneumococcus also cause IPD such as sepsis and meningitis in young children, causing more than half a million deaths in this younger population annually (Ingels, 2015).

Moreover, pneumococcus is the most common bacterial pathogen for community-acquired pneumonia (CAP), in both developed and developing countries (Song et al., 2011, Welte et al., 2012). Immunocompromised individuals (e.g. patients with HIV-1 infection) have increased incidence of severe pneumococcal infections (reviewed in (Kadioglu et al., 2008). In addition, pneumococcus is also responsible for infective exacerbations of chronic pulmonary diseases. For example, *S. pneumoniae*-associated bronchitis is responsible for 25% of infective exacerbations in chronic obstructive pulmonary disease (COPD) (Garcha et al., 2012). However, currently available vaccines (e.g. conjugate or polysaccharide vaccines) do not give complete protection against specific serotypes and only cover a limited number of serotypes. Moreover, antibiotic resistance to pneumococci raises further concerns and justifies further attention towards the pathogenicity of pneumococcal disease. Therefore, the host-defence mechanisms used

against pneumococci require better characterisation. Macrophages are an essential component in the first line of immune defense. Alveolar macrophages are particularly critical for responses against pneumococci in the lung and kill ingested bacteria using their large phagolysosomal capacity (Aberdein et al., 2013). My host group and other recent studies have demonstrated that macrophages mitochondria are a critical organelle involved in eradication of intracellular bacteria (Bewley et al., 2017, West et al., 2011a, Aberdein et al., 2013).

1.2. Pneumococcal disease prevalence and treatment

Streptococcus pneumoniae was first discovered and isolated by Griffith Sternberg in the United States (Watson et al., 1993, Sternberg, 1881) and by Pasteur in France, in 1881 (Pasteur, 1881). It is the most common bacterial pathogen causing CAP and results in more than 20% mortality in patients with concurrent bacteraemia, in the United Kingdom (Balakrishnan et al., 2000, Lim et al., 2001). It mostly colonises in the upper respiratory tract and more frequently colonise in early childhood. The pneumococcus has around 91 different serotypes, which are classified based on their cell surface polysaccharide capsule, which is structurally different and shows distinct antigenicity (reviewed in (Kadioglu et al., 2008)). The 23-valent polysaccharide vaccine (PPV23) replaced the earlier 14-valent polysaccharide pneumococcal vaccine, and contains 23 as opposed to the 14 purified capsular polysaccharide antigens of *S. pneumoniae* contained in the older vaccine.

However, this PPV23 polysaccharide vaccine shows moderate immune T-cell independent responses, does not induce memory T-cell responses or induce mucosal immunity and is not prescribed to those under two years old as it lacks efficacy in this group (reviewed in (Jedrzejas, 2001)). This has led to replacement of PPV23 with protein conjugate vaccines (PCV), initially containing 7 serotypes but now extended to 13 serotypes (Prevnar). This vaccine has replaced PPV23 in the childhood vaccine schedules and induces T-cell and mucosal immunity resulting in reduction in not only IPD but also reduction in pneumonia. The introduction of PCV has not only reduced pneumococcal infection in vaccinated children but also in older age groups through reduced transmission of bacteria (Simonsen et al., 2011). Pneumococcal vaccination with PCV has resulted in some replacement of vaccine serotypes with non-vaccine serotypes in the community but

this has not offset the overall reduction in IPD associated with PCV programmes. Moreover, some pneumococcal strains also show antibiotic resistance towards penicillin (Baquero et al., 1991, Spika et al., 1991). For example, 35% of pneumococcal strains are resistance to penicillin, as isolated from developed and developing countries, although penicillin resistance remains low in the United Kingdom (Arnold et al., 1996, Duchin et al., 1995, Hofmann et al., 1995). Therefore, it is essential to identify pneumococcal virulence factors, to identify new vaccine candidates and to better understand pathogenicity and host-pathogen interaction at the cellular level.

1.3. Pneumococcal virulence factors and their role in pathogenicity

Like other Gram-positive bacteria, pneumococcus displays a range of proteins and enzymes on the surface which significantly contribute to pathogenesis. Although the polysaccharide capsule is considered as the primary virulence factor, certain pneumococcal proteins such as pneumococcal surface protein A, hyaluronate lyase, pneumolysin, autolysin, pneumococcal surface antigen A, choline binding protein A, and neuraminidase (NanA/B), also have significant roles in the pneumococcal pathogenesis. Fortunately, some of them are immunogenic and display antigenicity (reviewed in (Jedrzejas, 2001). In this review of the literature, I have mainly focused on the polysaccharide capsule and the pneumolysin toxin.

1.3.1. Polysaccharide capsule

The polysaccharide capsule is the outermost layer of pneumococci and its thickness is approximately 200-400 nm (Sorensen et al., 1988). This capsular polysaccharide (CPS) is covalently attached to peptidoglycan – one of the major cell-wall components of Gram-positive bacteria, and pneumococci are known as encapsulated bacteria (Sørensen et al., 1990). So far, 91 types of distinctive CPS have been identified in pneumococci, which show distinct serological and morphological phenotypes (Henrichsen, 1995, Kadioglu et al., 2008). The CPS is a critical virulence factor of pneumococci and it plays a substantial role in their pathogenicity (Austrian, 1981). For example, the CPS diminishes the phagocytosis of non-immunised individuals. As a result, low numbers of colony forming units (cfu) of encapsulated pneumococci can establish lethal pneumococcal infection, whereas inocula of 10^6-10^8cfu of non-encapsulated pneumococci are required to establish the same level of

infection in mice (Austrian, 1981). Mechanistically the CPS forms an inert shield that seems to hinder bacteria opsonisation through blocking either the interactions between the Fc region of immunoglobulin G (IgG) with the Fcγ receptors of the phagocytic cells or inhibiting complement component iC3b deposition required for recognition by complement receptors (Winkelstein, 1981, Musher, 1992). Moreover, the pneumococcal capsule can also decrease the total amount of complement which is deposited on the bacterial surface (Abeyta et al., 2003). The pneumococcal capsule also helps pneumococci to evade mucus-associated entrapment in the respiratory tract, which allows them to colonise the epithelial surface (Nelson et al., 2007).

Collectively, it appears that the pneumococcal virulence factor CPS, prevents both clearance by the respiratory tract's mucociliary escalator but also limits the phagocytosis by immune cells and attack by complement. However, CPS also has immunogenicity and although the polyvalent purified CPS vaccine (PPV23) was effective against approximately 90% of pneumococcal disease-causing serotypes. The vaccine was poorly immunogenic, as discussed above, because CPS contained in PPV23 are T-cell independent antigens and do not stimulate immunological memory – which is essential for longer protection. Thus, the CPS-protein conjugate vaccine (PCV13, Prevnar) which also triggers T-cell dependent immune responses, has replaced PPV23 in childhood vaccine schedules. But the PCV13 only raises immune responses to specific serotypes of pneumococci (reviewed in (Kadioglu et al., 2008))

1.3.2. Pneumolysin

Pneumolysin is a potent, soluble protein virulence factor of *S. pneumoniae*. It is a family member of cholesterol-dependent cytolysins (CDCs). Pneumolysin is not secreted during pneumococcal growth due to the lack of a protein secretion-signal sequence. However, it is released from the bacterial cytoplasm through coupling with the pneumococcal enzyme, autolysin (LytA). Autolysin degrades the bacterial cell wall and permits pneumolysin secretion during the stationary phase of pneumococcal growth or treatment with antibiotics (Rubins and Janoff, 1998). Pneumolysin is usually produced as a 52 kDa protein, which triggers pore-formation, approximately 260 angstrom in diameter, in the target cells after oligomerisation in the plasma membrane. This creates a transmembrane pore with a spectacular conformational change in pneumolysin structure (Tilley et al., 2005).

Pneumolysin makes pores, causing plasma membrane lysis of target cells, unlike listeriolysin O (LLO), the CDC of *Listeria monocytogenes*. The latter can only lyse phagosomal membranes with its optimum pH 5.5 (Geoffroy et al., 1987).

Moreover, pneumolysin oligomers show toxicity, as observed by the effects seen with sub-lytic concentrations (Hirst et al., 2004). Apart from its membrane damaging effect, pneumolysin also inhibits ciliary beating and diminishes the respiratory bursts of phagocytes. While it also inhibits complement activation. In addition, it has been reported that pneumolysin interacts with TLR4 and induces cytokine production (Malley et al., 2003) and apoptosis (Srivastva et al., 2005) in peritoneal macrophages. In contrast, pneumolysin activates p38 MAPK in epithelial cells (Ratner et al., 2006) and nuclear factor of activated T cells (Koga et al., 2008) in a TLR4-independent manner. Besides, it has been demonstrated that pneumolysin induces humoral and cellular immunogenic mediators after recognition via nucleotide oligomerisation domain like receptor P3 (NLRP3) and related NLR (McNeela et al., 2010). For example, endotoxin free pneumolysin interacts with NLRP3 and induces proinflammatory cytokines in a TLR4-independent manner (McNeela et al., 2010).

1.4. Host response to *Streptococcus pneumoniae*

1.4.1. Innate immunity against pneumococcus

Innate immunity provides the first of line of defense. It involves a diverse array of protective components, including complement and mucociliary beating, as well as phagocytes (e.g. neutrophils and macrophages) which mediate humoral and cellular components of the innate immune response. The complement system performs three key functions; (i) opsonisation of bacterial surface to enhance bacterial phagocytosis by neutrophils or macrophages, (ii) chemotaxis of neutrophils to the site of infection and (iii) the direct killing of microbes by forming the ‘membrane attack complex’ on bacterial surfaces (Paterson and Orihuela, 2010). There are more than 30 serum and membrane proteins in the total complement system. C3 is the central complement component of the classical activation pathway. The genetic deficiency (Paterson and Orihuela, 2010) or loss of C3 complement causes recurrent pneumococcal infections, septicaemia and impaired macrophage activation (Jeremy et al., 2002). Whereas, mucociliary beating and clearance of bacteria prevents inhaled noxious particles coming in direct contact with epithelial cells and reaching the alveolar airspaces.

However, pneumococci and other airway pathogens either tightly adhere to epithelial surfaces and slow down mucociliary beating, or increase the viscosity of mucous through formation of biofilms and evade ciliary clearance (Marks et al., 2012).

On the other hand, phagocytic cells particularly neutrophils and macrophages, are essential cell-mediated host defence components against pneumococci. For example, alveolar macrophages (AMs) are the resident phagocytes that internalise and clear pneumococci from the small airway (Dockrell et al., 2003). However, this bacterial clearance capacity is diminished during other medical co-morbidities such as COPD (Taylor et al., 2010) or viral co-infection particularly with human immunodeficiency virus (HIV) (Collini et al., 2010). Thus, the finite AMs capacity to clear bacteria can be further compromised.

1.4.2. Macrophages

Macrophages originate from either bone marrow progenitors that mature to peripheral blood monocytes or from tissue macrophage intermediates that may replicate and mature in tissues (van Furth and Cohn, 1968, van Furth et al., 1972). Macrophages role is to engulf and digest cellular debris, foreign particles, microbes, and cancer cells in a process called phagocytosis. In addition, they are highly versatile cells and play major roles in embryonic development, homeostasis and wound healing in different tissues. Monocytes are attracted to a damaged site through chemotaxis, triggered by a range of stimuli, including damaged cells, pathogens and cytokines such as GM-CSF or G-CSF, released by resident macrophages and epithelial cells. The diverse characteristics of different resident macrophages are the result of additional micro-environment imprinting, as displayed in various tissues such as Langerhans cells in the epidermis, Kupffer cells in the liver, osteoclasts in the bone, microglia in the brain and alveolar macrophages in the lung.

Phenotypic differences in macrophages are further induced by transient changes in local stimuli, a phenomenon described as macrophage polarisation. Macrophages which are classically activated by Th1 cytokines such as IFN-γ encourage tissue inflammation and are called M1 macrophages. The M1 macrophages have microbicidal, tumoricidal and antigen presenting capacity (Edwards et al., 2006), whereas macrophages which are alternatively activated by Th2 cytokines, such as IL-4/IL-13, show anti-inflammatory effects and participate in tissue repair and are called M2 macrophages. The latter macrophages not only maintain tissue homeostasis through wound healing but also resolve inflammation with clearance of apoptotic cells and debris (Zizzo et al., 2012, Uderhardt et al., 2012, Sindrilaru

et al., 2011) (Figure 1.1). This is however a gross simplification and in practice many variations in these polarisation extremes exist and many unique stimuli provide mixed phenotypes with a combination of M1 and M2 associated gene.

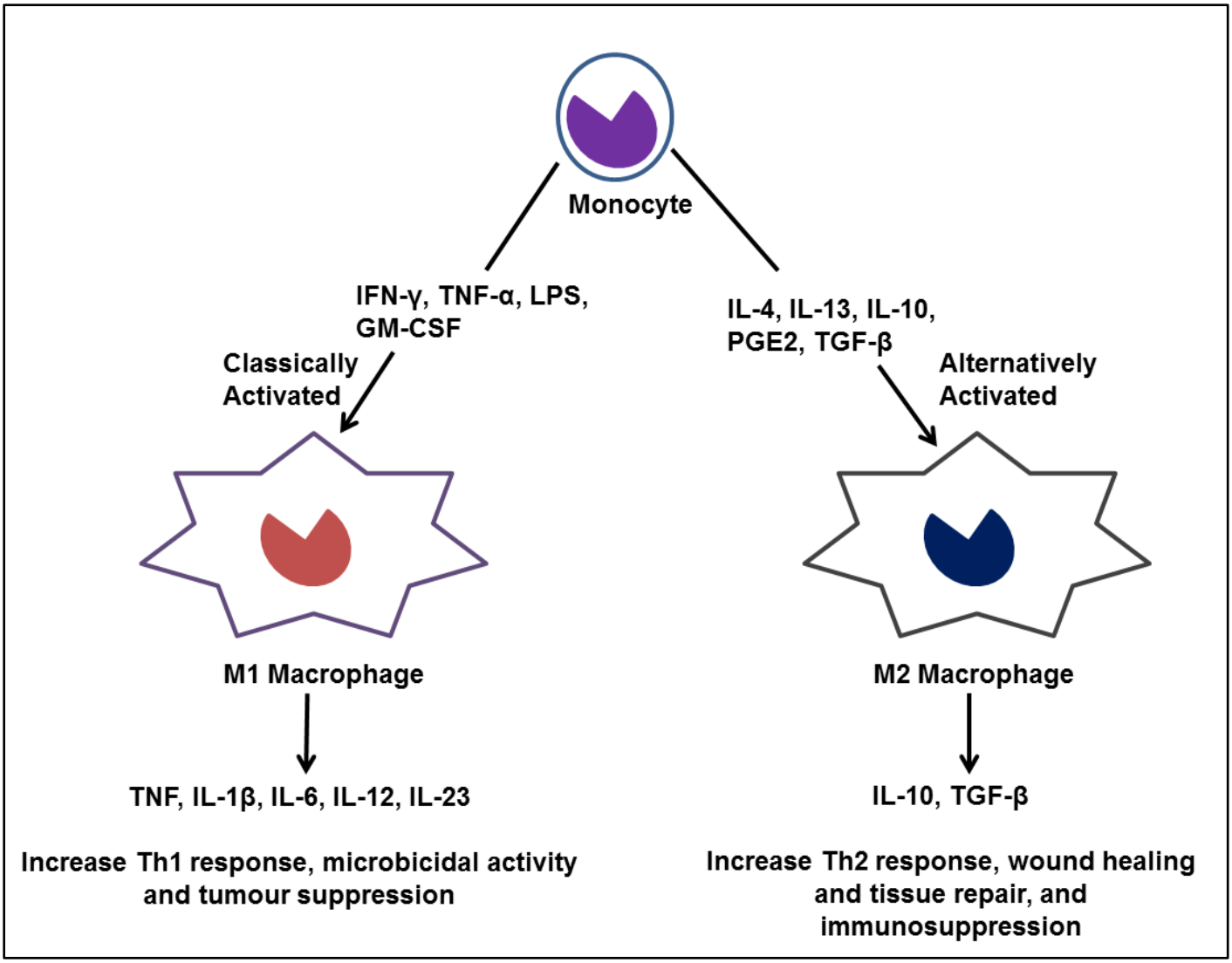

Figure 1.1. **Macrophage polarisation.** Monocytes are differentiated into either highly microbicidal and pro-inflammatory M1 macrophages or immunosuppressive and anti-inflammatory M2 macrophages, upon encountering distinct cytokines. Classically activated M1 macrophages secrete tumour necrosis factor-α (TNFα) and interleukin-1β (IL-1β). Whereas, alternatively activated M2 macrophages release IL-10 and transforming growth factor-β (TGF-β), the immune-regulatory cytokines. Figure is adapted from (Arango Duque and Descoteaux, 2014).

1.4.3. Macrophages in host defence

Macrophages play essential roles in host defence against microbial infection. They are ubiquitous in all tissues where they act as sentinels responding to pathogens. In addition, microbial infiltration of tissues triggers the release of a variety of chemotactic agents that alert the macrophages to the infection. Subsequently, macrophages bind with pathogens via phagocytic receptors that initiate the cytoskeleton rearrangements and membrane re-arrangements, which initiate the phagocytosis-mediated internalisation of pathogens. The internalised microbes should remain in a phagosome, which fuses with lysosomes and is converted into a phagolysosome where the pathogen is killed by a wide variety of microbicidal mechanisms such as oxidative or nitrosative stress involving reactive oxygen/nitrogen species and by proteases and cytotoxic peptides (Aderem and Underhill, 1999, Underhill and Ozinsky, 2002, Greenberg and Grinstein, 2002). Microbial peptides released from dead pathogens are processed by the action of hydrolases in the phagolysosomes. Subsequently, the microbial peptides are processed and expressed as immunogenic epitopes in association with the major histocompatibility complex (MHC)-II, thereby facilitating the activation of an adaptive immune response, involving T cell responses.

However, the capacity of macrophages to clear bacteria is limited and they may no longer be able to control bacteria in the airway if there is a high inoculum of, as suggested from studies of mice infection (Dockrell et al., 2003, Knapp et al., 2003). At this stage, macrophages play pivotal roles in regulating the inflammatory response in the lung. They produce inflammatory cytokines, such as IL-1β, which induce CXCL-8, also called interleukin 8 (IL-8), expression from epithelial cells. The chemokine, CXCL-8 attracts neutrophils which play a critical role in bacterial clearance (Knapp et al., 2003, Marriott et al., 2012). Moreover, macrophages not only induce apoptosis of inflammatory cells (such as neutrophils) but also remove apoptotic cells -by a process called efferocytosis, resulting in the down-regulation of pro-inflammatory cytokines and resolution of lung inflammation (Dockrell et al., 2001, Marriott et al., 2006).

1.4.4. Macrophage recognition of *Streptococcus pneumoniae*

The pattern recognition receptors (PRRs) are the pathogen sensors of the immune system. They are classified broadly based on their cellular location. These groups include the transmembrane Toll-like receptors (TLRs), cytosolic nucleotide-binding oligomerisation domain (NOD)-like receptors (NLRs), retinoic acid-inducible gene (RIG)-1-like receptors (RLRs), which detect double stranded RNA, and cytosolic DNA sensors. They can recognise or interact with invading pathogens through conserved microbial molecules - also called pathogen-associated molecular patterns (PAMPs) - as well as endogenous molecules (e.g. danger-associated molecular patterns (DAMPs)), produced during tissue damage (Medzhitov and Janeway, 2000, Vance et al., 2009, Rock et al., 2010). For example, Gram-negative bacterial lipopolysaccharide (LPS) interacts with TLR4 in innate immune cells (Hoshino et al., 1999). *S. pneumoniae* lack LPS, but TLR4 was suggested to interact with the pneumococcal virulence factor pneumolysin - a cholesterol-dependent cytolysin, however this interaction has been controversial and many authorities now believe pneumolysin is recognised by NLRs (see below), rather than by TLR4 (McNeela et al., 2010). Malley and colleagues who proposed the TLR4 pneumolysin interaction, suggest it harnesses macrophage immune responses which subsequently confer resistance to pneumococcal infection in mice (Malley et al., 2003).

In addition, pneumococcal lipoteichoic acid (LTA) is recognised by TLR2 and an *in vivo* study with $TLR2^{-/-}$ mice has shown a reduced clearance of pneumococci from their nasopharynx (Van Rossum et al., 2005). However, the mortality rate and the bacterial susceptibility of $TLR2^{-/-}$ mice is increased after challenge with pneumolysin-deficient pneumococci, but it shows comparable mortality after challenge with wild-type pneumococci (Dessing et al., 2008), suggesting that pneumolysin-PRR signalling could compensate for loss of the LTA/TLR2-mediated immune responses. Moreover, the unmethylated cytosine-phosphate-guanosine (CpG) motif of bacterial DNA interacts with the endosomal TLR9 receptor, which also harnesses the innate immune responses against bacteria (Ishii and Akira, 2006, Krieg, 2000). For example, TLR9 knockout mice show greater susceptibility to pneumococcal infection compared to either TLR2 or TLR4 deficient mice (Lee et al., 2007).

The TLRs engage with myeloid differentiation factor 88 (MyD88) – a key signalling adaptor protein, which activates NF-κB mediated inflammatory cytokines and chemokines, in the

presence of pneumococcal infection (e.g. TNFα, IL-6, IL-1β and CXCL1) (Figure 1.2) (Koppe et al., 2012). MyD88-deficient mice also show enhanced susceptibility to pneumococcal infection and more severe infection phenotypes were observed compared to the milder phenotypes, observed in single TLR2-, TLR4- and TLR9-knockout mice (Koedel et al., 2004). From these findings, Koppe and colleagues have speculated that during pneumococcal infection, TLRs may show functional redundancy or MyD88 itself may engage with other upstream signalling receptors (e.g. IL-1R or IL-8R) (Koppe et al., 2012). Moreover, internalised pneumococcal peptidoglycan fragments interact with NOD2 in the cytosol, which also activates NF-κB signal transduction (Opitz et al., 2004). In addition, internalised pneumococcal DNA in macrophages activates the adaptor molecule STING, which upregulates the transcription factor interferon regulatory factor (IRF) 3, a positive regulator of type I interferons (i.e. IFNα/β) (Nakamura et al., 2011).

In addition, other host cell PRRs, such as inflammasome-forming proteins NLRP3 and AIM2 (absent in melanoma-2), also recognise pneumococci which trigger host innate immune responses (reviewed by (Koppe et al., 2012). For example, pneumococcal pneumolysin stimulates IL-1β production in macrophages and dendritic cells through interaction with the NLRP3 inflammasome complex and in a TLR4-independent manner (McNeela et al., 2010, Witzenrath et al., 2011). However, $NLRP3^{-/-}$ cells or mice challenge with pneumococci also produce IL-1β (Witzenrath et al., 2011). Fang and colleagues have also demonstrated that NLRP3-deficient macrophages produce IL-1β through interaction of AIM2 - another inflammasome complex which interacts with pneumococcal DNA (Fang et al., 2011). Interestingly, both NLRP3 and AIM2 inflammasomes interact with the ASC [apoptosis-associated speck-like protein containing a CARD (caspase recruitment domain)] adapter molecule, and mice lacking ASC are more susceptible to pneumococcal pneumonia compared to wild-type or $NLRP3^{-/-}$ mice (Fang et al., 2011). Collectively, NOD2, NLRP3 and AIM2 are essential host cell PRRs, which stimulate innate immune responses and play critical roles against *S. pneumoniae*.

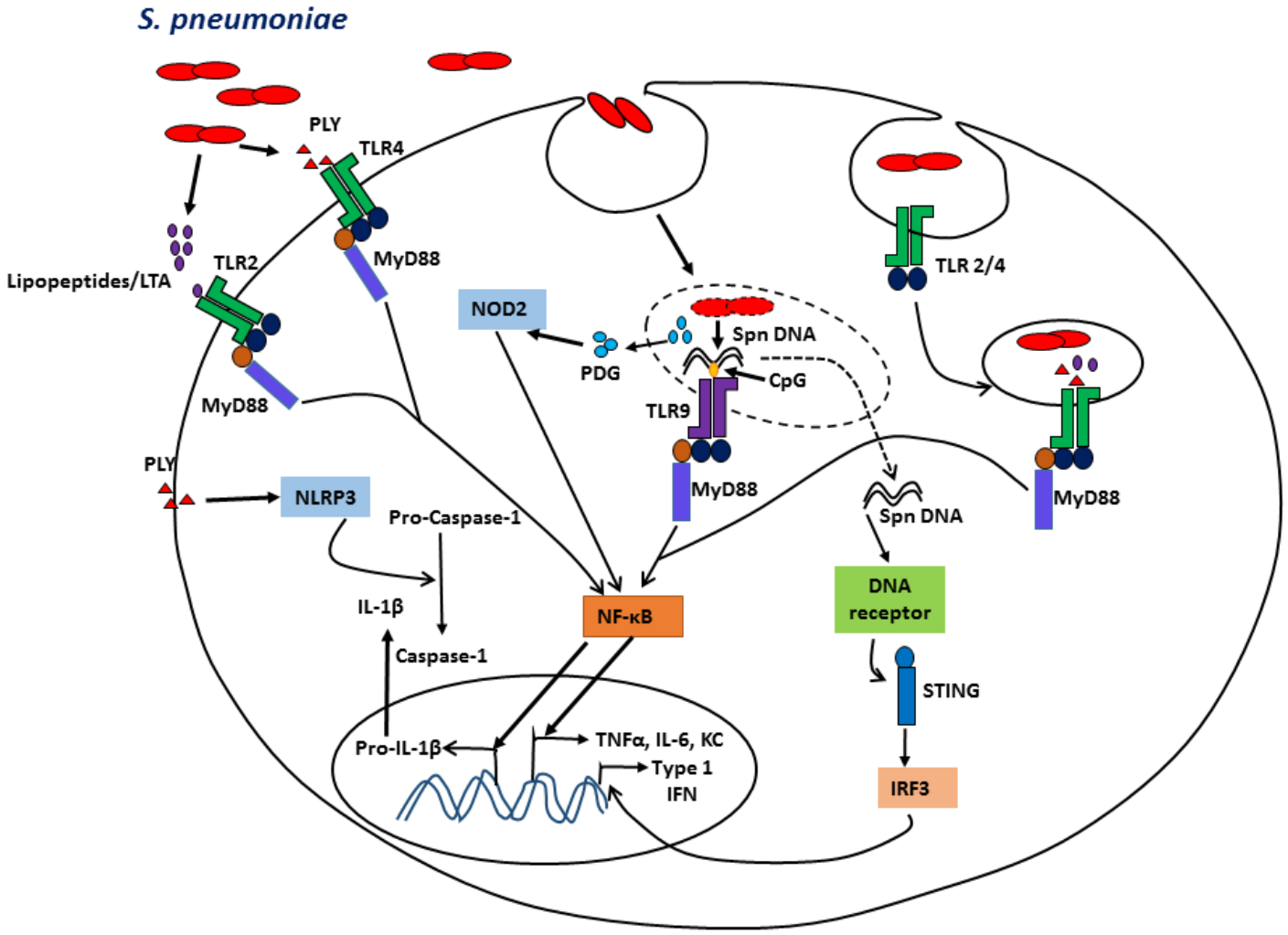

Figure 1.2. **Macrophage pattern recognition receptors sense *S. pneumoniae***. Pneumococcal lipopeptides or lipoteichoic acid (LTA) stimulate Toll-like receptor 2 (TLR2) and pneumolysin may stimulate macrophage cell surface receptor TLR4, although this is controversial. Whereas endosomal (e.g. phagosome/phagolysosome associated) TLR9 recognises unmethylated CpG of bacterial DNA (Sabroe et al., 2003). These TLRs engage MyD88, which upregulates inflammatory cytokine (e.g. TNFα, IL-6 and pro-IL-1β) and chemokine (e.g. CXCL1) expression, through turning on NF-κB mediated inflammatory gene transcription. Subsequently, the pro-interleukin-1β is converted into mature IL-1β by caspase-1-associated proteolytic cleavage. This cleavage is positively regulated by the NLRP3 inflammasome complex and AIM2 which are stimulated by pneumolysin (NLRP3 and AIM2) and pneumococcal DNA (AIM2). Moreover, internalised pneumococci are degraded in the phagosome, resulting in the release of bacterial peptidoglycan (PDG) and nucleic acid to the cytoplasm. Pneumococcal peptidoglycans are detected by the NOD2 within the cytosol, which

stimulates NF-κB dependent inflammatory cytokines. Whereas bacterial DNA interacts with a DNA receptor that turns on type I interferons (IFNs) expression, through inducing the STING/IRF3 signal transduction pathway. (TLR –toll-like receptor, MyD88 –myeloid differentiation factor 88, NF-κB –nuclear factor-kappa B, NLRP3 –the NOD-like receptor (NLR) family, pyrin domain-containing 3, NOD2 –nucleotide-binding oligomerisation domain containing protein 2, PDG-peptidoglycan, PLY-pneumolysin, STING –stimulator interferon genes, IRF3 –interferon regulatory factor 3). The figure is adapted from (Koppe et al., 2012).

1.4.5. Macrophages Phagocytosis

Phagocytosis is considered as an ancient adaptation process. While primitive organisms use phagocytosis as a strategy for the acquisition of nutrients, some specialised immune cells (macrophages and neutrophils etc.) in higher organisms use this process to bolster host defence while macrophages use it as a strategy to control inflammation through the removal of senescent cells which are produced either by programmed cell death or pathogen induced apoptosis (Cardelli, 2001). Dendritic cells also use phagocytosis to ingest particles, including micro-organism, as a source of antigens for presentation to T-cells. In addition, It is essential for embryonic development and tissue remodelling (Aderem and Underhill, 1999, Underhill and Ozinsky, 2002). Phagocytosis is a complex process which is initiated by the interaction of specific receptors on the surface of macrophages with ligands on the surface of microbes or other particles (Pommier et al., 1983). It leads to the polymerisation of actin at the site of ingestion which triggers internalisation of microbes, cells or other particles via an actin-based mechanism.

Subsequently, the actin surrounding the endosome containing the internalised particle is shed from the phagosome which matures by a series of fusion and fission events. This process involves the endocytic pathway and culminates in the formation of a mature phagolysosome (Aderem and Underhill, 1999), which enhances killing of microbes by different mechanisms.

Phagocytic cells can engulf either non-opsonic microbes through engaging related PRRs with microbial surface antigens, or they initiate opsonic-phagocytosis through deposition of proteins (e.g. antibodies or complement) on microbes, which are recognised by cell surface receptors of phagocytes (e.g. macrophages) (Underhill and Ozinsky, 2002). For example, lipoteichoic acid (LTA) of non-opsonised pneumococci is recognised by scavenger receptors SR-AI/II or MARCO (macrophage receptor with collagenous structure) of macrophages. Mice deficient in scavenger receptors SR-AI/II or MARCO show reduced bacterial clearance capacity and increased mortality because they increase cytokine responses and inflammation

in the lung following pneumococcal infection (Arredouani et al., 2006, Arredouani et al., 2004). On the other hand, anti-pneumococcal immunoglobulin G (IgG) mediates opsonisation and potentially enhances the Fc-gamma receptor (FcγR)-associated internalisation of pneumococci in macrophages (Ali et al., 2003). Interestingly, serum complement proteins also opsonise microbes (e.g. pneumococci) or particles in an antibody dependent or independent manner. For example, complement protein iC3b mediates the interaction of opsonised-pneumococci with CR3 (complement receptor 3), which increases pneumococcal phagocytosis by macrophages (Ali et al., 2003).

1.4.6. Microbicidal mechanisms of macrophages

Depending on the bacterial species, different phagocytic cells use different strategies for microbial killing. For example, ROS generated by nicotinamide adenine dinucleotide phosphate (NADPH) oxidase in phagocytic cells contributes to the killing of many bacteria. In addition, neutrophils express serine proteases such as cathepsin G and elastase for bacterial killing, which are not expressed in macrophages. Some species of bacteria, for example *S. pneumoniae*, evade oxidative stress with a variety of adaptive strategies.

For example, *S. pneumoniae* genes encode several enzymes, such as superoxide dismutase (SodA), which removes superoxide by encoding a manganese superoxide dismutase (MnSOD), a NADH oxidase (encoded by *Nox*), that converts O_2 to H_2O rather than superoxide, SpxB, a pyruvate oxidase that repletes cellular ATP during oxidative stress through conversion of acetyl phosphate to ATP, pneumococcal surface antigen (Psa) A and PsaD that encode a manganese permease and a putative glutathione reductase respectively, which together limit hydrogen peroxide generation by pyruvate oxidase (SpxB) and PsaD mitigates oxidative stress through glutathione reductase (Yesilkaya et al., 2000, Yu et al., 2001, Pericone et al., 2003, McAllister et al., 2004, Tseng et al., 2002, Potter et al., 2010). In this situation, macrophages need to change their antimicrobial strategies, for example, nitric oxide (NO) is generated via nitric oxide synthase (NOS) 2 and subsequently nitric oxide can react and form S-nitrosothiols such as S-nitrosoglutathione (GSNO) or react with ROS and generate peroxynitrite (one of reactive nitrogen species (RNS)), both of these make a significant contribution to early phagolysosomal killing of *S. pneumoniae* (Macmicking et al., 1997).

In addition, some virulence factors (pneumolysin or pneumococcal cell wall) of *S. pneumoniae* upregulate NO generation and stimulate NO-mediated bacterial killing (Orman et al., 1998, Braun et al., 1999, Marriott et al., 2004b). Other studies have also showed that NOS2 is indispensable for *S. pneumoniae* clearance from the lung of mice (Marriott et al., 2007, Dockrell et al., 2012b). Nevertheless, some bacterial genes help to evade and adapt to nitrosative stress (the effect of NO or RNS). For example, pneumococcal surface protein C (PspC) inhibits NOS2 mediated NO production, alcohol dehydrogenase C detoxifies S-nitrosoglutathione and caseinolytic peptidase P (ClpP) mitigates the effect of RNS (Peppoloni et al., 2006, Stroeher et al., 2007, Park et al., 2010). Therefore, it is clear that macrophages need to apply additional antimicrobial strategies with combinations of ROS and RNS, or with alternative strategies to mediate phagolysosomal killing to control lung infection with *S. pneumoniae*.

1.4.7. Apoptosis mediated microbial killing

Bacterial infection may induce pathogen-mediated apoptosis to allow the bacteria escape from the immune system (Zychlinsky and Sansonetti, 1997). Alternatively the host may activate macrophage apoptosis to maximise bacterial clearance and control detrimental inflammation (Bewley et al., 2014). Apoptosis-associated bacterial killing occurs after the exhaustion of initial macrophage microbicidal activity (in phagolysosomes).

The induction of apoptosis typically occur after 16-20 hours of bacterial ingestion *in vitro* (Marriott et al., 2004b). However, both *in vitro* and *in vivo* studies have demonstrated that macrophage apoptosis is involved with the clearance of *S. pneumoniae* (Dockrell et al., 2003, Dockrell et al., 2001). In addition, induction of apoptosis is positively correlated with the intracellular burden of bacteria in the case of pneumococci. The internalisation of pneumococci is increased by opsonisation (Ali et al., 2003).

Moreover, the pneumococcal capsule, which impedes bacterial internalisation or a caspase inhibitor down-regulates monocyte-derived macrophage (MDM) apoptosis (Ali et al., 2003), suggesting that intracellular bacteria induce caspase mediated macrophage apoptosis. A previous study also demonstrated that NO induces mitochondrial outer membrane permeabilisation and apoptosis mediated bacterial killing, whereas inhibition of NOS2 induces cell necrosis with decreased bacterial killing, suggesting the initial microbicidal response sensitised the macrophage for apoptosis (Marriott et al., 2004b). Recently Bewley

et al. demonstrated that the pneumococcal virulence protein pneumolysin activates both phagocytosis independent lysosomal membrane permeabilisation (LMP) and phagocytosis-dependent conversion of this signal to the later stages of apoptosis after bacterial internalisation.

Thus, the host response to this toxin promotes macrophage apoptosis rather than necrosis. The authors of this study also showed that cathepsin D plays a critical role in apoptosis induction which helps to downregulate the pro-inflammatory effects of LMP-mediated inflammasome activation through reduced pro-inflammatory cytokine generation (Bewley et al., 2014). In contrast, inhibition of the apoptotic response not only reduces bacterial killing but also increases pathogen-driven death by necrosis (Marriott et al., 2005, Bewley et al., 2011, Marriott et al., 2004b). Therefore, apoptotic macrophages down-regulate pro-inflammatory cytokine expression as well as the recruitment of other inflammatory cells and therefore they help control lung inflammation (Marriott et al., 2007, Marriott et al., 2006).

1.5. Macrophages role in COPD

The pulmonary macrophages help to maintain different anatomical compartments, including the alveolar spaces, airways and the interstitial lung space. Over 90% of pulmonary macrophages are AM in the alveolar spaces (van oud Alblas and van Furth, 1979), which were previously thought to originate from bone marrow progenitor cells or by local replication from interstitial lung macrophages. However, it now appears from the fate mapping experiments they are derived from foetal monocytes derived from haematopoietic stem cells (possibly from the foetal liver) that differentiate in an environment that contains GM-CSF, and that these cells maintain the resident population unless there is overwhelming depletion in which case adult monocytes can contribute to re-population (Epelman et al., 2014, Guilliams et al., 2013, Jakubzick et al., 2013). They are one of the most adept professional phagocytic cells and efficiently participate in limiting lung inflammation, with the clearance of lung irritants and pathogens in healthy subjects; whereas in COPD, AMs show phagocytic impairment with increased bacterial colonisation of the airway and subsequently patients suffer from persistent inflammation and declining lung function (Vlahos and Bozinovski, 2014).

Moreover, in COPD, recruited inflammatory macrophages are attracted to the lungs by alveolar epithelial cells (AECs) and resident macrophages through secretion of chemoattractants such as MCP-1 (Shapiro, 1999) in the presence of different noxious particles, complementing total numbers of macrophages in the alveolar space. Previous studies have also demonstrated that the upregulation of MCP-1 in sputum and BAL, which attracts a high number of macrophages (that originate from monocytes) into the alveoli and small airways of patients with COPD (Traves et al., 2002, Capelli et al., 1999, de Boer et al., 2000). These recruited inflammatory macrophages may be less able to regulate inflammatory responses in the lung.

Besides, a morphometric analysis showed a 25% increase of macrophage numbers in different respiratory compartments of emphysematous patients compared with smokers with normal lung function (Retamales et al., 2001). This indicates that AM numbers are positively associated with the severity of COPD. This assumption is strongly supported by an experimental model of COPD which demonstrated that depletion of pulmonary macrophages not only reduced smoke-induced airway remodelling and emphysema but also conferred protection against alteration of lung function (Beckett et al., 2013). However, either depletion of alveolar macrophages or impairment of their function causes

opportunistic infection and increases the susceptibility to *Streptococcus pneumoniae* colonisation and systemic invasion (Ghoneim et al., 2013).

In addition, AMs play indispensable role in the resolution of inflammation by scavenging exhausted neutrophils and cell debris (i.e. efferocytosis). Thus, it seems that the resident AMs play important protective roles in the lung, while a subset of recruited inflammatory macrophages in the airspace may contribute to disease pathogenesis. Although, at least in theory, it is possible that altered pro-inflammatory activation states in resident AM might also contribute to phenotype. From these enigmatic roles of AMs in the lungs, it is apparent that it is important to elucidate the role of macrophages organelles in their specific function, especially that of mitochondria.

Moreover, previous studies have shown that the upregulation of AMs mitochondrial ROS and the depletion of intracellular antioxidants (e.g. GSH) impair bacterial phagocytosis (Martí-Lliteras et al., 2009) and decrease efferocytosis (Hodge et al., 2007). The underlying mechanism of these phagocytosis impairments may be cigarette smoke - mediated oxidant-dependant RhoA activation (Richens et al., 2009) and Rac1 inhibition (Minematsu et al., 2011), which impedes actin polymerisation mediated efferocytosis. Interestingly, in the pulmonary milieu, both altered pro-inflammatory and anti-inflammatory functions of AMs could contribute to the overall phenotype of disease (Vlahos and Bozinovski, 2014), with an increase altered M1 AMs participating in the inflammatory role and an reduced M2 function limiting the resolution of inflammation (wound healing), as explained earlier.

1.5.1. Reactive oxygen/nitrogen species in COPD

Macrophages, along with other inflammatory cells (neutrophils, eosinophils) and structural cells (epithelial cells) are activated in the airways of COPD patients and produce ROS (MacNee, 2001), which contribute to the increased oxidative stress in the airways (Paredi et al., 2000, Montuschi et al., 2000, Rahman et al., 2002). Cigarette smoke extract and other stimuli cause activation and assembly of a multicomponent NADPH oxidase in the macrophage cell membrane which generates superoxide anion ($O_2.^-$). Then another enzyme, superoxide dismutase (SOD) converts the superoxide anion into hydrogen peroxide (H_2O_2) which is either detoxified to water by catalase or may form the highly reactive hydroxyl radical ($^{\cdot}OH$) by interacting with $O_2.^-$ in the presence of iron (Iles et al., 2002).

In addition, superoxide anion ($O_2.^-$) also combines strongly with NO to form peroxynitrite, causing an increase in 3-nitrotyrosine immunoreactivity in AMs of COPD patients (Ichinose et al., 2000). Peroxynitrite also generates the hydroxyl free radical (Beckman and Koppenol, 1996). NO is generated by NOS2 that is upregulated in AMs and lung parenchyma of patients with COPD (Ichinose et al., 2000, van Straaten et al., 1998, Maestrelli et al., 2003). Although the reactive oxygen/nitrogen species that are endogenously generated by the above mechanisms act as microbicidal molecules against pathogens, they also play an important role in cell signalling. For example, ROS also activate mitogen-activated protein (MAP) kinase signal transduction pathways and signalling pathways involving the GTPases Ras/Rac, c-Jun-NH_2-terminal kinase (JNK), p38 mitogen-activated MAPK, protein tyrosine kinase, as well as the transcription factors, such as NF-κB and activator protein (AP)-1 in COPD (Di Stefano et al., 2002) (Figure 1.3). These activated signalling pathways and transcription factors induce transcription of multiple inflammatory genes, including TNF-α, IL-8, GRO-α, MCP-1, GM-CSF, NOS2, proteases such as metalloproteinase (MMP)-9 and adhesion molecules (e.g. intercellular adhesion molecule (ICAM)-1).

In addition, oxidative stress also activates histone acetyltransferase (HAT) which subsequently modifies chromatin, allowing relaxation of chromatin structure, which enables the switching on of transcription of multiple inflammatory genes (Rahman, 2003, Tomita et al., 2003). Concomitantly, there is downregulation of histone deacetylase 2 (HDAC2) activity in COPD (Ito et al., 2005), suggesting the underlining cause of resistance to corticosteroid-mediated anti-inflammatory activity (steroid resistance) may involve epigenetic mechanisms involving oxidative stress (Meja et al., 2008, Ito et al., 2004). Indeed, oxidative stress activates phosphoinositide-3-kinase (PI-3K)–δ, which downregulates HDAC2 gene expression and decreases deacetylation activity (To et al., 2010). The expression and activity of nuclear factor erythroid 2-related factor2 (Nrf2), is also regulated by acetylation, but in this case a posttranslational acetylation of the protein, in contrast to acetylation of a gene, result in protein downregulation (Mercado et al., 2011). Nrf2 is an important transcription factor which controls expression of more than 200 cellular antioxidant and detoxifying enzymes through its interaction with antioxidant response elements within the promoters of these antioxidant and cytoprotective genes (Mercado et al., 2011). This indicates that ROS may undermine the endogenous anti-oxidant mediated cellular defences.

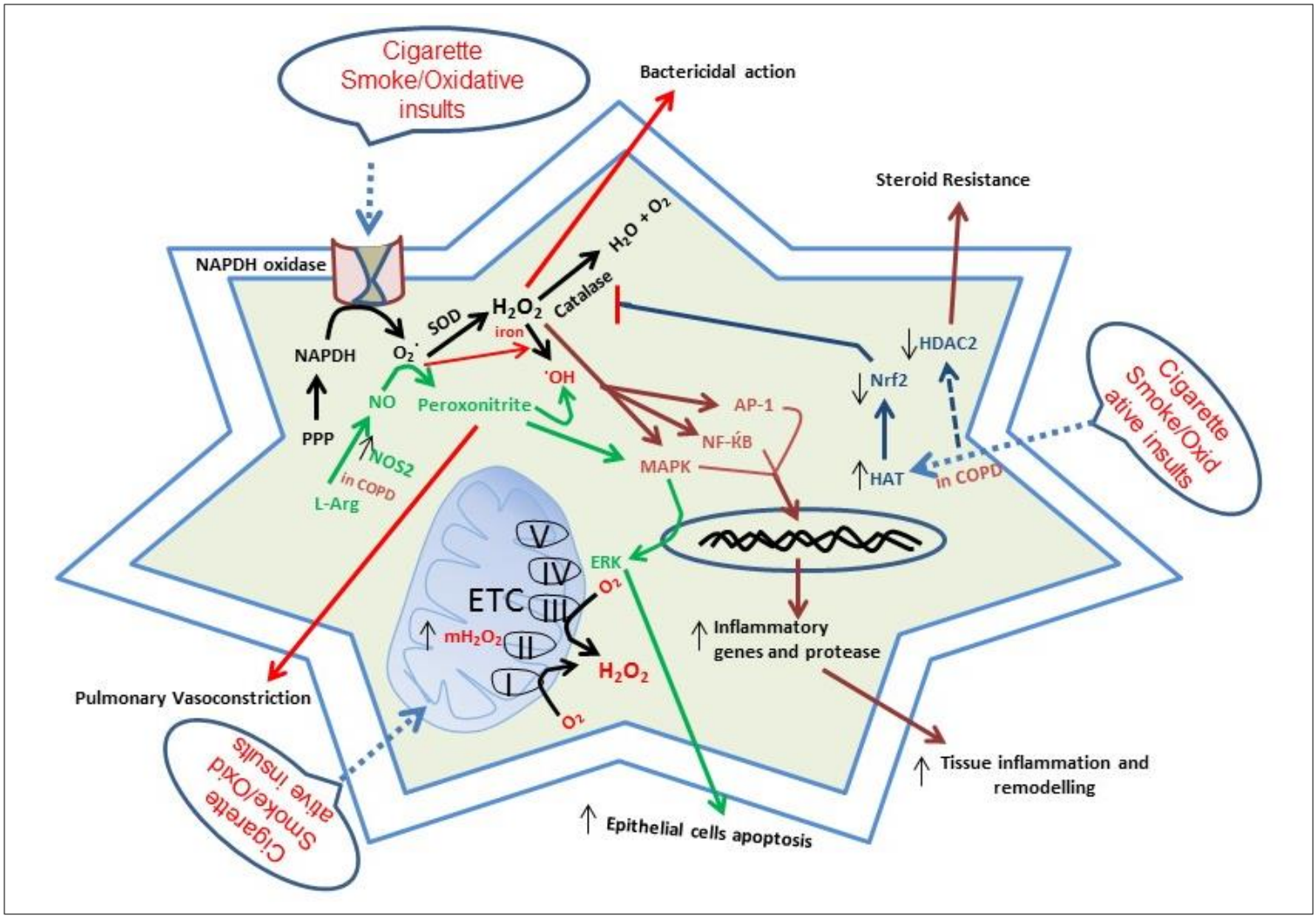

Figure 1.3. **Oxidative stresses in alveolar macrophages during COPD**. Cigarette smoke (CS) induces reactive oxygen/nitrogen species (ROS/RNS). CS also diminishes the antioxidant activity of cells. Subsequently ROS/RNS activates inflammatory genes and proteases. These reactive oxygen species also induce apoptosis of lung epithelial cells and trigger vasoconstriction. They deactivate nuclear factor erythroid 2-related factor 2 (Nrf2) and down-regulate histone deacetylase 2 (HDAC2), which inhibits anti-oxidants and corticosteroid activity, respectively. SOD-superoxide dismutase, NOS2- nitric oxide synthase 2, MAPK- mitogen activated protein kinase, AP-1- activator protein 1, NF-κB-nuclear factor kappa B, HAT-histone acetyl transferase.

Like ROS, peroxynitrite activates the MAP kinase pathway in airway epithelial cells and induces extracellular signal regulated kinase (ERK) signalling, which mediates epithelial cells apoptosis, adding to lung injury (Nabeyrat et al., 2003). In addition, peroxynitrite is also responsible for pulmonary vasoconstriction in normoxic rat lung but not in the hypoxic setting, suggesting a loss of normal physiological function (Nossaman et al., 2004). Furthermore, the lung is not only exposed to the above mentioned oxidative stress

but also other exogenous oxidants contained in cigarette smoke, itself an oxidant, and air pollutants, including ozone, nitrogen dioxide and diesel particulates, which may also increase the oxidative burden. These oxidative stresses are positively correlated with inflammatory gene expression, corticosteroid insensitivity, the prevalence of lung inflammation and COPD exacerbation (Sunyer, 2001).

1.6. Macrophages response to *S. pneumoniae* in HIV/AIDS compromised individuals

Pneumococcal pneumonia or invasive pneumococcal disease (IPD) is one of the leading causes of morbidity for human immunodeficiency virus (HIV) infected individuals (Gordin et al., 2008). Although the $CD4^+$ T-cell is main cellular reservoir for HIV-1, macrophages also provide an important site for cellular replication and cell-to-cell transmission to $CD4^-$- cells (e.g. epithelial/endothelial cells), which contributes to acquired immunodeficiency disease syndrome (AIDS) pathogenesis (Muratori et al., 2007). Moreover, the HIV-1 envelope glycoprotein (e.g. gp120) diminishes macrophage apoptosis by inducing the pro-survival cytokine macrophage colony stimulating factor (M-CSF), which upregulates the anti-apoptotic proteins Bfl-1 and Mcl-1 (Simon et al., 2007, Lum and Badley, 2003).

In addition, unlike most $CD4^+$ T cells, antiretroviral therapy (e.g. highly active anti-retroviral therapy (HAART)) does not penetrate into macrophages as effectively, hence HIV-1 can persist in macrophages and macrophages may form a cellular reservoir, in addition to that observed in $CD4^+$ memory T cells (Crowe and Sonza, 2000). Besides, HIV-1 infected monocyte-derived macrophages (MDM) are relatively resistant to the cytopathic effects of viral infection, and MDM can harbour the viral virions for prolonged periods in their cytosolic compartment (Cassol et al., 2006).

Furthermore, AMs from HIV-infected subjects exhibit a normal phagocytic index with opsonised *S. pneumoniae* (Gordon et al., 2001). However, AMs from HIV patients, who develop *Pneumocystis jirovecii* show decreased phagocytic capacity of *Staphylococcus aureus* (Musher et al., 1990). HIV-1 infection in bronchoalveolar lavage (BAL) also modulates mROS production, apoptosis and pneumococcal killing in AM (Collini et al., 2018), which might be one of the potential reasons for the increased susceptibility to IPD in people living with HIV. The HIV-1 envelope glycoprotein gp120 impinges macrophages function and inhibits apoptosis induction (Cummins et al., 2010, Cicala et al., 2002). Recently, it has been demonstrated that gp120 not only diminishes

mitochondrial respiration capacity but also remodels mitochondrial morphology, with increased mitochondrial size and length, as well as its dynamics in neurons (Avdoshina et al., 2016). A further study shows gp120 promotes mitochondrial fusion and downregulates the fission protein dynamin 1-like (DNM1L) in neurones (Fields et al., 2016). However, how gp120 in combination with *S. pneumoniae* effects macrophage function, particularly mitochondrial metabolism and dynamics needs to be elucidated.

1.7. Metabolic status and phenotype of Macrophages

The general purpose of catabolic metabolism is to generate units of energy in the form of adenosine triphosphate (ATP) from the breakdown of organic matter and this process is essential for sustaining life. A recent study demonstrated upregulation of metabolic processes such as oxidative phosphorylation, aerobic glycolysis and immune responses to infection by activated memory CD8 T cell as compared with naive (resting) CD8 T cells, illustrating that metabolic capacity is linked to immune functional capacity (Van Der Windt et al., 2013). Metabolic status is also considered a key aspect of macrophage polarisation. Macrophage activation by either classic or alternative pathways brings enormous changes in their metabolic profiles (Rodríguez-Prados et al., 2010). Metabolic impairments of macrophages are implicated in functional impairment. For instance, inhibition of the glycolytic enzymes PFK1 (phospho-fructo kinase 1) and PFK2 by glucocorticoids in macrophages, not only blocks glycolysis but also impedes cytokine production (Bustos and Sobrino, 1992).

In addition, macrophage's metabolic profile can depend on the type of activation, which influences metabolism of key molecules such as L-arginine, influencing macrophage function. For example, classical activation by LPS or INFγ (M1 phenotype) results in catabolism of arginine into microbicidal metabolites such as nitric oxide and generation of citrulline due to the upregulation of nitric oxide synthase (NOS2). In contrast, alternate activation by IL-4/13 (M2 phenotype) induces agrinase-1 (Arg1), which converts arginine into urea, polyamines and ornithine and facilitates wound healing (Corraliza et al., 1995, Munder et al., 1998). These findings emphasise the potential therapeutic target of immunometabolic reprogramming of macrophages in disease settings.

1.7.1. Metabolic profiles of M1 versus M2 macrophages

Cellular respiration involves a set of metabolic reactions which generate ATP for cellular activity. Recent studies have demonstrated that metabolic reactions in macrophages not

only maintain cellular homeostasis through the supply of energy (ATP) but also regulate function through generation of pro-inflammatory (M1) or anti-inflammatory (M2) macrophages (Corraliza et al., 1995, Munder et al., 1998). To achieve this there are distinct differences between M1 and M2 macrophage's cellular respiration. For instance, Gram negative bacterial LPS mediates classical macrophage activation (M1) and increases the extracellular acidification rate (ECAR) and decreases the oxygen consumption rate (OCR) (Haschemi et al., 2012), suggesting an increase in aerobic glycolysis, likely due to a modified 'Warburg' type effect. IFNγ/LPS also induces glutamine (Gln) uptake which is converted into succinate. The latter not only replenishes the Krebs cycle intermediate but also upregulates hypoxia inducible factor-1α (HIF-1α), a transcription factor which induces glycolytic flux through upregulation of genes involved in glycolytic metabolism (Tannahill et al., 2013). Others however have shown increases in glycolytic rate with enhanced cellular glucose uptake and conversion of pyruvate to lactate can also occur in a HIF-1α independent fashion, which is associated with downregulation of the rate of oxidative phosphorylation (Rodríguez-Prados et al., 2010). M1 macrophages also produce NADPH through the pentose phosphate pathway (PPP). Subsequently, NADPH plays an important role in the generation of cytosolic ROS and nitric oxide through NADPH oxidase and NOS2, respectively (Aktan, 2004).

On the other hand, IL-4 stimulated macrophages demonstrate only delayed and marginal upregulation of ECAR and no alteration in OCR (Haschemi et al., 2012), suggesting that the basal state in culture has a metabolic profile more similar to the M2 macrophage and it is classical activation that produces a transcriptional response to reprogramme macrophage metabolism towards a glycolytic pattern. M2 macrophages turn on fatty acid oxidation through β-oxidation and use respiration through oxidative phosphorylation with high expression of electron transport chain (ETC) components. In addition, M2 macrophages also stimulate the Krebs cycle through replenishment of its intermediates via pyruvate. The Krebs cycle produces both energy (ATP, GTP) and reducing equivalents (NADH, $FADH_2$) which also generate ATP through the ETC and OXPHOS. Moreover, previous studies demonstrated that oxidative metabolism is essential for the M2 phenotype because blocking metabolism through oxidative phosphorylation induces M1 characteristics in M2 macrophages. Similarly, inducing oxidative phosphorylation in M1 macrophages gives them a M2 phenotype (Rodríguez-Prados et al., 2010, Vats et al., 2006).

The different metabolic profiles are clearly distinguishable but the molecular mechanism by which different patterns of metabolic flux regulate macrophage polarisation is largely unknown. However, classically activated macrophages increase glycolytic flux through the transcriptional upregulation of the ubiquitous 6-phosphofructose-2-kinase/fructose-2,6-bisphosphatase (u-PFK2), a more active isoenzyme of PFK2 as compared to the liver-isoenzyme (L-PFK2) (Rodríguez-Prados et al., 2010). A recent study demonstrated that LPS upregulates the first and rate-limiting enzyme (glucose-6-phospate dehydrogenase) of the PPP pathway (Reales-Calderón et al., 2014). In addition, LPS mediated classical activation also downregulates the carbohydrate kinase like protein (CARKL) which enhances flow of glucose through the glycolytic and PPP pathway and limits the restriction of these pathways exerted by the CARKL product sedoheptulose-7-phosphate (S7P), which has the net effect of enhancing NADPH levels and thus ROS but also antioxidants such as glutathione (Haschemi et al., 2012).

High levels of CARKL in cells not only attenuates LPS-stimulated superoxide production but also downregulates pro-inflammatory cytokine (IL-6 and IL-1β) production, suggesting that CARKL over-expression may reverse a M1 phenotype and favour a M2 phenotype in macrophages (Haschemi et al., 2012). In contrast, alternatively activated macrophages, stimulated with IL-4, upregulate L-PFK2 and down-regulate fructose-2,6-bisphosphate (a positive modulator of phosphofructo-kinase1), thus they decrease the glycolytic flux, but this is compensated through oxidative metabolism, involving fatty acid oxidation and oxidative phosphorylation. IL-4 activates STAT6, a transcription factor which subsequently turns on the co-activator protein peroxisome proliferator-activated receptor (PPAR)γ-coactivator-1β (PGC-1β) and this upregulates mitochondrial respiration and biogenesis (St-pierre et al., 2003, Shao et al., 2010) (Figure 1.4).

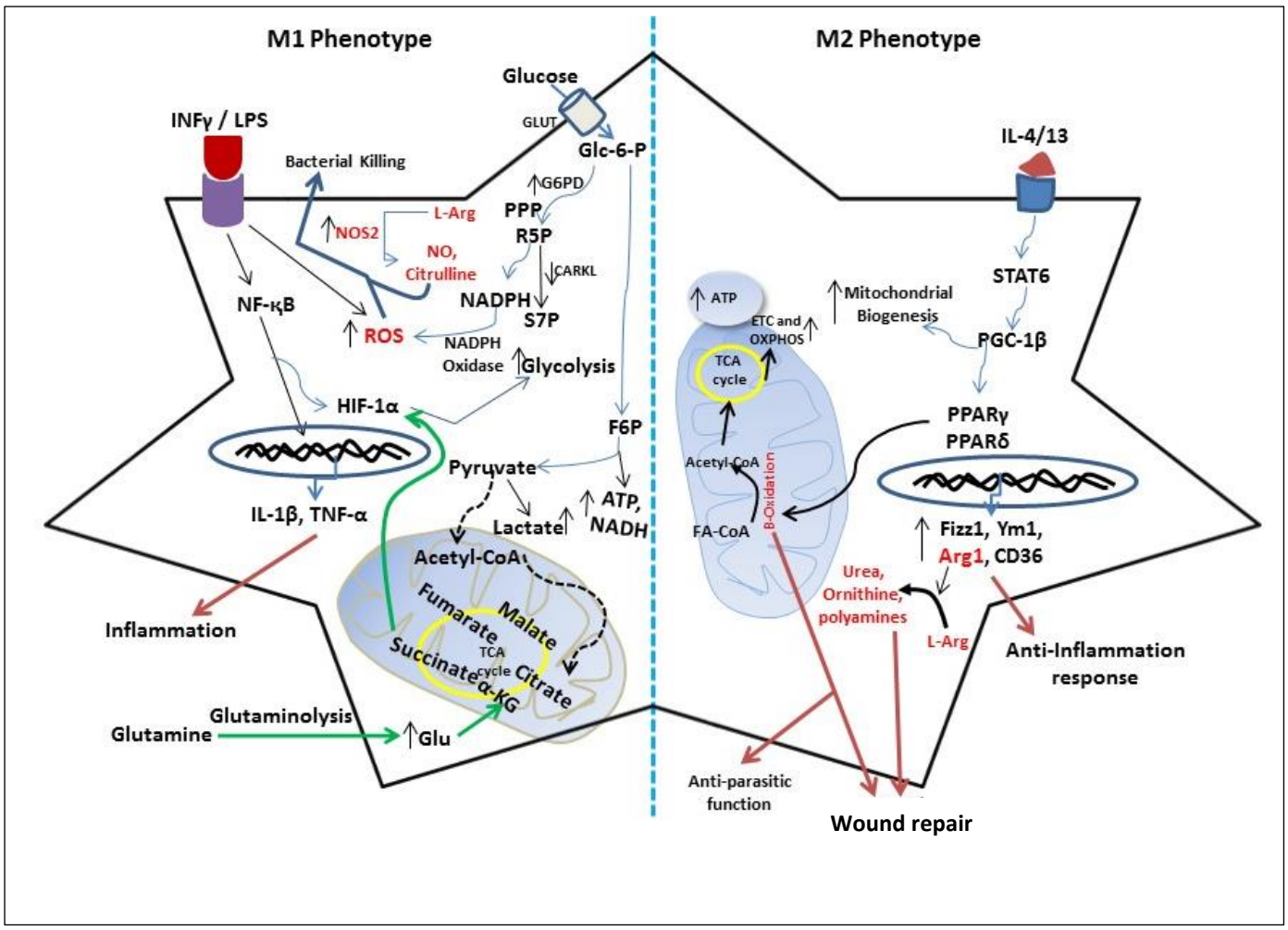

Figure 1.4. **Metabolic profile of M1 and M2 macrophages**. Lipopolysaccharide (LPS) and interferon-γ (IFNγ) mediate classical activated M1 macrophages, inducing glycolysis as well as the pentose phosphate pathway (PPP). M1 macrophages also upregulate inflammatory cytokines through stimulation of the NF-κB signal transduction pathway. In addition, LPS/TLR-4 also induce the glycolytic flux through stabilising hypoxia-inducible factor-1α (HIF-1α). HIF-1α is also stabilised by the Krebs cycle intermediate succinate. In the mitochondrial matrix, the level of succinate is increased through glutaminolysis of glutamine. The uptake of glutamine is also increased in M1 macrophages. On the other hand, IL-4 or IL-13 activates macrophages into an M2 phenotype (also called alternatively activated macrophages). In M2 macrophages, IL-4/IL-4R activates STAT6/PGC-1α signal transduction pathways which induce mitochondrial OXPHOS, fatty acid β-oxidation and mitochondrial biogenesis. Moreover, M2 macrophages also upregulate anti-parasitic and anti-inflammatory cytokines. STAT6 –Signal transducer and activator of transcription 6, PGC-1β –Peroxisome proliferator-activated receptor gamma coactivator-1β, PPP –pentose phosphate pathway, NOS2 –nitric oxide synthase 2, ROS –reactive oxygen species, Arg2 –arginase2, Glu –glutamate, GLUT –glucose transporter. Figure is adapted from (Galvan-Pena and O'Neill, 2014).

There is evidence that knock-out of the transcription factor PGC-1β alters the metabolic status and function of M2 macrophages since it is a key transcription factor for several genes encoding factors required for oxidative phosphorylation (Vats et al., 2006). Thus, PGC-1β plays a pivotal role in metabolic reprogramming of M2 macrophages. Apart from

this, a recent study demonstrated that the TNF-α induced protein 8-like 2 (TIPE2) can change M1 macrophages to a M2 phenotype by inducing arginase1 mediated arginine metabolism (Lou et al., 2014). Recent reviews have highlighted the positive correlation between the severity of COPD and mitochondrial ROS production with decreased expression of antioxidants and impaired metabolism by oxidative phosphorylation (Kirkham and Barnes, 2013, Meyer et al., 2013). Since the focus has been on muscle cells, epithelial cells and recruited inflammatory cells as sources of ROS it is unclear how macrophages contribute to this. Although elevated macrophage production of ROS might suggest the contribution of an M1 macrophage, this does not fit with evidence for an M2 bias amongst alveolar macrophages during COPD (Shaykhiev et al., 2009b). Modulating the mitochondrial bioenergetic flux and M1 and M2 phenotype of macrophages could be a therapeutic approach for the management of chronic inflammatory diseases such as COPD.

1.8. Mitochondrial Biology

1.8.1. Mitochondrial structure and its physiological importance

The mitochondrion (plural mitochondria) is a double-membrane containing organelle, which is ubiquitous in all eukaryotic organisms. It is called the metabolic hub and is considered as a power-house of the cell, because it links and regulates almost all metabolic pathways in the cell and produces most of the cellular energy as ATP. Mitochondria also occupy up to 25% of the volume of the cytoplasm, in amounts that vary by cell type. Structurally they are separated from the cytoplasm by the outer and inner membranes. However, these two-layer lipid membranes are separated by a ~20nm gap, called the intermembrane space, which is equivalent to the bacterial periplasm. An α-proteobacterium – a Gram-negative bacterium - seems to be the ancestor of mitochondria (Gray et al., 1999). Although conventional electron microscopy (EM) images with ultrathin plastic sections suggests that some sites have direct contact between outer and inner membranes (Schleyer and Neupert, 1985, Perkins et al., 1997), modern cryo-electron microscopy (cryo-EM) images of unfixed, unstained organelles demonstrate that proteins such as the translocases of outer membrane (TOM) and translocases of inner membrane (TIM) form a super-complex which spans the intermembrane space and are held together by the polypeptide chain in the transit (~20 nm in length) (Gold et al., 2014). The latter observation suggests that conventional electron tomography with fixed, dehydrated and heavy-metal stained cells could induce

the artefact contact sites between outer and inner membrane (reviewed in (Kuhlbrandt, 2015)).

In addition, the mitochondrial outer and inner membrane show a distinctive structural and functional phenotype. For example, the outer membrane is a permeable membrane which allows ions and small, uncharged molecules to move through porins - the pore-forming membrane proteins. For example, the voltage-dependent anion channel (VDAC) allows free movement of ions and small molecules, however larger molecules (e.g. proteins) are imported by special translocases (Bayrhuber et al., 2008). Hence there is no membrane potential resulting from movement of free ions across the outer membrane.

On the other hand, the inner mitochondrial membrane (IMM) has a tight diffusion barrier which does not allow free movement of ions or molecules without aid of specific transporters. For example, the mitochondrial electron transport chain's (ETC) complex I, III and IV pump out protons (H+) to the intermembrane space, from the mitochondrial innermost compartment - known as the mitochondrial matrix - to create an electrochemical gradient. This gradient is coupled with mitochondrial oxidative phosphorylation, which produces ATP by ATP synthase (complex V), and couples this to flux of protons from the intermembrane space to the matrix. Evolutionarily conserved mitochondrial matrix is similar to the bacterial cytoplasm, but its pH is quite high 7.9 to 8.0, much like chloroplast stroma (Llopis et al., 1998). Moreover, the IMM also builds up an electrochemical membrane potential (~ -180 mV) as a result of its ion selectivity. The high pH and electrochemical potential allow cationic marker probes (attached with a triphenyl phosphonium cationic group) such as Mitotracker (green or red), MitoSox red and JC-1 (5,5',6,6'-tetrachloro-1,1',3,3'-tetraethyl benzimidazolyl carbocyanine iodide) to stain mitochondria, mROS and the inner mitochondrial transmembrane potential ($\Delta\Psi_m$), respectively.

In addition, the IMM also forms a special folded structure called a crista (plural-cristae), which protrudes throughout the matrix. The crista lumen is also defined as the third compartment of mitochondria, which mostly holds the fully assembled electron transport complexes (i.e. complex I to V of mitochondrial ETC and OXPHOS) (Vogel et al., 2006). This lumen also contains large amounts of cytochrome c - a soluble electron carrier protein, which carries electrons from complex III (cytochrome oxidoreductase/reductase) to complex IV (cytochrome oxidase) of the ETC (Berg JM, 2002). Moreover, cristae play a pivotal role in cellular physiology. For example, in tissues which have a high energy demand (e.g. skeletal or heart muscle cells), the cristae form a highly stacked disk-like

lamellae which occupy most of the mitochondrial inner volume (Figure 1.5 is taken from (Kuhlbrandt, 2015)). Whereas in tissues with lower energy demands (e.g. liver, kidney), the cristae leave more room for the matrix and form a less compact structure. Moreover, it is postulated that cristae folding or invaginations prevent protons from escaping the mitochondrial intermembrane space, into the cytosol, which enhances ATP production by ATP synthase (reviewed in (Kuhlbrandt, 2015)).

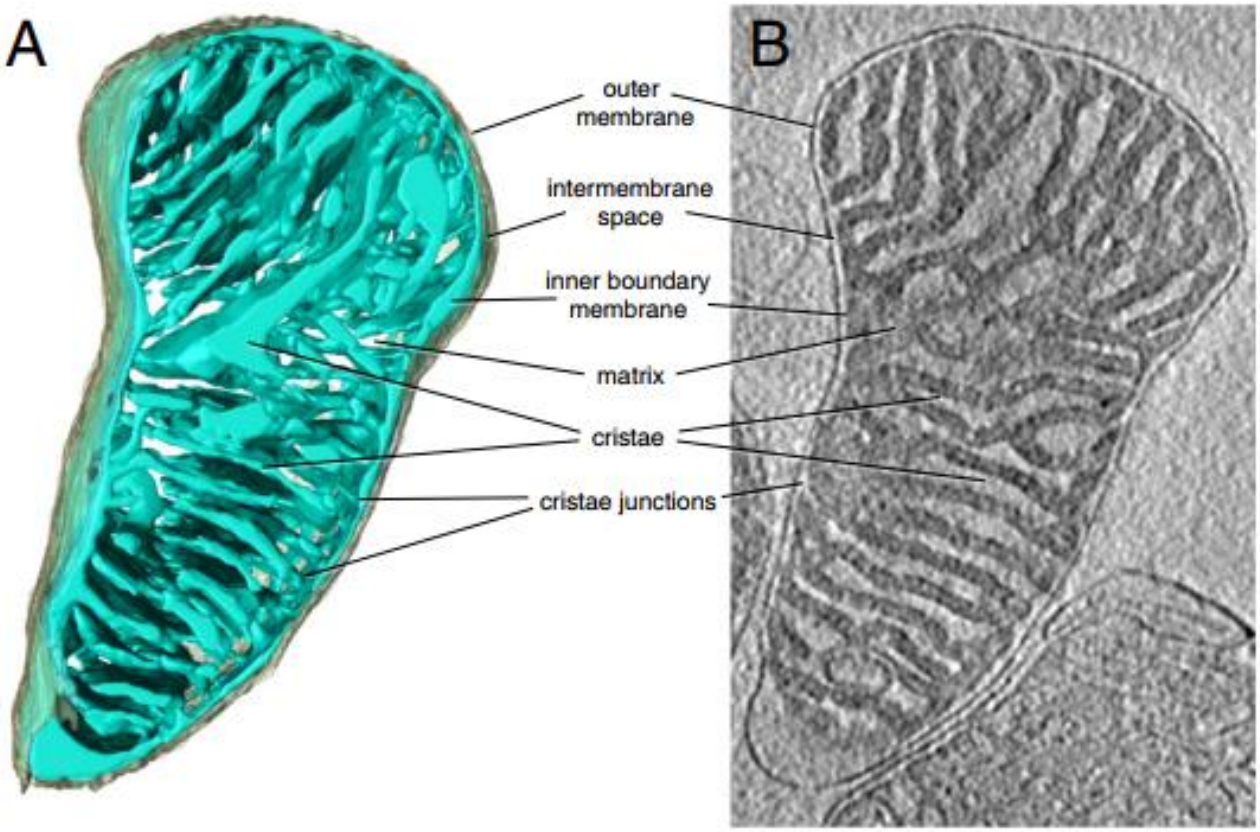

Figure 1.5. **Tomographic view of mouse heart mitochondrion**. Figure A shows the three dimensional volume of a mitochondrion, which is determined by modern Cryo-Electron microscopy (cryo-EM). It shows the outermost membrane (grey) surrounded by the inner membrane (light blue). Figure B shows the tomographic slice of a mitochondrion. Figure is copied from (Kuhlbrandt, 2015).

1.8.2. Mitochondrial genome

The mitochondrial genome is the only extra-chromosomal DNA within most eukaryotic cells (except for chloroplasts in plant cells). Its genome size is only 16.6kb in humans, which consists of a multicopy, circular double-strand DNA, similar to a bacterial genome. Its genome encodes 13 polypeptides within mitochondrial organelles, and these

polypeptides are indispensable for mitochondrial OXPHOS and RNA machineries (reviewed in (Taylor and Turnbull, 2005)). However, mitochondrial physiology is regulated by both nuclear and mitochondrial DNA. For example, the fully functional mitochondrial ETC (e.g. the OXPHOS) is comprised by nuclear-encoded genes and the above mentioned 13 mitochondrial polypeptides.

1.8.3. Mitochondrial metabolism

Eukaryotic cells maintain physiological functions in different anatomical compartments. However, the major metabolic pathways in different compartments are interlinked. The mitochondrion is the central point of cellular metabolism. For example, the end product of glycolysis, pyruvate, is converted into acetyl-CoA by pyruvate dehydrogenase in the mitochondrial matrix. Moreover, mitochondrial fatty acid metabolism, also called β-oxidation, produces acetyl-CoA (David and Michael, 2008). This acetyl-CoA combines with oxaloacetate to yield citrate and initiate the tricarboxylic acid cycle (TCA cycle, also called the Krebs cycle) which is the central pathway of cellular oxidative metabolism (Geoffrey, 2000). During each cycle, two carbon atoms of citrate are completely oxidised into two molecules of carbon-dioxide, producing one molecule of GTP, three molecules of NADH and one molecule of FADH2.

In the mitochondrial matrix, NADH is oxidised and releases electrons to complex I (i.e. NADH dehydrogenase), whilst FADH2 also releases electrons to complex II (i.e. succinate dehydrogenase) in the mitochondrial respiration chain. Electrons from these complexes (I and II) are transferred to complex III (i.e. cytochrome reductase) by the soluble electron carrier protein ubiquinone (Q). Then cytochrome c accepts electrons from complex III and transfers these to complex IV (i.e. cytochrome oxidase), where it is reduces molecular oxygen to water (David and Michael, 2008). During this electron passage, protons are pumped out (by complex I, III and IV) from the matrix to the intermembrane space and generate an electrochemical gradient, also known as the proton-motive force (Δp) (reviewed in (Jastroch et al., 2010)). This force drives protons back into the matrix through the nano-machine ATP synthase (complex V), and the resulting free energy is coupled with ATP production from ADP and inorganic phosphate (Mitchell, 1961). However, like a hydroelectric engine, this coupling is not one hundred percent efficient, because protons can return to the matrix without ATP synthase. This proton by-passing process is called proton leak. The rate of proton leak can be measured

indirectly, in the presence of oligomycin - an inhibitor of ATP synthase (Jastroch et al., 2010).

Besides, mitochondrial reactive oxygen species (mROS) are produced as a by-product of mitochondrial OXPHOS (Balaban et al., 2005). Superoxide is produced as a result of single electron leak from the ETC and transfer to dioxygen (O_2), instead of an electron pair mediating the reduction of oxygen to H_2O, at complex IV of the mitochondrial respiration chain (Murphy, 2009). Evidence suggests that electron leak (or slippage) happens at complex I, which produces superoxide only at the matrix, and at complex III, which produces superoxide both sides of the inner mitochondrial membrane (Raha and Robinson, 2000).

In addition, during different cellular physiological conditions, mitochondrial TCA cycle intermediates are removed to serve as biosynthesis precursors, or they are replenished by other metabolites. For example, one of the TCA cycle intermediates, α-ketoglutarate, is produced from glutamate, which is replenished from glutamine through glutaminolysis (David and Michael, 2008) (Figure 1.6).

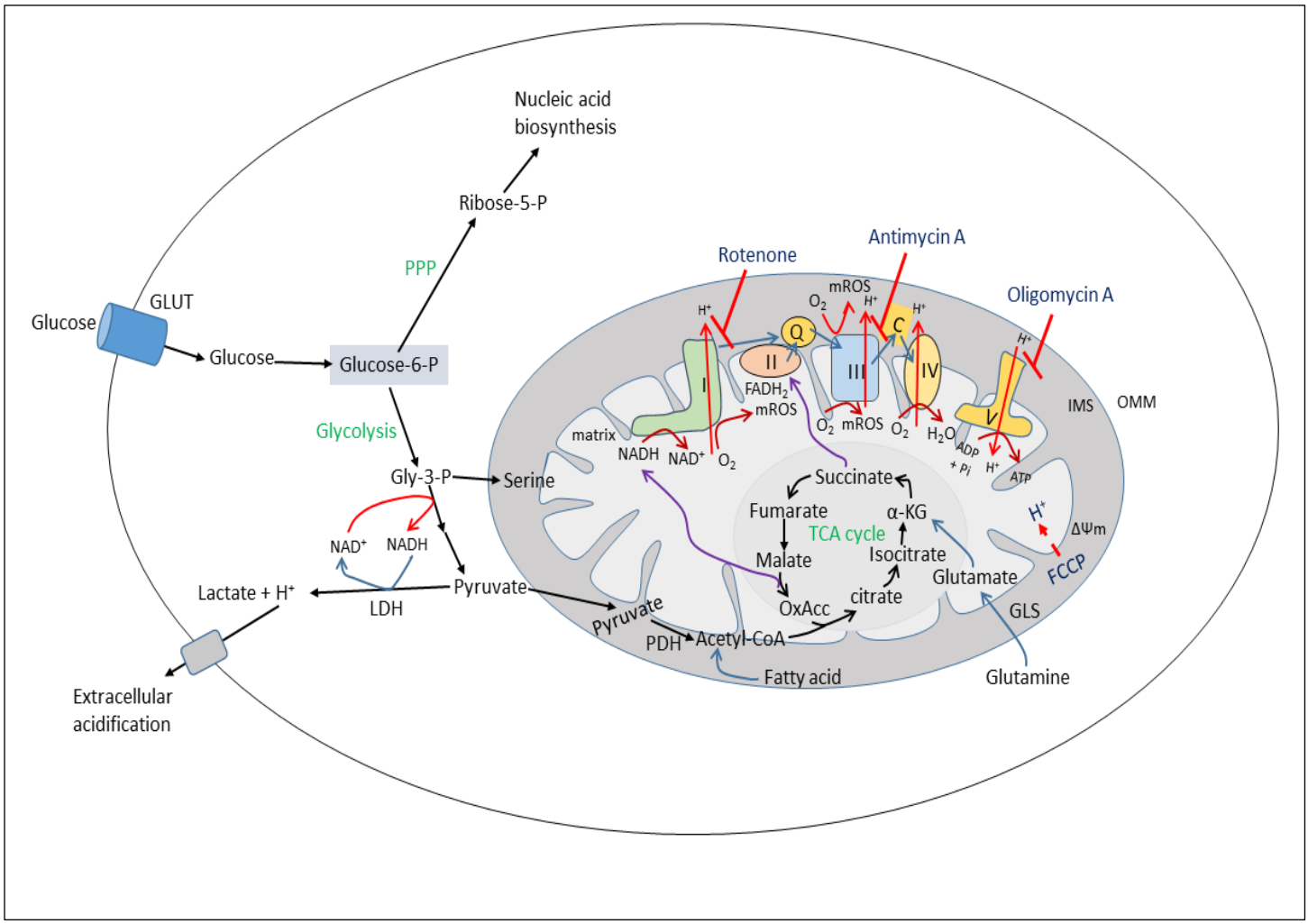

Figure 1.6. **Mitochondrial metabolism is interlinked.** In most eukaryotic cells glucose is oxidised to pyruvate by glycolysis or oxidised by the pentose phosphate pathway (PPP) to produce nucleic acids precursors. Pyruvate is converted to lactate under hypoxic or anaerobic conditions, resulting in extracellular acidification. Whereas, under aerobic conditions, pyruvate is converted into Acetyl-CoA by pyruvate dehydrogenase in the mitochondrial matrix. Acetyl-CoA and oxaloacetate produce citrate which enters into the Krebs cycle (i.e. TCA cycle). Acetyl-coA is also produced from β-oxidation of fatty acids which replenishes the TCA cycle intermediate citrate. Moreover, glutamine replenishes the TCA cycle intermediate, α-ketoglutarate (α-KG), which is converted into succinate. Both glycolysis and the TCA cycle produce reducing equivalents as NADH, which releases electrons to complex I of mitochondrial OXPHOS. The TCA cycle also produces FADH2 which donates electrons to complex II (succinate dehydrogenase). Electrons from complex I and II are carried to complex III by ubiquinone (Q). Then cytochrome c carries electrons from complex III to IV. At complex IV electrons reduce oxygen into water. The figure also shows that protons (H^+) are pumped out from the matrix to the intermembrane space (IMS) through complex I, III and IV. Moreover, premature release of free electrons from the ETC, mainly via complex I and III, produce superoxide (mROS). The mitochondrial ETC is inhibited by the complex I inhibitor rotenone or the complex III inhibitor antimycin A or the complex V inhibitor oligomycin A. Like uncoupler proteins, FCCP (is a synthetic OXPHOS uncoupler) that carries proton from IMS to the matrix and diminishes $\Delta\Psi_m$. OMM-outer mitochondrial membrane.

1.8.4. Physiological importance of proton and electron leak

The basal proton leak is quite variable from tissue to tissue, and it contributes significantly to the basal metabolic rate (BMR, also called the resting metabolic rate). This is the energy expenditure per unit time during the resting state. For example, approximately 20-30% of BMR is utilised as proton leak in rat hepatocytes, whereas it is up to 50% of BMR in skeletal muscle (Brand et al., 1999). This basal proton leak is induced by fatty acids and reactive alkenals (e.g. 4-hydroxynonenal), which upregulate IMM anion carrier proteins ANT (adenine nucleotide translocase) and UCPs (uncoupling proteins) (Parker et al., 2008).

Moreover, proton leak also implies the coupling efficiency of mitochondrial OXPHOS. Thus, more proton leak retrospectively produces less ATP, which is mostly observed during aging (Conley et al., 2007). However, proton leak is indispensable for heat production in brown adipose tissue, where high abundance UCP1 transports protons from intermembrane space to the matrix. Apparently, it seems that the futile proton cycle of proton pumping and leakage allows human infants, small rodents and hibernators to adapt in the winter season (Cannon and Nedergaard, 2004). In addition, UCP1 in brown adipocytes is also activated by catecholamine release from sympathetic nerves in the form of noradrenergic stimulation (Jastroch et al., 2010), which emphasises the importance of stimuli such as noradrenaline (norepinephrine) as a positive modulator of uncoupling and physiological thermal regulation.

On the other hand, electron leak from the mitochondrial ETC/complexes results in superoxide production. At low concentrations, the resulting mROS may be associated with signal transduction, but at high concentrations cause detrimental effects to cellular molecules (Murphy, 2009). Moreover, recent studies demonstrated that mROS has a role in innate immunity (West et al., 2011b). For example, mROS significantly contributes to intracellular bacterial killing in the phagolysosomes of macrophages (West et al., 2011a, Bewley et al., 2017).

1.9. Mitochondrial homeostasis and its role after bacterial infection

1.9.1. Mitochondrial complexity and its role in cellular homeostasis

The word ‘mitochondrion’ originates from the Greek words ‘mitos’ for thread and ‘chondros’ for grain. They are highly dynamic organelles in eukaryotic cells. Moreover, they frequently fuse (a process termed ‘fusion’) and divide (‘fission’), which dictates the

average size and degree of connectivity in the mitochondrial network. A typical mitochondrial population is quite variable in size (<1 to ≥15μm) and they maintain a complex network with a tubule-like structure. In cells, mitochondria are heterogeneous in both functional and morphological aspects (Collins et al., 2002). They regulate a number of cellular processes such as metabolism, proliferation and apoptosis. Mitochondrial fission and fusion ensure the quality of mitochondria. For example, a damaged mitochondrion can combat its functional failure through integration (i.e. fusion) with a healthy mitochondrion, which allows exchange of mitochondrial DNA and proteins between them (Chan, 2006, Tomoko et al., 2001).

In contrast, a severely damaged mitochondrion triggers fission or fragmentation to generate smaller mitochondria that also lose their inner mitochondrial transmembrane potential ($\Delta\psi_m$), which is critical since $\Delta\psi_m$ is indispensable for fusion (Legros et al., 2002). However, mitochondrial fission events often generate two populations of progeny mitochondria. One population exhibits increased $\Delta\psi_m$, which shows a high probability of subsequent fusion with nearby healthy mitochondria. Whilst another group shows decreased membrane potential and a lessened probability of fusion or integration with healthy mitochondria. Rather the latter population is either removed by selective autophagy (i.e. mitophagy) (Twig et al., 2008) or triggers programmed cell death (i.e. apoptosis) (Richard and Mariusz, 2005) (Figure 1.7).

1.9.2. Mitochondrial roles in innate immunity

Mitochondria originate from a symbiotic relationship between an α-proteobacterium and eukaryotic cell more than two billion years ago (Gray et al., 1999). They maintain a distinct double-membrane compartment and have their own circular genome. Moreover, mitochondria are the central hub of cellular metabolism and they show cell- and tissue-specific morphological phenotypes, and have dynamic behaviour with constant fission or fusion (Jonathan and Jodi, 2014). These mitochondrial dynamics are essential to maintain an interconnecting network and cellular homeostasis (Suen et al., 2008). Previous studies demonstrated that some specific TLR-agonists augment mROS production (West et al., 2011a) and downregulation of mROS production reduces the bactericidal activity of macrophages (Hall et al., 2013).

In addition, the metabolic rewiring of mitochondria, shifting metabolism from OXPHOS to glycolysis, disrupts the Krebs cycle and leads to the generation of pro-inflammatory cytokines. During this process, LPS-stimulated M1 macrophages accumulate succinate,

which acts as a signalling molecule to upregulate HIF-1α and induces IL-1β production (Tannahill et al., 2013). Moreover, the mitochondrial Krebs cycle intermediate citrate is converted into itaconic acid that limits the growth of intracellular bacteria, such as *Salmonella enterica* and *Mycobacterium tuberculosis* (Jha et al., 2015, Alessandro et al., 2013). Furthermore, succinate induces mROS production, by reverse electron transfer to complex I, rather than to the downstream electron carrier ubiquinone in the mitochondrial ETC (Lambert and Brand, 2004, Liu et al., 2002, Hansford et al., 1997). Thus, the shifts in immunometabolism associated with classical activation allow the mitochondria to generate metabolites that play a role in microbicidal responses or stimulate pro-inflammatory cytokines.

1.9.3. Mechanism of mitochondrial fission/fusion

Dynamic fission and fusion of mitochondria are indispensable for mitochondrial homeostasis and cellular viability (Chan DC, Cell, 2012). For example, interruption of mitochondrial fusion causes the loss of $\Delta\psi_m$, as well as hampering embryonic development (Chen et al., 2003). Whereas, defective mitochondrial fission is associated with increased inflammation in macrophages (Sangjun et al., 2015).

In addition, mitochondrial fission is universally linked with programmed cell death (i.e. apoptosis) (Suen et al., 2008). Mitochondrial fission is promoted by the recruitment of a GTPase, called dynamin-related protein 1 (Drp1), to the outer membrane. Subsequently, Drp1 forms a ring-like structure through oligomerisation. The ring-shaped Drp1-oligomers constrict both outer and inner membranes and produce smaller fragmented mitochondria (Scott and David, 2007). Drp1 is a cytosolic protein, which is translocated to the mitochondria during fission, and this recruitment is regulated by post-translational modifications. For example, cyclin-dependent kinase 1 (CDK1) or protein kinase c delta (PKCδ) mediates phosphorylation of Drp1 at serine 616 (S616 isoform 1 of Drp1 corresponds to 579 of isoform 3 in *H. sapiens*) promoting mitochondrial fission (Ishihara et al., 2007) during mitosis or oxidative stress, whilst phosphorylation at serine 637 by cyclic AMP-dependent protein kinase A (PKA) impairs its recruitment to the mitochondria (Chang and Blackstone, 2007). Moreover, Drp1 also interacts with multiple putative receptors such as mitochondrial fission factor (Mff), mitochondrial fission protein 1 (Fis1), mitochondrial dynamics protein 49 (MiD49) and MiD51 in the mitochondrial outer membrane, to execute fission (Loson et al., 2013).

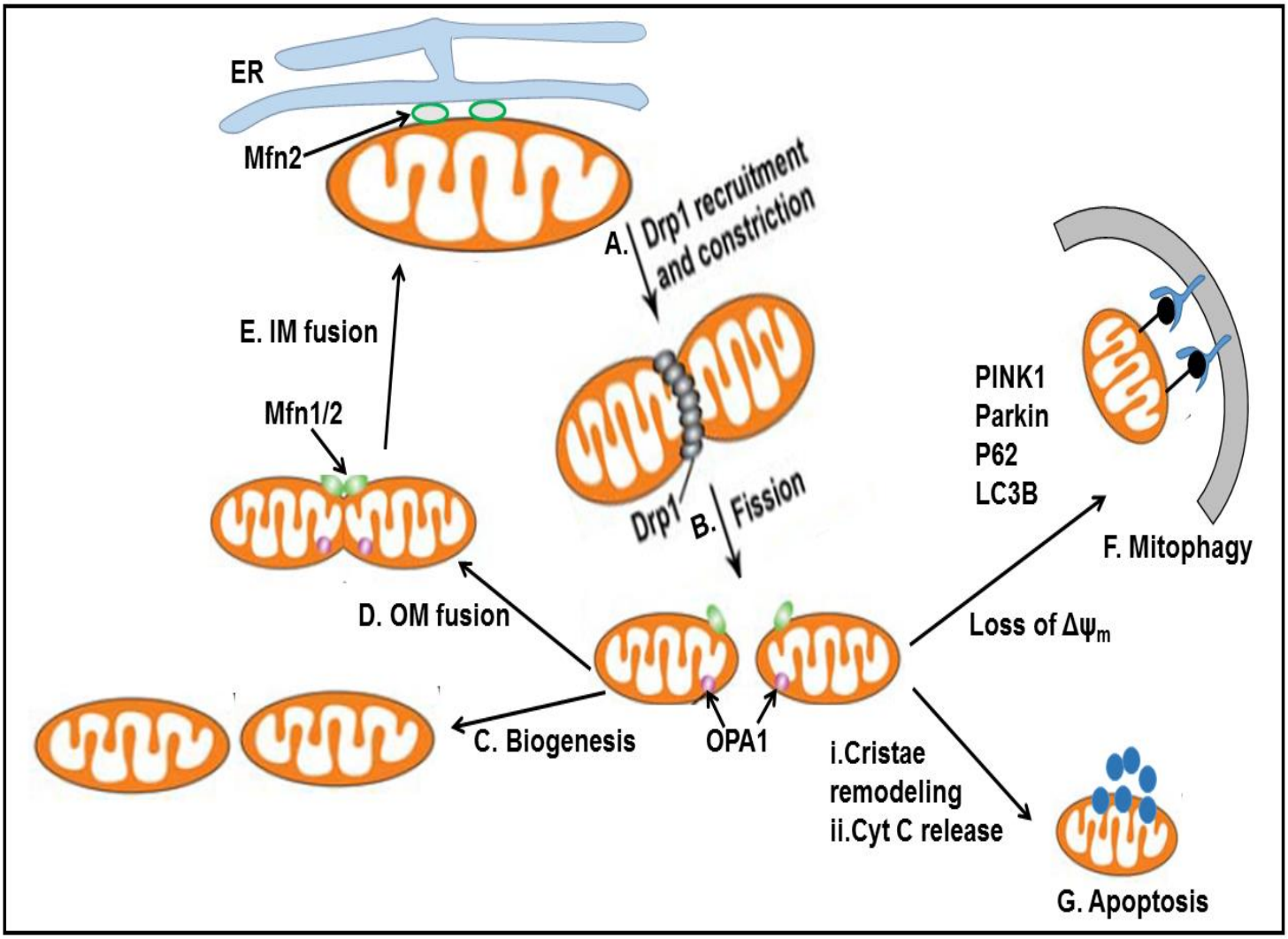

Figure 1.7**. Mechanisms of mitochondrial fission and fusion.** During fission (A-B), mitochondria recruit dynamin related protein 1 (Drp1) to their outer membrane from the cytosol. Then Drp1 assemble with Fis1 and form chain-like structures across the membrane through oligomerisation. This oligomer then constricts mitochondrial membranes, and mitochondrial fission divides one mitochondrion into two progeny mitochondria. The nascent mitochondria become like their parental mitochondrion by biogenesis (C). Mitochondria are mostly tethered with endoplasmic reticulum (ER) to mitofusin 2. Alternatively, mitochondrial fusion (D-E) is orchestrated by mitofusin 1 or 2 (Mfn1/2) in the outer membrane, and optic atrophy 1 (Opa1) in the inner membrane. Mfn1/2 works like glue, to merge the outer membrane of two neighbouring mitochondrion. Opa1 seals then the inner membrane and forms a fused mitochondrion. Physiological stress (e.g. oxidative stress) breaks the constitutive reversible fission/fusion cycle. Excessive fission either turns on mitophagy, through recruitment of Pink1/Parkin and the adapter molecule p62 and the cytoskeleton protein LC3B, or triggers apoptosis through release cytochrome c from fragmented mitochondria. Figure is adapted from (Cai and Tammineni, 2016).

In addition, Endoplasmic reticulum (ER)-mitochondria tethering is indispensable for mitochondrial fission (Friedman et al., 2011). F-actin filaments are required to regulate mitochondrial network fragmentation in DRP-1 dependent models of fission (De Vos et al., 2005). On the other hand, mitochondrial fusion is indispensable for the oxidative phosphorylation (Chen and Chan, 2010). The molecular players for mammalian cell mitochondrial fusion are mitofusin 1/2 (Mfn1/2), which are GTPases that localise to the outer mitochondrial membrane. Moreover, Opa1 (optic atrophy type 1) - another GTPase located in the IMM - is also essential for fusion (Chen et al., 2003). Mitochondrial fusion is initiated by the homotypic/heterotypic interactions of outer membrane proteins Mfn1/2 in adjacent mitochondria, triggering outer membrane fusion (Chen et al., 2003). Whereas, Opa1, on the opposing mitochondrion's inner membrane promotes their integration (Otera and Mihara, 2011) (Figure 1.7).

1.9.4. Mitochondrial fission's role in mitophagy

Autophagy (derived from the Greek autophagos which means 'eating of self') is a self-degradation or catabolic process which mostly acts as a survival mechanism for cells, during starvation and stress conditions. This process plays a housekeeping role through degradation of misfolded or aggregated intracellular proteins and damaged organelles, as well as intracellular pathogens, by forming a circular double membrane autophagosome (Glick et al., 2010). For example, when mitochondrial damage (e.g. through accumulation of misfolded polypeptides) is identified in a cell, mitochondrial quality surveillance pathways such as (i) protease-associated degradation and (ii) selective autophagy (also called mitophagy), perform the repair function based on the persistence of mitochondrial damage cues. For instance, if the mitochondrial damage is not sufficiently repaired, the damaged mitochondria show diminished respiration capacity and loss of $\Delta\psi_m$, so mitochondrial quality monitoring systems recruit mitophagy to selectively remove the damaged mitochondria from the population (Lazarou, 2015). Frank *et al.* demonstrated that transient mild oxidative stress induces Drp1-dependent mitochondrial fission which recruits LC3 to the fragmented mitochondria and triggers mitophagy in mammalian cells. They also showed that a dominant-negative Drp1 ($Drp1^{k38A}$) not only inhibits oxidative stress associated mitochondrial fission, but also prevents induction of mitophagy (Frank et al., 2012), suggesting that fission is an upstream process of mitophagy. In the same year another group demonstrated that mitophagy reduces mROS production, whilst mitophagy-deficient (autophagy-related protein Atg32 or Atg11 knockout) yeast produce

excessive mROS. This mROS damages mitochondria, which produces more mROS and creates a vicious cycle (Kurihara et al., 2012).

On the other hand, overexpression of Parkin (an E3 ubiquitin ligase) in an FCCP-treated depolarised mitochondria, triggers mitophagy (Narendra et al., 2008). Moreover, PINK1 (a mitochondrial kinase) (Ziviani et al., 2010), p62 and NIX are essential for Parkin-dependent oxidative stress mediated mitophagy (Ding et al., 2010). Interestingly, Parkin also has a positive role in innate immunity. For example, mutations in Parkin's regulatory regions increase the susceptibility to infectious disease in humans (Ali et al., 2006, Mira et al., 2004). In addition, Parkin also interacts with the mitochondrial translocator protein and voltage-dependent anion channel 1 protein complex (TSPO-VDAC1) and both factors are required for immunity during bacterial infection in Drosophila (Cho et al., 2015). However, Parkin's precise role in mitochondrial responses during innate immunity remain to be determined.

1.9.5. Relationship between mitochondrial dynamics and apoptosis

Mitochondrial dynamics (fission and fusion) are maintained by the cellular cytoskeleton, which governs mitochondrial number, morphology and subcellular distribution inside living cells (Bereiterhahn and Voth, 1994). Perturbation of these mitochondrial processes have profound influences on cellular viability (Karbowski and Youle, 2003). For example, inhibition of mitochondrial fission inhibits programmed cell death. Moreover, mitochondria trigger fragmentation before the activation of caspases, the family of apoptosis executioner cysteine proteases (Richard and Mariusz, 2005). Inhibition of Fis1, which triggers fission after combining with Drp1, respectively show inhibits apoptosis while overexpression of Fis1stimulates the mammalian mitochondrial apoptosis pathway (Lee et al., 2004, James et al., 2003). Collectively, this suggests that mitochondrial fission is essential for caspase-associated intrinsic (mitochondrial) pathway of apoptosis. This pathway of programmed cell death involves activation of caspase 9, by cytochrome c that is released from the mitochondrial intermembrane space after mitochondrial outer membrane permeabilisation (MOMP) and which forms an apoptosome with apoptotic protease activating factor (Apaf-1) to cleave caspase 9, which in turn activates the downstream executioner caspases such as caspase 3 (Xiong et al., 2014). However, excessive fission can occur without triggering apoptosis. For example, FCCP-induced mitochondrial fission does not alter cell viability (Richard and Mariusz, 2005). Rather

FCCP-mediated excessive mitochondrial fission activates the pro-survival process, autophagy (Narendra et al., 2008).

Moreover, viral infection, for instance with cytomegalovirus (CMV), also induces mitochondrial fission/fragmentation which also does not induce apoptosis (Damien et al., 2004, Poncet et al., 2004). Interestingly, HIV-1 viral protein R (vpr) and hepatitis B virus protein HBx interact with mitochondrial outer membrane proteins voltage dependent anion channel VDAC and VDAC3, resulting in the opening of the mitochondrial permeability transition pore (MPTP), loss of $\Delta\Psi_m$, massive mitochondrial fragmentation, and subsequent apoptosis (Jacotot et al., 2000, Rahmani et al., 2000). My host group has previously demonstrated that *Streptococcus pneumoniae* reduces mitochondrial $\Delta\Psi_m$ and induces intrinsic apoptosis in macrophages (Marriott et al., 2004b). Therefore, further investigation of mitochondrial dynamics was warranted, particularly to determine if there was a relationship between fission and macrophage apoptosis after challenge with pneumococci.

1.10. Hypothesis and aims

It is clear that macrophages are a critical cellular effector of innate immune responses against *S. pneumoniae*. Macrophages sense bacterial presence very rapidly by their cell membrane and cytoplasmic pattern recognition receptors, demonstrating plasticity in their morphology, functional phenotype and metabolism. Moreover, macrophages also need to adapt these responses to engage a range of antimicrobial strategies after phagocytosis of bacteria that include mitochondrial-mediated responses such as generation of mROS and apoptosis, to eradicate internalised bacteria.

I hypothesised that;

the macrophage response to *S. pneumoniae* involves changes in mitochondrial metabolism and dynamics, which optimises the microbicidal response to pneumococci by enhancing mROS generation and enhances the mitochondrial contribution to innate immunity in response to internalised bacteria.

On the basis of my hypothesis, the aims of my doctoral work were:

1. To investigate macrophage metabolic phenotypes during host-pathogen interactions between macrophages and *S. pneumoniae*

2. To observe any defects in the macrophages host response to *S. pneumoniae* mitochondrial respiration, during COPD or HIV-1 infection in macrophages, conditions associated with both altered mitochondrial dynamics and susceptibility to pneumococci.
3. To evaluate mROS and nitric oxide levels, investigating their interaction with the pneumococcus and their localisation relative to mitochondria and phagolysosomes.
4. To observe mitochondrial morphology and dynamics, after challenge with *S. pneumoniae* and
5. To examine the role and relationship of mitochondrial dynamics to microbicidal responses generated by macrophages during innate immunity to pneumococci.

Chapter 2. Methods and materials

2.1. Study site and ethical issue

The study was conducted in the Department of Infection, Immunity and Cardiovascular Disease, Medical School, University of Sheffield. Approval for mouse experiments was from the Sheffield Ethical Review Committee, University of Sheffield and were conducted in accordance with the Home Office Animals (Scientific Procedures) 1986 under Project license 40/3251. Human blood was drawn from healthy volunteers from Sheffield teaching hospital (STH), University of Sheffield. Recruitment of COPD patients and age-matched healthy volunteers were approved by the National Research Ethics Service (NRES) committee Yorkshire and the Humber (Sheffield cohort, reference number: 10/H1016/25). Written consent from STH's staff, students, COPD patients and age-matched healthy volunteers were obtained as a requirement of ethical guidelines.

2.2. Mouse Bone-Marrow cells culture

Bone-marrow progenitor cells (BMPC) were extracted from C57BL/6 mouse femurs and tibias and placed in Dulbecco's Modified Eagle's Media (BioWhittaker®DMEM, Lonza, BE12-604F). Cell clumps were removed by pipetting up and down gently with a 1mL pipette. BMPC were counted with a haemocytometer, centrifuged for 5 minutes at 200xg at 4°C and resuspended in 10% dimethyl sulfoxide (DMSO, Sigma-Aldrich, C67-68-5) + 90% heat inactivated fetal calf serum at 7.5×10^6 cells/mL and placed in vials at 1mL/vial. BMPC were frozen slowly to -80°C and then transferred for storage in liquid nitrogen. Cell vials were thawed under a running tap water and diluted in 50mL warm DMEM media supplemented with 10% heat inactivated fetal calf serum, 10% L929 conditional medium (source of M-CSF), penicillin (100U/mL) and streptomycin (100µg/mL). After counting in a haemocytometer, the cell suspension was re-adjusted to 2.0×10^5 cells/mL by adding DMEM culture medium. Subsequently, 25 mL was added to a T-75 cell culture flask or 1mL/well to a 24-well culture plate (Corning Inc. NY) with or without coverslips (size:13x13mm), and incubated in an incubator at 37°C and 5% CO_2. After 5 days, the medium was changed, non-adherent cells were removed, and media replaced with DMEM media supplemented with 10% heat inactivated fetal calf serum and 10% L929 conditional medium without penicillin/streptomycin. The medium was then replaced every other day up to 14 days. These differentiated BMPC, also called bone-marrow derived macrophages (BMDM) were used for extracellular flux assays and other experiments.

2.3. Human PBMCs culture and differentiated into monocyte-derived macrophages

Human peripheral blood mononuclear cells (PBMCs) were separated from whole blood by Ficoll-Paque^{TM} (GE Healthcare, Life Sciences) density centrifugation. Briefly, 25 mL of heparinised blood was gently added onto 12.5 mL of Ficoll-Paque^{TM} in a 50 mL centrifuge tube (Thermo-Fisher Scientific). Subsequently, blood was centrifuged at 1500 rpm for 23 minutes. Then the mononuclear cell layer was transferred to a sterile 50 mL centrifuge tube and diluted to 50 mL with phosphate buffered saline (PBS, Oxoid). The tube was then centrifuged at 1000 rpm (rotation per minute) for 10 minutes. The pellet was resuspended with PBS and centrifuged again at 1000 rpm for 10 minutes. Finally, PBMCs were counted by a haemocytometer and the cell number readjusted to 2 x 10^6 cells/mL with RPMI 1640 media (Lonza) supplemented with 10% fetal calf serum and 2mM L-glutamine (Gibco BRL). These PBMCs were seeded at 1 mL/well in 24 well plates or 20 mL/flask in T-75 flasks and differentiated into monocytes-derived macrophages (MDM) after 14 days culture, as described previously (Dockrell et al., 2001).

2.4. Culture and stock of *Streptococcus pneumoniae*

S. pneumoniae serotype 2 (wild type D39 strain, NCTC 7466) or pneumolysin deficient D39 [(STOP D39 or ΔD39, as described in (Bewley et al., 2014)] was plated onto Columbia blood agar (CBA) plates and incubated overnight in the incubator at 37^{o}C and 5% CO_2. Pneumococcal colonies were confirmed by observing their microbiological characteristics such as Gram stain positivity, catalase reaction negativity and optochin sensitivity. Moreover, it was also observed that the colonies were haemolytic on blood agar and form diplococci. Subsequently, 9-10 colony forming units (cfu) were selected from each blood agar plate and inoculated in culture broth of brain heart infusion (BHI, a mixture of 12.5g/L brain infusion solids and 5.0g/L beef heart infusion solids supplemented with 10.0g/L proteose peptone, 2.0g/L glucose, 5.0g/L NaCl, 2.5g/L Di-sodium phosphate (Oxoid, CM1135)). To make 250mL of BHI broth, 9.26g of BHI mixture powder was dissolved in 250mL distilled water and autoclaved at 121^{o}C for 15 minutes. 9-10 cfu were inoculated into 30mL BHI broth with 20% heat inactivated fetal calf serum (in a 50 mL centrifuge tube), then put on a shaker (at 250 rpm) in an incubator at 37^{o}C and 5% CO_2. Subsequently, optical density (OD at 610nm) was recorded at different time points. Simultaneously, serial dilutions of bacterial suspensions were added

onto blood agar plates to estimate the bacterial cfu at the comparable time points, a technique called the Miles-Misra surface viable count method (Miles et al., 1938). The growth curve from the recorded OD and Miles-Misra count was used to estimate the mid-log phase. The bacterial suspension at mid-log phase was then stored at -80^{o}C in an Eppendorf tube (1mL/vial).

2.4.1. Opsonisation and heat inactivation of *S. pneumoniae*

The stored aliquot of *S. pneumoniae* was thawed in running tap water and centrifuged at 9000 rpm for 3 minutes and washed twice with PBS. Subsequently, the bacterial suspension (in serum free DMEM/RPMI 1640 media) was opsonised either with 10% mouse pooled immune serum collected from the Pneumovax (PPV23) immunised mouse whole blood or 10% human pooled immune serum collected from the PPV23 immunised adult humans whole blood, incubated for 30 minutes at 200 rpm at 37^{o}C and 5% CO_2. For heat inactivation, freshly thawed bacterial suspension was kept in a heat block at 60^{o}C for 40 minutes. This was then centrifuged at 9000 rpm for 3 minutes and washed with PBS twice before opsonisation with mouse immune serum. The opsonised heat inactive pneumococci were washed twice with PBS, and centrifuged at 9000 rpm for 3 minutes. The bacterial pellet was re-suspended in 1mL DMEM medium. Finally, bacterial viability was re-checked by the Miles-Misra method (Miles et al., 1938) to confirm heat inactivation, with confirmation of no bacterial growth. Opsonised live bacteria and heat inactivated D39 were exposed to mouse BMDM or human MDM in subsequent experiments.

2.5. Optimisation of Seahorse extracellular flux assay conditions with BMDM

After 14 days of culture the supernatant was discarded from adherent BMDM in T-75 cell culture flasks and the cells washed once with 5mL sterile Dulbecco's PBS (Life Technologies). Cells were detached by incubating with 5mL/flask Accutase (Biolegend) for 15 minutes at 37^{o}C and 5% CO_2. After detachment, the cell suspension was centrifuged at 200xg for 10 minutes at 20^{o}C. The cell pellet was resuspended in DMEM medium at a concentration of $2x10^6$ BMDM/mL, after counting by haemocytometer. Subsequently, different concentrations of cell suspensions were prepared through diluting with DMEM medium, to get 1000,000 to 5000,000 cells/mL. 100μL/well of these cell suspensions were seeded in XF24 cell plates to get $1x10^5$, $2x10^5$, $3x10^5$ and $5x10^5$ BMDM/well unless other cell densities are stated.

The plates were incubated for 2 hours at 37ºC and 5% CO_2. 150µL/well DMEM medium was added without disturbing the seeded cells and the plates left overnight at 37ºC and 5% CO_2. The following day, the supernatant was removed, and wells washed once with XF assay medium (XFAM, Bioscience) supplemented with 25mM glucose (pH adjusted to 7.4) medium. Subsequently, 630µL/well XFAM with 25mM glucose was added and incubated at 37 ºC for an hour in a warm room. Simultaneously, the XF24 sensor cartridges (Seahorse Bioscience) were hydrated for consistent results. Thus, 1mL/well XF calibrant pH 7.4 (Seahorse Bioscience) was added to the Seahorse XF24 flux plate and a sensor cartridge applied to the top of the plate so that the sensors were submerged in calibrant solution. Then the plate was hydrated at 37ºC without CO_2 in a warm room for 16 hours. For titration of the cell number, 70µL of XFAM with 5.5mM (1 g/L) glucose medium was added in port A of the cartridge, and kept at 37ºC without CO_2 in a warm room for an hour. The cartridge contained 24 probes (with H^+ and O_2 sensors) along with 4 injection ports (A-D) attached to each probe. The injection ports inject pneumatically and deliver different substrates/inhibitors/stimulators simultaneously to all the wells of the Seahorse cell culture microplate. To start recordings from the experiment the Seahorse cartridge with flux plate was loaded into the Seahorse flux analyser. Then, a calibration step was performed for approximately 6 minutes, after this only the XF24 flux plate was removed and the cell plate loaded. Next, the equilibration was performed prior to initiation of the mixing, waiting and measuring cycle. The analyser measured both the extracellular acidification rate (ECAR) or proton production rate (PPR) by the H^+ sensor, and also the oxygen consumption rate (OCR) by the O_2 sensor, making measurements kinetically in real time in a non-invasive way.

2.5.1. Schematic work flow for the Seahorse Extracellular flux assay

As described in the section 2.5, XF24 cell plate was prepared through re-seeding either mouse BMDM or human MDM and the XF24 flux plate prepared simultaneously with the XF calibrant (1mL/well) and incubated overnight. Following day, cell plate was with mock-infected or challenged with opsonised *S. pneumoniae* and incubated for a specific time point (see below). Subsequently, the non-buffered XF assay medium (BD, Bioscience) with antibiotics (penicillin and streptomycin) and supplements was added onto the cell plate and incubated for 60 minutes at 37ºC without CO_2. Parallelly, the XF flux plate was prepared through adding either Glyco-stress test (i.e. measurement of glycolysis) inhibitors such as oligomycin A and 2-deoxy-D-glucose (2DG) in the

cartridge's injection port A and B, respectively or Mito-stress test (i.e. measurement of mitochondrial OXPHOS) inhibitors such as oligomycin A, FCCP and rotenone plus antimycin A in the cartridge's injection port A, B and C, respectively and incubated for 60 minutes at 37ºC without CO_2. Subsequently, the XF flux plate with the sensors (H^+ and O_2 sensors) cartridge was loaded into the XF24 flux analyser for calibration. After calibration, the flux plate was unloaded without the cartridge. Next, the cell plate was loaded into the flux analyser. Subsequently, the analyser automatically added either Glyco-stress test inhibitors or Mito-stress test inhibitors consecutively according to the customised command programme. The H^+ (proton) sensor measures the glycolytic metabolism as the rate of acidification or rate of the extracellular proton production (ECAR) and the O_2 sensor measures mitochondrial OXPHOS as the rate of oxygen consumption (OCR) in a non-invasive and real time manner. From the Glycol-stress or Mito-stress test kinetic data, we can measure the different glycolysis or mitochondrial OXPHOS related parameters using the following formulae (also labelled in Fig 2.1):

i. **Basal glycolysis (ECAR)** = Rate of baseline glycolysis – Rate of glycolysis after 2DG treatment.
ii. **Maximum glycolytic capacity** = Rate of glycolysis after oligomycin A treatment – Rate of glycolysis after 2DG treatment.
iii. **Glycolytic reserve** = Rate of glycolysis after oligomycin A treatment – Rate of basal glycolysis.
iv. **Non-glycolytic acidification** = Rate of glycolysis after 2DG treatment.

v. **Basal OXPHOS (OCR)** = Baseline OCR – OCR after rotenone plus antimycin A treatment.
vi. **ATP-linked OCR =** OCR after oligomycin treatment – Basal OCR.
vii. **Maximum respiration capacity** = OCR after FCCP treatment – OCR after rotenone plus antimycin A treatment.
viii. **Respiration reserve/spare =** OCR after FCCP treatment – Basal OCR
ix. **Proton (H^+) leak =** OCR after oligomycin treatment - OCR after rotenone plus antimycin A treatment.
x. **Non-mitochondrial OCR** = OCR after rotenone plus antimycin A treatment.

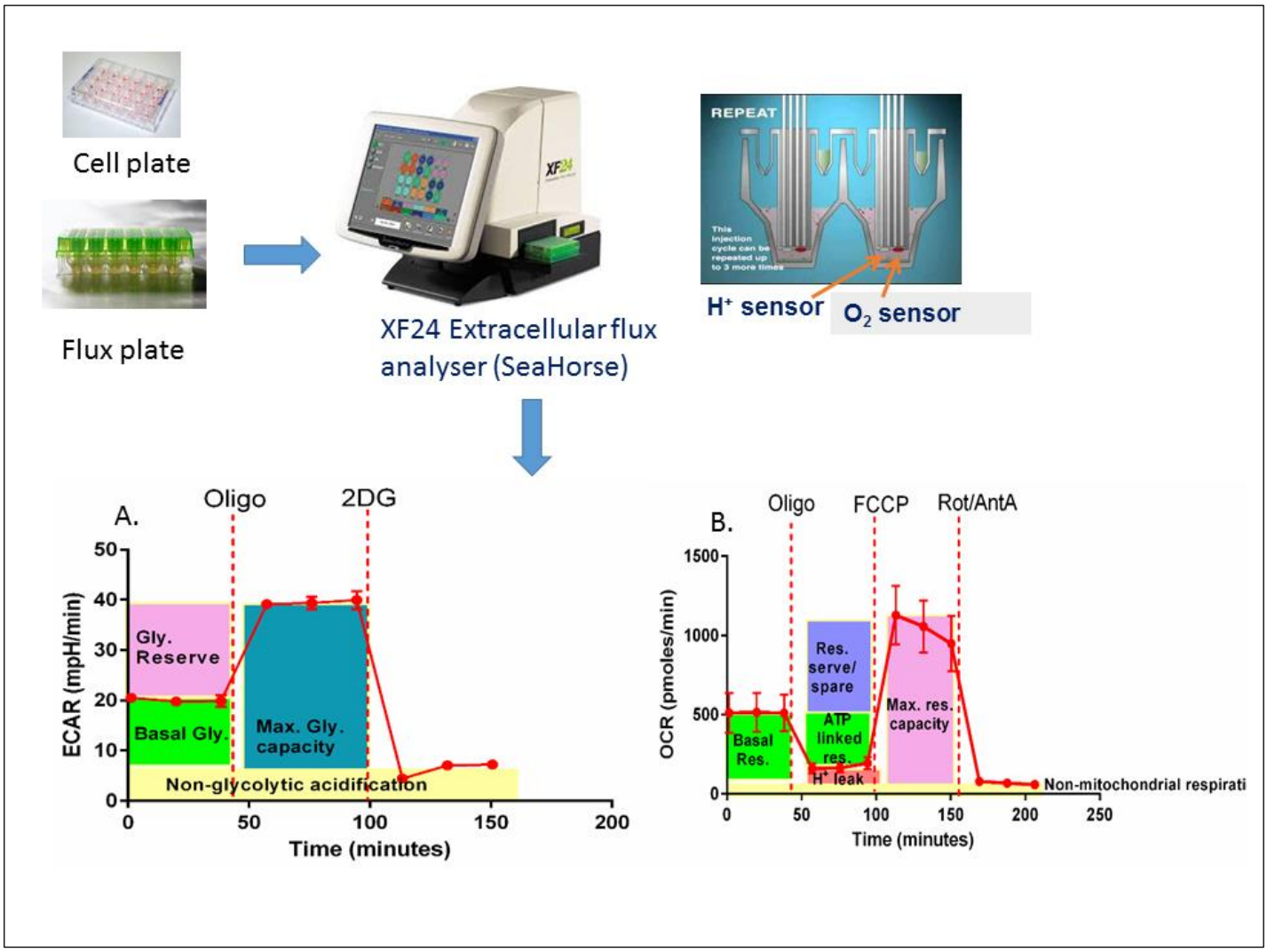

Figure 2.1. **Schematic diagram for the extracellular flux assay with the XF 24 flux analyser.** Figure shows the major steps of extracellular flux assay, briefly the flux plate with the cartridge is loaded into the XF24 flux analyser to complete the assay calibration. Subsequently, the cell plate is loaded into the analyser. Next, the XF24 flux analyser measures (A) the extracellular acidification rate (ECAR) as mpH/minute using the proton (H^+) sensor and (B) the oxygen consumption rate (OCR) as pmoles/minute using the oxygen (O_2) sensor. The diagram also shows different sets of glycolytic and OXPHOS parameters which are labelled in the respective kinetic data. Oligo –Oligomycin, 2DG –2-deoxy-D-glucose, FCCP –Carbonyl cyanide-4-(trifluromethoxy) phenylhydrazone, Rot –Rotenone, AntA –Antimycin A.

2.6. Normalisation of Seahorse data

2.6.1. Normalisation using total cell count

At the end of the Seahorse experiment, CyQuant® NF dye (Invitrogen, C35007) was used to estimate cell numbers. A stock solution was made up by adding 2µL of Cyquant dye/mL of 1x Hank's Balanced Salt Solution (HBSS) buffer and 200µL of this solution was added into each well of the Seahorse cell plate and the plate incubated for an hour at 37ºC without CO_2 in a warm room. Then, the plate was loaded in the InCell Analyser2000 to capture (20x) images from the central area of each well, capturing a total of 9 fields for each well. After acquisition, automated image analysis was performed with the InCell Developer toolbox 1.9 software (GE Healthcare) using custom-developed analysis protocol. For cell segmentation and nuclei count readout, images were captured in the eGFP/FITC channel using 490nm excitation and 525nm emission wavelength filters with a 0.1 second exposure time. The custom protocol developed for nuclei count readout identifies nuclei based on object segmentation and data is reported as the sum of the nuclei count for the whole well (*i.e.* central 9 fields).

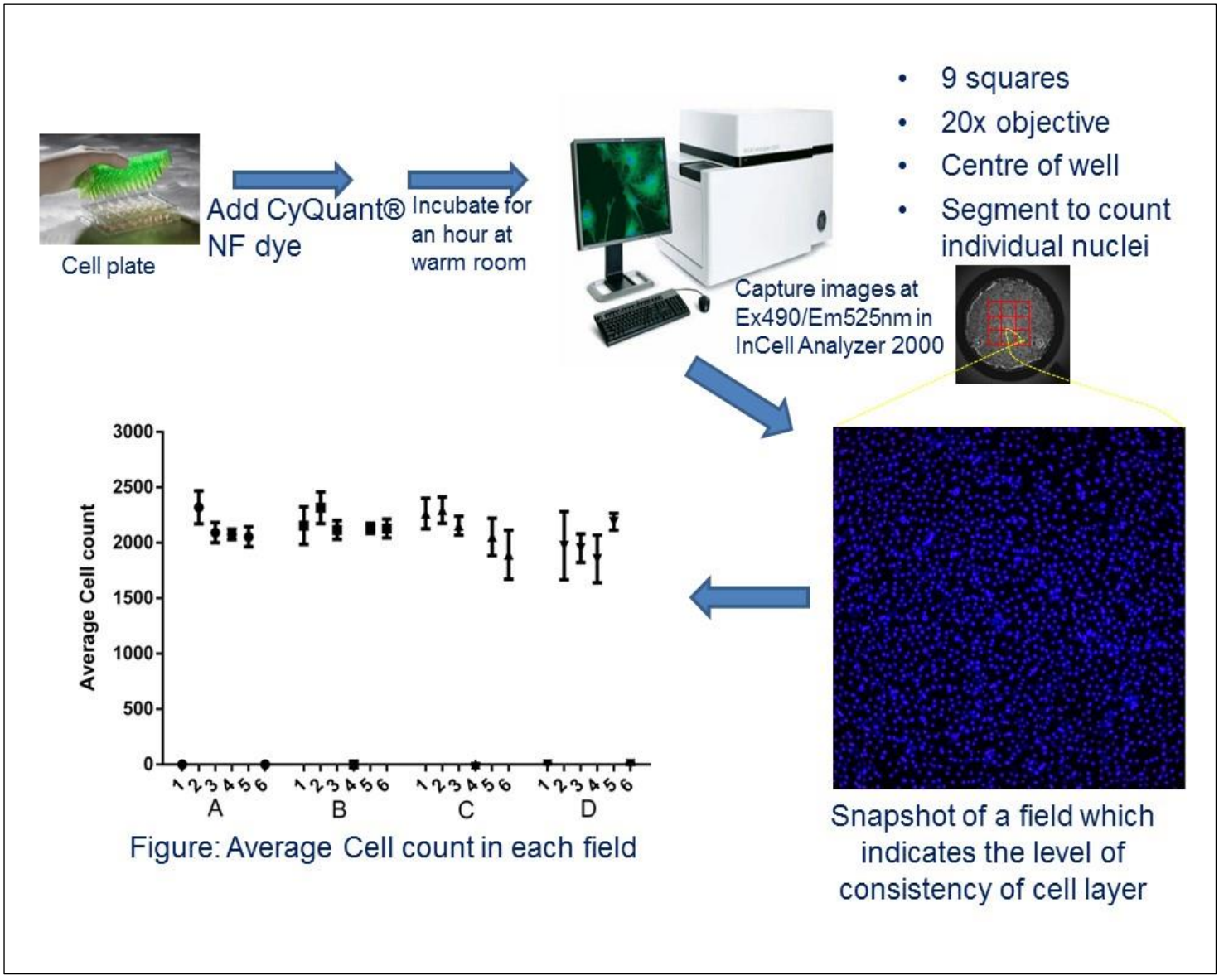

Figure 2.2. **Schematic diagram for cell counting through the Incell Analyser2000**. Figure shows BMDM cells counting and seeding density which also shows the consistency of the cell layer in the XF24 microplates, using InCell Analyser2000.

2.6.2. Normalisation using total cell protein

As an alternative to cell count, the Seahorse data was normalised by total protein of each well. At the end of the Seahorse experiment, each well was washed twice with PBS. Then 100 µL/well of lysis buffer (Profound™ lysis buffer, Thermo Scientific) with 1:25 protease inhibitor (Roche, Ref no. 04693132001) was added for 10 minutes at room temperature. The lysates of each well was preserved at -20°C. Subsequently, for total protein estimation the Bio-Rad protein assay kit (Bio-Rad) was used. 25µL of reagent A' (composed of 20µL Reagent S in 1mL Reagent A) was added into each well of 96 well plate. Then 5µL of each Seahorse well lysate was added into each well (duplicate well). In parallel, 5µL of bovine serum albumin (BSA) in a serial dilution (0-10mg/mL) was added to the plate for a standard curve. Then 200µL/well of Reagent B was added to each well and left for minimum 15 minutes to allow the colour development. The photometric assay protocol was used to measure the optical density of each well by a plate reader (Varioskan™ Flash multimode Reader with Skanlt™ software) at a wavelength of 630nm. A standard curve was created using the OD of BSA in GraphPad Prism™ v6.1 (GraphPad Software Inc.) and the amount of total protein (in µg) for each well was estimated by interpolating the known standard curve.

2.7. Optimisation of Seahorse glycolytic and mitochondrial stress tests inhibitors

2.7.1. Titration of oligomycin A

2mM stock solution of oligomycin A (Sigma-Aldrich) was prepared in DMSO. A range of different working concentrations initially 2.5-50µM then 5-25µM were obtained by diluting stock solution in XFAM + 25mM glucose medium and oligomycin A applied via the injecting port A (70µL/port) that attached to the cartridge. After injection of oligomycin A to the respective well of cell plate, it was diluted tenfold (630µL existing XFAM + glucose media + 70µL oligomycin A). Hence, the final oligomycin A concentrations in the wells were 0.25-5.0µM and 0.5-2.5µM. OCR and ECAR were measured three times before and after injecting oligomycin A by the Seahorse XF24 flux analyser. Three separate optimisation experiments were performed with a range of oligomycin A concentrations. Comparing these experiments, 1.0µM oligomycin A was

found to be the optimum concentration which was applied via the injecting port A in FCCP and 2-Deoxy-D-glucose titration in subsequent experiments.

2.7.2. Titration of FCCP

A 10mM stock solution of FCCP (Sigma-Aldrich, C370-86-5) was prepared in DMSO. A range of different working concentrations initially 6-25µM then 10-30µM were obtained by diluting stock solution in XFAM + 25mM glucose medium) and FCCP applied via the injecting port B (77µL/port) attached to the cartridge. Injection of FCCP into the wells of the plate resulted in a tenfold dilution (700µL existing XFAM+ 25mM glucose media per well + 77µL FCCP from injecting port). Hence, the final FCCP concentrations in the wells were 0.6-2.5µM and 1.0-3.0µM. OCR and ECAR were measured three times before and after injecting FCCP by the Seahorse XF24 flux analyser.

2.7.3. Titration of 2-deoxy-D-glucose

Like FCCP, 2-DG (Sigma-Aldrich) titration experiments were performed with a range of concentrations from 10mM to 200mM. The Seahorse protocol was adapted so that after the basal ECAR and OCR measurements were performed over three cycles, 70 µL of oligomycin A (10µm) was injected from port A to all wells and responses were measured for 3 more cycles. Then, 0mM (only XFAM+ 25mM glucose medium), 10mM, 25mM, 50mM, 100mM and 200mM 2-DG in XFAM + 25mM glucose medium (adjusted to pH 7.4 with 1.0M NaOH) was injected to the respective group of wells from port B and measurements performed over three more cycle. The 2-DG titration assay was also performed twice separately, with the same settings.

2.7.4. Titration of rotenone

First a range of different working concentrations of rotenone, initially 5-50µM then 5-25µM and 5-15µM, were obtained by diluting stock solution in XFAM + 25mM glucose medium) and rotenone applied via the injecting port C (85µL/port) that attached to the cartridge. After injection of optimised oligomycin and FCCP, rotenone was injected into the respective wells of the cell plate becoming diluted tenfold (777µL existing XFAM+ 25mM glucose media per well + 85µL rotenone from injecting port). Hence, the final rotenone concentrations in the wells were 0.5-5.0µM, 0.5-2.5µM and 0.5-1.5µM. OCR and ECAR were measured during basal conditions, oligomycin A and FCCP injections

and consecutively extracellular fluxes were measured three times after injecting rotenone.

2.7.5. Titration of antimycin A

Like rotenone, the concentration of antimycin A (Sigma-Aldrich) was optimised by testing a range of different concentrations of antimycin A, initially 10-200μM then 10-50μM were obtained by diluting stock solution in XFAM + 25mM glucose medium) and antimycin A applied via the injecting port C (85μL/port). Antimycin A was injected to the respective wells of cell plate, becoming diluted tenfold (777μL existing XFAM + 85μL antimycin A from injecting port). Hence, the final antimycin A concentrations in the wells were 1.0-20.0μM and 1.0-5.0μM. OCR and ECAR were measured during basal conditions, oligomycin A and FCCP injections and consecutively extracellular fluxes were measured three times after injecting antimycin A.

2.8. Measuring extracellular fluxes of BMDM in the presence of heat killed *S. pneumoniae.*

After 14 days of BMDM culture, $2x10^5$ BMDM/well were re-seeded in Seahorse cell plates and the Seahorse flux plate (cartridge with flux plate) also prepared as per section 2.5. On the day of the Seahorse experiment, the Seahorse cell plates were separated into 3 groups for analysis without bacteria, analysis of plates with heat-inactivated (HI) bacteria (multiplicity of infection, MOI=10) and plates exposed to HI bacteria (MOI =20) during the experiment (*i.e.* HI bacteria added from the cartridge port A). The flux plate injection port A was prepared either with HI *S. pneumoniae* (HISpn) (MOI=10 or 20 in XFAM with 25mM glucose) or without bacteria (XF medium with 25mM glucose only). Then oligomycin A (77μL at 10μM) and 2-deoxy-D-glucose (85μL at 1.0M) were added to injection port B and C, respectively. Like previous Seahorse experiments, cell plates and flux plates were kept at 37ºC without CO_2 for an hour before loading in the extracellular flux analyser.

2.9. Measuring glycolytic responses of mouse BMDM after stimulation with live *S. pneumoniae*, LPS, IFNγ and IL-4

Macrophage mediated real-time aerobic glycolytic respiration (e.g. Extracellular acidification) was measured by the XF24 extracellular flux analyser (Seahorse,

Bioscience). Briefly, after 14 days of culture of wild type mouse bone marrow cells into BMDM in the T-75 flask, cells were detached using Accutase solution (Biolegend) followed by re-seeding at $2x10^5$ BMDM/well into the XF24 cell plate. After overnight incubation to allow adherence, BMDM were challenged either with mock infection or opsonised D39 (MOI=10) or heat inactivated D39 (MOI=10, heat inactivated at 70^0C for 40 minutes) or stimulated with LPS (100ng/mL) and mouse IFNγ (20ng/mL) or mouse IL-4 (20ng/mL) for 4 hours at 37ºC with 5% CO_2. Subsequently, cells were washed twice by the XF medium (Seahorse, Bioscience) (supplemented with 4.5g/L D-glucose, 2mM L-glutamine and penicillin (100U/mL and streptomycin (100µg/mL), pH 7.4 adjusted with 1.0M NaOH, then the XF medium (630µL/well) was added and incubated for an hour at 37ºC without CO_2. Meanwhile, the XF24 utility plate containing cartridge with a sensors probe was submerged into the XF calibrant (Bioscience) and incubated overnight at 37ºC, afterwards the optimised concentration of ATP synthase inhibitor oligomycin A (70µL at 10µM), the glucose analogue 2-deoxy-D-glucose (77µL at 1M) were added in the cartridge containing injection port A and B, respectively and incubated for an hour at 37ºC. Finally, after successful calibration by calibrant containing plates, the cell plate was loaded into the XF24 analyser and the rate of oxygen consumption (OCR) and extracellular acidification (ECAR) were measured kinetically before and after injecting oligomycin, 2-deoxy-D-glucose (Sigma-Aldrich), respectively. From the kinetic data, the basal OCR, maximum glycolytic capacity and glycolytic reserve were calculated following Pelletier M et al. calculation formula (Pelletier et al., 2014).

2.10. Measurement of mitochondrial OXPHOS after challenge with pneumococci in wild type and Mcl-1 transgenic mouse BMDM

After 14 days culture and differentiation of wild-type and human CD68 Mcl-1 transgenic mouse bone marrow cells into BMDM (described in (Bewley et al., 2017)) in T-75 flasks, cells were detached using Accutase (Biolegend) for 15 minutes at 37ºC with 5% CO_2 followed by re-seeding at $2x10^5$ BMDM/well in the XF24 cell plate. After adhering overnight, cells were either mock-infected or exposed to opsonised D39 (MOI=10, opsonised with 10% mouse immune serum) for 4 hours at 37ºC with 5% CO_2. Subsequently cells were washed twice in XF medium (Seahorse, Bioscience) (supplemented with 4.5g/L D-glucose, 2mM L-glutamine, 1.0mM sodium-pyruvate, penicillin (100U/mL) and streptomycin (100µg/mL) at pH 7.4 adjusted with 1.0M NaOH), before the XF medium (630µL/well) was added and incubated for an hour at 37ºC without CO_2. ECAR and OCR were then measured using extracellular flux analyser.

2.11. Measurement of mitochondrial OXPHOS in human MDM after challenge with *S. pneumoniae*

Human MDM were culture in T-75 flask for 14 days. Cells were washed 3 times with PBS and treated with Accutase for 15 minutes at 37ºC and 5% CO_2. The detached cells were re-seeded in XF24 cell plate (at 150,000 MDM/well), then exposed to opsonised D39 (MOI =10) for 4 or 16 hours. Subsequently, cells were washed twice with XF medium (as in section 2.10) and the XF medium (630µL/well) was added and incubated for an hour at 37ºC without CO_2. At the same as the cell plate was being set up the XF24 utility plate containing sensors probes were submerged into the XF calibrant and incubated overnight at 37ºC. Then, 70µL oligomycin A (15µM), 77µL FCCP (20µM) and 85µL rotenone (10µM) plus antimycin A (10µM) were added in the cartridge containing injection port A, B and C, respectively, and incubated for an hour at 37ºC without CO_2. Finally, the calibration plate was loaded into the XF24 flux analyser. After calibration completion, the cell plate was loaded into the XF24 analyser and the OCR and ECAR were measured kinetically before and after injecting oligomycin, FCCP and rotenone plus antimycin A, respectively. The rate data were normalised using total cell protein and the key parameters of mitochondrial OXPHOS and ECAR were calculated, described in (Pelletier et al., 2014).

2.12. Measurement of mitochondrial OXPHOS in human MDM after stimulation with HIV-1 glycoprotein gp120 and *S. pneumoniae*

Human PBMCs were differentiated into monocyte derived macrophages (MDM) in T-75 flasks (Dockrell et al., 2001). MDM were detached using Accutase (Biolegend) for 15 minutes at 37ºC and 5% CO_2. Cells were then gently scrapped with a cell scrapper followed by re-seeding at $1.5x10^5$ cells/well into the XF24 cell plate and incubated overnight at 37ºC and 5% CO_2. Subsequently, cells were treated either with or without recombinant gp120 (100ng/mL in RPMI media) and incubated for 24 hours at 37ºC and 5% CO_2. Cells were either challenged with mock infection or opsonised pneumococci (D39, MOI=10) with or without recombinant gp120 for 4 or 16 hours at 37ºC and 5% CO_2. After incubation, cells washed 2 times with XF medium. Then 630µL of XF medium with or without recombinant gp120 was added to each well and incubated for an hour at 37ºC without CO_2. ECAR and OCR were then measured as in section 2.11.

2.13. Measurement of mitochondrial OXPHOS in COPD MDM in the presence of *S. pneumoniae*

Both COPD patients and age-matched healthy volunteers PBMCs were differentiated into monocyte-derived macrophage (MDM) in the T-75 flasks. MDM were gently detached using Accutase and gentle scrapping followed by re-seeding at $1.5x10^5$ MDM/well into the XF24 cell plate. After overnight incubation, cells were either mock-infected or exposed to opsonised pneumococci (MOI =10) for 4 hours at 37°C with 5% CO_2. Subsequently cells were washed twice with XF medium, 630µL XF medium was added to each well of XF24 cell plate and incubated for an hour at 37°C without CO_2. The OCR and ECAR was then measured as in section 2.11.

2.14. Measurement of mitochondrial OXPHOS in MitoTempo pre-treated mouse BMDM

Mouse bone marrow cells were culture in T-75 flask and differentiated into BMDM (detail protocol in 2.2). Then cells were re-seeded at 200,000 cells/well in the XF24 Seahorse cell plate and incubated overnight at 37°C and 5% CO_2. Cells were treated or untreated with MitoTempo (10µM) (Sigma-Aldrich) for an hour prior to pneumococcal (D39, MOI=10) exposure for 12 hours. Cells were then washed with XF medium (explained in 2.4). Next, 630µL/well of XF medium with/without MitoTempo were added and incubated for an hour at 37°C without CO_2. Subsequently oligomycin A, FCCP and the combination of rotenone and antimycin A were added to the inject ports of the flux plate, and incubated for an hour at 37°C without CO_2. The OCR and ECAR were measured kinetically before and after the consecutive injection of oligomycin, FCCP and rotenone plus antimycin A, using the XF24 extracellular flux analyser. From the OCR and ECAR rate data, the key parameters of mitochondrial OXPHOS and glycolysis were calculated. Data were normalised using total cell protein.

2.15. Flow cytometry

2.15.1. Evaluation of mitochondrial inner transmembrane potential ($\Delta\Psi_m$) in COPD MDM

Both COPD and age-matched healthy control volunteers MDM were exposed to *S. pneumoniae* (D39, MOI=10) or mock infected and left an hour on ice and incubated 3 hours at 37°C with 5% CO_2. They were then washed 3 times with pre-warmed HBSS followed by staining with 10µM of 5,5′,6,6′-tetrachloro-1,1′,3,3′-tetraethyl

benzimidazolyl carbocyanine iodide (JC-1, diluted in phenol red free RPMI media supplemented with 2mM L-glutamine) (eBioscience, 65-0851-38) for 30 minutes at 37ºC with 5% CO_2 and washed 3 times with HBSS before being resuspended in 300µL/well PBS. The loss of mitochondrial inner transmembrane potential ($\Delta\Psi_m$) is equivalent to the loss of JC-1 aggregates (red fluorescence) from mitochondrial matrix, was measured by the FACSCalibur (Becton Dickinson) using FL-2H channel. The forward and side scatter were used to distinguish the cell population and a total of 10,000 events for each sample were recorded. The settings were saved and the same instrumental settings were used for subsequent sample acquisition and analyses. Data were analysed using the FlowJo software, version 8.8.4 (Tree Star Inc.).

2.15.2. Evaluation of mitochondrial $\Delta\Psi_m$ in 3-methyladenine pre-treated mouse BMDM in the presence of pneumococci

Mouse BMDM were pre-treated with/without 3-methyladenine (10mM) for an hour. Then, *S. pneumoniae* (D39, MOI=10) was exposed to BMDM for 16 hours at 37ºC and 5% CO_2. Then macrophages washed 3 times with pre-warmed HBSS followed by staining with JC-1 (10µM) for 30 minutes at 37ºC and 5% CO_2. Subsequently cells were washed 3 times with HBSS before being gently scrapped and resuspended in 300µL/well PBS. The loss of mitochondrial inner transmembrane potential ($\Delta\Psi_m$) or loss of JC-1 aggregates (i.e. red intensity) from mitochondrial matrix was measured by the FACSCalibur (Becton Dickinson) using FL-2H channel (detail protocol in 2.15.1).

2.15.3. Measurement of mROS in mouse BMDM after challenge with pneumococci

Mouse BMDM were challenged with *S. pneumoniae* (D39, MOI=10) or mock-infected and left for an hour on ice and 3 hours at 37ºC and 5% CO_2, washed three times with PBS, then incubated in fresh DMEM+10% heat inactivated fetal calf serum for 12 hours at 37ºC and 5% CO_2. As a positive control, BMDM were treated with rotenone (2.0µM) and antimycin A (10 µM) for 30 minutes at 37ºC and 5% CO_2 followed by washed 3 times with pre-warmed HBSS. Subsequently, MitoSox red (2.5µM) (Invitrogen, M36008) was diluted in pre-warmed phenol red free RPMI media supplemented with 2mM L-glutamine, or Mito-tracker green FM (1:1000) (Invitrogen, cat. no. M7514) was added for 30 minutes at 37ºC and 5% CO_2. Cells were resuspended in PBS (300µL/well), after gentle scrapping and washed 3 times with HBSS. The oxidised Mitosox Red and Mito-tracker green were measured by the FACSCalibur (Becton Dickinson) using FL-2H and

FL-1H channels, respectively. The forward and side scatter were used to distinguish cell populations and a total of 10,000 events were recorded. The instrumental settings were saved and used for subsequent sample acquisition and analyses. Data were analysed using FlowJo software, version 8.8.4 (Tree Star Inc.).

2.15.4. Measurement of mROS in 3-methyladenine pre-treated mouse BMDM in the presence of pneumococci

Mouse BMDM were treated with/without 3-methyladenine (10mM) for an hour at 37ºC and 5% CO_2. *S. pneumoniae* (D39, MOI=10) was exposed to BMDM for 12 or 14 or 16 hours at 37ºC and 5% CO_2. Cells were washed 3 times with pre-warmed HBSS, before being treated with MitoSox red (2.5µM) for 30 minutes at 37ºC and 5% CO_2. Then, cells were washed 3 times with HBSS. Subsequently cells were resuspended in PBS (300µL/well) after gently detached with a cell scrapper. The oxidised MitoSox red was measured by the FACSCalibur (Becton Dickinson) using FL-2H channel. To measure MitoSox red fluorescence intensity, total 10,000 events per sample were recorded and data were analysed using FlowJo software, version 8.8.4 (Tree Star Inc.).

2.16. Immunofluorescence

2.16.1. Co-staining of mROS and mitochondrial outer membrane protein Tom20

Mouse BMDM were challenged with *S. pneumoniae* (D39, MOI=10) or mock-infected and incubated for an hour on ice, followed by 3 hours at 37ºC with 5% CO_2. After washing three times with PBS, cells were incubated for 12 hours at 37ºC with 5% CO_2. Cells were washed 3 times with pre-warmed HBSS and mROS were labelled using the live cell mROS staining probe MitoSox red (2.5µM). Cells were fixed with 2% paraformaldehyde (in PBS) for 20 minutes at room temperature (RT). Cells were permeablised using 50mM NH_4Cl with 0.1% Triton-X-100, and blocked with working solution PGAT (PGAT composition: 0.2% Gelatin with 0.02% Na-azide and 0.01% Triton X-100 in PBS) for 15 minutes each. Subsequently, the blocking solution was replaced with 200µL/well rabbit anti-Tom20 (FL-145) (Santa Cruz, cat no. sc-11415) at a 1:500 dilution in PGAT solution and incubated overnight at 4ºC. The following day, cells were washed 3 times with the PGAT solution, then, the secondary antibody Alexa Fluor 488-conjugated goat anti-rabbit IgG (Thermo-fisher scientific, cat. no. A32723) at a 1:500 dilution in PGAT solution was

added for an hour at RT. Cells were washed 3 times with the PGAT solution and 2 times with PBS. Finally, nuclei were stained with Draq5 (BioStatus LTD) with a 1:1000 dilution in PBS for 12 minutes at RT. After washing 3 times with PBS and once with distilled H_2O, cells were mounted with a glycerol free poly-(vinyl alcohol) (CITIFLUOR MOWIOL Tris-MWL 4-88) mounting agent in the microscopic slides. Images were acquired by the Zeiss LSM 510 inverted confocal fluorescence microscopy (ZEISS), using 63 X 1.4 NA oil objective (zoom 2) lens and 488nm, 568nm and 633nm excitations lasers and 500-530nm (for Alexa Fluor 488), 565-615nm (for MitoSox red) and 661-704nm (for Draq5) emission spectrums, respectively.

2.16.2. Labelling of *S. pneumoniae* with Alexa Fluor 647-conjugated succinimidyl ester

S. pneumoniae (D39) (3 x 10^8 cfu/mL) was thawed and washed twice with PBS, centrifuging at 9000 rpm for 3 minutes, then the bacterial pellet was resuspended in PBS to obtain a concentration of 10^8 cfu/mL. 18.8µL of Alexa Fluor 647-conjugated carboxylic acid succinimidyl ester (stock concentration was 0.5mg/mL in DMSO) (Life Technologies, A37573) (AF647-NHS-ester) was added to 500µL bacterial suspension and incubated for an hour at RT, with frequent mixing. This was then centrifuged at 2000xg for 10 minutes, and the pellet washed twice with PBS. Subsequently the pellet was resuspended in phenol red and serum free RPMI 1640 media (Sigma-Aldrich, R7509-500mL) and opsonised with 10% mouse or human pneumococcal immunised serum for 30 minutes at 37^{o}C and 5% CO_2. The Alexa Fluor-647 NHS ester labelled bacterial suspensions were subsequently either air dried on a microscopic slide to confirm the labelling (by fluorescence microscope) or used to challenge macrophages. Labelled bacterial images were captured by the Zeiss LSM510 inverted confocal microscopy using 63x1.4 oil (zoom 2) objective lens and 633nm excitation and 650-704nm emission spectrum.

2.16.3. Co-staining of Alexa Fluor-647 *S. pneumoniae* and mROS in macrophages

Mouse BMDM were pretreated with 10µM MitoTempo (Sigma-Aldrich, SML0737-5MG) for an hour, then, cells were challenged with Alexa Fluor-647-NHS ester (or vehicle) labelled opsonised *S. pneumoniae* (D39, MOI=10) and incubated for 16 hours. mROS specific 2.0µM of MitoSox red and, as a negative control endoplasmic reticulum

(ER) specific 500nM ER-tracker red (BODIPY TR Glibenclamide) (Thermo-Fisher scientific, E34250), were added for 15-30 minutes at 37°C and 5% CO_2. Cells were then washed 3 times with pre-warmed HBSS, and fixed with 4% paraformaldehyde for 20 minutes at RT, before being mounted onto microscopic slides with poly-(vinyl alcohol) mounting agent. Cells were visualised with Z-stack images which were captured by Zeiss LSM510 inverted confocal microscopy, using 63x1.4 oil (zoom 2) objective lens. 633nm excitation and 650-704nm emission spectrum was used for AF-647-NHS ester labelled D39, 488nm excitation and 565-615nm emission spectrum was used for MitoSox red, and 543nm excitation and 560nm emission was used for ER-tracker red. The Pearson's correlation coefficient was measured by ImageJ (v1.48, NIH) using the Pearson co-localisation test with the Costes threshold regression, described in (Bewley et al., 2017). In addition, the total corrected cellular fluorescence [TCCF = Integrated density – (area of selected cell x mean fluorescence of background readings)] was measured for MitoSox red from the maximum projected Z-stack images by ImageJ.

2.16.4. Co-staining of mROS and lysosome/phagolysosome in macrophages

Alexa Fluor 647-NHS ester-labelled opsonised *S. pneumoniae* (D39, MOI=10) was exposed to mouse BMDM for 16 hours. Cells were washed three times with HBSS, then, both mROS specific MitoSox red (2.0µM) and lysosome/phagolysosomes specific Cresyl violet (0.5µM) (Sigma-Aldrich, C10510540) were added for 30 minutes at 37°C and 5% CO_2. For negative controls, both lysosome/phagolysosome specific Cresyl violet and endoplasmic reticulum (ER) specific ER-tracker red (500nM) (BODIPY TR Glibenclamide) were added for 30 minutes at 37°C and 5% CO_2. All staining probes were diluted in phenol red and serum free RPMI media supplemented with 2mM L-glutamine. Cells were washed 3 times with HBSS, then cells were fixed with 4% paraformaldehyde for 20 minutes at RT, before being mounted onto microscopic slides with a drop of poly-vinyl alcohol mounting agent. Then, Z-stack images were captured by the above mentioned confocal microscope. The MitoSox red and Cresyl violet labelled mROS and lysosome/phagolysosomes images were acquired using 488nm and 633nm excitation lasers, and 565-615nm and 650-704nm emission spectrums, respectively. ER and lysosome/phagolysosome labelled ER-tracker red and Cresyl violet stains were acquired with 543nm and 633nm excitation lasers and 560nm and 650-704nm emission spectrums, respectively. The Pearson's correlation coefficient was measured by ImageJ using the

Pearson co-localisation test with Costes threshold regression, described in (Bewley et al., 2017).

2.16.5. Co-staining of mROS, nitric oxide and lysosome/phagolysosomes in macrophages

Alexa Fluor 647-NHS ester-labelled opsonised *S. pneumoniae* (D39, MOI=10) was exposed to mouse BMDM for 16 hours. Cells were washed three times with HBSS, then nitric oxide (NO)-specific DAF-FM diacetate (4-Amino-5-Methylamino-2',7'-Difluorofluorescein-Diacetate) (Thermo-Fisher Scientific, Cat. no. D23844) (10µM) was added for 30 minutes at 37ºC and 5% CO_2. Cells were washed three times with HBSS before being treated with mROS-specific MitoSox red (2.0µM) and lysosome/phagolysosome-specific Cresyl violet (0.5µM) for 30 minutes at 37ºC and 5% CO_2. For negative controls, either NO-specific DAF-FM diacetate and ER-specific ER-tracker red (BODIPY TR Glibenclamide), or lysosome/phagolysosome-specific Cresyl violet and ER-tracker were used for 30 minutes, at 37ºC and 5% CO_2. All staining probes were diluted in phenol red and serum free RPMI media, supplemented with 2mM L-glutamine. Cells were also separately stained with each of these specific probes (single staining) to compensate the overlapping excitation and emission spectrums. Subsequently cells were washed 3 times with pre-warmed HBSS. The MitoSox red, DAF-FM and Cresyl violet labelled mROS, NO and lysosome/phagolysosomes cells, respectively were visualised with 543nm, 488nm and 633nm excitation lasers, and 565-615nm (for MitoSox red), 500-530nm (for DAF-FM) and 650-704nm (for Cresyl violet) emission spectrums. ER tracker red and DAF-FM labelled ER and NO stained cells images were acquired with 543nm and 488nm excitation lasers and 560nm and 500-530nm emission spectrums, respectively. From three independent experiments, the percentage of macrophages showing co-localisation signal for mROS (red), NO (green) and lysosome/phagolysosome (pink) was measured by ImageJ.

2.16.6. Co-staining of mROS, NO and Alexa-Fluor 647-labelled *S. pneumoniae* in macrophages

Alexa Fluor 647 NHS ester-labelled opsonised *S. pneumoniae* (D39, MOI=10) was exposed to mouse BMDM and incubated for 16 hours. Cells were washed three times with HBSS and NO-specific DAF-FM diacetate (10µM) was added for 30 minutes at

37ºC and 5% CO_2. Subsequently, cells were washed three times with HBSS before being treated with mROS-specific MitoSox red (2.0µM) for 30 minutes at 37ºC and 5% CO_2. For negative control, both mock-infected and Alexa Fluor 647-labelled pneumococci exposed BMDM were stained with NO-specific DAF-FM and ER-specific ER-tracker red together, or only ER-tracker for 30 minutes at 37ºC and 5% CO_2. All staining dyes were diluted in phenol red and serum free RPMI media, supplemented with 2mM L-glutamine. Subsequently, macrophages were washed 3 times with HBSS before being fixed with 4% paraformaldehyde for 20 minutes at RT. Cells were washed with PBS, and mounted in microscopic slides with poly-vinyl alcohol mounting agent. Z-stack images were captured by Zeiss LSM510 inverted confocal microscopy using 63x1.4 oil (zoom 2) objective lens. The images of MitoSox red and DAF-FM stained macrophages with or without Alexa Fluor 647-labelled pneumococci were visualised with 543nm, 488nm and 633nm excitation lasers, and 565-615nm or 500-530nm and 650-704nm emission spectrums, respectively. Whilst as a control, the ER-tracker red and DAF-FM labelled ER and NO stained images were captured with 543nm and 488nm excitation lasers and 560nm and 500-530nm emission spectrums, respectively. From three independent experiments, the percentage of macrophages showing co-localisation signal for mROS (red), NO (green) and Alexa Fluor 647-labelled intracellular D39 (blue) was counted by ImageJ. The co-localisation of the negative comparator, ER with NO, was also observed in mock-infected and Alexa Fluor 647-labelled D39 exposed macrophages. In addition, single stained cells images were also visualised to compensate the overlapping excitation and emission spectrums

2.17. Evaluation of Mitochondrial morphological features

2.17.1a. Staining of mitochondrial outer membrane protein TOM20

Mouse bone marrow cells on coverslips (13x13mm) in 24 well plate and differentiated into bone marrow-derived macrophages (BMDM). Cells were treated with Mdivi-1 (25µM) (Sigma-Aldrich, M0199) or 3-methyladenine (10mM) (Sigma, M9281) for an hour prior to mock-infection or challenged with opsonised *S. pneumoniae* (D39, MOI=10), and then the plate left on ice for an hour and 3 hours at 37ºC and 5% CO_2. Cells were washed 3 times with PBS, and added fresh DMEM media with the respective inhibitors and incubated for 4, 8 and 10 hours at 37ºC and 5% CO_2. Subsequently, cells were washed 3 times with PBS, before being fixed with 4% paraformaldehyde for 20

minutes at RT. Next, they were washed once with quenching solution and 250µL/well quenching solution [50mM NH_4CL (1.34g in 500mL PBS) in 0.1% Triton-x-100 (500µL in 500mL PBS)] added for 15 minutes at RT. Cells were washed once with blocking solution (PGAT solution) and 250µL/well blocking solution [PGAT solution: 0.2% Gelatin (sigma-aldrich) + 0.02% Na-Azide (Sigma-Aldrich) + 0.01% Triton-x-100 (promega) in PBS] added for 15 minutes at RT. The blocking solution was replaced with 200µL/well rabbit anti-Tom20 (FL-145) (Santa Cruz, cat no. sc-11415) at 1:500 dilution in PGAT solution and incubated overnight at 4^oC. Cells were washed 3 times with PGAT solution with 1-2 minute intervals and Alexa Fluor 488-conjugated goat anti-rabbit IgG (H+L) (Life technologies, A11034) secondary antibody was added for an hour (in the dark) at RT. Next cells were washed 3 times with PGAT solution and 2 times with PBS. Finally, nuclei were stained with Draq5 (BioStatus LTD) with 1:1000 in PBS for 12 minutes at RT. Cells were washed 3 times with PBS and once with distilled H_2O followed by mounting on poly-vinyl alcohol mounting agent and left overnight at RT. Cells were visualised by the Zeiss LSM 510 inverted confocal fluorescence microscopy using 63 X 1.4 oil objective (zoom 2) lens, and 488nm and 633nm excitations with 500-530nm and 660-704nm emission spectrums for Tom20 and nuclei, respectively.

2.17.1b. Quantification of mitochondrial network complexity by ImageJ

To assess mitochondrial network complexity, the Z-stack images of mitochondrial outer membrane protein, Tom20 were acquired by LSM510 inverted confocal fluorescence microscopy (Zeiss). Z-stack images were converted into maximum projected images by ImageJ. Subsequently, individual cell was duplicated and adjusted its brightness and contrast. The resolution of mitochondrial population was fine-tuned with a 13 x 13 hat filter (matrix developed by Dr. De Vos Kurt), described in (De Vos et al., 2005). The total population of mitochondria were skeletonised after threshold level optimisation. Subsequently the binary connectivity were quantified by the Morphology plugins of ImageJ software, this procedure shows schematically in figure 2.2. As an output it returns 0, 1, 2, 3, 4 and so on for the total number of background pixels, single pixels, end points, junctions with two neighbouring pixels, branch points (value is ≥ 4), respectively (Figure 2.3). The network complexity of mitochondrial population of individual cell was measured as the ratio of total branch points and total end points.

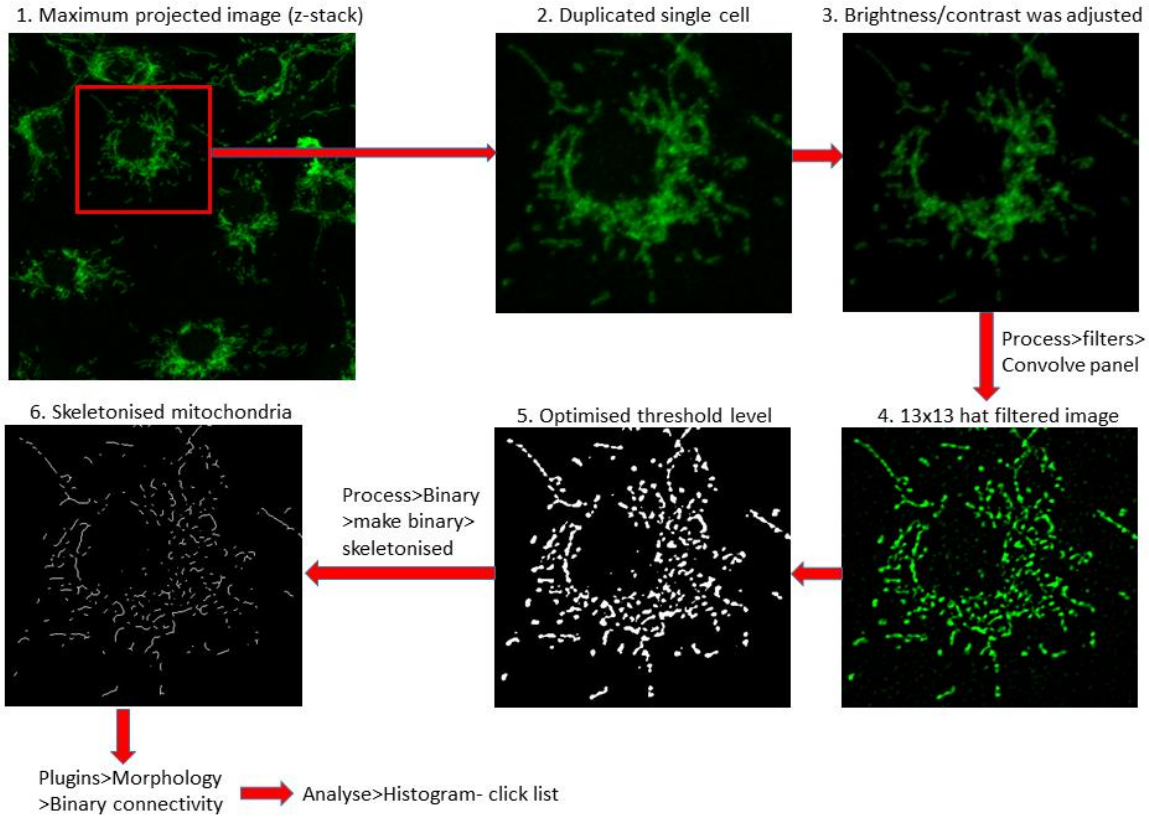

Figure 2.3. **Schematic diagram for mitochondrial image processing by ImageJ.** It quantifies the network complexity of total mitochondrial population in a macrophage. Figure shows (1-6) how a single cell was skeletonised by ImageJ. Free hand selection and then duplication of each cell from the maximum projected Z-stack image. The background noise is minimised by adjusting brightness/contrast. The hat filter (13 x 13) was increased the resolution of signal pixels. Then the binary image was skeletonised after threshold level optimisation. Subsequently the voxels binary connectivity was quantified using morphology plugins.

A.

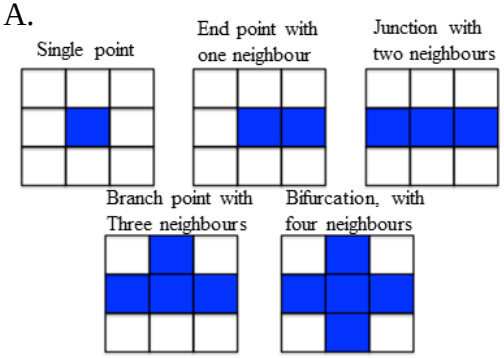

B.

Value (WT-Mock infected)	Count	Description	Network complexity
0	62232	Background	Ratio of total number of Branch points(value ≥4) and End points(value =2) (187+33+3)/322= 0.69
1	4	Single pixels	
2	322	End points	
3	1708	Junction with two neighbours (more count higher the length)	
4	187	Triple point with three neighbour (Branch point)	
5	33	Bifurcation with four neighbours (Branch point)	
6	3	Five neighbours (branch point)	

Figure 2.4. **Mitochondrial network complexity in a typical macrophage**. The total population of mitochondria were skeletonised, then ran the connectivity morphology plugins by ImageJ. Figure A shows the visual explanation of skeletonised voxel's connectivity. The blue quadrant represents the single pixel of binary skeletonised images. It also shows the end point which represents single pixel with one neighbouring pixel, junction pixel shows the length of skeletonised voxel. Whereas branch point shows single pixel's with three or more than three neighbours. Table B shows an example of mitochondrial network complexity of a typical wild-type (WT) mouse BMDM as a ratio of total branch points and end points, which was 0.69.

2.17.2. Co-staining of mitochondrial Tom20 and phosphorylated-Drp1 (serine 616)

Human PBMCs were culture on coverslip in a 24-well plate and differentiated into MDM. *S. pneumoniae* (D39, MOI=10) were exposed to MDM and the plate left on ice for an hour and 3 hours at 37ºC and 5% CO_2. Cells were washed 3 times with PBS and added fresh RPMI media, and incubated for 12 hours at 37ºC and 5% CO_2. In the positive control wells, MDM were treated with the mitochondrial OXPHOS uncoupler FCCP (20µM) for 8 hours. Cells were then washed 3 times with PBS before being fixed with 4% paraformaldehyde for 20 minutes at RT. Next, cells were washed once with quenching solution and added 250µL/well quenching solution for 15 minutes at RT. Cells were washed once with PGAT solution and added 250µL/well PGAT solution for 15 minutes at RT. Subsequently the PGAT solution was replaced with primary antibodies, 200µL/well mouse monoclonal anti-Tom20 (F-10) (Santa Cruz, cat no. sc-17764) at 1:500 dilution to give a final concentration of0.4µg/mL in PGAT solution and rabbit anti-

phospho-Drp1 (Ser616) (Cell signalling Tech, cat no. 3455) at 1:500 dilution (in PGAT solution) and incubated overnight at 4^{o}C. Cells were washed 3 times with PGAT solution with 1-2 minutes intervals. Alexa Fluor 488 and 568-conjugated goat monoclonal anti-mouse (Molecular probes, A11001) and goat anti-rabbit IgG (H+L) (Thermo-fisher scientific, A11011) secondary antibodies were added for an hour at RT. Subsequently cells were washed 3 times with PGAT solution and twice with PBS. Finally, cells nuclei were stained with Draq5 (BioStatus LTD) with 1:1000 in PBS for 12 minutes at RT, washed 3 times with PBS and once with dH_2O followed by mounting in microscopic slides with a drop of glycerol-free poly-vinyl alcohol mounting agent. Cells were visualised by the Zeiss LSM 510 confocal fluorescence microscopy using 63 X 1.4 oil objective (zoom 2) and 488nm, 543nm and 633nm excitations with 500-530nm 565-615nm and 660-704nm emission spectrums, respectively.

2.17.3. Co-staining of mitochondrial Tom20 and E3 ubiquitin ligase Parkin

Mouse BMDM were untreated or treated with Mdivi-1 (25µM) or 3-MA (10mM) for an hour, then exposed to *S. pneumoniae* (D39, MOI=10), and the plates left on ice for an hour and 3 hours at 37^{o}C and 5% CO_2. Cells were washed 3 times with PBS and fresh DMEM media added with respective inhibitors and incubated for 8 hours at 37^{o}C and 5% CO_2. Cells were fixed with 4% paraformaldehyde for 20 minutes at RT. After quenching and blocking, the primary antibodies, rabbit anti-Tom20 (200µL/well) at 1:500 dilution and mouse monoclonal anti-Parkin IgG2 (PARK8) (Santa-Cruz, cat no. SC-32282) at 1:100 dilution in PGAT solution were added and incubated overnight at 4^{o}C. Cells were washed 3 times with PGAT solution before being treated with secondary antibodies, Alexa Fluor 568-conjugated goat anti-rabbit IgG (H+L) and Alexa Fluor 488 goat anti-mouse IgG for an hour at RT. Cells were washed and nuclei were stained with Draq5 before being mounted in microscopic slides. Cells were visualised by the Zeiss LSM 510 confocal fluorescence microscopy using 63 X 1.4 oil objective (zoom 2) lens. Images were acquired using 568nm, 488nm and 633nm excitation lasers, and respectively with 565-615nmm, 500-530nm and 660-704nm emissions for Tom20, Parkin and nuclei stains. For quantification, Parkin's fluorescence intensity for each condition, was measured as the corrected total cell fluorescence (CTCF) by ImageJ (NIH). Moreover, the Pearson's correlation coefficient for mitochondrial outer membrane protein Tom20 and Parkin in mock-infected and D39 exposed BMDM was quantified by ImageJ.

2.17.4. Co-staining of mitochondrial Tom20 and autophagy marker LC3B

Human MDM were exposed to *S. pneumoniae* (D39, MOI=10) and the plates left on ice for an hour and 3 hours at 37ºC and 5% CO_2. Cells were washed 3 times with PBS and fresh RPMI media added for 12 hours at 37ºC and 5% CO_2. In the positive control wells, MDM were treated with FCCP (20µM) for 12 hours, then washed 3 times with PBS and fixed with 4% paraformaldehyde for 20 minutes at RT. After quenching and blocking, the blocking solution was replaced with the primary antibodies, mouse anti-Tom20 at 1:500 dilution (Santa Cruz) and rabbit polyclonal anti-LC3B (Abcam, cat no. ab48394) at 1:500 dilution in PGAT and incubated overnight at 4ºC. They were then washed 3 times with PGAT solution and treated with secondary antibodies, Alexa Fluor 488 conjugated goat anti-mouse IgG (H+L) and Alexa Fluor 568 goat anti-rabbit IgG for an hour at RT. Cells were washed 3 times with PGAT and twice with PBS followed by nuclei staining with Draq5. Images were acquired by the Zeiss LSM 510 confocal fluorescence microscopy using 63 X 1.4 oil objective (zoom 2) lens. To capture images, 568nm, 488nm and 633nm excitation lasers, respectively used with 565-615nmm, 500-530nm and 661-704nm emission spectrums for Tom20, LC3B and nuclei stains.

2.17.5. Co-staining mitochondrial Tom20 and phagolysosomal LAMP1

Human MDM were exposed to *S. pneumoniae* (D39, MOI=10) and the plates left on ice for an hour and 3 hours at 37ºC and 5% CO_2. Then cells washed 3 times with PBS and fresh RPMI media added for 12 hours at 37ºC and 5% CO_2. After washing 3 times with PBS the cells were fixed with 4% paraformaldehyde for 20 minutes at RT. Cells were quenched and blocked followed by treated with the primary antibodies, rabbit polyclonal anti-Tom20 at 1:500 dilution (Santa Cruz) and mouse monoclonal anti-LAMP1 (H4A3) (Abcam, cat no. ab25630) at 1:100 dilution in PGAT solution and incubated overnight at 4ºC. After washing 3 times with PGAT solution, secondary antibodies Alexa Fluor 568-conjugated goat anti-rabbit IgG and Alexa Fluor 488-conjugated goat anti-mouse IgG (H+L) were added for an hour at RT. Cells were washed 3 times with PGAT and twice with PBS followed by stained with Draq5 at RT. Cells were washed 3 times with PBS and once with distilled H_2O followed by mounting in microscopic slides. Images were acquired by the Zeiss LSM 510 confocal fluorescence microscopy using 63 X 1.4 oil objective (zoom 2) lens, and 568nm, 488nm and 633nm excitations, and respectively with

565-615nmm, 500-530nm and 661-704nm emissions for Tom20, LAMP1 and nuclei stains.

2.17.6. Mitochondrial fission/fragmentation in pneumolysin deficient and heat inactivated pneumococci exposed macrophages

Metabolically active *S. pneumoniae* (D39, MOI=10), D39 was heat inactivated (at 60^{o}c for 40 minutes) (MOI=10 to 40), pneumolysin deficient D39 [ΔPLY D39 or PLYSTOP D39, MOI=10 to 50)] (Bewley et al., 2014) or 0.5µg/mL-5µg/mL exogenous purified pneumolysin (source: E. coli, using a HIS tag, and purified by the HPLC) (Gift from Timothy J. Mitchell's lab, University of Birmingham) were exposed to mouse BMDM and the plates were left on ice for an hour and 3 hours at 37^{o}C and 5% CO_2. Macrophages were washed 3 times with PBS and fresh DMEM media added with or without exogenous pneumolysin and incubated for 8 hours at 37^{o}C and 5% CO_2. Cells were washed 3 times with PBS before being fixed with 4% paraformaldehyde for 20 minutes at RT. As described in section 2.17.1a cells were treated with quenching and blocking solution. Blocking solution was replaced with primary antibody rabbit anti-Tom20 (200µL/well) at 1:500 dilution and incubated overnight at 4^{o}C. Subsequently cells were washed 3 times with PGAT solution before being treated with secondary antibody, goat anti-rabbit IgG (H+L)-conjugated with Alexa Fluor-488 for an hour at RT. Cells were washed 3 times with PGAT and twice with PBS. Cell nuclei were stained with Draq5 with 1:1000 in PBS for 12 minutes at RT. Cells were then washed 3 times with PBS and once with distilled H_2O followed by mounting in microscopic slides with glycerol-free poly-vinyl alcohol mounting agent. Images were acquired by the Zeiss LSM 510 inverted confocal fluorescence microscopy using 63 X 1.4 oil objective (zoom 2) lens. And 488nm and 633nm excitations with 500-530nm and 660-704nm emission spectrums for Tom20 and nuclei stains, respectively. At least 300 macrophages with or without fission/fragmented mitochondria were counted (in each condition) from the acquired images and data were shown as the percentage of macrophages with fission/fragmented mitochondrial population.

2.18. Western blotting with subcellular fractions

2.18.1. Isolation of cytosolic and mitochondrial fractions

Mouse bone-marrow cells were culture in T-25 flasks (2 million cells/flask) for 14 days and differentiated into BMDM as described in section 2.2. BMDM were treated with or without 3MA (10mM, 3 mL/flask) for an hour followed by exposed to opsonised *S. pneumoniae* (D39, MOI=10) and left on ice for an hour and 3 hours at 37^{o}C and 5% CO_2. Cells were washed 3 times with PBS and fresh DMEM media with or without 3MA added and incubated for 8 hours at 37^{o}C and 5% CO_2. BMDM were washed 3 times with ice cold PBS followed by 100µL lysis buffer (lysis buffer compositions: 0.1M NaH_2PO_4, 0.2M Na_2HPO_4 and 1.0M NaCl in PBS) containing complete protease inhibitor cocktail (Roche, reference no. 05892970001), and 9.38µg per million cells digitonin and kept on ice. Cells were scrapped into the lysis buffer, placed into a 1.5mL Eppendorf tube and vortexed for 30 seconds, then centrifuged at 13000 rpm for 60 seconds. The supernatant containing the cytosolic fraction was collected and put into a fresh tube and stored at -80^{o}C. The pellet was resuspended in 100µL lysis buffer containing complete protease inhibitor but without digitonin and centrifuged at 13000 rpm for 60 seconds. The supernatant was discarded and the pellet containing the mitochondrial fraction was resuspended in the lysis buffer without digitonin and stored at -80^{o}C.

2.18.2. Protein quantification assay

The protein concentration of the cytosolic and mitochondrial lysates were estimated using DC protein assay (Bio-Rad) described in section 2.6.2.

2.18.3. Sodium dodecyl sulphate-Polyacrylamide gel electrophoresis (SDS-PAGE)

12% resolving gels and 4% stacking gels were prepared (for recipe see Appendix 7.6 iii and iv) to give 1.5mm thick gels with ammonium persulphate (APS) and tetramethyl ethylene diamine (TEMED) being added immediately before the gels were poured. After the resolving gel was poured isopropanol was added to form a small layer on the top. After polymerisation the isopropanol was removed and the gel rinsed with distilled water. The sacking gel was poured on top of the resolving gel and immediately 10 well combs were inserted into the stacking gels and after setting they were placed into a tank with running buffer (Appendix 7.6 vi) and the combs carefully removed. To achieve equal loading of samples the same quantity of protein of each sample was loaded on the gel by adjusting all samples to the same concentration using 1.5M Tris base and then adding

20µL of each sample. Equal volumes of reducing sample buffer (also called Laemmli buffer (Laemmli, 1970), Appendix 7.6 ii) were added to the samples (cytosolic or mitochondrial) and were denatured by heating at 95^{o}C for 1-2 minutes. The denatured samples with a protein ladder (Geneflow Ltd, UK) were loaded into the wells. The electric current was applied at 80V for 15 minutes or until the samples was passed the stacking gel, then at 125V until the loading dye in the sample reached to the bottom of the resolving gel.

2.18.4. Semi-dry electro transfer and protein detection by chemiluminescence

To detect specific proteins, the proteins separated by SDS-PAGE were transfer to poly-vinylidene difluoride (PVDF) membrane (Bio-Rad laboratories Ltd., UK) using semi-dry blotting. The PVDF membrane was activated by soaking in methanol for 1-2 minutes at RT. Three pieces of blotting paper (Whatman International, Maidstone, UK) were soaked in transfer buffer (25mM Tris-Base, 192mM glycine and 20% methanol, Appendix 7.6 vii), on top of these pieces of filter papers were placed the membranes and the gels were placed on the top of the membranes. Then three more pre-soaked pieces of blotting papers were placed on top of each gel, like a sandwich, which was placed in a semi-dry transfer blotter (Trans-Blot SD transfer cell, Bio-Rad). Air bubbles within the stack were removed by rolling a stripette over the top, and 15V constant voltage applied for 45 minutes (Towbin et al., 1992). Transfer of proteins to the PVDF membrane was checked by Ponceau S staining dye. After confirmed proteins transfer, the Ponceau S dye was cleaned with the Tris buffered saline (TBS)-tween for 5 minutes. The membrane was blocked with 5% skim milk in TBS-tween for an hour at RT on a plate shaker. The membrane was then put into a 50mL centrifuge tube with 5mL of mouse anti-Parkin IgG2 (PARK8) (Santa-Cruz, cat no. SC-32282) (1:200 dilution in 5% milk TBS-tween) antibody or rabbit polyclonal anti-actin (1:10000 dilution in 5% milk TBS-tween) (Sigma-Aldrich) or rabbit anti-VDAC (1:1000 dilution) (Cell Signaling Tech. lot-4) and incubated overnight at 4^{o}C on a rolling platform. The membranes were washed 3 times for 10 minutes with TBS-tween. Next, the membranes were put into 50ml tube with 5mL secondary antibodies, either horseradish peroxidase (HRP)-conjugated goat anti-mouse IgG (Dako, P0447) with 1:2500 dilution in 5% milk TBS-tween or goat anti-rabbit IgG (Dako, P0448) with 1:2500 dilution and incubated for one hour on a rolling platform at RT. Then the membrane was washed three times with TBS-tween. Equal volumes of ECLs substrate (GE Healthcare)

were mixed together, added to the membrane for 5 minutes at RT and excess substrate removed from the membrane. Finally the specific proteins bands were detected by enhanced chemiluminescence. Chemiluminescence -high resolution images were acquired by the Chemidoc^{TM} XRS machine using Image lab software (Rio-Rad), using 30 seconds first exposure, then images (total 20) were captured with 200 seconds exposure-interval. Colorimetric images were acquired to record the ladder.

2.18.5. Densitometry

Western blotting allows to measure the level of specific protein expression in a semi-quantitative manner. The intensity of each band area was measured using the ImageJ (v1.8 NIH) software. Then the intensity ratio of Parkin to cytosolic loading control actin, and Parkin to mitochondrial loading control VDAC were calculated from individual protein band intensity.

2.19. Transmission electron microscopy (TEM)

Mouse bone-marrow cells were culture in T-25 flasks (2 million cells/flask) for 14 days and differentiated into BMDM. Then BMDM were mock-infected or exposed to *S. pneumoniae* (D39, MOI=10) and flasks left on ice for an hour and 3 hours at 37^{o}C and 5% CO_2. Cells were washed 3 times with PBS, fresh DMEM media added and cells incubated for 8 hours at 37^{o}C and 5% CO_2. BMDM were washed 3 times with HBSS and 2.0mL/flask Accutase added for 15 minutes at 37^{o}C and 5% CO_2. The cell suspensions were centrifuged at 2000xg for 10 minutes, the pellets washed once with HBSS and centrifuged again at 2000xg for 10 minutes and the pellet fixed with 3% glutaraldehyde in 0.1M cacodylate buffer at 4^{o}C overnight. Cells were washed twice with 0.1M cacodylate buffer in a 30 minutes incubation at 4^{o}C. Secondary fixation was carried out with 3% aqueous osmium tetroxide for 2 hours at RT. The fixative was washed out twice with 0.1M cacodylate buffer in a 30 minutes incubation at 4^{o}C. The cells were dehydrated twice using a graded series of ethanol; 75% for 15 minutes, 95% for 15 minutes, and 100% for 15 minutes and 100% ethanol with anhydrous copper sulphate for 15 minutes at RT. Then the specimen pellets were placed in an intermediate solvent of propylene oxide for 15 minutes twice at RT. Each specimen was infiltrated by placing the specimen pellets in a 50/50 mixture of propylene oxide/araldite resin and incubated overnight at RT with a rota mix. The mixture was mostly discarded, then the specimen left in the full strength araldite resin for 6-8 hours at RT. Subsequently the specimen pellets were embedded in fresh araldite resin (in the hexagonal blocks) for 48-72 hours at 60^{o}C. The resin blocks were cut and confirmed cells section by an ultra-microtome with a binocular

microscopy. The ultrathin (thickness was 90nm) tissue sections were cut on a Reichert Ultracut E ultramicrotome with a diamond knife. The sections were transferred to a copper wire girds (3.05µm diameter). These sections were respectively stained with Uranyl acetate for 30 minutes and Lead citrate for 10 minutes. After the sections were washed twice, electron micrographs were acquired by a transmission electron microscopy using a Gatan digital camera at an accelerating voltage of 80Kv.

2.20. Evaluation of apoptotic macrophages after challenged with *S. pneumoniae*

Mouse bone marrow cells were culture on coverslips (13x13mm) in 24 well plates and differentiated into BMDM. Cells were pre-treated with/without 3MA (10mM) for an hour at 37^{o}C and 5% CO_2. BMDM exposed to *S. pneumoniae* (MOI=10) for 12, 14 and 16 hours at 37^{o}C and 5% CO_2. Cells were washed 3 times with pre-warmed HBSS and 200µL/well NucView^{TM} 530 (1:500 dilution in phenol red and serum free RMPI media) (Biotium, cat no. 10406) was added for 30 minutes at 37^{o}C and 5% CO_2. Cells were fixed with 2% paraformaldehyde for 15 minutes at RT after being washed 3 times with HBSS. Then, the nuclei staining dye DAPI, 0.5µg/mL in PBS, was added for 12 minutes at RT. Subsequently cells were mounted on microscope slides with a drop of glycerol-free polyvinyl alcohol. NucView^{TM} 530 is comprised of a fluorogenic high-affinity DNA dye and a DEVD caspase substrate moiety. In the caspase 3/7 positive macrophages the fluorogenic DNA dye is cleaved from the DEVD substrate, and the fluorogenic intercalating DNA dye binds with nucleus and emits red fluorescence. The NucView^{TM} 530 (red) positive and DAPI (blue) positive cell counted as an apoptotic cell. Whereas NucView^{TM} 530 (red) negative and DAPI positive cell counted as a non-apoptotic cell. At least 300 nuclei were counted for each condition using the Zeiss LSM510 inverted fluorescence microscope.

2.21. Intracellular bacterial killing assay

Mouse BMDM were pre-treated with/without 3MA (10mM) or Mdivi-1 (25µM) or bafilomycin A1 (100nM) (Sigma, 88899-55-2) for an hour at 37^{o}C and 5% CO_2. Cells were exposed to *S. pneumoniae* (D39, MOI=10) and the plates were left on ice for an hour followed by 3 hours at 37^{o}C and 5% CO_2. After washing 3 times with PBS cells were incubated for 4 hours at 37^{o}C with 5% CO_2. In one set of experiment (total 8 hours

post-bacterial challenge), cells were treated with gentamicin (20µg/mL) and penicillin G (40U/mL) (Sigma, PENNA-100MU) for half an hour at 37°C and 5% CO_2, to kill the extracellular bacteria. Viable intracellular bacteria were measured by treating cells with 250µL/well 0.02% saponin diluted in distilled water (Sigma, S4521) for 15 minutes at 37°C and 5% CO_2. 750µL PBS was then added to each well and macrophages lysed with vigorous pipetting and scrapping across the wells. Subsequently the lysates were 5-fold serial diluted and plated on blood agar plates, described in (Miles et al., 1938).

In another set of experiment, after first 4 hours incubation, cells were incubated for 8 hours more at 37°C and 5% CO_2. Cells were washed 3 times with PBS followed by treatment with gentamicin (20µg/mL) and penicillin G (40U/mL) for half an hour at 37°C and 5% CO_2. Subsequently cells were washed 3 times with PBS before being either treated with 0.02% saponin for viable count as above or incubated 4 hours more with vancomycin hydrochloride (0.75µg/mL) (Sigma, V2002) at 37°C and 5% CO_2. Cells were washed 3 times with PBS followed by treatment with 0.02% saponin for 15 minutes and Miles-Mirsa as above. The intracellular survival bacterial colonies were counted after 16 hours incubation at 37°C and 5% CO_2 and data were calculated as cfu/mL.

2.22. Statistical analysis

Flow cytometry data were analysed using FlowJo software version 8.8.4 (Tree Star Inc.). Western blotting and immunofluorescence images were analysed using ImageJ (v1.8 NIH) image processing software. Data were analysed by One-way ANOVA with Bonferroni post-hoc test for multiple comparison or pair t-test for pair-wise comparison, unless otherwise stated. All statistical tests were performed using GraphPad Prism 6.0 (GraphPad Software Inc, San Diego, CA). Data were shown as mean ± standard error mean (SEM) and $p<0.5$ were considered to be statistical significance, with a 95% CI (confidence interval).

Chapter 3. Optimisation of extracellular flux assay with mouse BMDM and human MDM

3.1. Introduction

Macrophage's metabolism and functional phenotype are interconnected. Two decades ago Murphy and Newsholme demonstrated that BCG-activated macrophages in glutamine and L-arginine rich media increase to nitric oxide (NO) production (Murphy and Newsholme, 1997), and later on Gross and co-workers showed that NO induces phagocytosis and antimicrobial function in macrophages (Gross et al., 1998). Recent studies have observed that infectious stimuli alter the metabolic phenotype of macrophages or dendritic cell and a switch in metabolism to glycolysis from mitochondrial oxidative phosphorylation (OXPHOS), is essential for innate immunity (Tannahill et al., 2013, Pantel et al., 2014, Krawczyk et al., 2010). Distinct stimuli result in macrophage polarisation, for example, TLR-agonists (e.g. LPS) or IFN-γ mediate classical activation and IL-4 plus IL-13 mediate alternative activation of macrophages (Mantovani et al., 2004, Stein et al., 1992). These activated macrophages are often referred to as M1 and M2 macrophages, respectively. As part of these distinct phenotypes there are specific changes in molecules associated with metabolism. M1 macrophages upregulate hypoxia-inducible factor (HIF)-1α, glucose transporter channel-1 (GLUT1) and ubiquitous phosphofructokinase 2 (PFK2), a positive regulator of glycolysis, promoting glycolysis (Rodríguez-Prados et al., 2010).

Moreover, M1 macrophages also induce expression of the mitochondrial citrate carrier, which is essential for NO, ROS and prostaglandin production (Jha et al., 2015, O'neill, 2015, Infantino et al., 2011), along with IL-6, IL-12 and TNF-α (Mills et al., 2000), promoting their antimicrobial and inflammatory phenotype, respectively. M2 macrophages, however, induce mitochondrial oxidative phosphorylation through upregulation of Peroxisome proliferator-activated receptor-γ co-activator 1β (PGC-Iβ) and components of the electron transport chain (St-pierre et al., 2003, Shao et al., 2010). These studies highlighted the metabolic and phenotypic differences between macrophages after classical activation with Th1 cytokines or TLR-agonists, as compared with alternative activation by Th2 cytokines. Despite this, detailed analysis of metabolic phenotypes and features of mitochondrial homeostasis in macrophages during host-pathogen interactions with live bacteria are yet to be elucidated in detail. Presumably, since mitochondria are the metabolic hub of eukaryotic cells and the major source of energy production that is essential for immune cells functions such as migration and phagocytosis, mitochondrial metabolism and homeostasis must be carefully regulated and aligned to functional phenotype (Buttgereit et al., 2000). Mitochondria are also an

important effector of innate immune functions beyond their role as a source of ATP production. Recently, Bewley and colleagues demonstrated that COPD alveolar macrophages fail to upregulate mitochondrial reactive oxygen species (mROS) production and that inhibiting mROS, decreased intracellular *S. pneumoniae* killing in healthy but not COPD alveolar macrophages (Bewley et al., 2017). Therefore, it is also essential to elucidate how macrophages metabolic phenotype and mitochondrial homeostasis influences microbicidal responses during host-pathogen interactions perspective.

To investigate the overall cellular metabolic phenotype rather than specific metabolites by NMR spectroscopy or mass spectrometry, the Extracellular Flux Analyser (XF24, Seahorse Bioscience), has proven a useful method. This technique is the latest and simplest method of analysis but also represents a non-invasive way to measure the cellular bioenergetic status of living cells in a real time manner. Seahorse simultaneously measures the major metabolic fluxes, such as glycolysis and mitochondrial OXPHOS through extracellular proton production or acidification rate (i.e. extracellular acidification rate (ECAR)) and oxygen consumption rate (OCR), respectively.

Moreover, the mitochondrial stress test reveals a range of mitochondrial metabolic parameters, such as ATP linked OXPHOS, proton leak, respiration reserve and maximal respiration capacity. These important parameters can be quantified through performing the mitochondrial-stress test with sequential addition of oligomycin A (as an ATP synthase inhibitor), trifluoro-carbonyl cyanide phenylhydrazone [(FCCP), as a mitochondrial OXPHOS uncoupler] and a mixture of rotenone (inhibitor of complex I) and antimycin A (inhibitor of complex III). On the other hand, the glycolytic stress test reveals baseline glycolysis, glycolytic respiration capacity or reserve through sequential addition of oligomycin A and 2-deoxy-D-glucose, which has the 2-hydroxyl group replaced by hydrogen, and which blocks conversion of glucose to glucose-6-phosphate, therefore enabling it to function as an effective inhibitor of glycolysis.

The aims of this chapter were therefore to optimise the extracellular flux assay for use with mouse bone marrow-derived macrophages (BMDM) and human monocyte-derived macrophages (MDM). This would allow me to investigate the metabolic phenotype of activated mouse BMDM and then to analyse the metabolic and bioenergetic status of non-transgenic and human Mcl-1 transgenic mouse BMDM after exposure to *S. pneumoniae*.

3.2. Optimisation of BMDM cell density and other conditions for the Seahorse Extracellular Flux Assay

3.2.1. Cell density optimisation

To perform the extracellular flux assay a consistent monolayer of cells is essential to get reproducible kinetic metabolic flux measurements in a real time basis. Since the sensors (*i.e.* proton and oxygen sensors) of the Seahorse extracellular flux analyser measure both glycolytic flux (*i.e.* proton production rate) and oxidative phosphorylation flux (*i.e.* oxygen consumption rate) in a small microenvironment, it is important that the microenvironment is truly representative of the whole culture and not influenced by regional differences in cell density. To determine the consistency of seeding in the microenvironment likely to be sampled in the XF microplate, representative images were captured and the number of cells were counted using the InCell analyser 2000 and InCell Developer Toolbox 1.9 (GE Healthcare). This approach is not only useful for normalisation of the extracellular flux assay data with the total cell count, it also demonstrates the consistency of cell layers in each well of the XF microplate. Figures 3.1D, 3.1E and 3.1F show that 200,000 BMDM/well was the optimal seeding density and provided consistent, confluent, clumping-free cell layers in the XF24 cell plate's microenvironment.

In contrast, as shown in Figure 3.1A, 3.1B and 3.1C 500,000 BMDM/well yielded more variation in cell density with fluctuating cell number and clumping of cells in the microenvironment of the XF24 microplate. In addition, as shown in Figure 3.2A and 3.2B, the glycolytic rate data also demonstrated that 200,000 and 300,000 cells/well produced similar trends in ECAR after addition of equal amounts of glucose. In contrast, despite the increasing cell density the ECAR was similar with 500,000 cells/well as compared to 200,000 or 300,000 cells/well. Therefore, the cell density/count with the InCell analyser and the real time metabolic responses demonstrated that 200,000 BMDM/well was the optimum cell density for the 24 well format extracellular flux analyser.

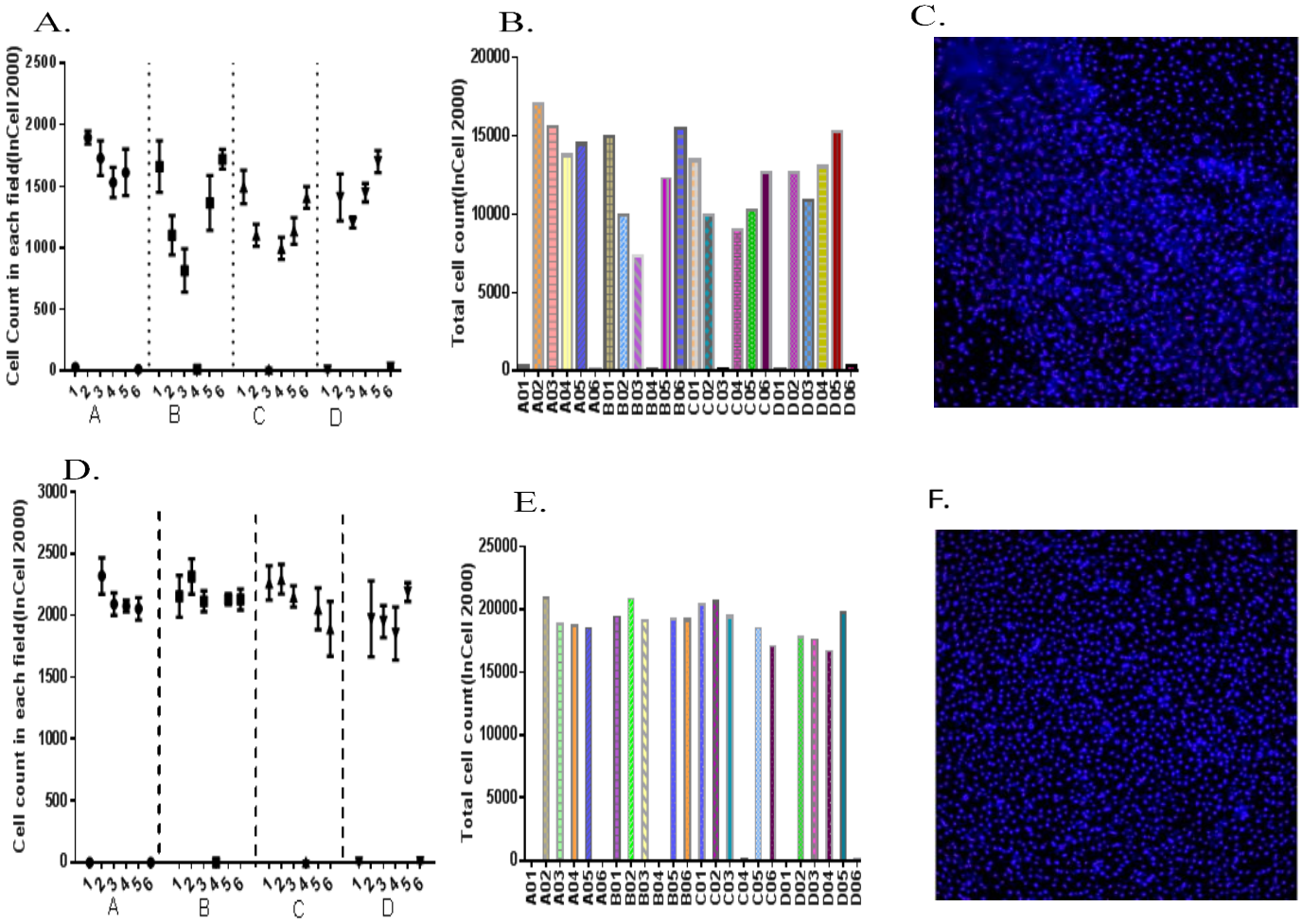

Figure 3.1. **Mouse BMDM cell density titration with Seahorse XF24 flux plate**. Different densities of BMDM were seeded in the XF24 cell plate, after overnight incubation and the SeaHorse extracellular flux measurements, CyQuant® NF dye was added and cell images (x20) were captured at Ex490/Em525nm wavelength (*i.e.* FITC channel). Figure A, B and C show the average cell count of each field, total cell count of each well and a representative field's captured image using the InCell analyser2000 technology, respectively, for 500,000 BMDM/well in the XF24 cell culture microplate. Figures D, E and F demonstrate the same parameters for 200,000 BMDM/well. Figure shows two representative experiments results with 500,000 and 200,000 BMDM/well seeding density. Images were created by using InCell Developer Toolbox 1.9.

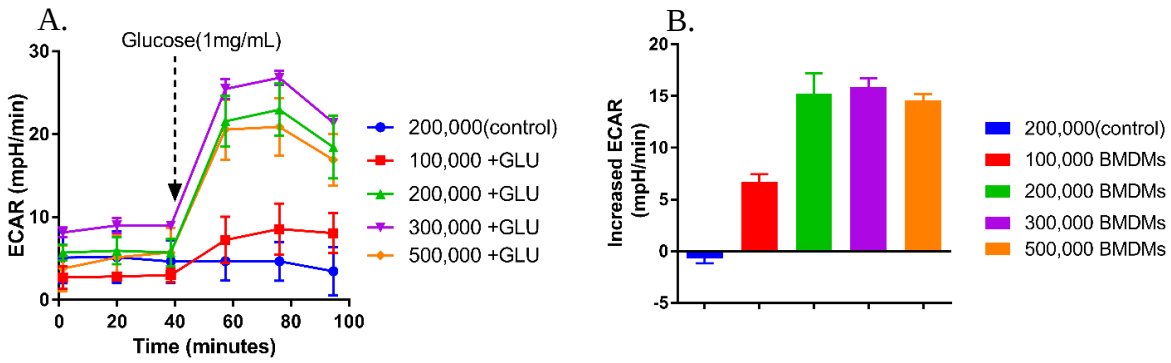

Figure 3.2. **Cell density titration and measurement of the rate of extracellular acidification**. Different densities of BMDM were seeded in the XF24 cell plate, after overnight incubation the ECAR was measured by XF24 flux analyser. Figure A shows the representative extracellular acidification rate (ECAR) as mpH/min for 100,000-500,000/well of BMDM before and after adding glucose (1mg/mL). Figure B shows the average increased ECAR after adding glucose (mean ± SD, n=3).

3.3.2. Oxygen tension and pH optimisation

The settings used will also introduce variation into measurements of changes in O_2 tension, measured in mmHg and changes in pH over time, which are recorded as the OCR and ECAR, respectively. Figure 3.3 represents the change in oxygen tension with respect to time in each group of wells. Typically, these parameters show at the starting point of each measurement, therefore, the microenvironment of each well needs to have an adequate amount of time to allow re-equilibaration during the mixing and waiting stages. This allows the O_2 sensor to re-equilibrate and yield reproducible OCR data with the ambient O_2 tension in the microenvironment. Figure 3.3A and 3.3B show that before the injection of the compound of interest, the O_2 level returned to the initial level (*i.e.* the ambient level), however, after an injection of glucose containing XFAM medium, the starting O_2 levels decreased at each successive measurement. This indicated that the cells consumed oxygen at an increased rate after injection of glucose and that with the mixing time (2.5 minutes) and waiting time (8 minutes) were inadequate to allow the system to reach equilibrium again before the O_2 sensors made their measurements.

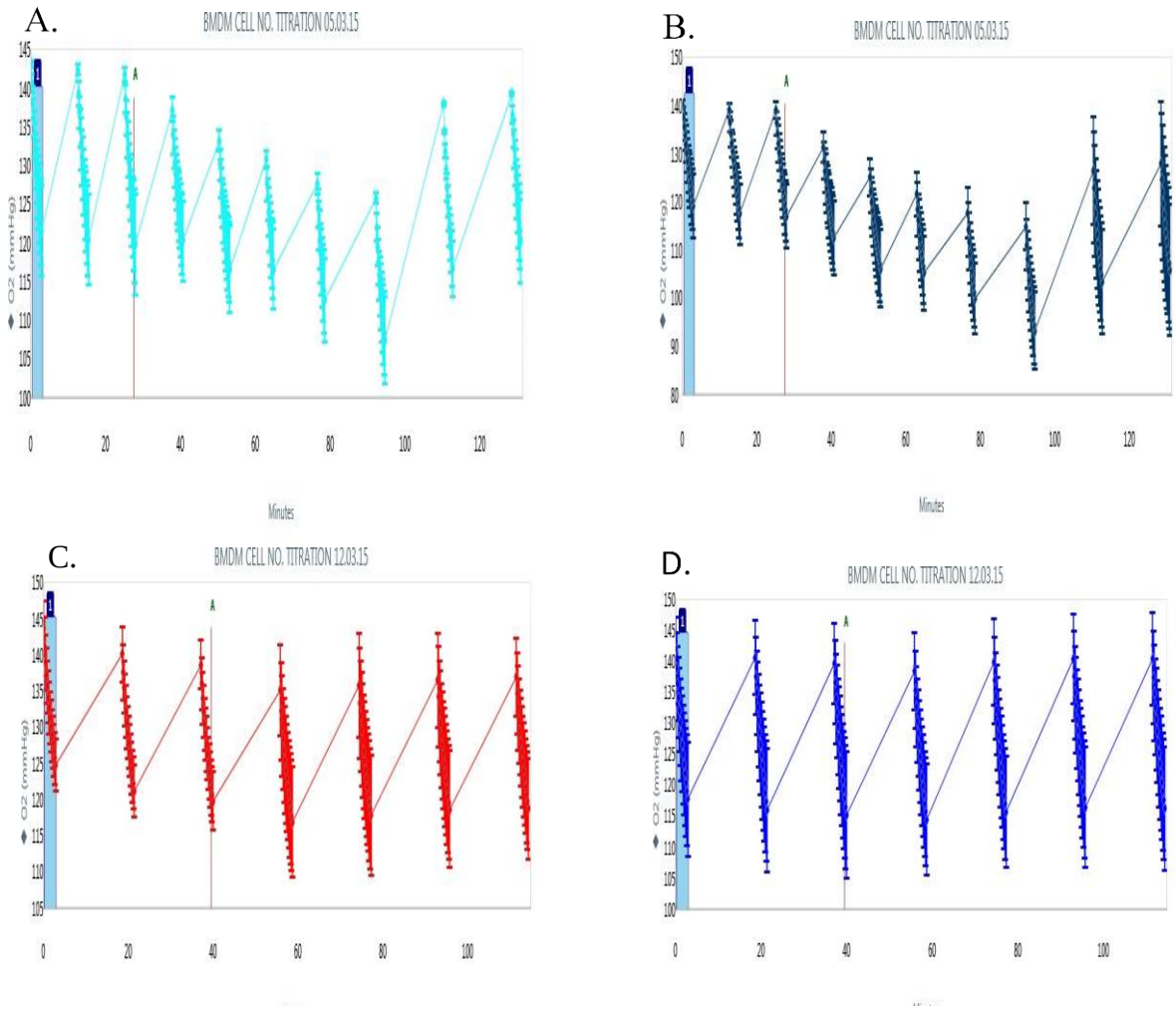

Figure 3.3. **Oxygen pressure optimisation through modification of the Seahorse execution protocol**. Figure (A) 200,000 BMDM/well and (B) 300,000 BMDM/well were seeded in Seahorse XF24 microplate. Figure A and B demonstrate that the oxygen tension (in mmHg) dropped from baseline after injecting XFAM+ 25mM glucose medium (XF assay medium) from injection port A (marked as vertical line). However, after 4 times measurement with 8 minutes waiting time, the oxygen tension returned to baseline level after changing the waiting time from 8 to 12 minutes. After modifying the protocol with 3 minutes mixing, 12 minutes waiting and 3 minutes measuring time, both (C) 200,000 BMDM/well and (D) 300,000 BMDM/well showed consistent oxygen tension before and after injecting the XF assay medium. The figure was created by the Seahorse Bioscience data analysis software Wave 2.2.0.

However, after changing the mixing and waiting times at measuring point 9 and 10 to 3 and 12 minutes respectively, the oxygen tensions returned to the basal level removing the variation in measures before equilibration was reached. Figure 3.3C and 3.3D demonstrate that pre- and post-injection of glucose supplemented XF medium, the oxygen tension returned to the starting point just before each measurement. Similarly, the pH of each injecting compound was adjusted. This was essential to get reproducible ECAR or proton production rate (PPR) data through the proton or pH sensor. In the case of the pH, the injecting compounds pH was adjusted to that of the Seahorse running medium (XF assay medium at pH 7.4).

3.3. Titration of oligomycin A, FCCP, 2-deoxy-D-glucose, Rotenone and Antimycin A for the Seahorse extracellular flux assay

3.3.1. Oligomycin A titration

Oligomycin is an antibiotic that inhibits ATP synthase (inhibiting complex V of the electron transport chain (ETC)) by blocking the proton channel (F_o subunit), which is essential for normal oxidative phosphorylation and the ATPase activity of F_1. Consequently, the presence of oligomycin A increases the rate of glycolysis of cells to compensate for the loss of oxidative phosphorylation and to maintain cellular energy requirements. Hence, oligomycin A is used to measure ATP-linked oxygen consumption by oxidative phosphorylation. Moreover, oligomycin A induces cellular glycolytic capacity to the maximum level. Figure 3.4A and 3.4C show that different concentrations of oligomycin A (0.5 to 2.5μM) increased ECAR and decreased OCR noticeably. These graphs illustrated that 0.5 and 1.0μM oligomycin A increased glycolysis (measured by increased production of extracellular protons) and decreased oxidative phosphorylation (measured by decreased oxygen consumption) consistently. In addition, the bar graphs 3.4B and 3.4D show 0.5μM oligomycin A raised ECAR to 22 mpH/min (the highest level) and reduced OCR by approximately 154 pmoles/min, whereas, 1.0μM increased ECAR to 21.75 mpH/min and decreased OCR approximately 175 pmoles/min. Therefore, 0.5-1.0μM was identified to be the optimum concentration of oligomycin A for mouse BMDM in the extracellular flux assay.

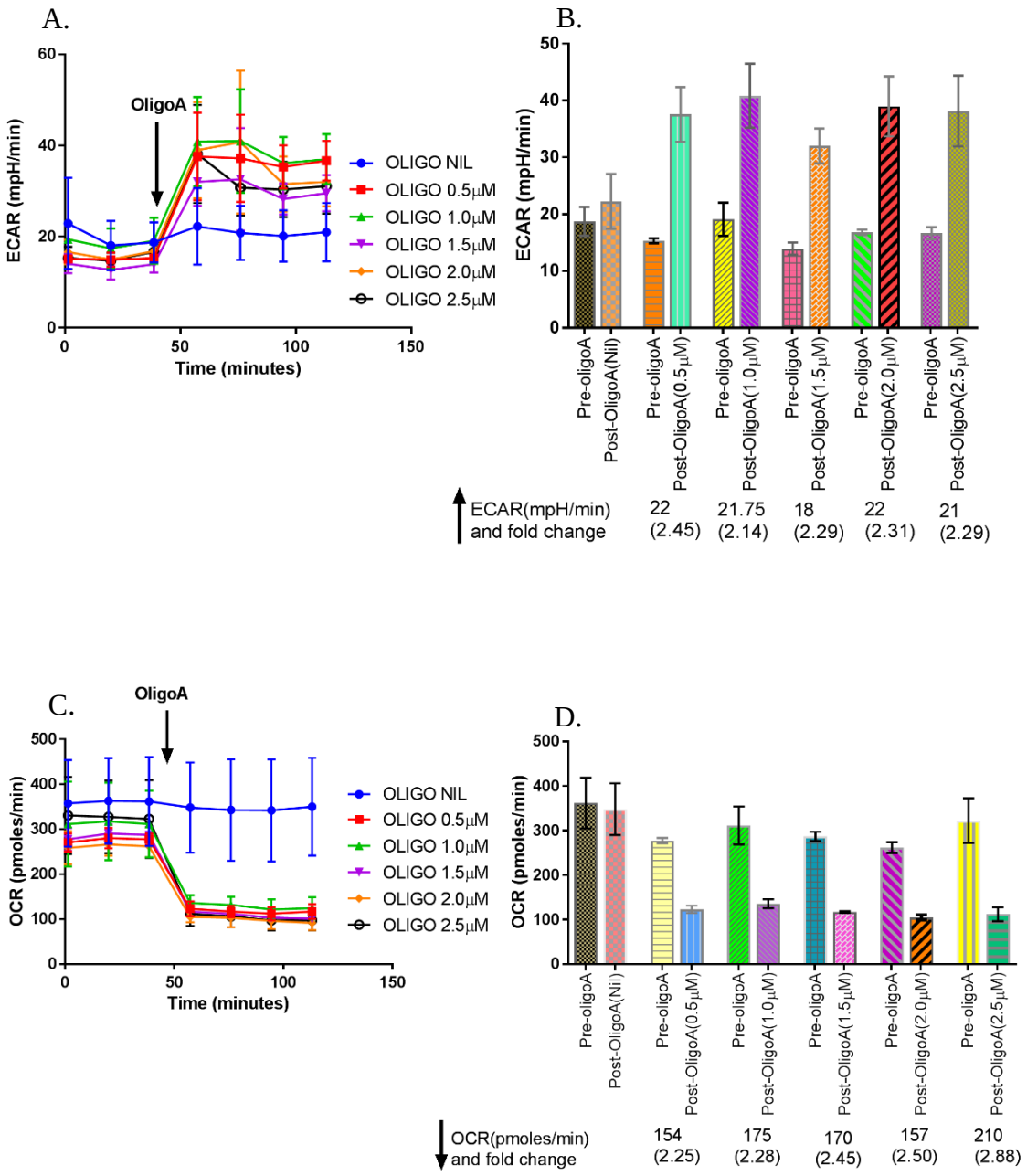

Figure 3.4. **Oligomycin A titration for the extracellular flux assay using mouse BMDM**. 200,000 BMDM/well were seeded onto XF24 cell plates with XF assay medium. Figure A and B show the conversion rate of pyruvate to lactate, as recorded by extracellular acidification rate (ECAR) and the absolute effect of each oligomycin A strength on glycolytic flux. Figure C depicts the kinetics of the oxygen consumption rate (OCR in pmoles/minute) before and after injecting different concentrations of oligomycin A to respective groups and Figure D shows the OCR before and after treatment of each concentration of oligomycin A. The error bar indicates standard error of the mean (n=3).

3.3.2. FCCP titration

Electron transport chain (ETC) and oxidative phosphorylation are interrelated aspects of mitochondrial metabolism. Compounds which stimulate oxygen consumption without a concomitant increase in ATP production, are called 'uncouplers'. It is a natural process in brown adipose tissue mitochondria where uncoupler protein (UCP1) disrupts the ETC mediated proton (H^+) gradient across the inner mitochondrial membrane and generates heat instead of energy (*i.e.* ATP). However, FCCP is an ionophore and a protein-independent mitochondrial oxidative phosphorylation uncoupler which carries protons across the mitochondrial inner membrane phospholipid bilayer.

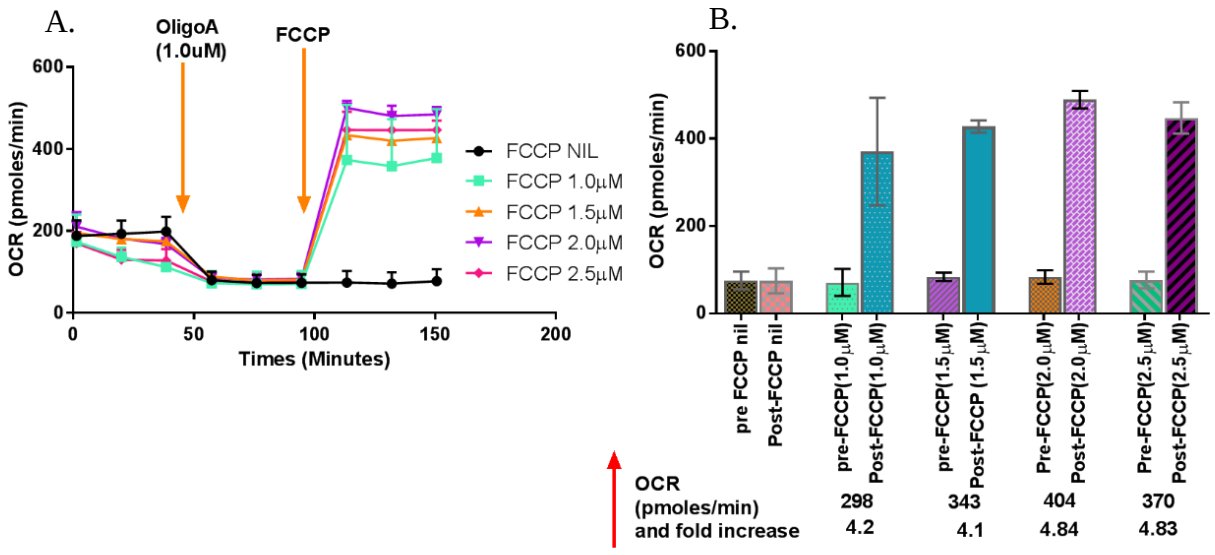

Figure 3.5. **FCCP titration for use in the extracellular flux assay using mouse BMDM**. FCCP was dissolved in DMSO following the supplier's instructions. Then a range of working concentrations 10-25µM (10x intended final concentrations) were prepared in XF assay medium. Figure A and B show the kinetics and the pre- and post-FCCP treated oxygen consumption rate (OCR), respectively. The error bar indicates the standard error of the mean (SEM), (n=3).

Consequently, the maximum amount of oxygen is consumed or converted into water by cytochrome oxidase, complex IV of the ETC. Figure 3.5A shows that 2.0µM FCCP elevated the OCR to a maximum level and levels remained consistently high over the next couple of measuring cycles. Figure 3.5B shows the absolute effect of oligomycin A (1.0µM) and FCCP on OCR. After comparing different strengths of FCCP, I determined

that 2.0µM also gives the highest increment in oxygen consumption of 404 pmoles/minute or around 5 fold the level observed with oligomycin A treated OCR.

3.3.3. 2-deoxy-D-glucose titration

2-deoxy-D-glucose is an analogue of D-glucose and inhibits glycolysis by binding to glucose hexokinase and inhibiting this enzyme, which normally phosphorylates D-glucose to 6-phospho-glucose in one of the rate limiting steps in the glycolytic pathway. Figure 3.6A shows that 0.5µM oligomycin A increased the rate of glycolysis to the maximum level from baseline, whereas, 2-deoxy-D-glucose reduced ECAR sharply below the baseline level of glycolysis. The difference between ECAR before and after oligomycin A treatment is equal to the glycolytic reserve capacity of cells. 2-DG inhibited the rate of glycolysis and decreased the level below baseline ECAR by ⩾20 mpH/minute. Moreover, 2-DG insensitive ECAR is the non-glycolytic acidification which was around 6-8mpH/minute with these settings. Figure 3.6B shows that 2-DG downregulated the rate of glycolysis in a concentration dependent manner up to a concentration of 100mM, which decreased ECAR to the greatest extent (24mpH/minute).

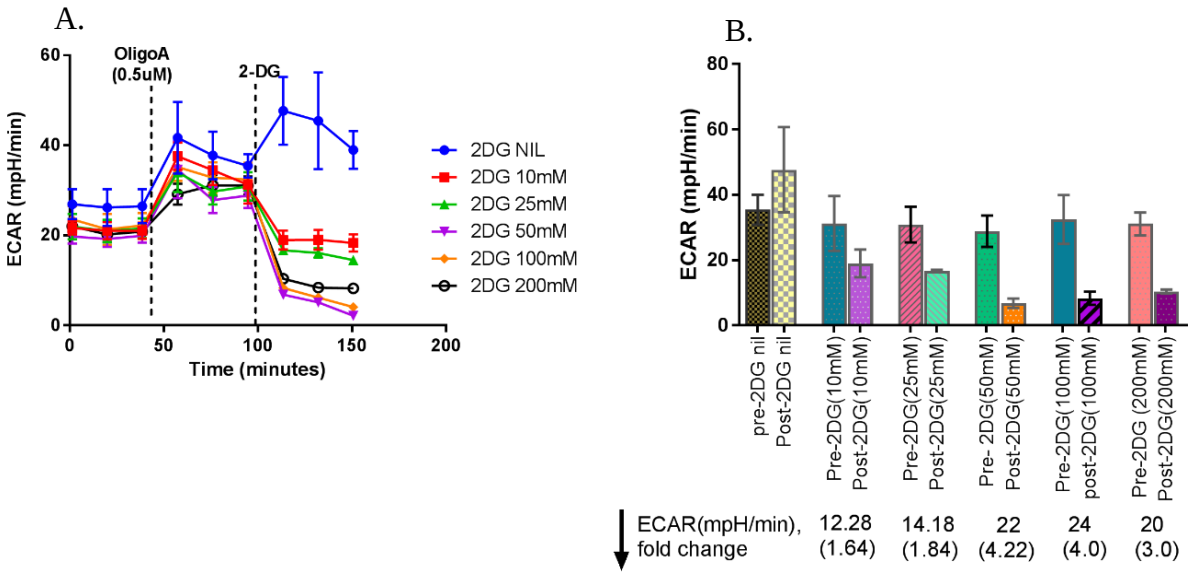

Figure 3.6. **2-deoxy-D-glucose titration using mouse BMDM in the extracellular flux assay**. After baseline flux measurements 10µM oligomycin A (1.0µM working concentration) was injected to all wells, then different concentration of 2-DG were added to respective wells except control wells. Figure A represents the kinetic data for a range of concentrations from a representative experiment. Figure B represents the mean and standard error of the mean of the

extracellular acidification rate (ECAR) values in mpH/min for each concentration pre- and post-addition of 2DG. The absolute reduction and fold change in ECAR is shown below for each concentration of 2DG. The error bar indicates the standard error of the mean (SEM), (n= 3).

3.3.4. Rotenone and Antimycin A titration

The mitochondrial electron transport chain (ETC) and oxidative phosphorylation are tightly linked via the five complexes that make up the ETC. Rotenone is a plant product which is used as an insecticide and pesticide. It blocks electron flow from complex I (i.e. NADH dehydrogenase) to CoQ of ETC. Consequently, rotenone inhibits NADH oxidation (Corbett, 1984). However, it does not affect FADH2 oxidation by complex II (i.e. Succinate dehydrogenase). Antimycin A is an antibiotic which blocks electron flow from cytochrome b_H in Complex III (i.e. Cytochrome C oxidoreductase) to CoQ. Therefore, a combination of rotenone and antimycin A effectively limits electron flow through the mitochondrial ETC and disrupts OXPHOS. Moreover, the non-mitochondrial respiration or oxygen consumption can be measured in the presence of rotenone and antimycin A. From analysis of OCR data and the absolute rate of OCR in the presence of different concentrations of rotenone and antimycin A, 1.0µM of rotenone or antimycin A was found to be the optimum concentration for mouse BMDM (Figure 3.7A-D).

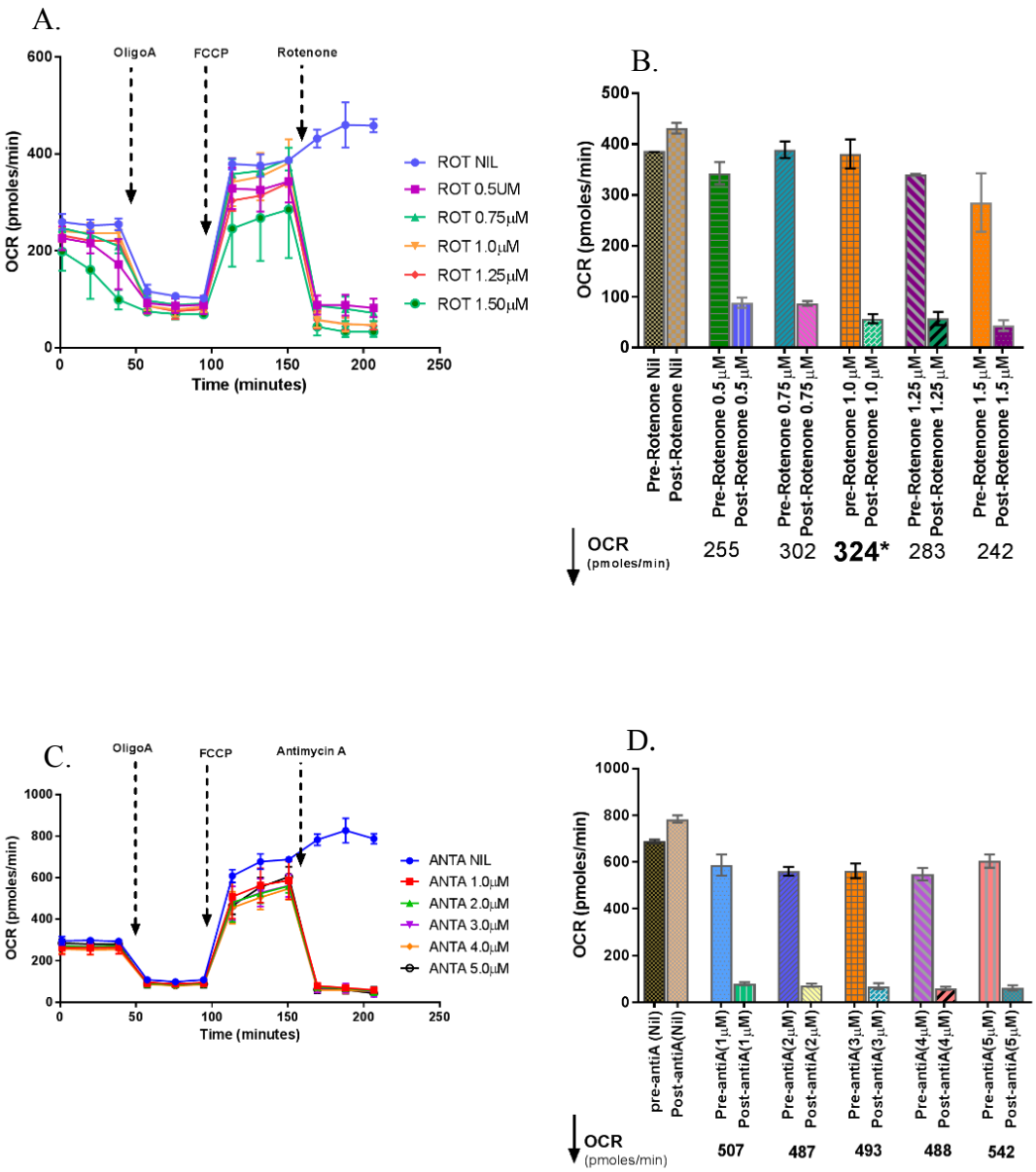

Figure 3.7. **Rotenone and antimycin A titration using mouse BMDM in the extracellular flux assay.** Rotenone and antimycin A were dissolved in DMSO following the supplier's instructions. Then a range of working concentrations 5-15µM (10 fold the final working solutions in media) for Rotenone and 10-50µM (10 fold the final working solutions in media) for antimycin A were prepared in XF assay medium. Figure A and B show the kinetics and the pre- and post-rotenone treated oxygen consumption rate (OCR), respectively. Figure C and D show the kinetics and the pre- and post-antimycin A treated oxygen consumption rate (OCR), respectively. The error bar indicates the standard error of the mean (SEM), (n=3).

3.4. Optimising the Extracellular flux assay with human monocyte-derived macrophages (MDM)

As I had performed for mouse BMDM, I also analysed the optimal parameters for assays of human MDM, specifically adjusting cell density and oxygen tension for mitochondrial stress and glycolysis stress tests in the XF24 flux analyser.

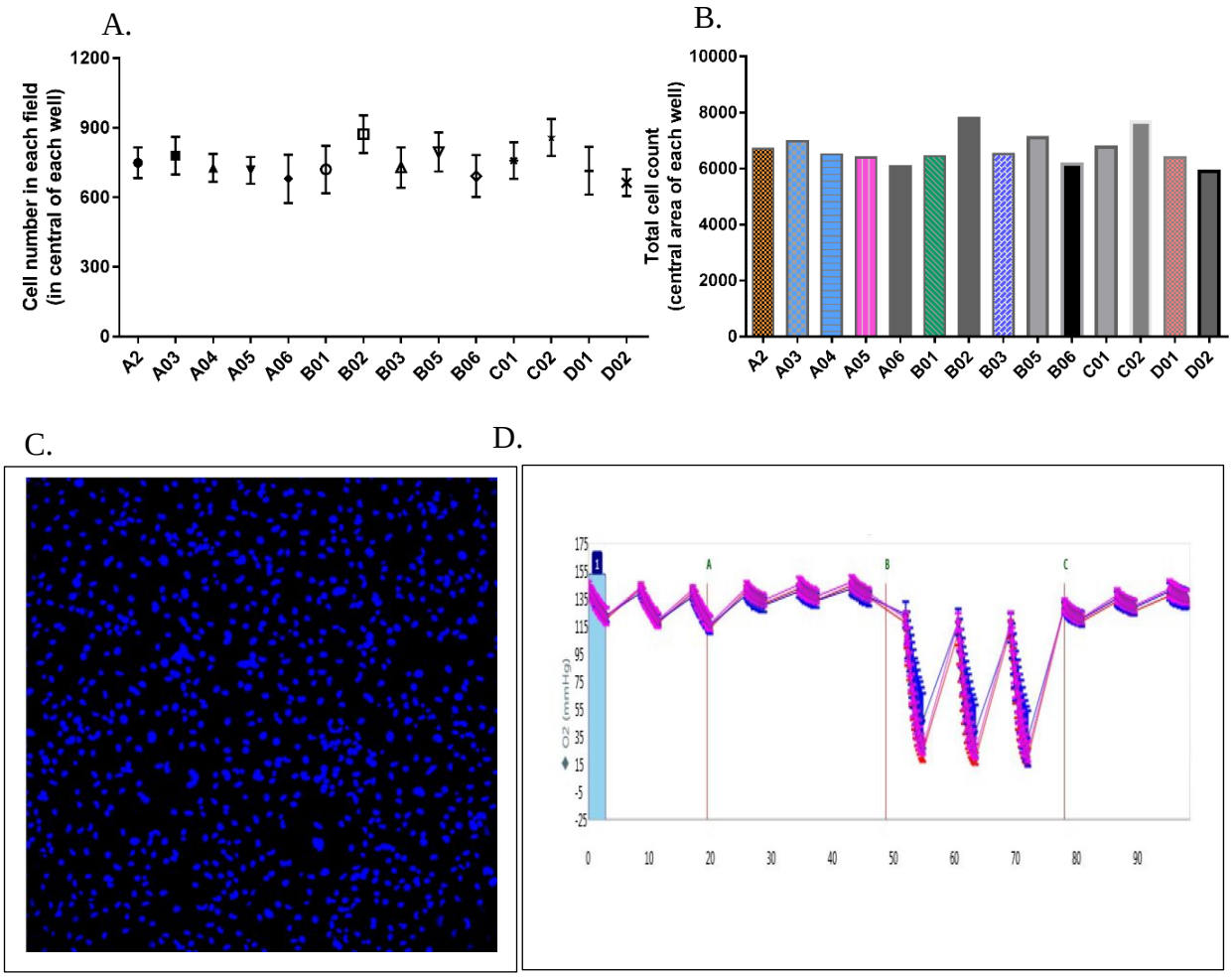

Figure 3.8. **Human MDM cell density, oxygen tension optimisation for the EX24 flux assay**. Human monocyte-derived macrophages (MDM) (150,000 cells/well) were seeded in the XF24 cell plate and incubated overnight at 37ºC and 5% CO_2. Following day, DNA staining dye CyQuant® NF dye was added for 1 hour. Subsequently, CyQuant stained cells images of each well's central representative area (e.g. 9 fields of each well) were captured by the InCell Analyser 2000, using 490nm excitation laser and 525nm emission spectrum with a 20x objective lens. Next, the cell number of each field was automatically counted by the InCell Developer Toolbox 1.9. Figure A shows the average cell count for each field and figure B shows the total cell count for the central representative area of each well (total 9 fields). Figure C illustrates a representative image of a field which was captured by the InCell Analyser 2000. In another set of experiment, 150,000 MDM/well were seeded in the XF24 cell plate and incubated overnight at 37ºC and 5% CO_2. Following day, MDM cell culture medium was replaced with XF assay medium. Subsequently, the cell plate was loaded into the XF24 flux analyser and subsequently the oxygen tension was recorded with 3 minutes mixing, 12 minutes waiting and 3 minutes measuring

interval. Figure D shows the baseline ambient oxygen tension, oxygen tension after oligomycin (vertical line A), FCCP (vertical line B) and rotenone plus antimycin A (vertical line C) injection to XF24 cell plate with 150,000 MDM/well. Figure D was created by the Seahorse Bioscience data analysis software Wave 2.2.0.

3.4.1. MDM glycolytic and mitochondrial stress test inhibitor optimisation

As previously performed for mouse BMDM, I next optimised the doses of inhibitors used in the glycolytic and mitochondrial stress tests for human MDM. The optimum concentration of each inhibitor used for the analysis of glycolytic and mitochondrial respiration, as quantified by the extracellular flux analyser. The titration assay data has shown that 1.5 µM oligomycin, 75 mM 2-DG, 2.0 µM FCCP and 1.0 µM rotenone plus antimycin A were optimum concentration for the XF24 extracellular flux assay with human MDM. The optimum concentration of each inhibitor for the Glyco-stress and Mito-stress test are shown in the following tables:

a. Glyco-stress test:

Name of inhibitors	Optimum concentration
Oligomycin A (2 mM stock in DMSO)	1.5 µM
2-deoxy-D-glucose	75 mM

b. Mito-stress test:

Name of inhibitors	Optimum concentration
Oligomycin A (2 mM stock in DMSO)	1.5 µM
FCCP (10 mM stock in DMSO)	2.0 µM
Rotenone (1 mM stock in DMSO)	1.0 µM
Antimycin A (3 mM stock in DMSO)	1.0 µM

3.5. Characterisation of *Streptococcus pneumoniae* for macrophages challenge

To observe how *S. pneumoniae* alters macrophage's metabolic profile, serotype 2 (strain D39) were grown and characterised to confirm key microbiological features of

pneumococci, such as optochin sensitivity, gram positive staining and catalase negativity. Figure 3.9A and 3.9B show that *S. pneumoniae* started growing exponentially after 2 hours lag phase growth and reached the stationary phase after 6 hours incubation. The mid-log phase was reached after 5 hours of culture and its optical density was approximately 0.4 to 0.5. Figure 3.9C shows the Gram-stained *S. pneumoniae* retained crystal violet dye (i.e. deep violet to blue) instead of counter stain dye safranin (i.e. red). Figure 3.9D shows a representative surface colony forming units of serotype 2 *S. pneumoniae* grown overnight in the Columbia blood agar plate after serial dilution. Figure 3.9E shows the zone of inhibition of optochin sensitivity test with *S. pneumoniae*.

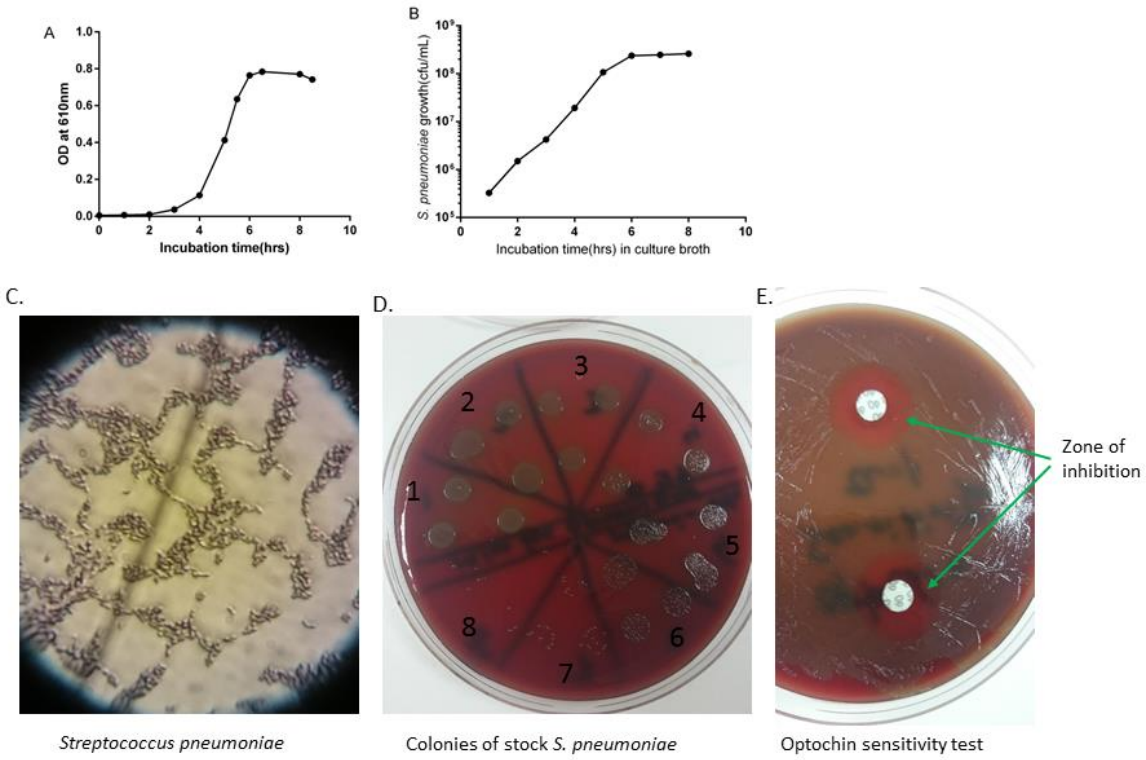

Figure 3.9. ***Streptococcus pneumoniae*** **D39 growth curve and microbiological characteristics**. Figure A shows the optical density at 610 nm at different time points and figure B shows the viable *S. pneumonie* as colony forming units (cfu)/mL after overnight incubation on a Columbia blood agar plate (Miles-Misra serial dilution). Both curves show that after 5 hours incubation *S. pneumoniae* reached the mid-log phase and after 6 hours the stationary phase was reached. Figure C shows the colonies of *S. pneumoniae* after gram staining. Figure D shows the colonies of serially diluted stock *S. pneumoniae* using surface viability counting and figure E shows the zone of inhibition around the optochin disks, confirming optochin sensitivity.

Table 3.1. Microbiological characteristics of *Streptococcus pneumoniae*

Name of experiment	Observation	Results/comments
1. Gram Staining	After staining of *S. pneumoniae* on microscope slides with crystal violet and iodine and then counter staining with safranin, bacteria retained deep violet to blue colour, whereas *E. coli,* stained for comparison, lost violet and showed pink to red staining.	*S. pneumoniae* is a Gram-positive bacteria
2. Catalase test	No noticeable reaction was observed after adding a few colonies of *S. pneumoniae* on a 4% H_2O_2 droplet on a microscopic slide, whereas *Staphylococcus aureus* generated bubbles.	*S. pneumoniae* is catalase negative
3. Pattern of growth on blood agar and hemolysis	*S. pneumoniae* were streaked onto blood agar plates and after overnight incubation it produced greyish colonies rather than clear or transparent colonies with an area of hemolysis around the colonies which was not transparent.	*S. pneumoniae* is α- hemolytic
4. Optochin (Ethylhydrocupreine hydrochloride) sensitivity test	After overnight incubation of *S. pneumoniae* streaked onto blood agar plates with an optochin (Sigma-Aldrich) impregnated disc there was more than a 15mm clear area (i.e. zone of inhibition) observed around the disc.	*S. pneumoniae* is sensitive to optochin

3.6. Optimisation of extracellular flux assay with macrophages challenged with *S. pneumoniae*

To assess macrophages metabolic status after bacterial challenge, either heat inactivated *S. pneumoniae* exposed after baseline ECAR/OCR measurement, or heat inactivated and live *S. pneumoniae* were used to challenge macrophages for 5 hours.

3.6.1. Heat-inactivated *S. pneumoniae's* effect on macrophage metabolism

Acutely injected heat inactivated *S. pneumoniae* (MOI of 10) caused a modest increase baseline glycolytic flux (Figure 3.10A) and reduction in OCR (Figure 3.10C) of mouse BMDM, but this level of bacterial challenge was not sufficient to alter the maximum glycolytic capacity or the glycolytic reserve of cells (Oligomycin treated ECAR, Figure 3.10A). Therefore, the stimulation with bacteria was repeated after baseline measurement

using a bacterial challenge increased to an MOI of 20. It was then observed that the basal glycolytic rate was increased by 10 mpH/min, whereas at an MOI of 10 the ECAR increase was only 6.5mpH/min (Figure 3.10B). In addition, the rate of oxidative phosphorylation was also further reduced, compared to baseline, by addition of heat-killed bacteria at an MOI of 20, falling by 48 pmoles/min compared to the MOI of 10 experiments where the reduction was 33 units pmoles/min (Figure 3.10D). However, the maximum glycolytic capacity was comparable between mock infected cultures and those acutely exposed to heat inactivated *S. pneumoniae*, irrespective of MOI (Oligomycin A treated ECAR, Figure 3.10A).

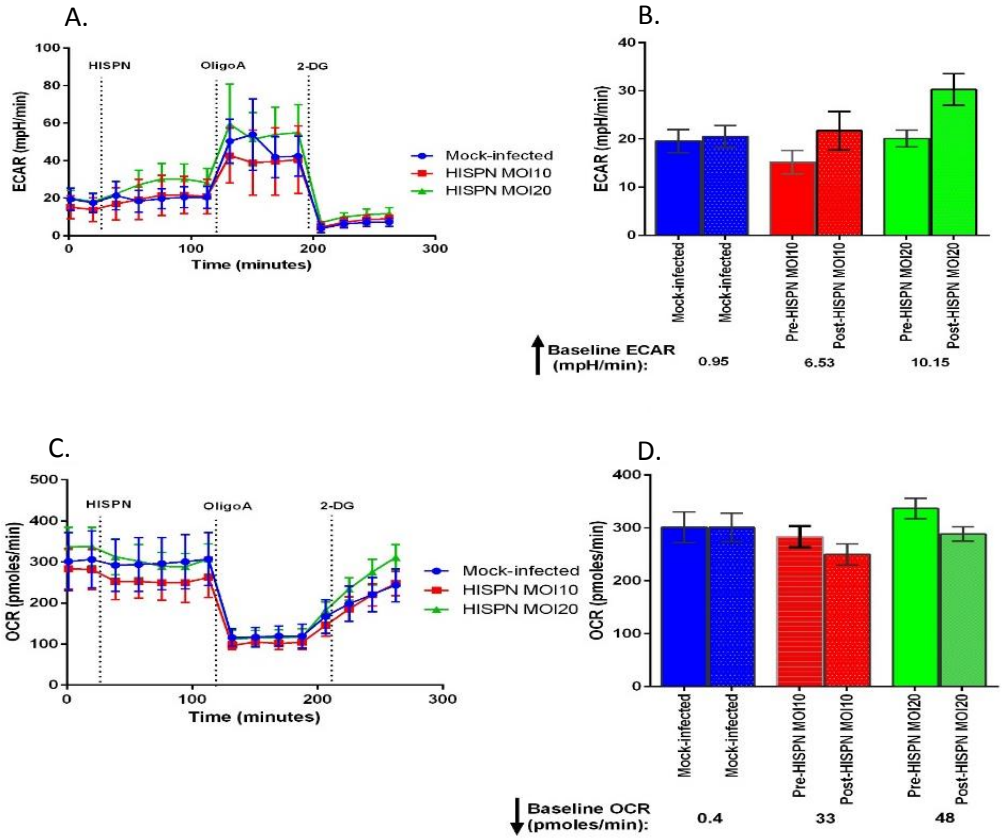

Figure 3.10. **Effect of different inocula of heat inactivated *S. pneumoniae* on mouse BMDM's metabolism**. Wells were seeded with 200,000 BMDM/well in an XF24 microplate and BMDM mock-infected or challenged with heat inactivated *S. pneumoniae* (HISPN), at a multiplicity of infection (MOI) of 10 or 20, after the baseline extracellular flux measurements, at 36 minutes. Subsequently, oligomycin A (Oligo A; final concentration 1µM) was added at 126 minutes and 2-deoxy-D-glucose (2-DG; final concentration 100mM) was added was subsequently added at 216 minutes to measure the maximum level of glycolysis and non-glycolytic ECAR. Figure A shows the representative extracellular acidification rate (ECAR) from pre- to post-bacterial exposure, illustrating the mean and standard error of the mean, respectively. Figure B shows the

ECAR level before the BMDM challenge (mock infection or HISPN at an MOI of 10 or 20). Figure C shows a representative measure of oxygen consumption rate (OCR) kinetics under each condition and Figure D shows the absolute change from pre- to post-bacterial stimulation values, illustrating the mean and standard error of the mean of the duplicating wells.

3.6.1. Metabolically active *S. pneumoniae's* effect on glycolytic metabolism in macrophages

I next addressed whether the impact of live bacteria might be more significant on macrophage metabolism and how this compared to classical activation stimuli. In conducting these experiments, I added both live and heat-inactivated *S. pneumoniae* for a more prolonged time (5 hours) before the metabolic measures were conducted to also examine if this would allow more impact on metabolism. Metabolically active and heat inactivated opsonised *S. pneumoniae* significantly altered various parameters of glycolytic metabolism (Figure 3.11A-D). Live, but not heat inactivated bacteria, decreased baseline OCR (Figure 3.11B), whereas it significantly increased basal glycolytic rate (Figure 3.11C). Both live and heat inactivated bacteria significantly increased maximum glycolytic respiration (Figure 3.11D). The effect of live bacteria was similar to that observed in macrophages that underwent classical activation with LPS and IFN-γ that also showed significant increases in basal and maximal glycolytic metabolism (Figure 3.11E-F). In contrast IL-4, an alternative activation stimulus, did not significantly alter basal or maximum ECAR (Figure 3.11E-F).

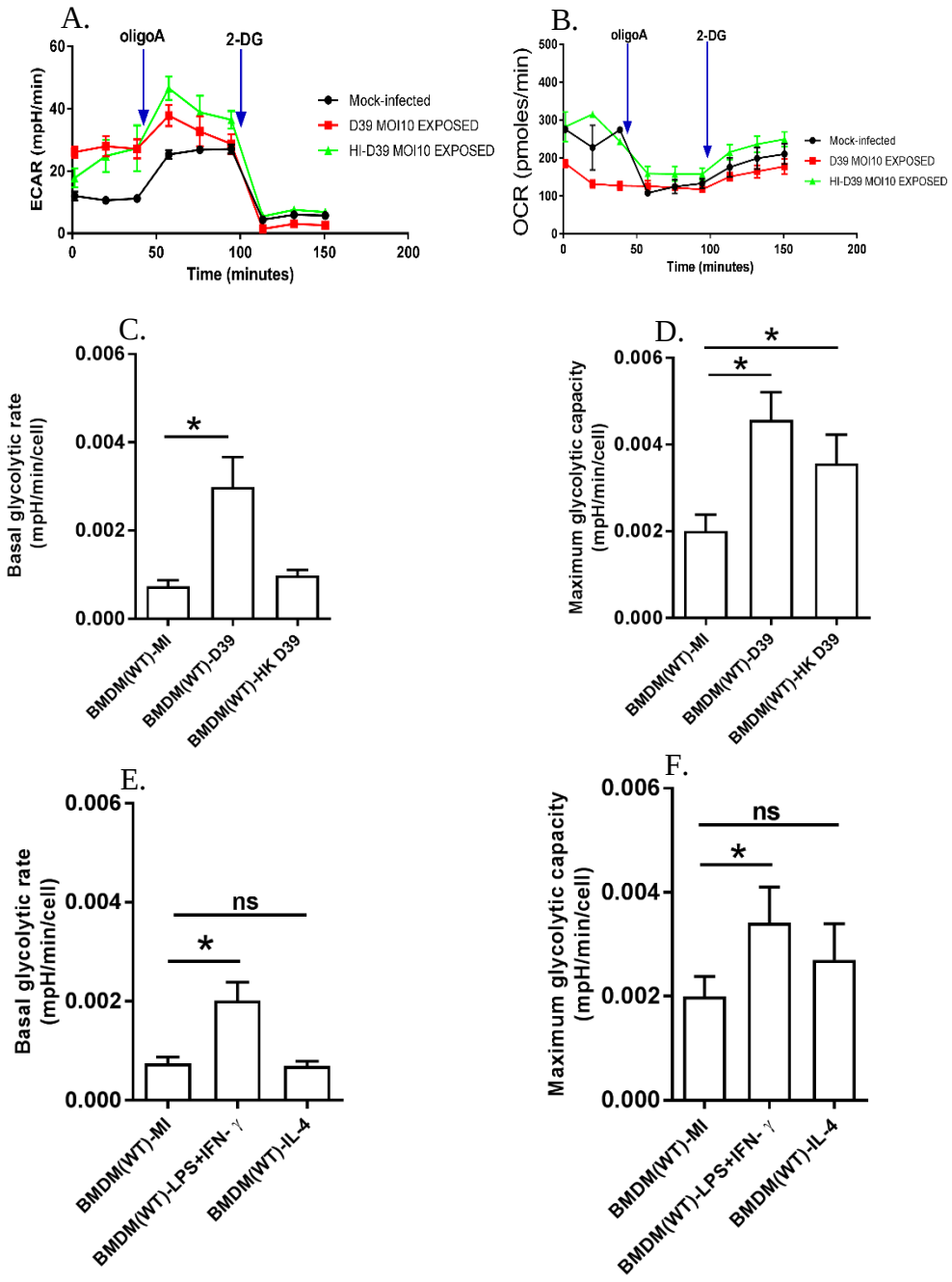

Figure 3.11. **Metabolically active *S. penumoniae* upregulated macrophage glycolytic respiration**. Mouse bone marrow-derived macrophages (BMDM), were either mock-infected (MI), exposed to opsonised live or heat inactivated (HI) *S. pneumoniae* (D39, MOI of 10) or treated with LPS (100ng/mL) plus IFN-γ (20ng/mL) or with IL-4 (20ng/mL) for 5 hours, then the basal glycolytic rate and the maximum glycolytic capacity were measured by the XF24 extracellular flux analyser. Figure A demonstrates the representative extracellular acidification rate (ECAR) and figure B the mitochondrial oxygen consumption rate (OCR) rate data for *S. pneumoniae* exposed BMDM respectively. Figure C shows the normalised basal glycolytic rate and Figure D the maximum glycolytic capacity of mock-infected or heat inactivated or live *S. pneumoniae* exposed macrophages, respectively. Figure E shows the normalised basal ECAR and Figure F the maximum glycolytic capacity of LPS+ IFN-γ and IL-4 treated BMDM, respectively. Data were normalized by total cell count with InCell analyser 2000 and show mean and standard error of the mean values and were analysed by One-way ANOVA with Bonferroni multiple comparison test (*p≤0.05, n=4).

3.7. Macrophages over expressing Mcl-1 show enhanced rates of mitochondrial oxidative phosphorylation

The mitochondrial electron transport chain (ETC) acquires electrons from reducing equivalents (e.g. NADH and FADH2 from the Krebs cycle). These electrons are transferred to cytochrome C oxidase which reduces molecular oxygen into water. During this process, protons are pumped out from the mitochondrial matrix to the intermembrane space, generating a proton gradient. This gradient drives phosphorylation of ADP to ATP and this process coupling a proton gradient to ATP generation is called mitochondrial oxidative phosphorylation (OXPHOS). OXPHOS is the major source of cellular energy (i.e. ATP) production, which is in turn proportional to the mitochondrial oxygen consumption rate (i.e OCR). Mcl-1 is an anti-apoptotic protein, a recent study demonstrated that matrix Mcl-1 increases OXPHOS and maintains mitochondrial homeostasis (Perciavalle, 2012). Our group developed a human CD68.Mcl-1 transgenic mouse (manuscript in review).

I therefore utilised these cells to and performed the metabolic profile assays described earlier in this chapter to test whether the Mcl-1 transgene influenced macrophage metabolism. I observed that human Mcl-1 transgenic mouse BMDM significantly increased baseline OCR (Figure 3.12A), maximum respiration capacity (Figure 3.12C), ATP-linked OCR (Figure 3.12D) and proton leak (Figure 3.12F) compared to non-transgenic littermate's BMDM. *S. pneumoniae* exposure for 4 hours decreased basal OCR in both wild-type and Mcl-1 transgenic BMDM compared to mock-infected BMDM (Figure 4.12A). It also reduced ATP-linked OCR (Figure 4.12D) and proton leak (Figure 3.12F) in the transgenic BMDM though there were also less marked and non-significant decreases seen in the wild-type cells. Overall; the transgene did not appear to have a major influence on the infection-related changes in metabolism. On the other hand, baseline glycolytic rate (Figure 3.13B) and maximum glycolytic capacity (Figure 3.13C) were comparable between wild-type and transgenic BMDM. *S. pneumoniae* exposure, however, significantly increased both basal glycolytic respiration (Figure 3.13B) and maximum glycolytic capacity (Figure 3.13C) of wild type and transgenic BMDM.

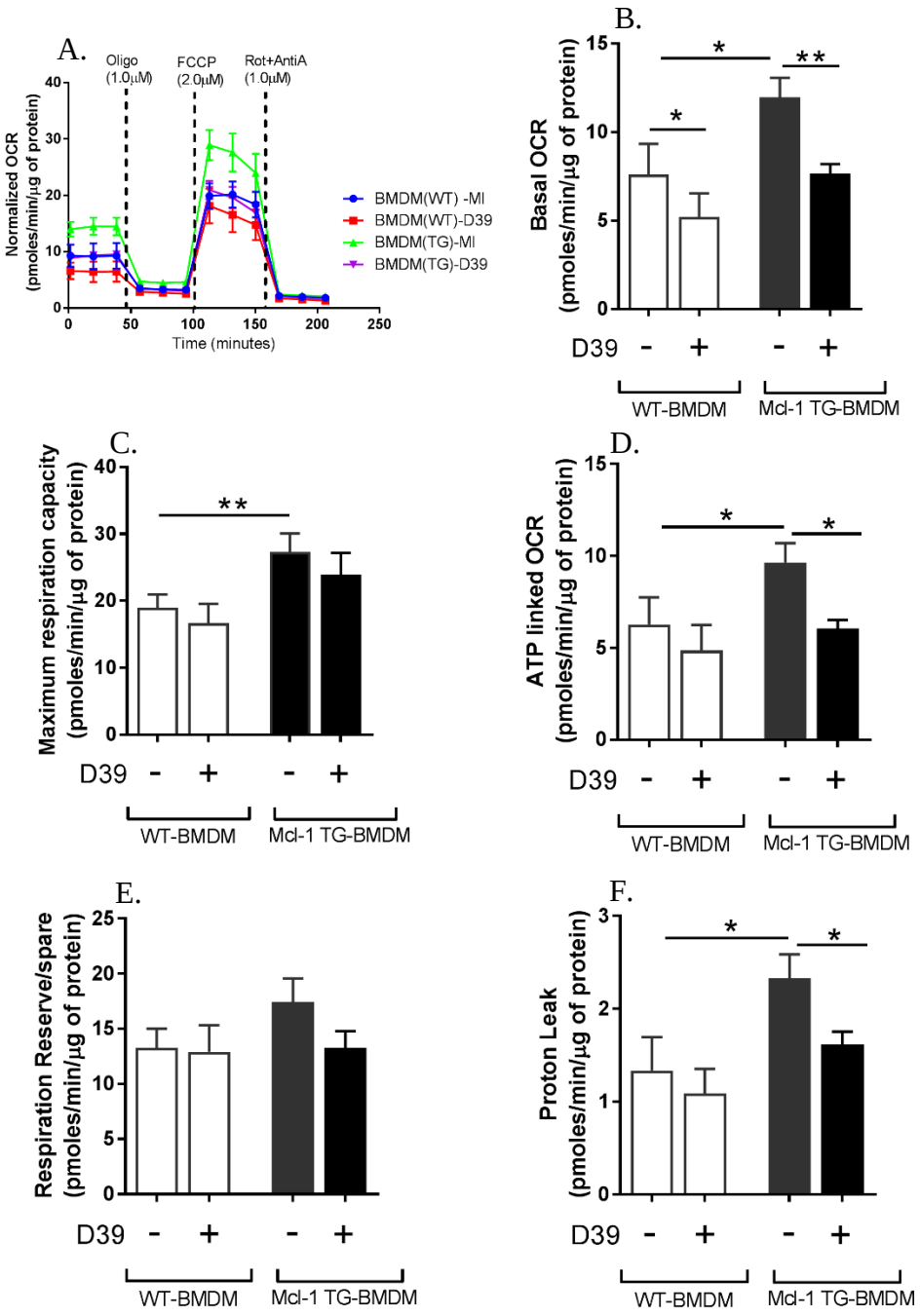

Figure 3.12. **Mitochondrial oxidative phosphorylation in macrophages is modified by a Mcl-1 transgene.** Both wild type (WT) and human Mcl-1 transgenic (TG) mouse bone marrow derived macrophages (BMDM) were exposed to opsonised serotype 2 *S. pneumoniae* (D39) or mock infected (MI) for 5 hours, then mitochondrial oxygen consumption rate (OCR) was measured using the X24 Seahorse extracellular flux analyser. (A) Representative normalised OCR for one experiment, summary data for, (B) basal OCR, (C) maximum respiration capacity, (D) ATP linked OCR, (E) respiration reserve and (F) proton leak calculated from the OCR data is depicted. Oligomycin A (1.0μM) was added to measure ATP-linked OCR, maximum respiration capacity was estimated by subtracting non-mitochondrial OCR with rotenone (1.0μM) plus antimycin A (1.0μM) from FCCP (2.0μM) OCR data (details in method-materials section). Data were normalized by total protein and are shown as mean ± standard error of the mean and

analysed by one-way ANOVA with Sidak's multiple comparison test. (*p≤0.05, **p ≤0.01, n=6).

3.8. Human Mcl-1 transgenic mouse BMDM and non-transgenic BMDM show comparable baseline and bacterial induced glycolysis

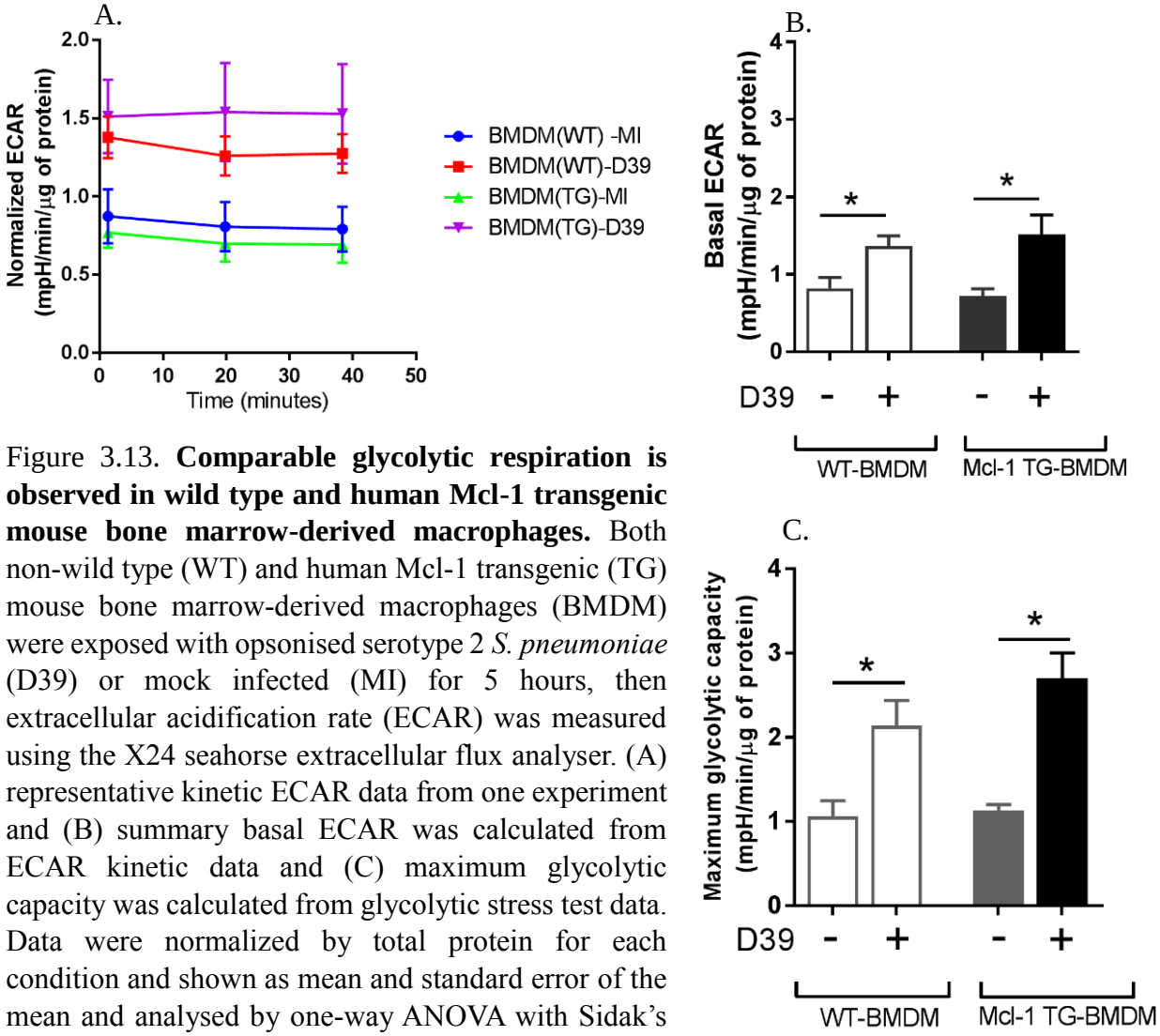

Figure 3.13. **Comparable glycolytic respiration is observed in wild type and human Mcl-1 transgenic mouse bone marrow-derived macrophages.** Both non-wild type (WT) and human Mcl-1 transgenic (TG) mouse bone marrow-derived macrophages (BMDM) were exposed with opsonised serotype 2 *S. pneumoniae* (D39) or mock infected (MI) for 5 hours, then extracellular acidification rate (ECAR) was measured using the X24 seahorse extracellular flux analyser. (A) representative kinetic ECAR data from one experiment and (B) summary basal ECAR was calculated from ECAR kinetic data and (C) maximum glycolytic capacity was calculated from glycolytic stress test data. Data were normalized by total protein for each condition and shown as mean and standard error of the mean and analysed by one-way ANOVA with Sidak's multiple comparison test. (*p≤0.05, n=6 for A and B and n=4 for C).

3.9. Discussion

Immune cells, especially macrophages, consume energy for metabolically demanding functions that require ATP. Some of these functions include cell migration and phagocytosis, antigen processing and presentation, cell proliferation and immune effector

functions such as bacterial killing, cytokine and chemokine generation and induction of cell apoptosis (Buttgereit et al., 2000). Macrophages show high plasticity and they are highly adapted to environmental cues. Moreover, macrophages exhibit varying forms of activation and show variations in polarisation from the *in-vitro* extremes of M1 and M2 phenotype, which show distinct metabolic profiles (Haschemi et al., 2012, Tannahill et al., 2013). Jacobs et al. and Rathmell et al. both demonstrated that inhibition of cell metabolism may lead to impaired function and apoptosis, whereas excessive metabolic function may also alter functional phenotype and predispose to disease conditions such as autoimmunity and inflammatory diseases (Jacobs et al., 2008, Rathmell et al., 2003). It will be important to determine in the future whether clinical conditions such as chronic obstructive pulmonary disease (COPD), which are associated with altered host-pathogen responses such as reduced phagocytosis of bacteria (Taylor et al., 2010, Bewley et al., 2016), are also associated with altered metabolic responses whether these are mechanistically linked.

To further investigate the metabolic profiles of macrophages and their relationship to susceptibility to infection, the XF24 Seahorse extracellular flux assay was thoroughly optimised for use with differentiated mouse BMDM and human MDM. From the titration experiments, 200,000 BMDM/well and 150,000 MDM/well were observed as the optimum cell density for the XF24 microplate. To get an optimum ambient oxygen tension inside the XF24 microenvironment, 3 minutes measuring time was identified as the best option after 3 minutes of mixing time and 12 minutes of waiting time. To assess the glycolytic metabolism (*i.e.* ECAR) of macrophages, oligomycin A and 2-deoxy-D-glucose, and for mitochondrial OXPHOS assessment, oligomycin A, FCCP and rotenone/antimycin A were titrated against response in the XF24 flux analyser. These compounds formed the glycolytic stress test and the mitochondrial stress tests and a range of concentrations was tested to get the most accurate bioenergetic profiles for macrophages as evidenced by the ability to produce the expected changes in key bioenergetics measurements (Pelletier et al., 2014).

The titration experiments showed that 0.5-1.5µM oligomycin A, 75-100mM 2-deoxy-D-glucose, 2.0µM FCCP and 1.0 µM rotenone/antimycin A are optimum for the extracellular flux assay with mouse BMDM and human MDM. Oligomycin A inhibits ATP synthase (complex V), hence it decreases oxygen consumption via complex IV (*i.e.* cytochrome oxidase) of the mitochondrial ETC, resulting in oxidation of molecular oxygen to water in the presence of protons (Hong and Pedersen, 2008). To compensate

for the inhibition of ATP synthesis, cellular energy production is maintained through increases in the rate of glycolysis, and increases in glycolysis occur to the maximum level in the presence of oligomycin A. Therefore, oligomycin A is not only used to determine the mitochondrial ATP-linked oxygen consumption and proton leakage but also to measure the maximum glycolytic capacity and glycolytic reserve of the cell. In contrast, 2-deoxy-D-glucose is a glucose analogue which inhibits hexokinase (*i.e.* glucokinase) competitively, hence it is used to determine the basal glycolytic rate, and the non-glycolytic acidification rate.

On the other hand, FCCP is an uncoupler of mitochondrial oxidative phosphorylation from ETC. It upregulates oxygen consumption rate massively without ATP synthesis, because it disrupts the proton gradient across the mitochondrial membranes by transferring protons across the inner mitochondrial membrane to the matrix. Like uncoupling proteins (UCP1/2), FCCP breaks coupling between substrate oxidation and mitochondrial oxidative phosphorylation (OXPHOS) of ADP to ATP (Heytler, 1980). Hence it is called an ‘‘uncoupler’’ and is used to measure the maximum mitochondrial respiration rate. All of the inhibitors including rotenone (complex I inhibitor) and antimycin A (complex III inhibitor) were optimised separately to avoid artefacts.

Metabolically active *S. pneumoniae* increased BMDM basal and maximum glycolytic respiration with decreased basal OXPHOS at an earlier time point (5 hours post-infection). But at this stage, the maximum respiration capacity of mitochondria was unaltered, suggesting that the earlier metabolic switch to glycolysis is not due to mitochondrial impairment, but rather is activated to compensate for the high energy demand required for coping with intracellular bacteria. This metabolic shift is like a Warburg type-effect, as has been observed in LPS-activated macrophages (Palsson-Mcdermott et al., 2015) or as has been mediated by various TLR stimuli (TLR 2, 4 and 9) in dendritic cells (Krawczyk et al., 2010). Moreover, like LPS, heat inactivated or metabolically active *S. pneumoniae* increased the maximum glycolytic capacity of macrophages when exposure was sustained for several hours. The baseline glycolytic rate was comparable between mock-infected and heat inactivated bacteria exposed macrophages, suggesting that metabolically active bacteria could be contributory to increased baseline ECAR. Presumably heat inactivated Gram positive pneumococci provide peptidoglycan whose degradation products may signal via pattern recognition receptors, such as nucleotide-binding oligomerisation domain containing protein 2 (Nod

2), to generate similar results on metabolism to that provided by LPS-mediated TLR4 activation (Sriskandan and Cohen, 1999).

Moreover, it appeared that *S. pneumoniae* stimulate macrophages similarly to classic activation by LPS and IFN-γ and showed metabolic signatures similar to M1 polarised macrophages, in that they upregulate glycolysis. Recently Rodriguez-Prados and colleagues demonstrated that classical activation with LPS and IFN-γ or TLR-2,3,4 or 9-agonists increase glycolytic fluxes through shifting the expression pattern of phosphofructokinase 2 (PFK2) isoforms, resulting in an increase in ubiquitous PFK2 (uPFK2) expression and a decrease in the liver PFK2 (L-PFK2) isoform. This decreases phosphatase activity and causes accumulation of fructose-2,6-bisphosphate in macrophages, a positive regulator of one of the rate limiting enzymes of glycolysis called phosphofructokinase 1 (PFK1) (Rodríguez-Prados et al., 2010). On the other hand, human Mcl-1 transgenic mouse BMDM increased mitochondrial respiration capacity and ATP-linked OXPHOS with unaltered glycolytic respiration, in the mock infected condition. This is consistent with data from Perciavalle and co-workers, concerning mitochondrial bioenergetics in Mcl-1 transgenic murine embryonic fibroblasts (Perciavalle, 2012). *S. pneumoniae* reduced several OCR related parameters in the transgenic BMDM though there were similar trends in the wild type cells, so these changes were probably not specifically because of the transgene but are likely to reflect a modest reduction in OCR in the context of bacteria.

Overall, this section shows that the Seahorse XF24 extracellular flux analyser can be used to analyse metabolic responses of macrophages to *S. pneumoniae*. The data shown here suggests that like classical activation stimuli macrophages upregulate glycolytic metabolism in response to pneumococci, while my data also suggests that Mcl-1 can enhance oxidative phosphorylation. Further chapters in this thesis will explore potential alterations in macrophage metabolism following bacterial challenge with clinical disease states and relate these changes to other aspects of mitochondrial homeostasis.

Chapter 4. Evaluation of macrophages metabolic phenotype and their metabolites mROS or NO interactions with *S. pneumoniae* in the phagolysosomes

4.1. Introduction

Metabolic reprogramming is a signature of most immune cell's activation, and it is a pivotal part of immunometabolism that is linked to immune-regulation (Loftus and Finlay, 2016). For example, Gram-negative bacterial lipopolysaccharide (LPS) activates murine peritoneal macrophages, which absorb more glucose, upregulating glucose transporter 1 (GLUT1) (Fukuzumi et al., 1996), and LPS shifts the metabolic profile by increasing reliance on glycolysis, which is required to induce a proinflammatory macrophage phenotype (Jha et al., 2015). Moreover, the innate activation with LPS and interferon (IFN)-γ also upregulates inducible nitric oxide synthase (iNOS) in macrophages, which produces reactive nitrogen species (eg. nitric oxide radical, NO) (Lorsbach et al., 1993). NO inhibits mitochondrial oxidative phosphorylation (OXPHOS) by nitrosylating iron-sulfur rich proteins in complex I (NADH dehydrogenase) (Emilio et al., 1998, Drapier and Hibbs Jr, 1988) and complex IV (cytochrome oxidase) (Cleeter et al., 1994) of the electron transport chain (ETC) involved in mitochondrial oxidative phosphorylation (OXPHOS).

Furthermore, the metabolic reprogramming induces glycolysis and disrupts the Krebs cycle, inducing breaks in the Krebs cycle and diverts substrates, which are involved in the reprogramming that leads to the generation of proinflammatory cytokines. For example, breaks in the Krebs cycle in LPS-stimulated macrophages (M1), result in accumulation of the intermediate succinate, which acts as a signalling molecule to upregulate HIF-1α and induces IL-1β production (Tannahill et al., 2013). Moreover, Krebs cycle disruption also elevates citrate levels, which is converted into itaconic acid that limits the growth of bacteria, such as *Salmonella enterica* and *Mycobacterium tuberculosis* (Jha et al., 2015, Alessandro et al., 2013). However, it is not fully understood how elevated succinate or itaconic acid inhibit bacterial growth. Interestingly, several studies have demonstrated that succinate, the substrate of complex II (in the mitochondrial respiration chain) induces mitochondrial superoxide (i.e. mROS) production by transferring electrons in a reverse manner to complex I, rather than direct electron transferring to ubiquinone then complex III. This succinate-driven mROS production is also sensitive to complex I inhibitors (e.g. rotenone or piericidin) (Lambert and Brand, 2004, Liu et al., 2002, Hansford et al., 1997), suggesting that this is generated at the complex I site rather than in complex II. Besides, the Dockrell group have recently demonstrated that human immunodeficiency virus (HIV-1) (Collini et al., 2018) or chronic obstructive pulmonary disease (COPD) alveolar macrophages show impaired

intracellular *S. pneumoniae* killing (Bewley et al., 2017), which could be causes of increased susceptibility to pneumococcal pneumonia in HIV-1 infection or infection-mediated exacerbations in COPD respectively. Both of these studies also observed that in patients with COPD or HIV-1 infection, *S. pneumoniae* fails to trigger adequate induction of mROS over baseline and fails to activate a delayed mitochondrial pathway of apoptosis, which is essential for intracellular bacterial killing and inflammation resolution.

Typically, 0.2-2% of cellular consumed oxygen is converted into mROS, during mitochondrial OXPHOS, as a by-product due to electron leak from complex I and complex III of ETC (Balaban et al., 2005). But this *de novo* electron leak and subsequent mROS generation is augmented by TLR-agonists (e.g. LPS), which induce TRAF6 signalling associated with complex I inactivation (West et al., 2011a), or by triggering RIP1/RIP3 signalling pathway in macrophages, as shown following challenge with *Mycobacterium tuberculosis* (Roca and Ramakrishnan, 2013). This induction of mROS is also be caused by IFNγ/STAT1 signalling, as seen in macrophages challenged with *Listeria monocytogenes* (Sonoda et al., 2007).

Moreover, recently it has been shown that HIV envelope glycoprotein gp120 not only alters mitochondrial dynamics but also decreases mitochondrial respiration capacity in neurons (Avdoshina et al., 2016). Similarly, oxidative stress or COPD diminishes mitochondrial respiration capacity, respiration reserve and ATP-linked respiration in airway small muscle cells (Wiegman et al., 2015). Thus both COPD and HIV-1 infection may stimulate reduced OXPHOS and conditions that might allow increased baseline mROS, and potentially reduced induction of mROS during infection. Therefore, it is important to determine the exact metabolic phenotype - especially mitochondrial OXPHOS - after challenge in *S. pneumoniae* in COPD macrophages or macrophages stimulated with recombinant glycoprotein gp120, as the work of Collini and colleagues suggests this phenocopies the defect of mROS induction following *S. pneumoniae* challenge in HIV-1 infection (Collini et al., 2018). Overall, this complex scenario might aid our understanding of the mitochondrial role in innate immunity beyond energy supply, through its role as an effector of microbicidal responses. Therefore, in this section I will explore the mitochondrial bioenergetic profile of human monocyte-derived macrophages after challenge with *S. pneumoniae*. I will also investigate the metabolic phenotype of COPD macrophages or recombinant gp120 pre-treated macrophages challenged with or

without *S. pneumoniae*. Moreover, I will also evaluate the mitochondrial ROS and nitric oxide levels and investigate their interaction with bacteria in phagolysosomes.

4.2. *S. pneumoniae* decreased mitochondrial OXPHOS of human monocyte-derived macrophages

Cellular oxygen consumption is an integral part of mitochondrial OXPHOS and this process is the major site of ATP production. Recently it has been demonstrated that, unlike classical activation (i.e. M1 macrophage), macrophages with parasitic infection (e.g. *Leishmania infantum*) diverted an early increase in aerobic glycolysis to a later increase in mitochondrial OXPHOS (Moreira et al., 2015), which results in an M2 metabolic phenotype in macrophages. Whereas, LPS stimulated or Gram-positive (*e.g. S. aureus*) or Gram-negative bacteria (e.g. *E. coli*) exposed monocytes show increased glycolysis, but varied mitochondrial metabolic responses, characteristic of an M1 metabolic phenotype (Moreira et al., 2015).

To assess the metabolic responses in human monocytes-derived macrophages (MDM) in the presence of the lung pathogen *S. pneumoniae*, MDM were exposed to opsonised serotype 2 *S. pneumoniae* (D39) for 4 hours or 16 hours, then the mitochondrial OXPHOS and glycolytic responses were evaluated by the extracellular flux analyser (Seahorse, Bioscience). *S. pneumoniae* significantly increased the basal glycolysis of human MDM at both time points (Basal ECAR in the Figure 4.1A and ECAR rate data in Figure 4.1H and Figure 4.1I). Although the baseline OXPHOS was comparable between mock infected MDM and pneumococcal challenged MDM at the later time point, and although it was significantly decreased at the earlier time point the change was of small magnitude suggesting that basal OCR was not altered to a large extent (OCR rate data in Figure 4.1B and 4.1C and basal OCR in Figure 4.1D). Other changes were more marked at the 16 hour time point after bacterial challenge; *S. pneumoniae* decreased mitochondrial respiration capacity by approximately two-thirds (Figure 4.1E) and ATP-linked OXPHOS by one-third (Figure 4.1F), with increased proton leak (by approximately 3-fold) through the mitochondrial inner membrane at the later time (Figure 4.1G).

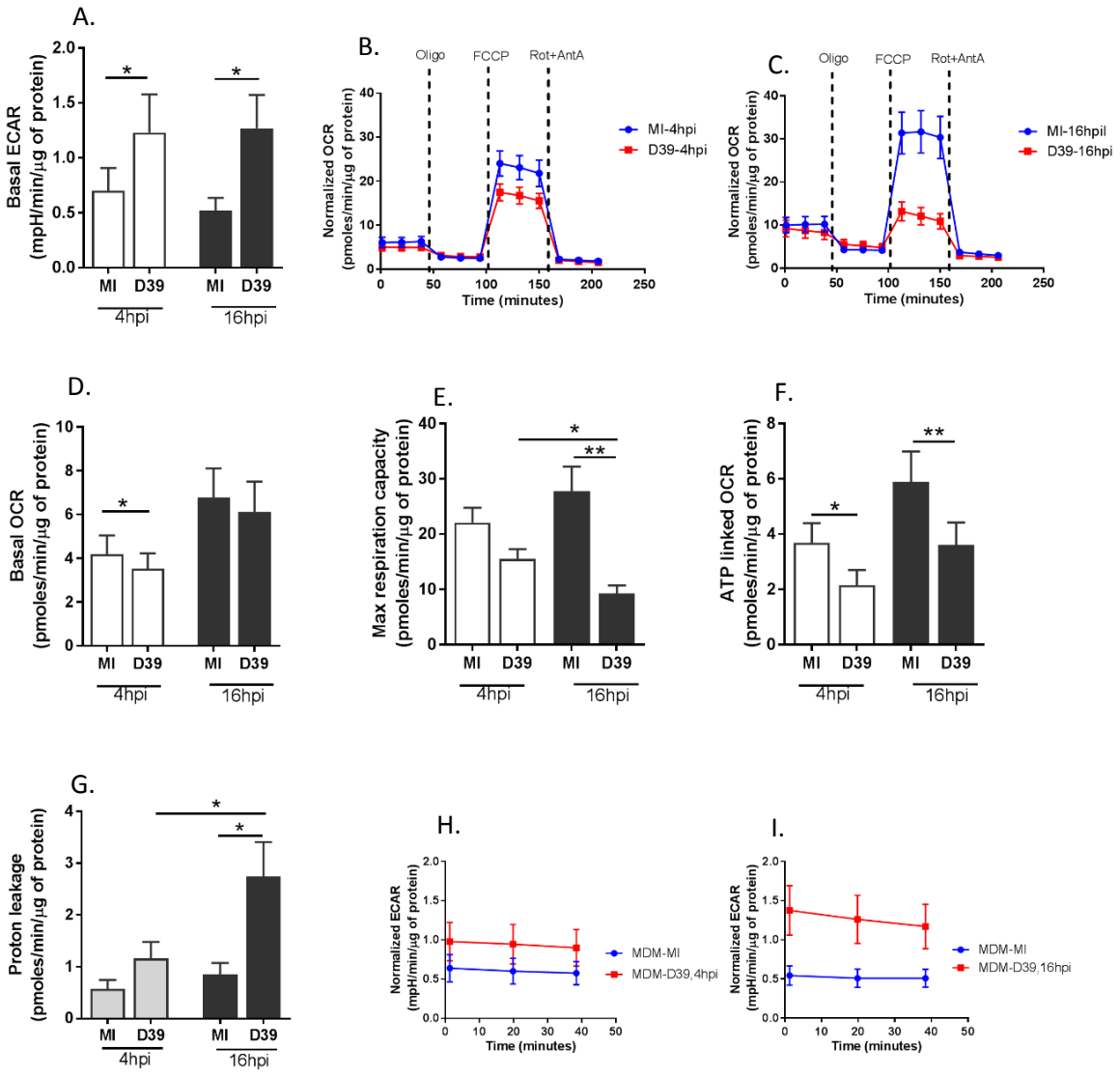

Figure 4.1. ***S. pneumoniae* decreased mitochondrial respiration capacity and increased mitochondrial inner membrane proton leak in human MDM.** Human monocyte-derived macrophages (MDM) were challenged with opsonised serotype 2 *S. pneumoniae* (D39) for 4 hours or 16 hours. Subsequently, the glycolysis (i.e. extracellular acidification rate (ECAR)) and mitochondrial OXPHOS (i.e. oxygen consumption rate (OCR)) were measured by the XF24 extracellular flux analyser. From the ECAR rate data (Figure H for 4 hours and figure I for 16 hours post-infection (hpi)), the basal glycolytic rate (ECAR) was calculated (A), and from OCR rate data (Figure B for 4 hours and Figure C for 16 hours post-challenge), the mitochondrial basal respiration (D), maximum respiration capacity (E), ATP-linked OCR (F), and proton leak (G) were calculated. Oligomycin A (Oligo) is an ATP synthase inhibitor (Complex V) that was added after the baseline ECAR and OCR measurement to measure ATP-linked OCR. The maximum respiration capacity is calculated by subtracting non-mitochondrial OCR with rotenone (Rot) plus antimycin A (AntA) from the FCCP treated OCR. Data were normalized by total protein of MDM, and shown as mean ± SEM for ECAR (mpH/minute/µg of protein) and OCR (pmoles/minute/µg of protein). Statistical analysis was performed using a one-way ANOVA and Sidak's post-hoc test for multiple comparison, and student paired *t-test* for time point comparisons. (*p≤0.05, **p ≤0.01, n=6).

4.3. HIV-1 envelop glycoprotein gp120 and *S. pneumoniae* alter mitochondrial metabolism in human monocyte-derived macrophages

Human immunodeficiency virus (HIV-1) can penetrate and replicate in macrophages like in its more common reservior the CD4+T-cell (Lum and Badley, 2003). HIV-1 envelop glycoprotein gp120 itself is sufficient to disrupt macrophage function and delay macrophage apoptosis,which produces a congenial milieu for viral replication (Cummins et al., 2010, Cicala et al., 2002). Moreover, HIV-1 patients are more susceptible to bacterial lung infection (Gordin et al., 2008, Yin et al., 2012).

To observe HIV-1 effects on macrophages metabolism, recombinant gp120 was used to pre-treat cells, prior to stimulation with the lung pathogen *S. pneumoniae*. Then, macrophage glycolysis and mitochondrial OXPHOS were evaluated using the extracellular flux analyser. The glycolytic response showed an increased trend in pneumococcal challenged MDM at the same time point (Figure 4.2A-B), although not to a significant level unlike Figure 4.1, likley due to donor variation, intensity of infection and other experimental variables. The mitchondrial OXPHOS was comparable between mock-infected and gp120 treated human macrophages (i.e. MDM), whether challenged with or without pneumococci when studied at an earlier time point (e.g. 4 hours) (Figure 4.2C-H).

On the other hand, pneumococcal challenge significantly upregulated the basal glycolytic response in MDM, whether treated or untreated with gp120 at 16 hours (Figure 4.3A-B). In contrast, at this later time point, the mitochondrial maximum respiration capacity (Figure 4.3E), respiration reserve (Figure 4.3F) and ATP-linked OXPHOS (Figure 4.3G) were significantly decreased in MDM after challenge with *S. pneumoniae*, irrespective of gp120 prior treatment. Moreover, *S. pneumoniae* significantly increased the proton leak in mitochondrial inner membrane (Figure 4.3H). Interestingly, HIV-1 gp120 decreased the proton leak at baseline, and significantly diminished pneumococcal induced proton leak (Figure 4.3H).

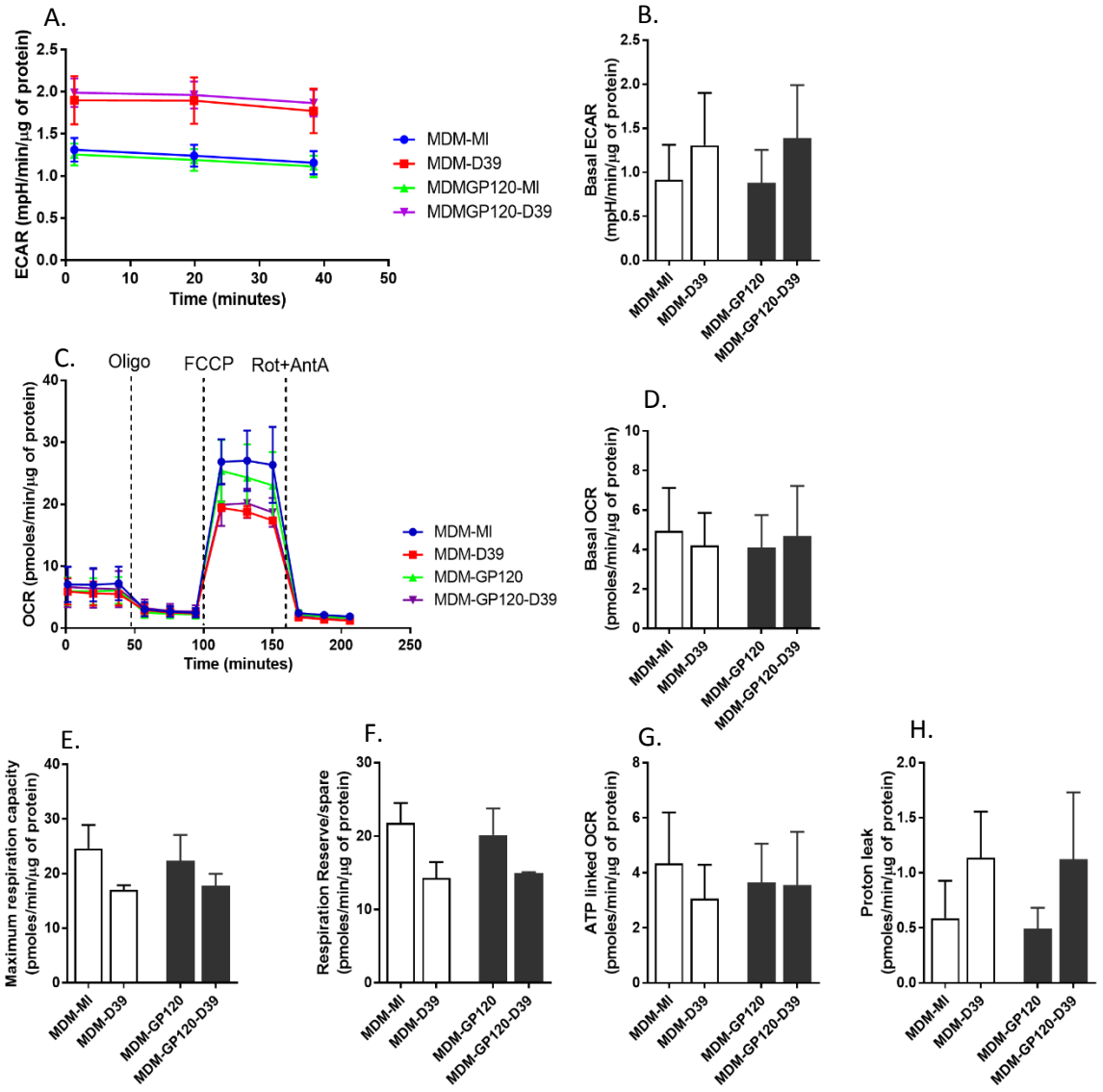

Figure 4.2. **Human Immunodeficiency virus (HIV-1) envelop glycoprotein gp120 and *S. pneumoniae* effects on human MDM's metabolism after 4 hours.** Human MDM were pre-treated with recombinant gp120 (100ng/mL) for an hour. Then, MDM were challenged with opsonised *S. pneumoniae* (D39) with a MOI (multiplicity of infection) of 10 for 4 hours. The glycolytic rate (ECAR) and mitochondrial OXPHOS (OCR) were measured by the XF24 extracellular flux analyser. From the ECAR rate data (A), the basal glycolytic rate was calculated (B), and from the OCR rate data (C), the mitochondrial basal respiration (D), maximum respiration capacity (E), respiration reserve (F), ATP-linked OCR (G), and proton leak (H) were calculated. ATP synthase inhibitor oligomycin A (Oligo) was added after baseline ECAR and OCR measurement to measure ATP-linked OCR. The maximum respiration capacity was calculated by subtracting non-mitochondrial OCR with rotenone (Rot) plus antimycin A (antA) from FCCP treated OCR. Data were normalized by total protein of respective MDM and shown as mean ± SEM for ECAR (mpH/minute/µg of protein) and OCR (pmoles/minute/µg of protein) n=2.

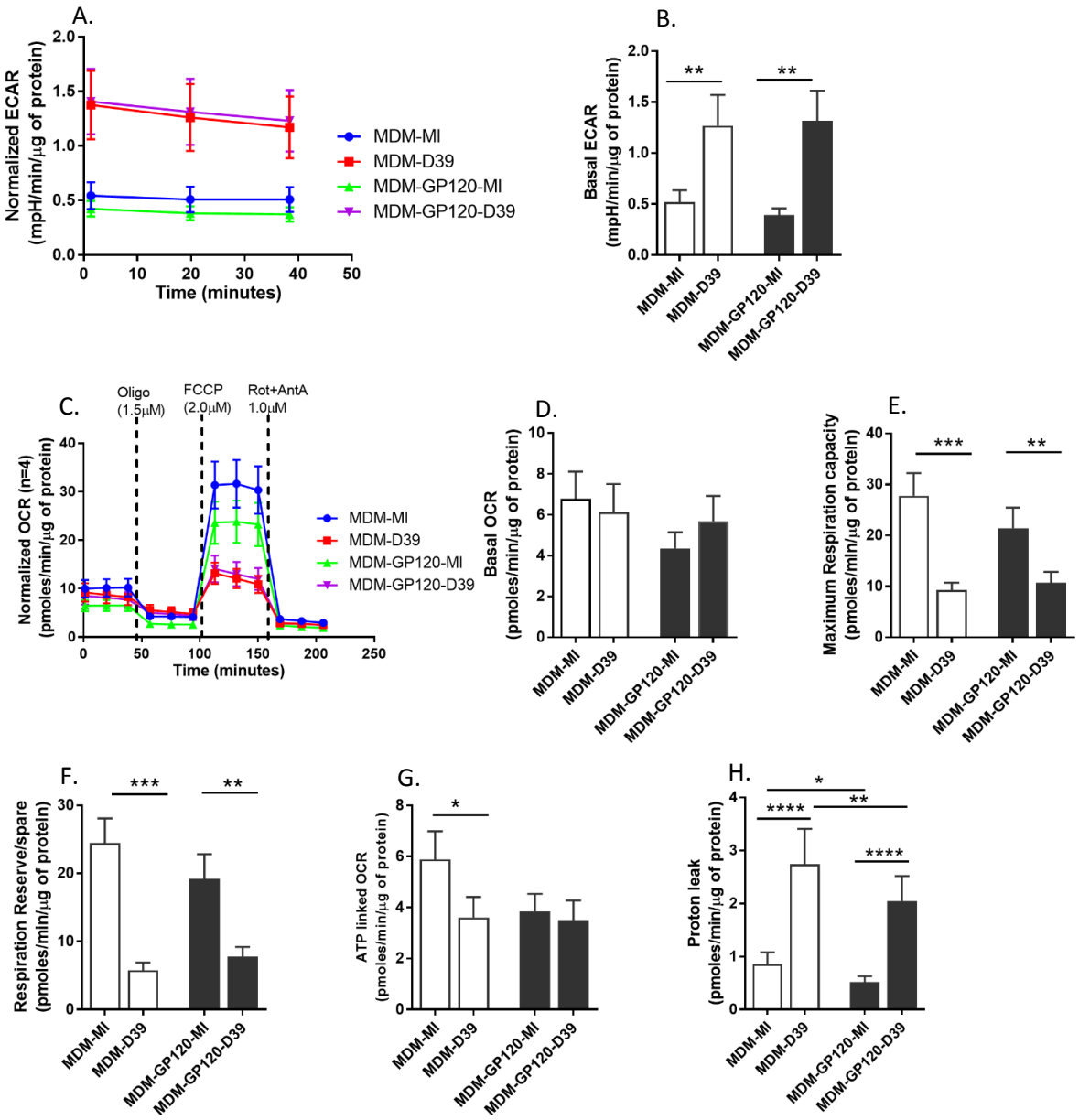

Figure 4.3. **Human Immunodeficiency virus (HIV-1) envelop glycoprotein gp120 and pneumococcal effects on mitochondrial respiration after 16 hours.** Human MDM were pre-treated with recombinant gp120 (100ng/mL) for 24 hours. Then, MDM were challenged with opsonised *S. pneumoniae* (D39) at an MOI of 10, for 16 hours. The glycolytic (defined as ECAR) and mitochondrial OXPHOS (OCR) were measured by the XF24 extracellular flux analyser. From the ECAR baseline rate data (A), the basal glycolytic rate was calculated (B), and from the OCR rate data (C), the mitochondrial basal respiration (D), maximum respiration capacity (E), respiration reserve (F), ATP-linked OCR (G), and proton leak (H) were calculated. Oligomycin A (Oligo) was added after baseline ECAR and OCR measurement. The ATP-linked OCR was calculated by subtracting oligo treated OCR from basal OCR. The maximum respiration capacity was calculated by subtracting the non-mitochondrial OCR [rotenone (Rot) plus antimycin A (AntA) treated OCR] from FCCP treated OCR. Data were normalized by total protein and are shown as mean ± SEM for ECAR (mpH/minute/µg of protein) and OCR (pmoles/minute/µg of protein). Statistical analysis was performed with two-way ANOVA and Holm-Sidak's post-hoc test for multiple comparisons, and Mann-Whitney paired test for pair-wise comparisons. (*p≤0.05, **p ≤0.01, n=6).

4.4. *S. pneumoniae* diminishes mitochondrial respiration capacity in COPD macrophages

Cigarette smoking is the primary cause of chronic obstructive pulmonary disease (COPD), and *S. pneumoniae*, nontypeable *Haemophilus influenzae* and *Moraxella caterrhalis* are the common causes of infection-induced COPD exacerbations (Sapey and Stockley, 2006, Torres et al., 1996). COPD also causes functional impairment of pulmonary parenchyma resulting in damage to the airways. In the COPD MAP study investigators have demonstrated that in COPD airway small muscle cells (ASM) the mitochondrial respiration capacity and mitochondrial inner transmembrane potential are diminished compared to healthy ASM (Wiegman et al., 2015). These observations prompted me to hypothesise that COPD-MDM may also have mitochondrial impairment, or have altered mitochondrial metabolism after challenge with pneumococcus.

To assess COPD-MDM mitochondrial metabolism, COPD patients and age-matched healthy control monocytes were differentiated into MDM. Subsequently, MDM were challenged with opsonised *S. pneumoniae* (D39) for 4 hours and then the mitochondrial OXPHOS and glycolytic respiration were measured by the extracellular flux analyser. The baseline mitochondrial respiration capacity (Figure 4.4C) and respiration reserve (Figure 4.4D) were significantly decreased in COPD-MDM compared to age-matched healthy MDM. Interestingly, *S. pneumoniae* further declined the mitochondrial respiration capacity (Figure 4.4C), respiration reserve (Figure 4.4D) and ATP-linked OXPHOS (Figure 4.4E). Apart from these observations, proton leak was unaltered in COPD-MDM with pneumococci in contrast to COPD mock-infected MDM, while it was an increase trend for healthy MDM challenged with pneumococci versus the mock-infected sample. However, the baseline proton leak was significantly elevated in COPD MDM compared to healthy MDM (Figure 4.4F), which was consistent with a trend towards lower baseline mitochondrial inner transmembrane potential ($\Delta\Psi_m$) in COPD-MDM compared to healthy-MDM (Figure 4.6A-B). On the other hand, the baseline glycolytic rate was comparable between COPD and healthy-MDM and pneumococcal challenge gave an increased trend in the basal glycolysis in both COPD and healthy MDM (Figure 4.5B), although in this small dataset this difference did not reach statistical significance unlike other data in this chapter, again emphasising the donor variability and experimental variation in the infection in MDM cultures.

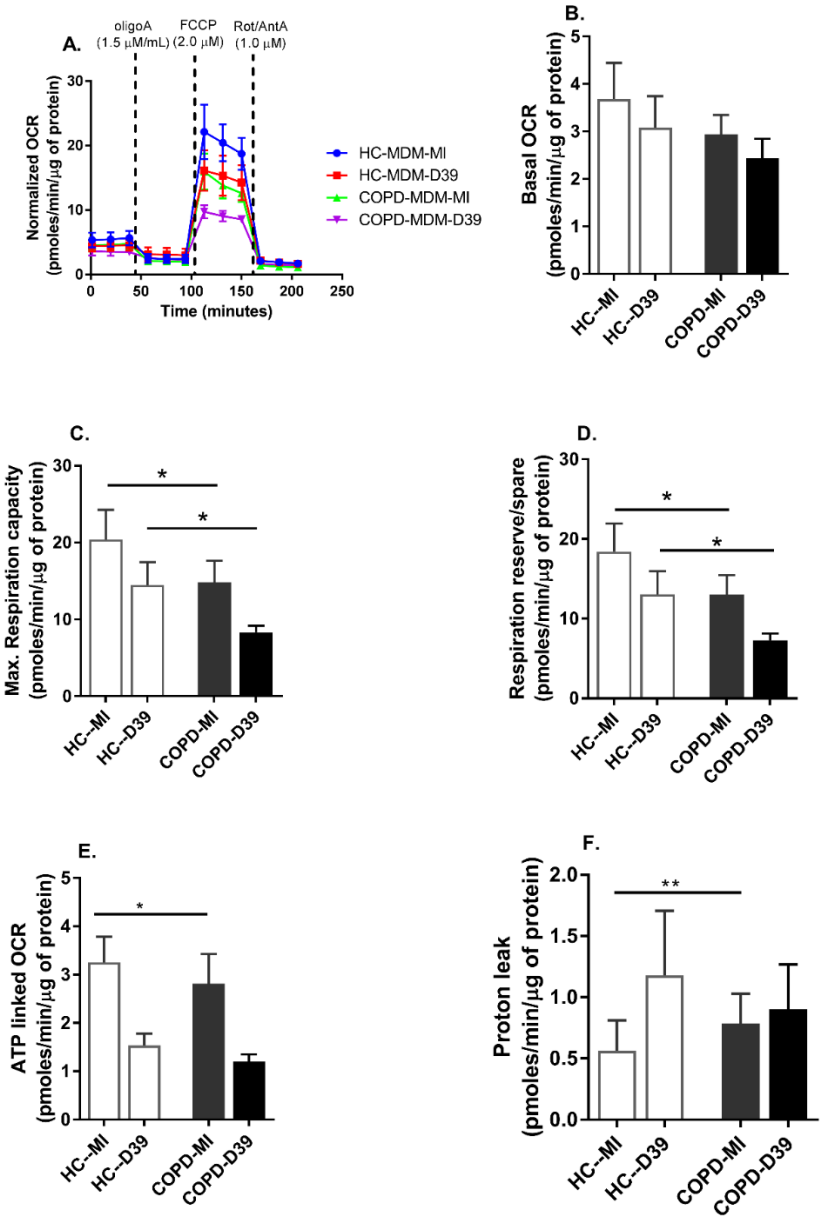

Figure 4.4. **Mitochondrial metabolic phenotype of COPD and healthy MDM**. Both COPD and age-matched healthy control volunteers MDM (HC-MDM) were challenged with opsonised *S. pneumoniae* (D39, MOI of 10) for 4 hours, then the basal oxygen consumption rate (OCR) (B), maximum respiration capacity (C), respiration reserve (D), ATP-linked OCR (E) and the proton leak (F) were calculated from the OCR kinetic data (A). Oligomycin A (oligo), Rotenone (Rot), antimycin A (AntA). Data were normalized by total protein of MDM and are shown as mean ± SEM. Results were analysed with one-way ANOVA and Dunnett's post-hoc test. (*p≤0.05, **p ≤0.01, n=3).

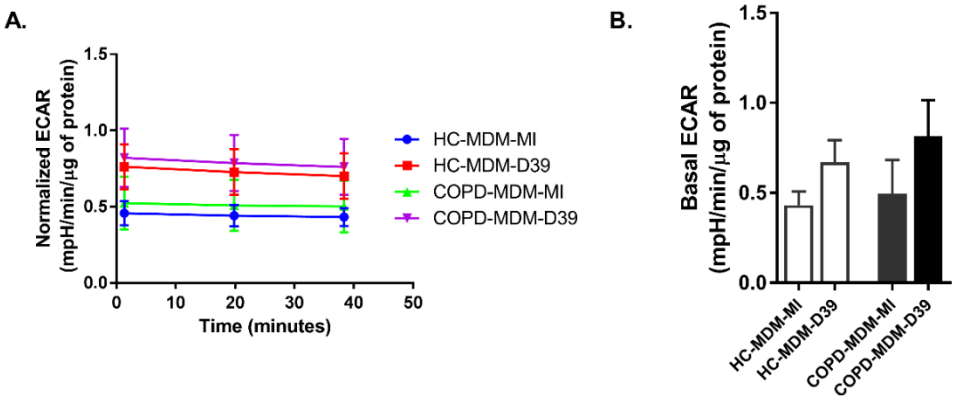

Figure 4.5. **Glycolytic metabolism of COPD and healthy monocyte derived macrophages**. COPD and age-matched healthy volunteer's MDM were challenged with opsonised *S. pneumoniae* (D39, MOI of 10) for 4 hours. Then, the baseline glycolytic rate (B) was calculated from the baseline extracllular acidification rate (ECAR) kinetic data (A), measured by the XF24 extracellular flux analyser. Healthy control MDM (HC MDM) were either mock-infected (MI) or challenged with D39 and were labelled in the figures as HC-MDM-MI and HC-MDM-D39, respectively. Mock-infected and D39 challenged COPD MDM were labelled in the figures as COPD-MDM-MI and COPD-MDM-D39, respectively. Data are shown as mean ± SEM (n=3).

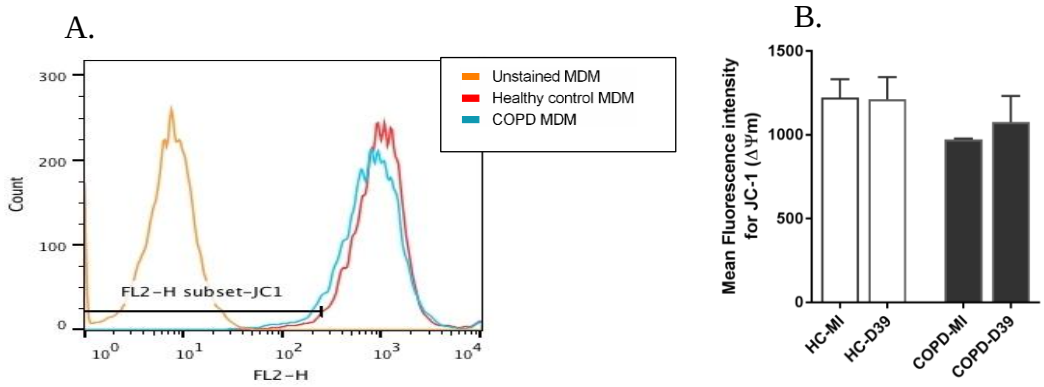

Figure 4.6. **Mitochondrial inner transmembrane potential of COPD and healthy MDM**. Both COPD and age-matched healthy control volunteers MDM (HC MDM) were exposed to opsonised *S. pneumoniae* (D39, MOI of 10) for 4 hours, loss of mitochondrial inner membrane potential ($\Delta\Psi_m$) was measured by flow cytometry after staining with 5,5′,6,6′-tetrachloro-1,1′,3,3′-tetraethylbenzimidazolylcarbocyanine iodide (JC-1, 10µM). Figure A shows the representative FL2-H subset for the baseline JC-1 counts of healthy and COPD MDM (orange, red and blue histograms for unstained, healthy and COPD mock-infected (MI) MDM, respectively) and Figure B shows the mean fluorescence intensity (MFI) for JC-1. Loss of fluorescence (MFI) refers to loss of $\Delta\Psi_m$. Data are shown as mean ± SEM, (n=3).

4.5. *Streptococcus pneumoniae* induces mitochondrial reactive oxygen species

Mitochondria produce superoxide (mROS) as a by-product, mainly due to electron slippage from complex I or III to the mitochondrial matrix or intermembrane space, during oxidative phosphorylation (Balaban et al., 2005, Lagouge and Larsson, 2013). Recently it has been demonstrated that mROS especially from complex I is augmented by Toll like receptor (TLR)-agonists or bacterial infection, and subsequently, this mROS is released into the phagolysosomal compartment for intracellular bacterial killing (West et al., 2011a).

To observe pneumococcal effects on mROS production, mouse bone marrow derived macrophages (BMDM) were challenged with *S. pneumoniae* (D39) for 16 hours and stained with an mROS probe (MitoSox red). The MitoSox-stained macrophages demonstrate that *S. pneumoniae* significantly increased mROS production. Similarly, rotenone (an inhibitor of complex I) and antimycin A (an inhibitor of complex III) treated macrophages also increased mROS production (Figure 4.7A-B). Additionally, neither pneumococcal challenge nor treatment with inhibitors of complex I and III altered mitochondrial density (Figure 4.7C-D), suggesting that observed mROS production was not caused by changes in mitochondrial density, rather it could be linked with the aforementioned mitochondrial metabolic reprogramming. Moreover, co-stained images of mROS and the mitochondrial marker Tom20, illustrate that mROS and mitochondria are co-localised (Figure 4.8), which reduces the concern of non-specific ROS staining by MitoSox Red.

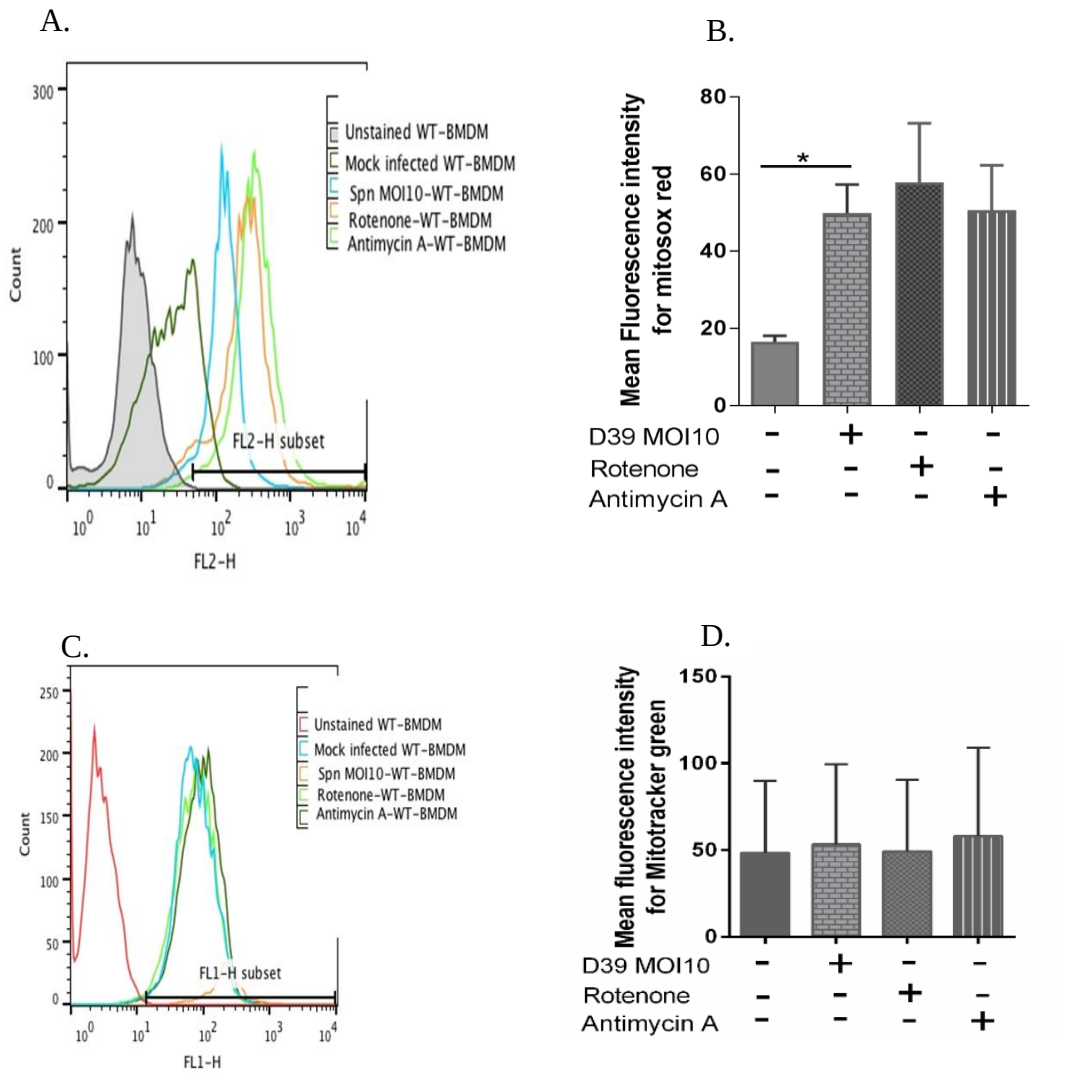

Figure 4.7. ***S. pneumoniae* triggers mitochondrial ROS in macrophages.** Mouse BMDM were challenged with *S. pneumoniae* (D39, MOI of 10) or mock-infected (MI) for 16 hours, then stained with MitoSox red (an mROS specific probe) or mitotracker green (a mitochondria specific probe) followed by flow cytometry. Figure A shows a representative histogram for FL2-H of unstained control or MitoSox red stained BMDM (grey, deep green, blue, orange and green line represent unstained and stained mock-infected, *S. pneumoniae* (Spn) exposed, rotenone and antimycin A treated BMDM, respectively). Figure B shows the mean fluorescence intensity (MFI) for MitoSox red stained mock-infected, *S. pneumoniae* exposed, rotenone and antimycin A treated BMDM. Figure C shows the representative histogram for FL1-H of unstained control and mitotracker green stained BMDM (red line shows unstained BMDM and blue, orange, green and deep green lines shows the stained BMDM that were mock-infected, *S. pneumoniae* exposed, rotenone and antimycin A treated, respectively). Figure D shows the mean fluorescence intensity (MFI) for mitotracker green stained BMDM with the same treatments. Data are shown as mean ± SEM and results were analysed with One-way ANOVA and Bonferroni multiple comparison test. *$p<0.05$, n=5). [Note: During flow cytometry acquisition, mouse BMDM were labelled as wild-type (WT)-BMDM and *S. pneumoniae* exposed BMDM labelled as Spn MOI 10-WT-BMDM].

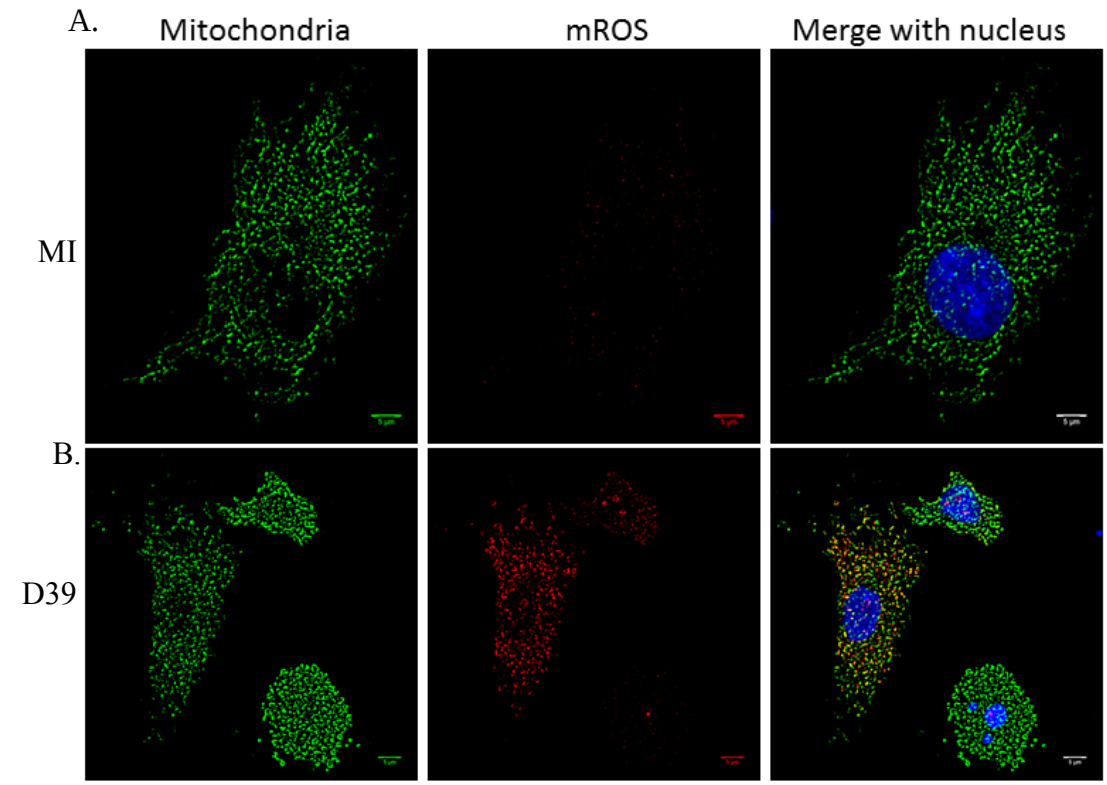

Figure 4.8. **Mitochondrial ROS are co-localised with mitochondria**. Mouse BMDM were incubated with *S. pneumoniae* (D39, MOI of 10) or mock-infected (MI) for 16 hours. Then, stained with MitoSox red. Subsequently, the mitochondrial specific marker Tom20 was labelled by rabbit anti-Tom20 (0.4µg/mL) primary antibody and goat anti-rabbit IgG (H+L) (4µg/mL) conjugated with Alexa Fluor 488. Figure A (top panel) shows the representative co-stained images of BMDM after mock-infection (MI), mitochondria (green pixels), mROS (red) and both merged with nucleus (blue, stained with Draq5). Figure B (bottom panel) shows the representative co-stained images of macrophages challenged with *S. pneumoniae*, mitochondria (green), mROS (red) and co-localised signal (yellow, merged image). The immunofluorescence images were captured by Zeiss LSM510 inverted confocal microscopy with 488nm excitation and 500-530nm emission spectrum for Alexa Fluor 488 and 543nm excitation and 565-615nm emission spectrum for MitoSox red, and 63x1.4 NA oil with zoom 2 objective. Images were reconstituted by imagej using 13x13 hat filter. Scale bar is 5µm.

4.6. *S. pneumoniae* upregulates mitochondrial ROS, which are co-localised with intracellular bacteria

Mitochondria play a pivotal role in innate immunity beyond cellular metabolism. Recently West and colleagues have demonstrated that mROS are localised adjacent to the phagosome to kill intracellular bacteria (West et al., 2011a). In section 4.5, it is shown that *S. pneumoniae* upregulates mROS in macrophages, but it is not clear whether mROS is directly in the vicinity of the phagosome and subsequently involved in killing of intracellular bacteria in macrophages, when other canonical killing strategies are exhausted. To observe mROS interactions with *S. pneumoniae* and phagolysosomes, Alexa Fluor-647 labelled opsonised *S. pneumoniae* (Figure 4.9A) was used to challenge

macrophages for 16 hours (Figure 4.9B). The co-staining images illustrate that the mROS stain co-localised or was adjacent to *S. pneumoniae* (Figure 4.10A). Moreover, the quantification data from macrophages with internalised bacteria shows that around 40% of internalised bacteria were co-localised and 46% were adjacent to mROS in macrophages (Figure 4.13A). Similarly, the mROS stain was co-localised or adjacent with phagolysosomes in macrophages challenged with pneumococci compared to mock-infected macrophages (Figure 4.11A-B and correlation quantification in Figure 4.13B). Whereas, mock-infected or *S. pneumoniae* exposed macrophages lysosomal compartment did not co-localised with the negative comparator ER (Figure 4.12).

In contrast, neither mROS nor pneumococci were co-localised with the endoplasmic reticulum (Figure 4.10B and quantification in Figure 4.13B). Moreover, inhibiting mROS with a superoxide scavenger MitoTempo significantly decreased the MitoSox fluorescence intensity in macrophages after challenge with *S. pneumoniae* (Figure 4.14A (V), and quantification data in figure 4.14D), suggesting the mithochondrial ROS species were selectively stained. Like mouse BMDM (Figure 4.14B), MitoSox also co-localised with pneumococci in human MDM (Figure 4.14C). These results corroborated our group's recent observations, that inhibiting mROS with MitoTempo decreases the delayed phase of intracellular bacterial killing and therefore that mROS play a role in the microbical response against *S. pneumoniae* (Bewley et al., 2017). I also confirmed that macrophages stained with cresyl violet to label lysosomes and phagolysosomes did not produce any background influencing the detection of mROS with MitosSox red (Figure 4.15A) or ER with ER tracker (Figure 4.15B) and that conversely these stains did not pick up any signal when trying to detect phagolysosomes. The broad emission spectrum of MitoSox red prevented at 565-615 nm that I could not perform similar localisation experiments with mROS and ER due to overlapping detection spectra.

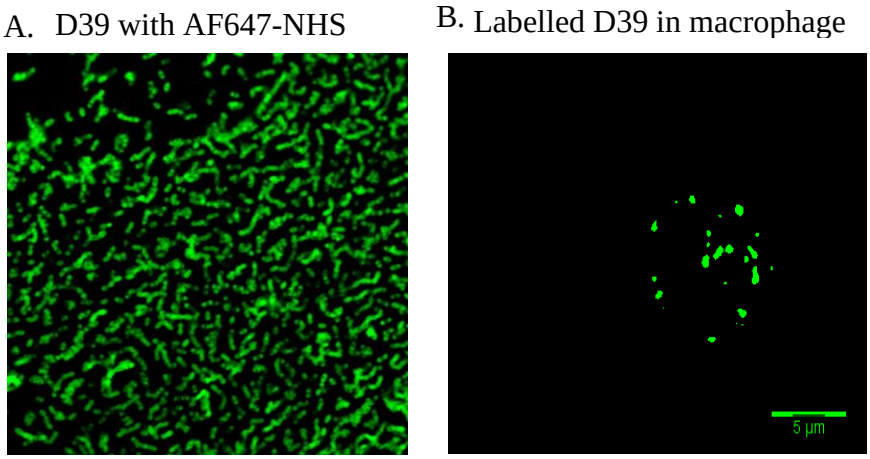

Figure 4.9. ***S. pneumoniae* labelled with Alexa Fluor tagged succinimidyl ester**. *S. pneumoniae* (D39) was labelled with Alexa Fluor 647-succinimidyl ester (AF647-NHS ester, 0.05mg/mL) for an hour. Figure A illustrates the representative confocal fluorescence image of AF647-NHS ester labelled D39 (green pixel). Figure B shows the representative image of intracellular AF647-NHS ester labelled D39 in mouse BMDM. Images were captured by Zeiss LSM510 inverted confocal microscopy with 633nm excitation and 650-704nm emission spectrum and 63x1.4 NA oil with zoom 2 objective lens. Scale bar is 5µm.

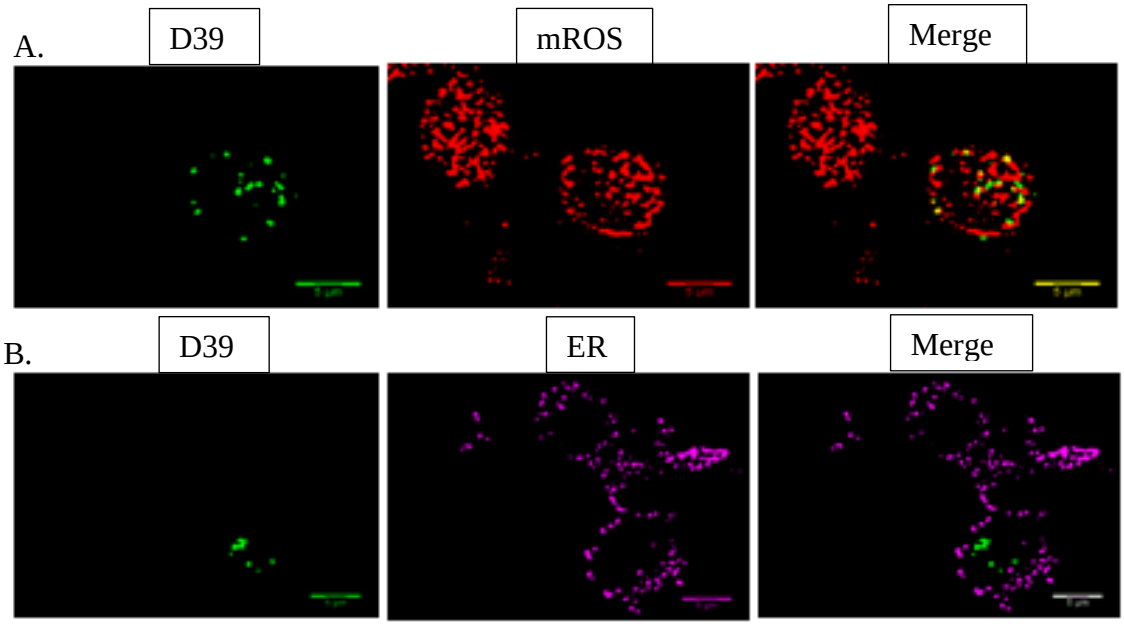

Figure 4.10. ***S. pneumoniae* and mitochondrial ROS are co-localised in macrophages**. Mouse BMDM were challenged with Alexa Fluor-647 (AF-647) labelled opsonised *S. pneumoniae* (D39) and incubated for 16 hours. Then, mitochondrial ROS (mROS) and endoplasmic reticulum (ER) were stained with MitoSox-red and ER-tracker red (BODIPY TR Glibenclamide), respectively. Figure A (top panel) shows the representative images of AF-647 labelled D39 (green), mROS (red) and the co-localised signal (yellow, merged image) in mouse BMDM. Figure B (bottom panel) shows the representative control images of D39 (green), ER (pink) in mouse BMDM. Images were captured by Zeiss LSM510 inverted confocal microscopy with 633nm excitation and 650-704nm emission spectrum for AF-647, 488nm excitation and 565-615nm emission spectrum for MitoSox red and 543nm excitation and 560nm emission for ER-tracker. The representative images were created from the maximum projected Z-stack images (Size scaling: 0.07X0.07X0.48µm, 63x1.4 NA oil, Scan zoom 2 and the average line 4) using a 17x17 hat filter with intermodes black and white threshold correction by ImageJ. Scale bar is 5µm.

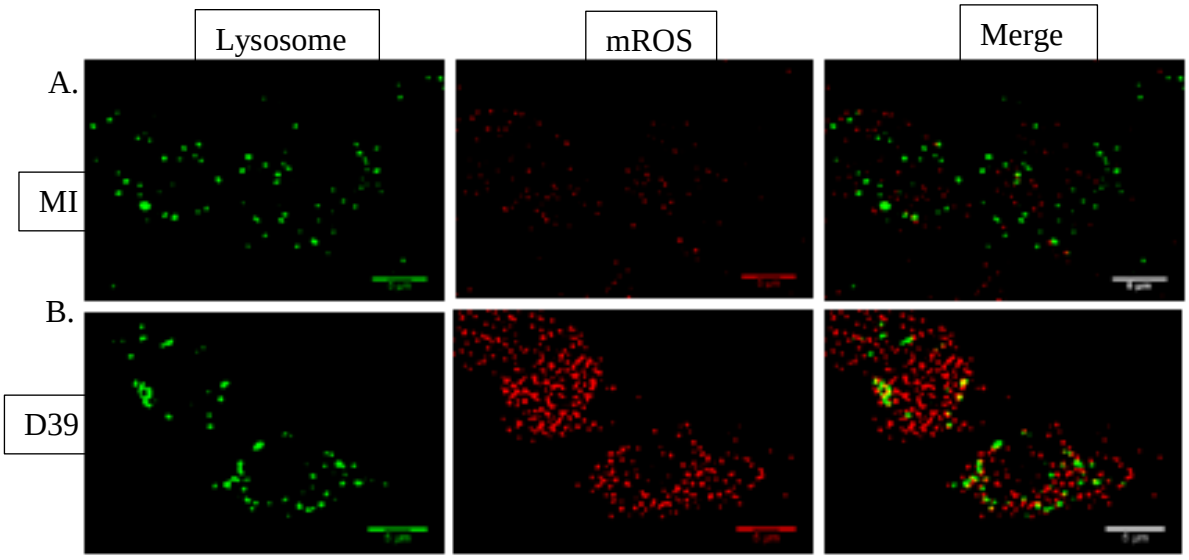

Figure 4.11**. Lysosome/phagolysosome are co-localised with mitochondrial ROS in macrophages**. Mouse BMDM were mock-infected or challenged with opsonised *S. pneumoniae* (D39) for 16 hours. Then lysosomal/phagolysosomal compartment and mitochondrial ROS (mROS) were co-stained with cresyl violet and MitoSox-red, respectively. Figure A (top panel) shows the representative images of lysosomes/phagolysosomes (green pixels), mROS (red) and merged image in mock-infected mouse BMDM. Figure B (bottom panel) shows the representative images of lysosomes/phagolysosomes (green), mROS (red) and co-localised signal (yellow, merged image) in mouse BMDM after challenge with D39. Images were captured by Zeiss LSM510 inverted confocal microscopy with 633nm excitation and 650-704nm emission spectrum for cresyl violet, 488nm excitation and 565-615nm emission spectrum for mitosox red. 63x1.4 NA oil with zoom 2 objective, images were reconstituted by ImageJ using a 17x17 hat filter with intermodes black and white threshold correction by ImageJ. The scale bar is 5µm.

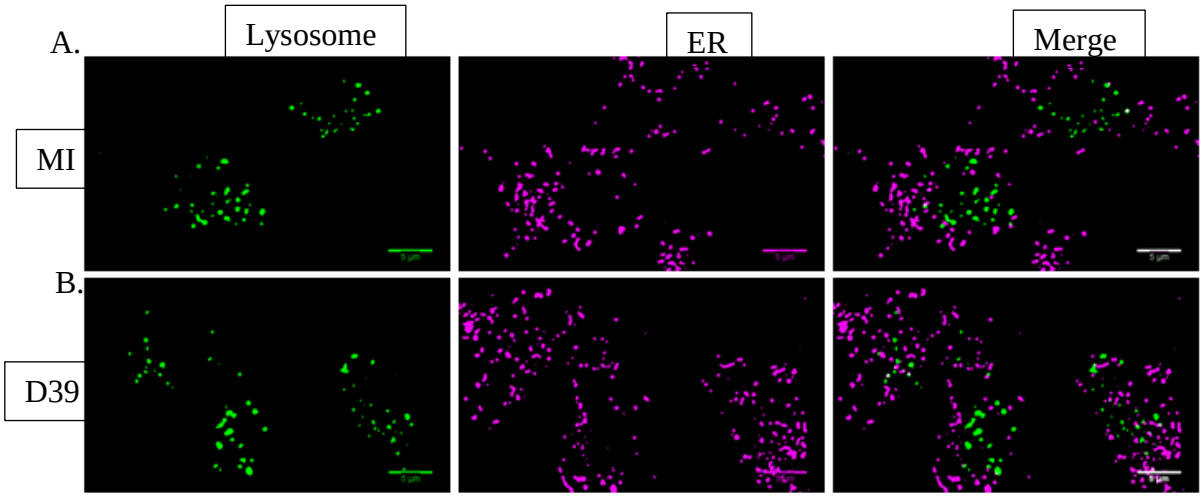

Figure 4.12. **Lysosomes and endoplasmic reticulum are not co-localised**. Mouse BMDM were mock-infected or challenged with opsonised *S. pneumoniae* (D39) for 16 hours. Then the lysosomal compartment and endoplasmic reticulum (ER) were co-stained with cresyl violet and ER-tracker red, respectively. Figure A (upper panel) shows the representative images of lysosomal compartments (green pixels), ER (pink) and the merged image in mock-infected mouse BMDM. Figure B (bottom panel) shows the representative images of lysosomal compartments (green), ER (pink) and merged image in mouse BMDM exposed to D39. Images were captured by Zeiss LSM510 inverted confocal microscopy with 633nm excitation and 650-704nm emission spectrum for cresyl violet, 543nm excitation and 560nm emission spectrum for ER-tracker red. 63x1.4 oil with zoom 2 objective lens. Images were reconstituted by ImageJ using 17x17 hat filter. The scale bar is 5µm.

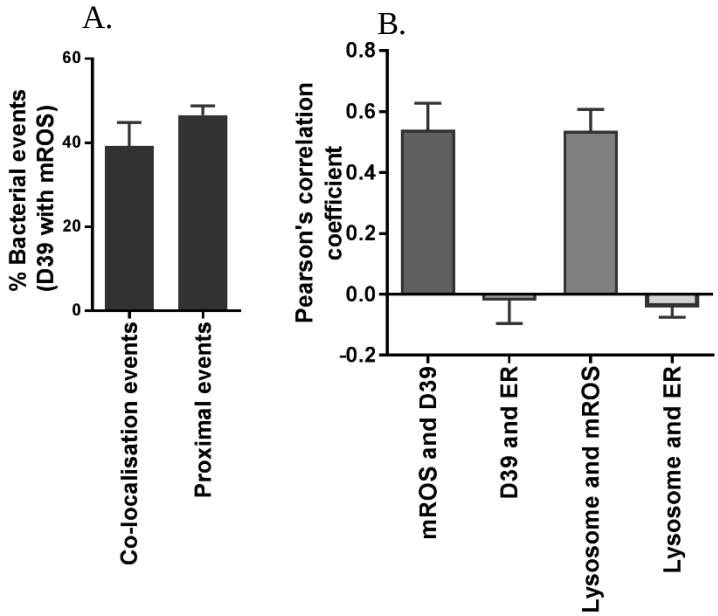

Figure 4.13. **Mitochondrial ROS and internalised *S. pneumoniae* are co-localised with phagolysosome in macrophages**. Mouse BMDM were mock-infected or challenged with opsonised *S. pneumoniae* (D39) for 16 hours. Figure A shows the percentage of *S. pneumoniae* (D39), from the data represented in Figure 4.10 that were co-localised or adjacent to mROS was calculated. In these experiments internalised bacteria were observed in 15.46 ± 3.50 % of BMDM. Figure A shows the percentage of bacteria showing a co-localised signal or proximal signal with

mROS was evaluated by a co-localisation test and digital distance measurement algorithms in ImageJ were used with adjacent bacteria defined as the average R value (Pearson's correlation coefficient) close to zero, and co-localised as average R value is ≥0.5. Figure B shows the Pearson's correlation coefficient for mROS with D39, D39 with ER, mROS with lysosomes/phagolysosomes, and lysosomes/phagolysosomes with ER co-staining images. Data was derived from experimental data from which Figures 4.10 to 4.12 are representative images and was quantified by the co-localisation test with ImageJ as described above. Data are depicted as mean ± SEM, n=3.

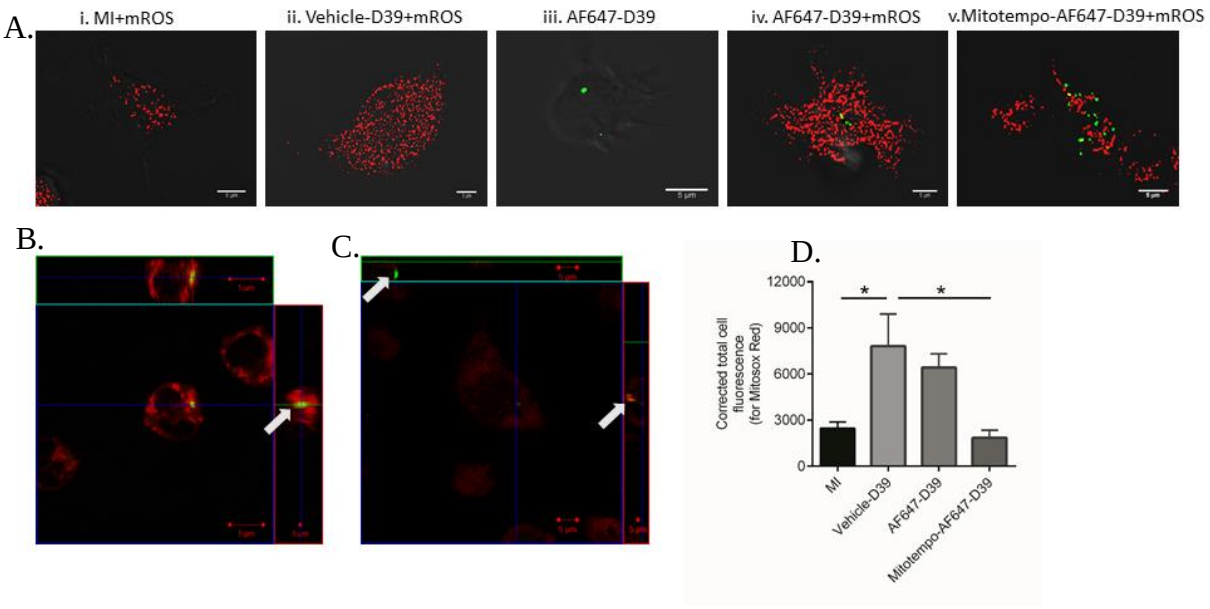

Figure 4.14. **Mitochondrial ROS are co-localised with *S. pneumoniae* in macrophages.** Mouse BMDM or human MDM were mock-infected (MI) or challenged with Alexa Fluor 647 labelled opsonised *S. pneumoniae* (D39) or unlabelled D39 and incubated for 16 hours. Then, mitochondrial ROS (mROS) were stained with MitoSox red. Figure A (top panel) shows mROS (red pixels) with or without labelled D39 in mouse BMDM. BMDM were (i) mock-infected (MI) or (ii) challenged with unlabelled D39, or (iii) exposed with Alexa Fluor 647 labelled D39 (in BMDM not stained for mROS), or (iv) exposed with labelled D39 (green) in cells stained with MitoSox (red) or (v) challenged with labelled D39 and stained with MitoSox (red) in MitoTempo pre-treated cells. Figure B and C show the orthogonal view of mouse BMDM and human MDM, respectively, with the Alexa fluor 647 labelled D39 (green) either co-localised with mROS (yellow pixel) or proximal to mROS (red). Images were captured by a Zeiss LSM510 confocal microscopy with zoom 2 and 63x1.4 oil objective lens and 488nm excitation and 565-615nm emission spectrum for MitoSox red, and 633nm excitation and 650-704nm emission for Alexa Fluor 647 labelled D39. Figure D shows the corrected total cell fluorescence for MitoSox red stained BMDM. Data are shown as mean ± SEM with one-way ANOVA and Sidak's post-hoc test (n=3, *$p<0.05$). The scale bar is 5µm.

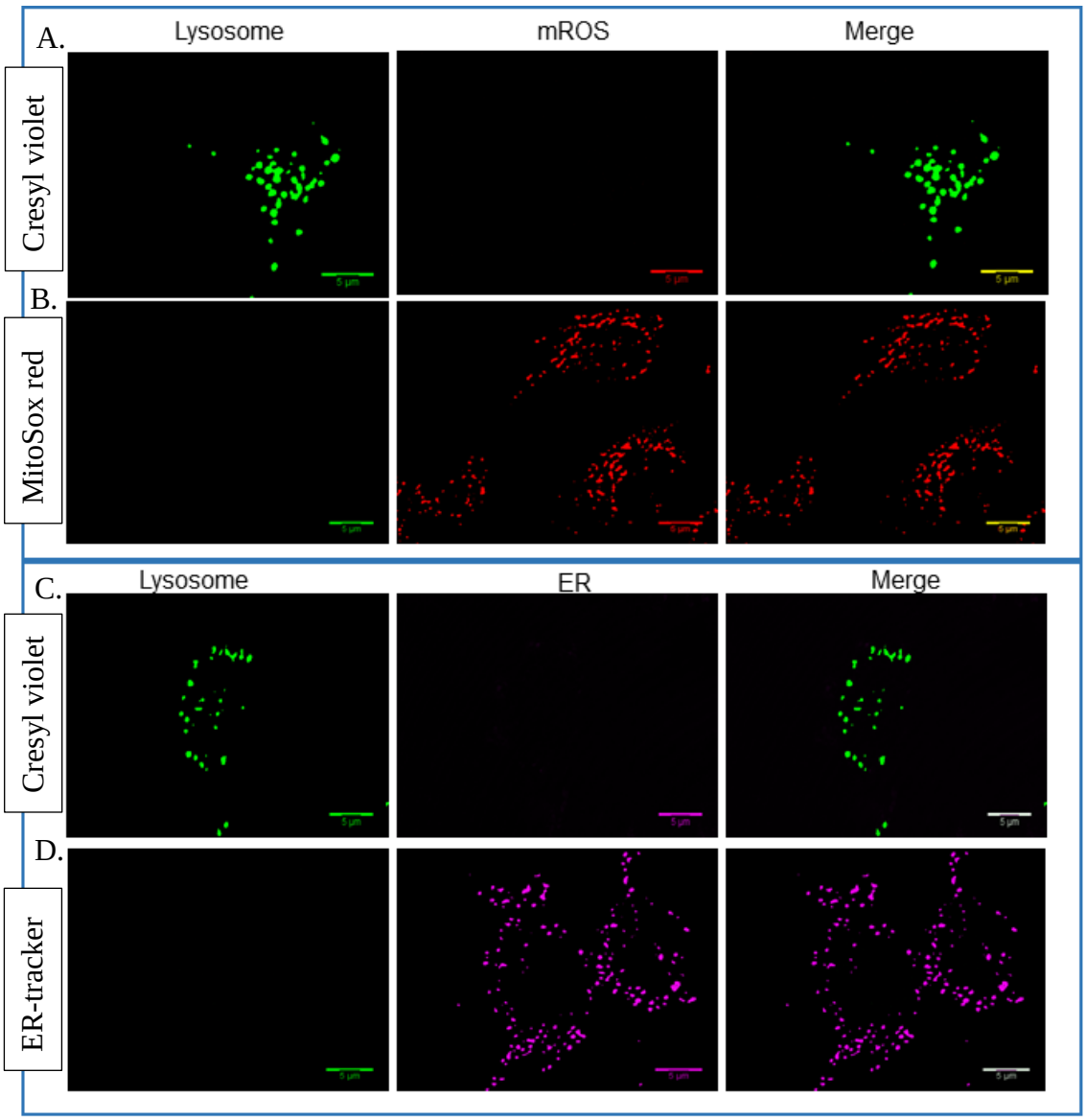

Figure 4.15. **Lysosome/phagolysosome specific cresyl violet staining does not influence mROS or endoplasmic reticulum detection.** Mouse BMDM were challenged with *S. pneumoniae* and incubated for 16 hours. Then, BMDM were stained with cresyl violet to stain lysosomes/phagolysosomes and separately alone with either MitoSox red to detect mitochondrial ROS (mROS) or ER-Tracker™ Red to detect endoplasmic reticulum (ER) for 15 minutes. Panel A shows no mROS signal in lysosome/phagolysosome cresyl violet (green) single stained B MDM. Panel B shows no lysosome/phagolysosome signal in mROS (red) MitoSox red single stained cells. Panel C shows no ER signal in lysosome (green) cresyl violet single stained cells. Panel D shows no lysosome/phagolysosome signal from ER (pink) c ER-tracker single stained cells. Panel A and B images were captured with 488nm and 633nm excitation lasers and 565-615nm and 650-704nm emission spectrums. Panel C and D images were captured with 543nm and 633nm excitation lasers and 560 and 650-704nm emission spectrums. Images were reconstituted by Imagej using 17x17 hat filter. Images are representative of three independent experiments. The scale bar is 5µm.

4.7. *S. pneumoniae* induces nitric oxide and mROS that co-localise with bacteria in the phagolysosomal compartment

Macrophages initiate bacterial internalisation via phagocytosis through forming a phagosome at the plasma membrane. Subsequently the phagosome fuses with the early endosome, then late endosomes and finally with lysosomes to form a phagolysosome (Aderem and Underhill, 1999). The phagosome plasma membrane contains NADPH oxidase (NOX2) which generate an oxidative burst, producing reactive oxygen species (ROS) and inducible nitrogen oxide synthase (iNOS), generating the nitric oxide (NO) radical. Moreover, ROS and NO radicals are able to interact and generate reactive nitrogen species (RNS), such as peroxynitrite ($ONOO^-$), which is a more potent intracellular bactericidal mediator (Fang, 2004). The NADPH oxidase generates a more vigorous oxidative burst in neutrophils compared to macrophages.

In contrast macrophages generate more vigorous NO responses, particularly rodent macrophages (Nathan and Shiloh, 2000), and have more mitochondria that produce mROS, which have an antimicrobial role in macrophages (West et al., 2011a). Although in the earlier sections of this chapter, I have shown that macrophage mROS are co-localised with bacteria in the phagolysosome, it was important to show whether mROS interacts with NO in the phagolysosome to form more potent RNS like peroxinitrite, since macrophages fail to generate the more potent halogenated ROS species as they usually lack myeloperoxidase and many bacteria like *S. pneumoniae* have well developed antioxidant defences against ROS (Aberdein et al., 2013). Thus it was important to establish if mROS was being generated in the vicinity of NO, with which it could react to form RNS, and whether both of these were adjacent to bacteria.

To observe mROS and NO co-localisation with *S. pneumoniae* or with the phagolysosome, Alexa Fluor-647 labelled opsonised *S. pneumoniae* was used to challenge mouse BMDM for 16 hours. mROS and NO were co-stained with Alexa Fluor labelled pneumococci and images illustrate that most of the NO signal was co-localised with mROS (yellow pixel), and some of this signal either co-localised or was located proximally to *S. pneumoniae* (blue) (Figure 4.16A-B). Similarly, the mROS, NO and phagolysosome co-stained images demonstrate that mROS and NO were frequently co-localised (yellow pixels) and these microbicidals were co-localised or juxtaposed with the phagolysosome in macrophages challenged with *S. pneumoniae*, while mock-infected macrophages had very little staining for mROS or NO (Figure 4.17A-B). Quantification of this data also showed that *S. pneumoniae* significantly increased the fluorescence

intensity of DAF-FM diacetate-labelled NO in macrophages challenged with *S. pneumoniae* compared with mock-infected macrophages (Figure 4.17C). Moreover, the co-localisation quantification data also demonstrated that most of the mROS colocalised with NO (Figure 4.17D), while approximately 20% of macrophages with mROS and NO were either co-localised or proximally stained with *S. pneumoniae* and 40% were co-localised or proximal to phagolysosomes (Figure 4.17D). I also confirmed that macrophages stained with cresyl violet to label lysosomes and phagolysosomes did not produce any background influencing the detection of mROS with MitosSox red (Figure 4.18A) or NO with DAF-FM diacetate (Figure 4.18B) and that conversely these stains did not pick up any signal when trying to detect phagolysosomes (Figure 4.18C).

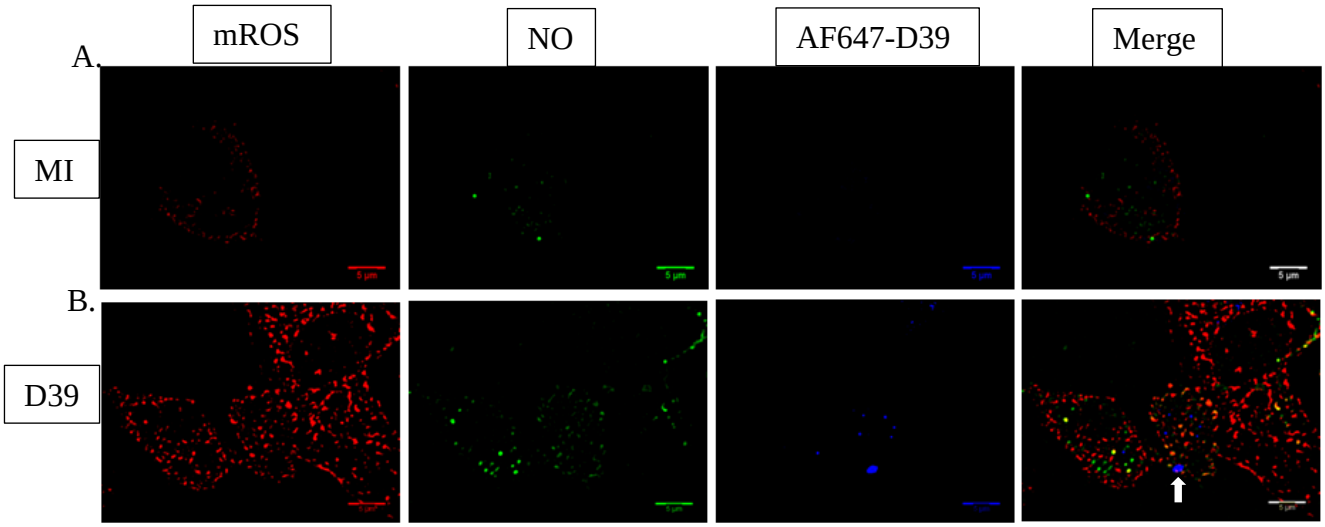

Figure 4.16. **Mitochondrial ROS and nitric oxide are co-localised with *S. pneumoniae* in macrophages**. Mouse BMDM were challenged with Alexa Fluor 647 labelled opsonised *S. pneumoniae* (D39) and incubated for 16 hours. Then mitochondrial ROS (mROS) and nitric oxide (NO) were stained with MitoSox-red and DAF-FM diacetate, respectively. Panel A (top panel) shows the representative fluorescence images of mROS (red) and NO (green) in mock-infected BMDM. Panel B (bottom panel) shows the representative fluorescence images of mROS (red), NO (green) and alexa fluor 647 labelled D39 (blue) in BMDM challenged with D39. Images were captured by Zeiss LSM510 inverted confocal microscopy with 488nm excitation and 565-615nm emission spectrum for MitoSox red, and 633nm excitation and 650-704nm emission spectrum for Alexa Fluor 647 labelled D39. 63x1.4 oil with zoom 2 objective images were reconstituted by ImageJ using 17x17 hat filter. In the merged image the arrow shows mROS and NO are adjacent to bacterial clumps. The scale bar is 5µm.

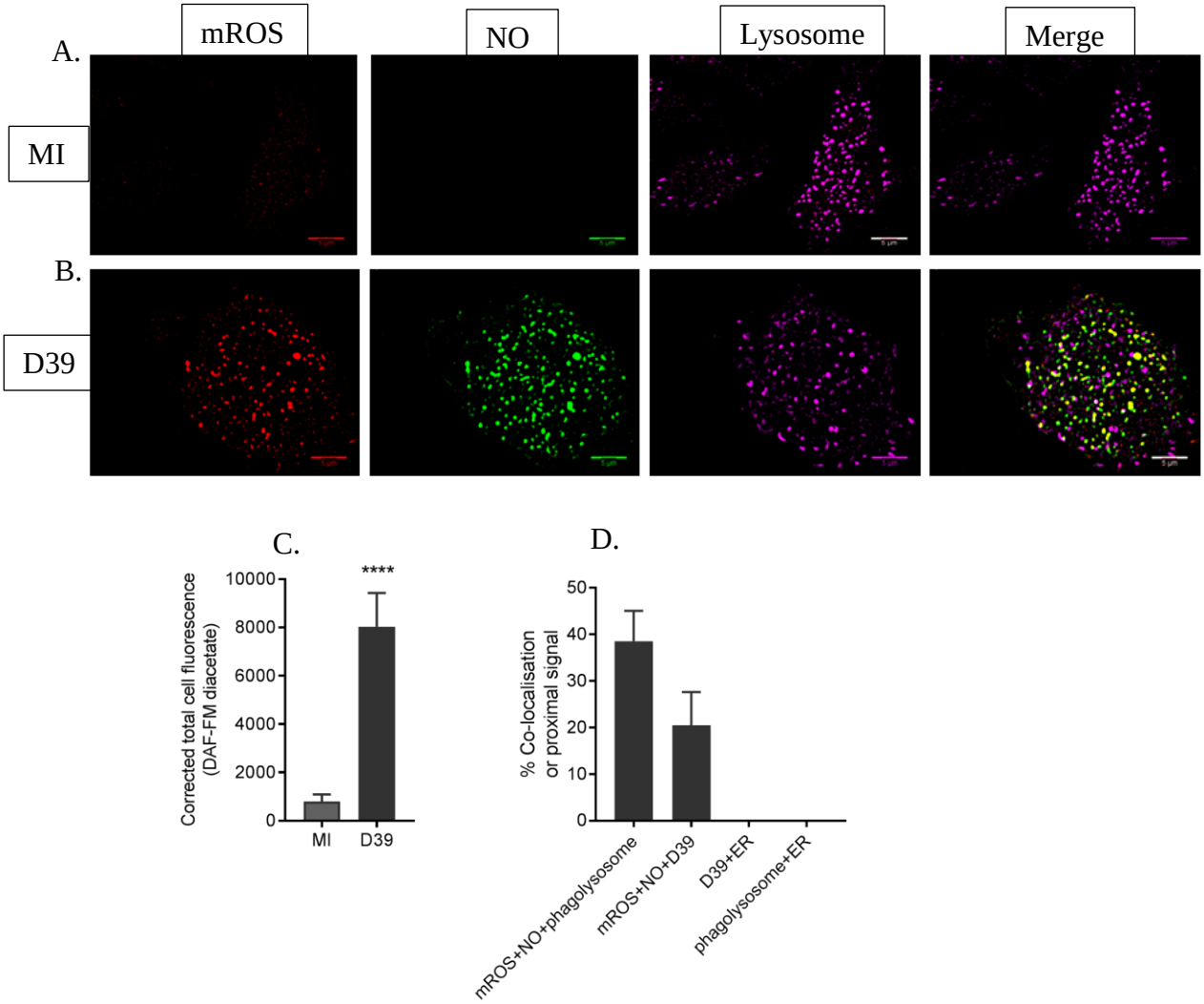

Figure 4.17. **Mitochondrial ROS and NO are co-localised with phagolysosomes**. Mouse BMDM were challenged with opsonised *S. pneumoniae* (D39) for 16 hours followed by staining with nitric oxide (NO) using DAF-FM diacetate, mitochondrial ROS (mROS) using MitoSox-red and lysosome/phagolysosome using cresyl violet. Panel A (top panel) shows the representative fluorescence images of mROS (red), NO (green) and lysosome/phagolysosome (pink) in mock-infected (MI) BMDM. Panel B (bottom panel) shows the representative fluorescence images of mROS (red), NO (green) and lysosome/phagolysosome (pink) in BMDM after challenge with D39. Images were captured by Zeiss LSM510 inverted confocal microscopy with 543nm excitation and 565-615nm emission spectrum for MitoSox red, 488nm excitation and 500-530nm emission spectrum for DAF-FM diacetate, and 633nm excitation and 650-704nm emission spectrum for cresyl violet. 63x1.4 NA oil with zoom 2 objective images were reconstituted by ImageJ using 17x17 hat filter. The scale bar is 5µm. Figure C shows the corrected total cell fluorescence for NO, measured by ImageJ from DAF-FM diacetate stained mock-infected (MI) and D39 exposed mouse BMDM. Figure D shows the percentage of macrophages with co-localisaed signal or proximal signal in mROS with either NO or D39, and mROS with either NO or lysosome/phagolysosome, and D39 or phagolysosome with ER as negative comparators. Data are shown as mean ± SEM and statistical analysis was performed with student paired *t-test* (n=3, *p<0.05).

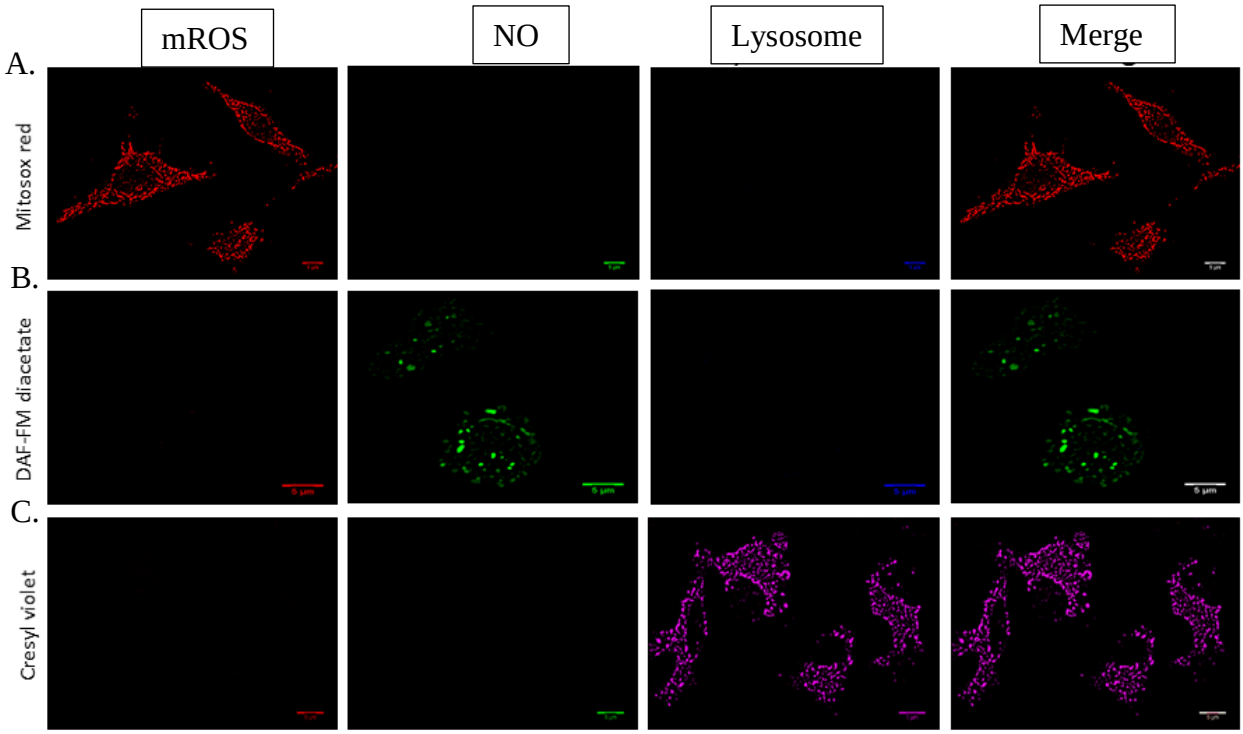

Figure 4.18. **Mitochondrial ROS signal does not influence NO or lysosome/phagolysosome detection in macrophages.** Mouse BMDM were challenged with opsonised *S. pneumoniae* (D39) for 16 hours. Then BMDM were co-stained with MitoSox red to stain mitochondrial ROS **(**mROS) and either with DAF-FM diacetate to detect nitric oxide (NO) or cresyl violet to detect lysosomes/phagolysosomes. Panel A (top row) shows no detectable NO or lysosomal signal in mROS MitoSox red (red) single stained BMDM. Panel B (middle row) shows no detectable mROS or lysosomal signal in the NO (green) DAF-FM diacetate single stained macrophages. Panel C (bottom row) shows no detectable mROS or NO signal in the lysosome/phagolysosome (pink) cresyl violet single stained cell. All representative images were taken from three independent experiments and these were captured with 488nm excitation laser and 500-530nm (for NO), 543nm excitation and 565-615nm (for mROS), and 633nm excitation laser with 650-704nm emission spectrum (for lysosomes/phagolysosome). Representative images were reconstituted by Imagej using a 17x17 hat filter. The scale bar is 5µm.

4.8. Inhibiting mitochondrial ROS restores mitochondrial respiration capacity

Reactive oxygen species (ROS) act as a redox signalling molecule. This signalling is essential for cellular homeostasis, which is maintained with low levels of ROS. But excessive ROS is detrimental for cell physiological function. This causes oxidative damage of macromolecules such as DNA and protein, which ultimately promotes cell death (Circu and Aw, 2010). I next investigated whether mROS generated in macrophages in response to *S. pneumoniae* modulates mitochondrial metabolism beyond its earlier reported bactericidal effect.

To observe mROS effect on mitochondrial metabolism, especially on mitochondrial OXPHOS, mouse BMDM were pre-treated with MitoTempo, which abrogates production of mitochondrial matrix-specific superoxide and alkyl radicals. Subsequently, BMDM were challenged with opsonised *S. pneumoniae* for 12 hours, and then the mitochondrial metabolic outputs were observed by the extracellular flux analyser. MitoTempo failed to alter the significant increase in glycolysis associated with *S. pneumoniae* in macrophages (Figure 4.19A-B) and did not alter the increase in non-mitochondrial OCR associated with *S. pneumoniae* (Figure 4.19C). Mitochondrial ROS abrogation with MitoTempo had no effect on basal oxygen consumption rate (Figure 4.20B) but significantly increased maximal mitochondrial respiration capacity in pneumococcal challenged mouse BMDM compared to mock-infected BMDM (Figure 4.20C and 4.20D), although this only represented partial restoration. However, inhibiting mROS production neither ameliorated ATP-linked OXPHOS (Figure 4.20E) nor altered proton leak (Figure 4.20F) in pneumococcal challenged macrophages.

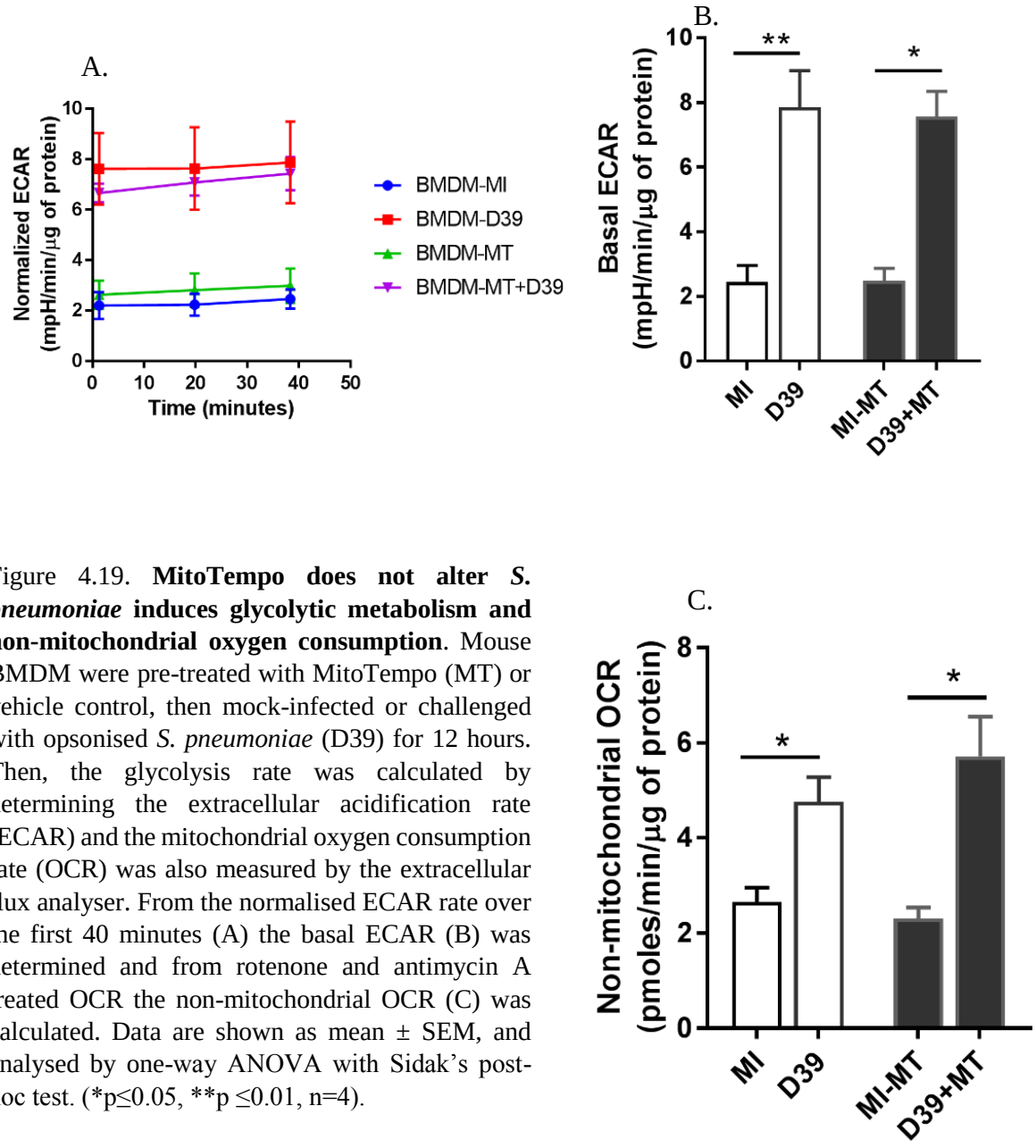

Figure 4.19. **MitoTempo does not alter *S. pneumoniae* induces glycolytic metabolism and non-mitochondrial oxygen consumption**. Mouse BMDM were pre-treated with MitoTempo (MT) or vehicle control, then mock-infected or challenged with opsonised *S. pneumoniae* (D39) for 12 hours. Then, the glycolysis rate was calculated by determining the extracellular acidification rate (ECAR) and the mitochondrial oxygen consumption rate (OCR) was also measured by the extracellular flux analyser. From the normalised ECAR rate over the first 40 minutes (A) the basal ECAR (B) was determined and from rotenone and antimycin A treated OCR the non-mitochondrial OCR (C) was calculated. Data are shown as mean ± SEM, and analysed by one-way ANOVA with Sidak's post-hoc test. (*p≤0.05, **p ≤0.01, n=4).

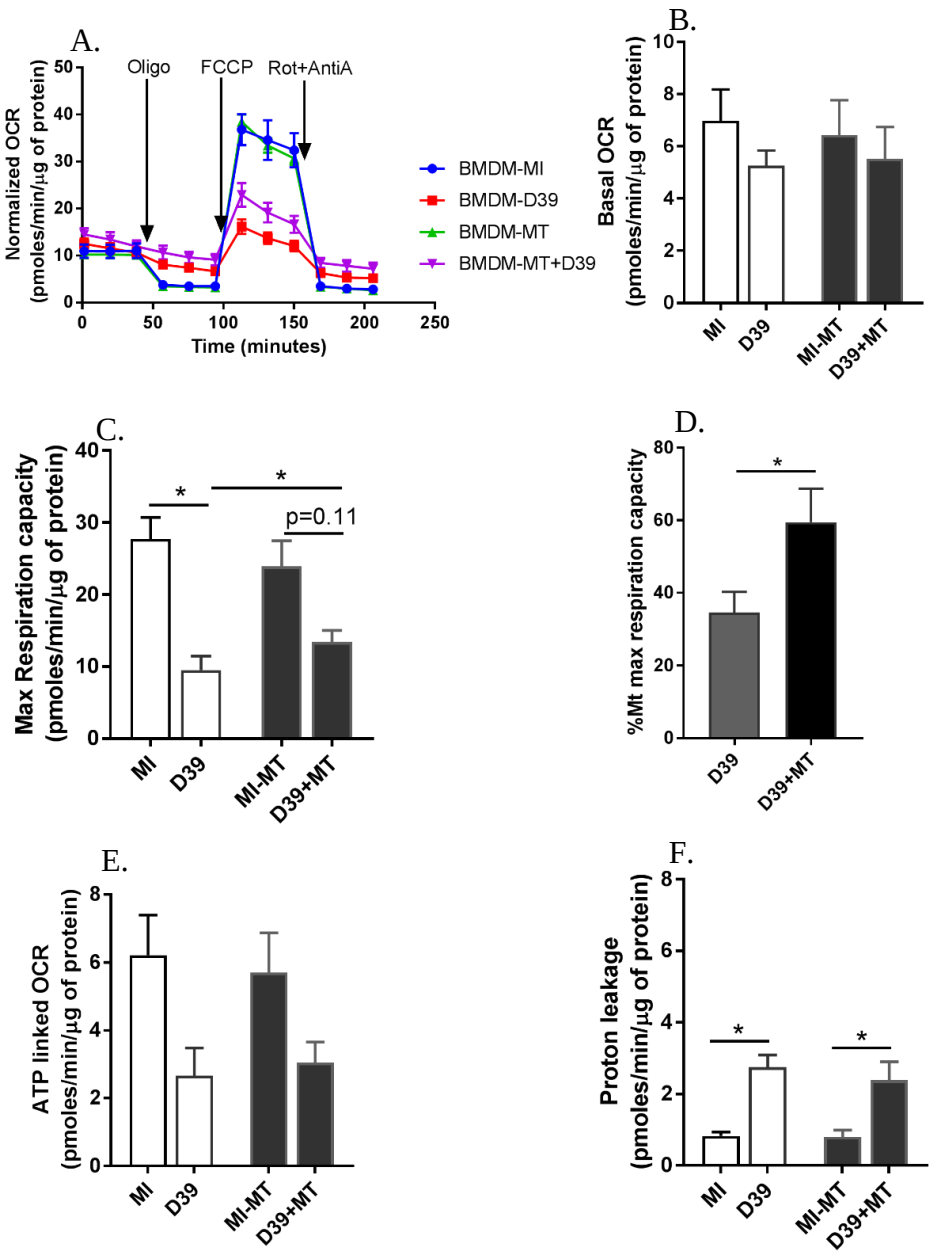

Figure 4.20. **Inhibiting mROS partially restores mitochondrial maximal respiration capacity after pneumococcal challenge.** Mouse BMDM were pre-treated with MitoTempo (MT) or vehicle control, then mock-infected (MI) exposed to opsonised *S. pneumoniae* (D39) for 12 hours. Subsequently, the mitochondrial oxygen consumption rate (OCR) was measured by extracellular flux analyser. From OCR rate data (A) the mitochondrial basal respiration (B), maximum respiration capacity (MRC) (C), % of mitochondrial MRC in macrophages challenged with D39 or D39 with MT treatment was compared to MRC in mock-infected macrophages in the same experiments, (D), ATP-linked OCR (E), and proton leakage (F) were calculated. The ATP synthase inhibitor oligomycin A (oligo) was added after baseline OCR acquisition, to measure ATP-linked OCR. The maximum respiration capacity was measured by subtracting non-mitochondrial OCR with rotenone (Rot) plus antimycin A (AntA) from FCCP treated OCR. Data were normalized by total protein of BMDM and shown as mean ± SEM. Statistical analysis was performed with one-way ANOVA with Sidak's post-hoc test for multiple comparisons and student paired *t-test* for pair-wise comparisons. (*p≤0.05, **p ≤0.01, n=4).

4.9. Discussion

In this chapter, I have observed that *S. pneumoniae* diminishes a variety of parameters associated with mitochondrial respiration capacity in human MDM and murine BMDM after a sustained period of bacterial exposure (16 hours). This include reductions in maximal respiration capacity and ATP-linked OCR while enhancing proton leakage. Challenge with *S. pneumoniae* also induced a switch to glycolytic metabolism and this was apparent from 4 hours after bacterial exposure. While some of the changes in mitochondrial metabolism were apparent either with statistical significance or with a non-significant trend at 4 hours the proton leakage was really only noted at the later 16 hour time point. I have also observed that mitochondrial maximal respiration capacity and ATP-linked oxygen consumption rate is downregulated in COPD MDM and proton leakage is higher. The maximal respiration capacity and respiratory reserve fell further after challenge with *S. pneumoniae* in COPD MDM. Moreover, I have also assessed the metabolic phenotype of human MDM pre-treated with a physiologically relevant concentration of recombinant HIV-1 envelop glycoprotein gp120 (100ng/mL), which is observed in HIV-1 seropositive bronchoalveolar lavage (BAL) specimens (Collini et al., 2018).

In addition, I have also observed that *S. pneumoniae* triggers mROS and NO, which were concentrated in the vicinity of the phagolysosomes and co-localised with intracellular bacteria. The latter observation support a role for mROS and NO in the delayed-phase of bacterial killing in the phagolysosome, when other initial canonical killing strategies such as phagosomal oxidative burst are exhausted. A recent study by West et al. has also demonstrated that TLR-agonists induce a TRAF6 signalling pathway which upregulates the post-translational modification involving ubiquitination of ECSIT which is involved in the assembly of the mitochondrial OXPHOS component complex I (NADH ubiquinone oxidoreductase), that augments mROS production. mROS are subsequently produced adjacent to the phagosome, where it participates in intracellular bacterial killing (West et al., 2011a). Presumably, the mitochondrial electron transfer complexes especially complex I and III (cytochrome c reductase) are the major sites of mROS production, which are upregulated with aging and pathological stress conditions (Raha and Robinson, 2000). In addition, a previous study also demonstrated that during apoptosis mitochondrial outer membrane permeabilisation (MOMP) causes caspase 9, and subsequently 3 activation, which induces mROS production when caspase 3 inhibits complex I and complex II (succinate dehydrogenase) of mitochondrial OXPHOS (Ricci

et al., 2003), suggesting that mROS production in macrophages challenged with *S. pneumoniae* could be a downstream process of apoptosis. This provides potential evidence that mROS may function both as a microbicidal and may be induced by apoptosis thus linking the observation of mROS production and apoptosis-associated bacterial killing in macrophages with intracellular pneumococci.

In contrast, a previous observation has shown that *S. pneumoniae* also augments NO and reactive nitrogen species (RNS) production, and their accumulation initiates MOMP and loss of mitochondrial membrane potential in macrophages (Marriott et al., 2004a), which implies that RNS is probably involved as an upstream stimulus for apoptosis. NADPH oxidase (NOX2) generates the oxidative burst which is an early microbicidal response but as discussed this is a less well developed response in macrophages as compared to neutrophils or even monocytes (Aberdein et al., 2013). Macrophages also utilise other reactive microbicidals such as NO and RNS (Flannagan et al., 2009), but these can be produced with slower kinetics than the initial oxidative burst, especially in response to bacteria such as *S. pneumoniae* (Marriott et al., 2004a). Thus, canonical intracellular bacterial killing via NOX2 may not adequately explain the later generation of RNS. However, mROS and NO peaks have been observed at the same time point (i.e. 16 hours post-bacterial challenge) in macrophages after challenge with *S. pneumoniae* (Preston and Bewley et al., in revision). Their accumulation or co-localisation with the phagolysosome suggests they could either form potent RNS (e.g. peroxynitrite) to kill intracellular bacteria or could lead to indirect effects since mROS, NO and RNS can act as signalling molecules and might indirectly activate alternative microbicidal strategies, such as generation of proteases or transcription of antimicrobial peptides for example.

This microbicidal response involving mROS generation is linked with the metabolic reprogramming of macrophages in the presence of *S. pneumoniae*, which alters macrophages metabolic phenotype from OXPHOS to glycolysis with a decreased mitochondrial oxygen consumption and increased non-mitochondrial oxygen consumption. It is well established that the mitochondrial respiration chain and OXPHOS component cytochrome oxidase (Complex IV) reduces molecular oxygen (i.e. mitochondrial consumed oxygen) into water by addition of two pairs of electrons. The origin of these electrons is NADH and FADH2 reducing equivalents, which gained electrons from substrate oxidation, particularly during the Krebs cycle. Subsequently, the electrons pass through the electron carriers of the mitochondrial electron transport chain (ETC), which is coupled with pumping out protons from the mitochondrial matrix to the

intermembrane space, creating a proton gradient or proton motive force (Δp). This force drives protons back into the matrix by a nanomachine called ATP synthase (complex v), which generates energy (i.e. ATP from ADP and P_i) like a hydroelectric pump (Mitchell, 1961). On the other hand, non-mitochondrial consumed oxygen also has lots of physiological roles apart from the oxidation of non-respirational derived substrates. For example, non-mitochondrial consumed oxygen can be utilised by NADPH oxidase and iNOS to generate reactive oxygen and nitrogen species, respectively. These species are well recognised immune components in the first line of microbicidal defence. In addition, macrophage consumed non-mitochondrial oxygen can be either reduced to oxygen anion (e.g. superoxide, mROS) by single electron leakage from the mitochondrial respiration chain, or used to produce NO by the inducible nitric oxide synthase (iNOS) at later points of infection. Presumably, NO has a negative effect on mitochondrial OXPHOS by nitrosylating iron-sulfur rich proteins in complex I of ETC (Emilio et al., 1998, Drapier and Hibbs Jr, 1988).

Interesting, I have also observed that *S. pneumoniae* induces proton leak through the mitochondrial inner membrane, which could be a plausible reason of our group's previous observation, regarding the loss of mitochondrial inner transmembrane potential ($\Delta\Psi_m$) and subsequent induction of mitochondrial apoptosis (Marriott et al., 2004a). However, it is not clearly established how intracellular bacteria induce proton leak and electron leak from the mitochondrial ETC. The basal proton leak is a natural process and it is indispensable for heat generation and acclimatisation (Brand et al., 2005). The basal proton leak contributes significantly to the maintenance of basal metabolic rate (BMR) and involves mitochondrial anion carrier proteins such as the adenine nucleotide translocase (ANT) uncoupling protein I (UCP1), especially in brown adipose tissue (Brand et al., 2005, Parker et al., 2009). The basal proton leak is induced by fatty acids and reactive alkenals (e.g. hydroxynonenal), which upregulate ANT and UCPs (Parker et al., 2008). The proton leak causes loss of proton motive force (Δp), which is essential for mitochondrial ATP generation.

Moreover, mROS production is highly sensitive to the decreased Δp and is reduced by proton leak (Papa and Skulachev, 1997). These observations led me to hypothesise that *S. pneumoniae* enhanced mROS and NO generation, and induced proton leak (i.e. mitochondrial uncoupling). NO could do this by stimulating loss of $\Delta\Psi_m$ while proton leak could limit excessive mROS generation. A consequence of this increased proton leak would, however, be to shift metabolism away from OXPHOS would be result in

mitochondrial metabolic reprogramming. To reconstitute the disrupted mitochondrial respiration, I have applied MitoTempo, a superoxide dismutase mimetic and observed that it restored approximately 25% of mitochondrial respiration capacity in pneumococcal challenged macrophages. However, MitoTempo neither rescued the loss of ATP-linked OCR nor reversed the proton leak across the mitochondrial inner membrane in pneumococcal challenged macrophages. However, since NO can drive loss of $\Delta\Psi_m$, (Belén et al., 2000) a role for NO in inducing proton leak it might be that both microbicidals need to be inhibited to more effectively restore mitochondrial metabolism. This suggests a paradigm in which infection not only activates glycolytic metabolism but that the mitochondrial metabolic reprogramming also results in mitochondria becoming key effectors of microbicidal responses. But that mitochondrial responses to these changes ultimately result in further adaptions OXPHOS, such as increased proton leak and loss of $\Delta\Psi$m, which ultimately leads to apoptosis. Mitochondrial homeostasis is not only regulated by metabolism, but also by active changes in mitochondrial dynamics (Mishra and Chan, 2016), which will be focused on in the next chapter.

A recent study has demonstrated that oxidative stress with HIV-1 glycoprotein gp120 not only diminishes mitochondrial respiration capacity but also alters mitochondrial dynamics in neurons (Avdoshina et al., 2016), suggesting that changes in mitochondrial dynamics may also be a feature of the conditions I studied. Moreover, HIV-1 seropositive patients are more susceptible to lung infection and bacterial colonisation (Gordin et al., 2008, Yin et al., 2012), so these mitochondrial changes may have functional changes of physiological relevance to host defence. Recently, our group has observed that recombinant gp120 increases mROS at baseline, but *S. pneumoniae* fails to induce further increases of mROS production in human MDM pre-treated with gp120 (Collini et al., 2018), as seen for COPD alveolar macrophages responses following pneumococcal challenge (Bewley et al., 2017). Thus it appears an increased level of production is not sufficient for acute responses to bacteria and what is required in acute induction. It may be that chronic increases in HIV or COPD result in compensatory increases in aspects of the antioxidant defence that limit the capacity for acute induction of mROS. Interestingly, I have observed that recombinant gp120 not only decreases basal proton leak but also diminishes the upregulation of proton leak in pneumococcal challenged macrophages (Figure 4.3H). This modification is predicted to be linked with a limited mROS production from complex I and downregulation of MOMP and caspase 3 activation in macrophages (Ricci et al., 2003).

Apart from other comorbidities, *S. pneumoniae* is a major cause of community-acquired pneumonia in COPD and lung pathogens especially *Haemophilus influenzae*, *S. pneumoniae* and *Moroxella catarrhalis* are involved in infection-associated exacerbations in COPD (Sapey and Stockley, 2006, Torres et al., 1996). Furthermore, recently we have demonstrated that COPD alveolar macrophages (AM) have increased mROS at baseline, but pneumococcal challenge does not induce mROS production, in contrast to the mROS induction in healthy AM (Bewley et al., 2017). Besides, this observation with COPD AM another contemporary observation in the COPD MAP consortium study with COPD airway small muscle cells (ASM) was that ASM also were to have increased mROS at baseline. The latter study has also observed mitochondrial metabolic impairments. In particular the investigators observed a diminished mitochondrial respiration capacity, an increased proton leak and loss of inner mitochondrial transmembrane potential ($\Delta\Psi m$) in COPD ASM (Wiegman et al., 2015). Interestingly, my findings have also shown mitochondrial metabolic impairments in COPD MDM. For instance, I observed that COPD MDM have a decreased mitochondrial respiration capacity and ATP-linked OCR, and an increased proton leak, suggesting that circulatory MDM in COPD also carry the signature of metabolic impairment, similar to that seen for lung structural cells in COPD, such as ASM.

However, most of my COPD MDM metabolic data did not reach statistical significance because the metabolic response was quite variable between donors and the sample size was small. It would have been desirable to obtain access to more samples but this was not possible before the end of that consortium. In addition, I also acknowledge a caveat to my study, which was that my observations were limited only to human circulatory MDM or mouse BMDM rather than tissue macrophages (e.g. alveolar macrophages). Besides, I was unable to check the metabolic phenotype of AM either in COPD or HIV-1 seropositive patients, since investigating the metabolic phenotype with the XF24 flux analyser needs approximately 3 million macrophages from each donor. Practically these numbers weren't readily available in BAL specimens due to limited yields particularly in COPD and competing demands for samples as part of the COPD MAP consortium. However, every technique has some pros and cons, and other techniques such as NMR or mass spectrometry could be applied to confirm my observed metabolic phenotype with tissue macrophages.

Overall, this section shows that *S. pneumoniae* not only impairs mitochondrial respiration capacity but also stimulates increased mROS production in human MDM as well mouse

BMDM. The confocal images and respective quantitative data suggest that mROS along with NO accumulate proximal to the phagolysosome and co-localise with intracellular pneumococci. Moreover, this chapter has emphasised a role for alterations in macrophage mitochondrial metabolism in COPD and HIV-1 glycoprotein gp120 pre-treated macrophages, which implies that these diseases not only impair macrophage mitochondrial oxidative phosphorylation but also impinges mitochondrial innate immune responses to *S. pneumoniae*. Finally, regulation of mitochondrial bioenergetics responses appears a necessary component of arming the mitochondria to become more effective at becoming effectors of the microbicidal response to pneumococci. Since mitochondrial bioenergetics is only one aspect of mitochondrial homeostasis, which is also influenced by mitochondrial dynamics, I next addressed the latter process in a later chapter of my thesis.

Chapter 5. Mitochondrial fission triggers antimicrobial response in macrophages

5.1. Introduction

Mitochondria play a pivotal role in cellular homeostasis mainly by maintaining cellular metabolism, proliferation and apoptosis. These functions are regulated by mitochondrial dynamics including division (i.e. fission) or integration (i.e. fusion) (Benedikt, 2010). In addition, morphologically mitochondria are extended throughout the cytosol and mostly are interconnected to maintain dynamic behaviour through constant fission and fusion (Prashant and David, 2014). Recently, it has been shown that Dynamin-related protein 1 (Drp1) and endoplasmic reticulum (ER)-mitochondrial tethering is essential to trigger mitochondrial fission (Sesaki et al., 2014, Kornmann et al., 2009). In addition to homeostatic roles, Stavru et al. have demonstrated that bacterial pore-forming toxins (e.g. listeriolysin O, a cholesterol dependent cytolysin) induce mitochondrial fission by a Drp1 independent non-canonical manner. They have also shown that this non-canonical fission is rather dependent on calcium efflux from ER, which is regulated at points of ER-mitochondrial tethering by F-actin polymerisation (Stavru et al., 2013).

Moreover, oxidative stress also triggers uncontrolled mitochondrial fission or fragmentation, which accentuates excessive mitochondrial ROS (mROS) production and results in subsequent loss of inner mitochondrial transmembrane potential. The loss of inner transmembrane potential in turn can induce either apoptosis or aberrant autophagy (Qi et al., 2013). LPS upregulates mROS production and induces mitochondrial fission via a Drp1-dependent mechanism (e.g. phosphorylation of Drp1 at serine 616), which is inhibited by the ROS scavenger N-acetyl cysteine (Katoh et al., 2017), suggesting that ROS is mechanistically linked to mitochondrial fission and may be triggered by bacterial components. On the other hand, inhibition of mitochondrial fission inhibits ROS overproduction in hyperglycaemia-associated disorder (Yu et al., 2006). Collectively, this indicates that excessive fission and ROS production can produce a vicious cycle and that ROS is not only a factor that triggers fission but also a result of increased fission. Mitochondrial fission is also associated with metabolic reprogramming from mitochondrial OXPHOS to glycolysis in activated T cells (e.g. effector T cells) (Buck et al., 2016).

Mitochondrial fission/fusion plays a critical role in determining cell fate since it is associated with apoptosis induction. For example, inhibition of Fission 1 protein (Fis1) – which binds activated Drp1 to initiate mitochondrial fission - inhibits apoptosis (Lee et al., 2004) whilst overexpression of Fis1 upregulates apoptosis (James et al., 2003).

Inhibition of mitochondrial fission also inhibits cytochrome c release from the mitochondrial intermembrane space to the cytosol (Richard and Mariusz, 2005). Cytosolic cytochrome c activates caspase-9, which activates apoptosis executioners caspase-3 and caspase-7 (Stephen and Douglas, 2010), suggesting that mitochondrial fission is an upstream process of apoptosis.

Furthermore, it has been demonstrated that depolarised mitochondria recruit Parkin (an E3 ubiquitin ligase), which acts in concert with Phosphatase and tensin homolog (PTEN)-induced kinase 1 (PINK1) upregulates apoptosis through switching on the degradation of anti-apoptotic protein Mcl-1 by polyubiquitination (Carroll et al., 2014). In contrast, Parkin and PINK1 accumulation on depolarised mitochondria also plays a role in mitophagy and triggers mitochondrial disintegration and elimination by mitophagy through recruiting microtubule-associated protein 1- light chain 3 (LC3)-binding adaptor protein p62 and neighbour of breast cancer 1 (BRCA1) protein (NBR1). These then form a double membrane around the fragmented mitochondria (i.e. an autophagosome) and subsequently fuse with lysosomes. This is called selective autophagy or macroautophagy/mitophagy (Narendra et al., 2008). The extent to which the cells complement of mitochondria are depolarised and decorated with parkin appears to influence whether the cell activates apoptosis and dies or mitophagy as a survival strategy (Carroll et al., 2014). Overall, this implies that eukaryotic cells mitochondria not only supply energy but also act as a molecular check point for cell death.

Aside from these concepts, recent research has revealed a role for mitochondria in innate immunity, separate from energy production (Manan et al., 2017). However, to the best of my knowledge, little research has examined mitochondrial dynamics during innate immune responses, during host-pathogen interactions. Hence, I observed mitochondrial morphology after challenge with bacteria (*S. pneumoniae*) and related these to key steps during the host-pathogen interaction such as metabolic reprogramming, mROS production in macrophages and its role in intracellular bacterial killing.

5.2. *S. pneumoniae* upregulated Drp1-independent mitochondrial fission in macrophages

Constitutive mitochondrial division (i.e. fission) and fusion processes are not only essential to preserve mitochondria function but also regulate cellular life-death decisions (Chan, 2012). Normal mitochondrial homeostasis is perturbed by excessive fission due to oxidative cues (Qi et al., 2013) or bacterial pore-forming toxins (Stavru et al., 2011). Our group previously has shown that fully differentiated macrophages have greater

mitochondrial volume compared to undifferentiated monocytes or less differentiated macrophages (Daigneault et al., 2010).

To assess mitochondrial morphological features of differentiated macrophages, mouse bone marrow-derived macrophages were challenged with *S. pneumoniae* for 12 hours, subsequently the mitochondrial outer membrane protein, Tom20, was labelled using immunofluorescence. Confocal microscopy images and ImageJ-processed skeletonised images illustrated that morphologically mitochondria are mostly tubular, maintain an inter-connected network and extend throughout the cytoplasm in mock-infected macrophages (Figure 5.1A and C). Whereas, mitochondria of pneumococci exposed macrophages are mostly fragmented and dispersed throughout the cytosol (Figure 5.1B and D). Moreover, pneumococci significantly decreased mitochondrial network complexity whether prior treated with or without Drp1 assembly inhibitor, Mdivi-1 (Figure 5.1E for the individual macrophages mitochondrial population and 5.1F of average network complexity), suggesting that pneumococci induced mitochondrial fission occurs in a Drp-1 independent manner. The time course fission frequency data demonstrate that pneumococci triggers mitochondrial fission from 12 hours onwards (Figure 5.1G). As a control, Mdivi-1 alone had no effect on mitochondrial complexity.

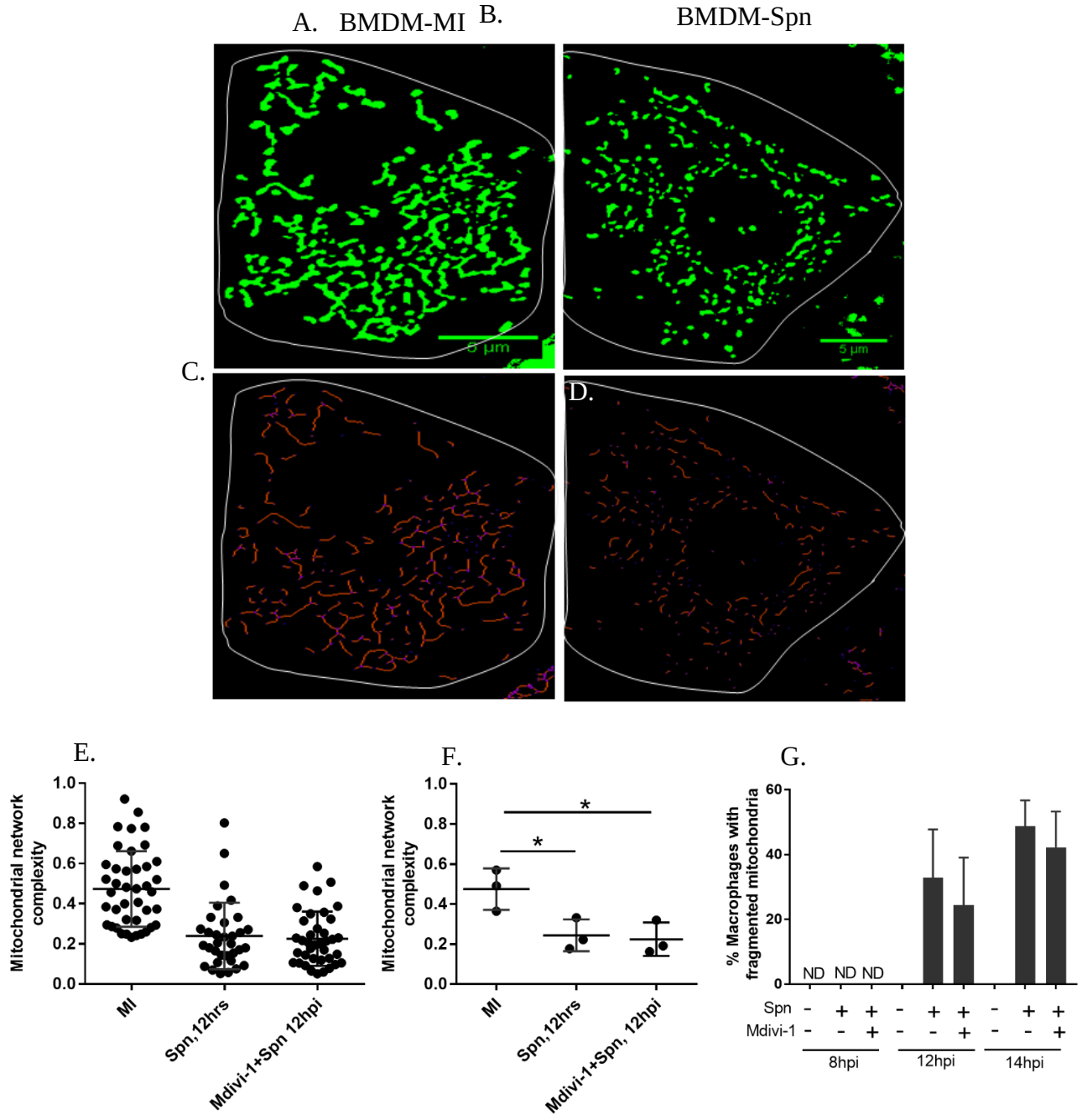

Figure 5.1. ***S. pneumoniae*** **induces mitochondrial fission in a Drp1 independent manner.** Mouse BMDM were exposed to serotype 2 *S. pneumoniae* (D39, MOI of 10) for 8, 12 and 14 hours. Then, cells were fixed, permeablised and blocked with 4% paraformaldehyde, 0.1% triton-x-100 and 0.2% gelatin in PBS, respectively. Subsequently, the mitochondria specific marker Tom20 was labelled with rabbit anti-Tom20 primary antibody (0.4µg/mL) and goat anti-rabbit IgG (H+L) (4µg/mL) conjugated with Alexa Fluor 488. Images were captured by Zeiss LSM510 confocal microscopy using 488nm excitation and 500-530nm emission spectrum. Figure A shows the representative mitochondrial images of mock-infected and B shows the mitochondrial image of D39 exposed BMDMs after 12 hours. Figure C and D illustrate the representative skeletonised mitochondrial images rebuilt by ImageJ from the corresponding images in figures A and B. Figure E shows the mitochondrial network complexity, with each dot representing the ratio of total branch points and end points of the total mitochondrial population of each macrophage. Figure F shows the average network complexity of total mitochondrial population of each donor mouse

BMDM. The network complexity was quantified by ImageJ from the mitochondrial images of mock-infected or D39 exposed BMDM after 12 hours, with or without pre-treatment with the Drp1 assembly inhibitor Mdivi-1. Figure G shows the percentage of macrophages with fragmented mitochondria at 8, 12 and 14 hours post-bacterial challenge. Mitochondrial network complexity and percentage of macrophages with fragmented mitochondria were calculated from three independent experiments. Data are shown as mean ± SD. Statistical analysis was performed with One-way ANOVA and Bonferroni post-hoc test, *$p<0.05$). Scale bars = 5µm.

5.3. Activated Drp1 is not recruited on fragmented mitochondria after pneumococcal challenge

Mitochondrial fission is positively regulated by Drp1. Drp1 phosphorylated at serine 616 is essential for mitochondrial division/fission (Mishra and Chan, 2016). This activated Drp1 (Ser616 phosphorylated-Drp1) binds with Fis1 on mitochondrial outer membranes and oligomerises, to constrict the mitochondrial membranes and trigger fission or division. This process is inhibited by Mdivi-1, a Drp1 assembly inhibitor (Cassidy-Stone et al., 2008). In the previous section, I showed that macrophages pre-treated with Mdivi-1 did not have a reduction in mitochondrial fission (Fig 1E-F). To further confirm Drp-1 independent fission, human MDM were challenged with *S. pneumoniae*. Subsequently mitochondria and serine-616 phosphorylated-Drp1 were co-stained using immunofluorescence method. Mitochondria and P-Drp1 co-staining images illustrated that there is no association of phosphorylated Drp1 with mock-infected macrophages mitochondria or mitochondria from pneumococcal challenged macrophages (Fig 5.2A-B). Whereas MDM treated with FCCP, a known activator for mitochondrial fission, show phosphorylated Drp1 associated with fragmented mitochondria (Fig 5.2C).

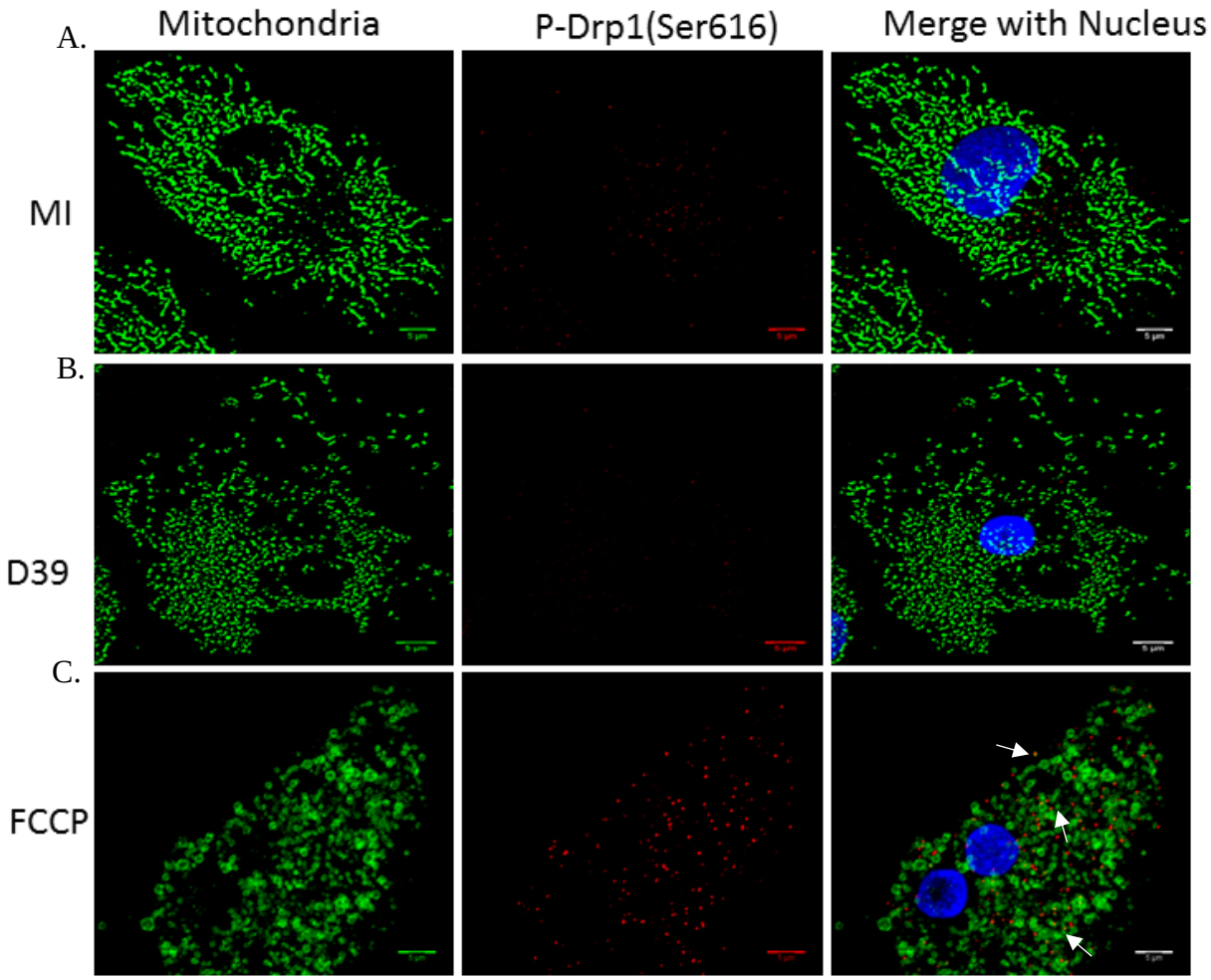

Figure 5.2. ***S. pneumoniae*** **induces p-Drp-1 independent mitochondrial fission.** Human MDM were exposed to *S. pneumoniae* (D39, MOI of 10) for 16 hours. Then the mitochondria specific marker Tom20 and serine-616 phosphorylation (p-Drp1) specific dynamin related protein-1 (p-Drp1) were labelled by mouse anti-Tom20 and rabbit anti-p-Drp1 primary antibodies. The following respective secondary antibodies were also used: goat anti-mouse IgG conjugated with Alexa Fluor 488 and goat anti-rabbit IgG conjugated with Alexa Fluor 568. The figure shows the representative images of mitochondria and p-Drp1 in macrophages with mock-infected (A, top panel) and macrophages challenged with D39 for 16 hours (B, middle panel). Panel C illustrates the representative images of mitochondria and p-Drp1 in macrophages treated with the mitochondrial OXPHOS uncoupler Carbonyl cyanide 4-(trifluoromethoxy) phenylhydrazone (FCCP, 20µM). Images were captured by Zeiss LSM510 confocal microscopy using 488nm and 543nm excitation with 500-530nm and 565-615nm emission spectrum, respectively. White arrows in the panel C merge image show the mitochondrial and p-Drp1 co-localised pixels (yellow). Images are representative of images from three independent experiments. Scale bars = 5µm.

5.4. Pneumolysin is not essential for mitochondrial fission but metabolically active *S. pneumoniae* is

Pneumolysin is a critical virulence factor for pneumococci and it belongs to the family of cholesterol-dependent cytolysins. Prior reports suggested that this family of pore-forming toxins, for example listeriolysin O from *Listeria monocytogenes,* triggers mitochondria fission in a Drp1-independent manner (Stavru, 2011 and Stavru, 2013). To assess the microbiological requirements for mitochondrial fission particularly pneumolysin's role in mitochondrial fission, mouse BMDM were challenged with heat inactivated pneumococci or a pneumolysin deficient pneumococcal (pneumolysin stop *S. pneumoniae*) strain (Bewley et al., 2014), at a comparable MOI to the wild-type. Mitochondrial morphological images demonstrated that live bacteria are essential to trigger mitochondrial fission (Figure 5.3B-C), and the pneumolysin deficient mutant could also trigger mitochondrial fission/fragmentation when a higher multiplicity of infection (MOI) of 40 or more was used, as compared to the MOI=10 used for wild-type pneumococci (Figure 5.3A-G). Moreover, exogenous pneumolysin also induced mitochondrial fission but only with a higher concentration (2.0µg/mL or more) (Figure 5.3H). Together, these data suggest that pneumolysin could enhance mitochondrial fission but it is not essential to trigger mitochondrial fission with metabolically active intracellular bacteria. However, it is warranted to validate the pneumolysin's effect on mitochondrial fission with exogenous pneumolysin a comparable cfu fo *S. pneumonaie.* Presumably, the sandwich ELISA is more applicable method to check the concentration of extracted pneumolysin and the hemolytic assay with rabbit red blood cell would be the best option to check the lytic concentration of exogenous pneumolysin and pneumolysin from the comparable cfu of pneumocococci (Sanders et al., 2008). Moreover, it is also essential to check the purity of *E. coli* source exogenous pneumolysin. Although I used apparently pure exogenous pneumolysin which was produced from the His tagged *E. coli* followed by HPLC purification (Timothy J. Mitchell lab, Birmingham university) (Bewley et al., 2014), I would not check its comparable level produced by pneumococci (e.g. MOI of 10) which I was exposed to mouse BMDM.

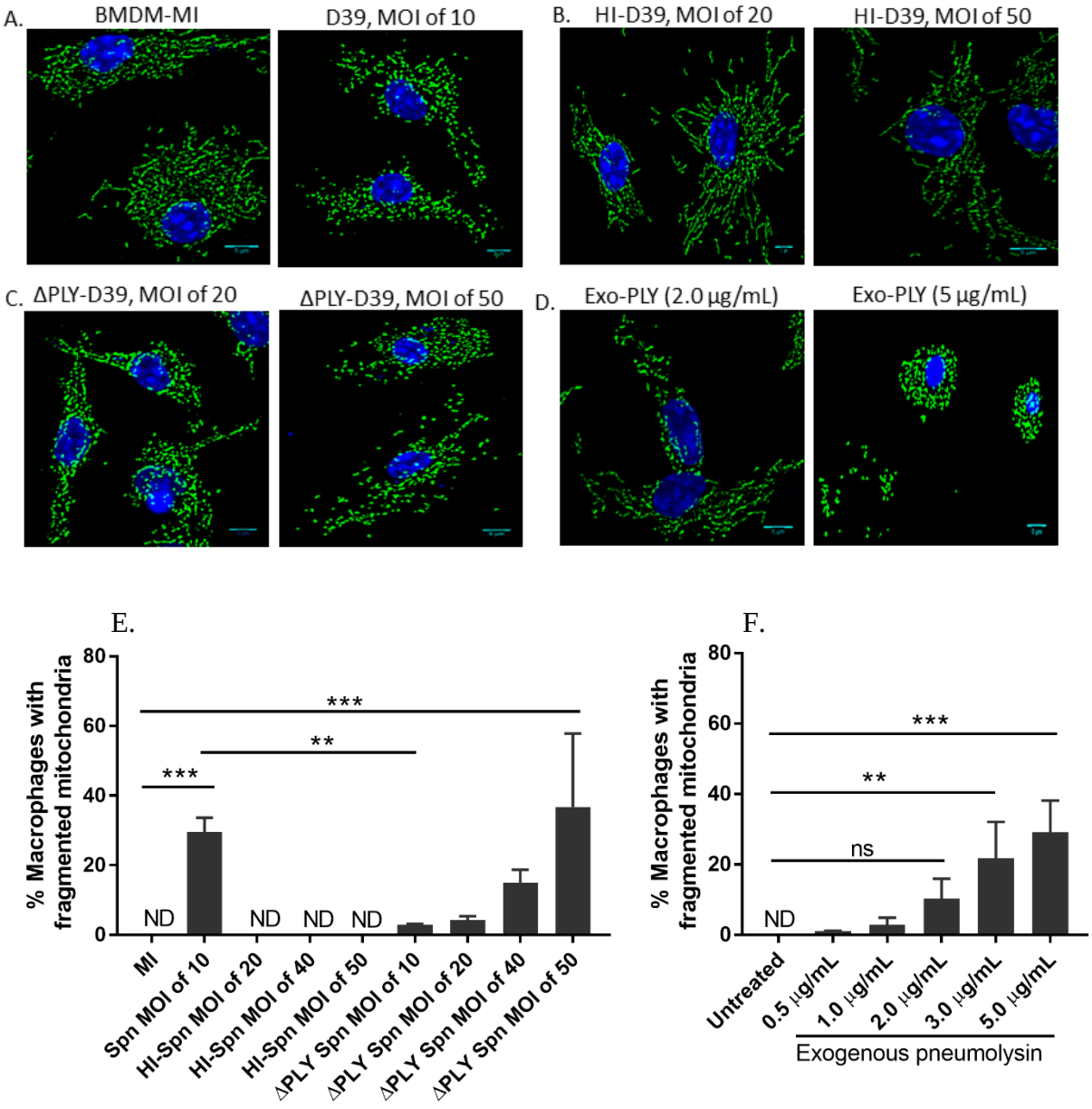

Figure 5.3. **Pore-forming toxin pneumolysin is not essential to trigger mitochondrial fission**. Metabolically active *S. pneumoniae* (D39), heat inactivated D39, pneumolysin deficient D39 (ΔPLY D39) or exogenous pneumolysin (0.5µg/mL-5µg/mL) were used to challenge mouse BMDM for 12 hours. The mitochondria specific marker Tom20 was labelled with rabbit anti-Tom20 primary antibody and goat anti-rabbit IgG conjugated with Alexa Fluor 488, and nuclei were stained with Draq5. Images were captured by Zeiss LSM510 confocal microscopy using 488nm excitation and 500-530nm emission spectrum. Panel A shows the representative mitochondrial images of mock-infected and metabolically active D39 (MOI of 10) exposed macrophages. Panel B shows the representative mitochondrial images of heat inactivated D39 (MOI of 20 and 50) exposed macrophages. Panel C shows the representative mitochondrial images of pneumolysin deficient mutant D39 (MOI of 20 and 50) exposed BMDM. Figure D shows the mitochondrial representative images of exogenous pneumolysin (2.0 and 5µg/mL) treated macrophages. Scale bars = 5µm. Figure E shows the percentage of macrophages with fragmented mitochondria after mock-infection or challenge with metabolically active wild type

D39 (MOI of 10) or heat inactivated D39 (MOI of 10 to 50) or pneumolysin mutant D39 (MOI of 10 to 50). Figure F shows the percentage of macrophages with fragmented mitochondria after treatment with 0.5µg/mL-5µg/mL of exogenous pneumolysin for 12 hours. Data were analysed with One-way ANOVA and Sidak's post-hoc test and are shown as mean ± SD, n=3. ***$p<0.001$, **$p<0.01$, ns- non-significant $p>0.05$.

5.5. *S. pneumoniae* exposure upregulates E3 ligase Parkin expression on fragmented mitochondria in macrophages

Parkin is a cytosolic E3 ligase protein and mostly responsible for ubiquitination of misfolded or damaged proteins expressed on the outer mitochondrial membrane, which are subsequently removed via the 26S proteasome system (Trempe et al., 2013). It is well established that during mitochondrial stress conditions, Parkin is recruited to damaged mitochondria and triggers selective autophagy or mitophagy, to minimise cellular toxicity (Narendra et al., 2008). Genetic defects or mutations in Parkin causes mitochondrial dysfunction and leads to development of juvenile Parkinson disease (Tohru et al., 1998). Moreover, a few studies have also demonstrated roles for Parkin in innate immunity. For example, single nucleotide polymorphisms (SNPs) in the Parkin (PARK2) regulatory regions have been associated with increased susceptibility to intracellular bacteria, such as typhoid and leprosy in humans (Ali et al., 2006, Mira et al., 2004). Recently, it has also been shown that Parkin interacts with the mitochondrial TSPO-VDAC1 (translocator protein and voltage-dependent anion channel 1) protein complex to mediate innate defence against bacterial infection in Drosophila (Cho et al., 2015).

Therefore, next I tested whether Parkin is involved with mitochondrial fission in macrophages in response to pneumococci. To assess this association, macrophages were challenged with pneumococci and then co-stained with anti-Parkin and anti-Tom20 antibodies, and were assessed by immunofluorescence microscopy. Mitochondria and Parkin co-staining showed that pneumococci upregulated Parkin expression in macrophages compared to mock-infected cells (Figure 5.4A-B and 5.5A-B), and Parkin was mostly co-localised with fragmented mitochondria (Figure 5.5C). Moreover, the Drp1 assembly inhibitor, Mdivi-1 did not modulate Parkin expression after bacterial challenge (Figure 5.4C and 5.5A-B). In contrast, 3-methyladenine, a type I/III phosphatidyl-inositol-3 kinase (PI-3K) inhibitor reversed Parkin activation in response to pneumococci (Figure 5.4D and 5.5A-B). This observation is also corroborated by immunoblotting with subcellular fractions. Mouse BMDM challenge with pneumococci has shown a trend towards increased Parkin expression in both cytosolic and

mitochondrial fractions compared to mock-infected macrophage fractions (Figure 5.5D-F). Moreover, 3-MA shows a trend towards decreased Parkin activation in the mitochondrial compartment of pneumococci exposed macrophages, compared to mock-infected macrophages (Figure 5.5D-F).

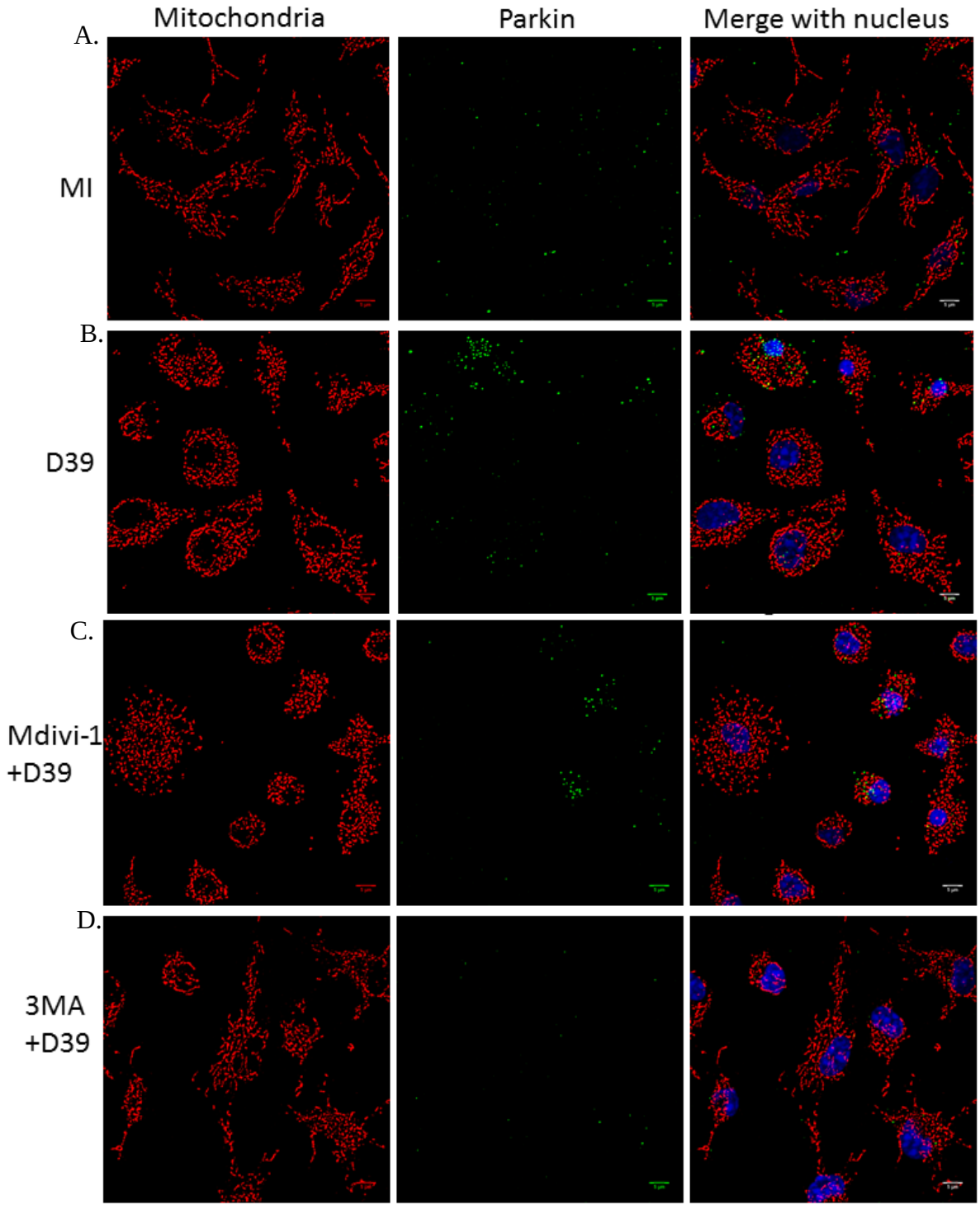

Figure 5.4. **Macrophage exposure to *S. pneumoniae* induces mitochondrial E3 ligase parkin expression in association with fragmentation**. Mouse BMDM were treated with Mdivi-1 or 3-

MA for an hour, then exposed to *S. pneumoniae* (D39, MOI of 10) for 12 hours. Then, mitochondria and parkin were co-stained using rabbit anti-Tom20 (tagged with Alexa Fluor 568 labelled-red) and mouse anti-Parkin antibody (tagged with Alexa Fluor 488-green). Each panel figure shows the representative images of mitochondria and Parkin in mock-infected (A), or pneumococci exposed macrophages (B), or in Mdivi-1 treated (C), or 3-MA treated pneumococcal exposed BMDM (D). Images were taken as the representative images from three independent experiments.

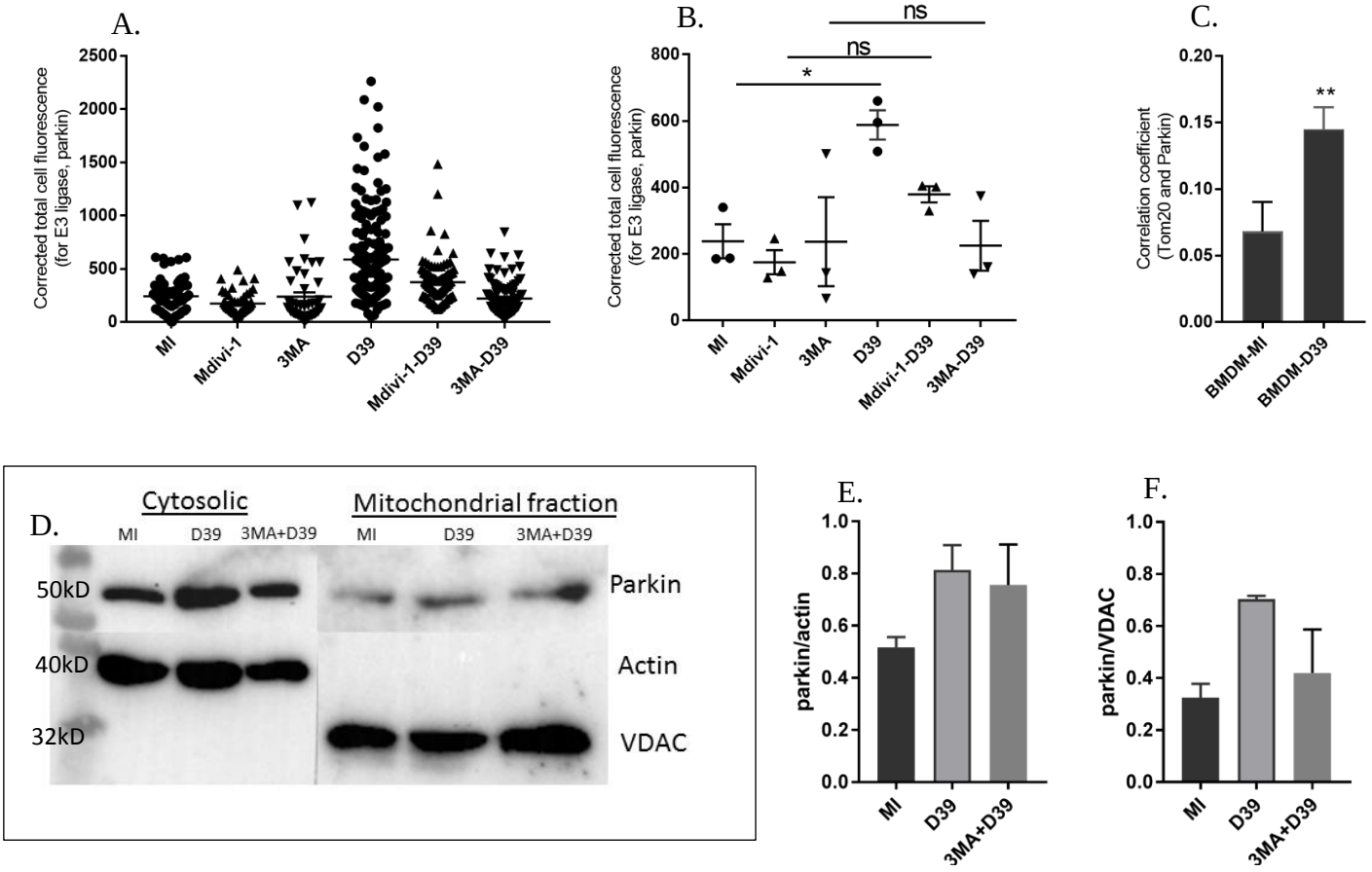

Figure 5.5. **Macrophages exposure to *S. pneumoniae* induces E3 ligase Parkin expression which translocate to mitochondria.** Mouse BMDM were treated with 3-MA or Mdivi-1 for an hour, then exposed to *S. pneumoniae* (D39, MOI of 10) for 12 hours. Figure A shows the quantitative data obtained from figure 5.4, and shows the corrected total cell fluorescence (CTCF) for Parkin in each macrophages after pre-treatment with or without Mdivi-1 or 3MA, followed by mock infection or D39 exposure. Figure B shows the average CTCF for Parkin. Figure C shows the co-localisation quantification data as the Pearson's correlation coefficient for mitochondrial outer membrane protein Tom20 and Parkin in mock-infected and D39 exposed BMDM from the same experiments. Immunoblotting was also performed after SDS-PAGE with the extracted cytosolic and mitochondrial fractions (n=2). Figure D shows the representative Immunoblots' of the cytosolic fraction where it shows the bands for Parkin (50kD) and alpha-actin (40kD), and the mitochondrial fraction shows the bands for Parkin and voltage-dependent anion-selective channel 1 (VDAC1; 32kD), used as a mitochondrial fraction loading control. Figure E and F show the ratio of Parkin/Actin and Parkin/VDAC1 for cytosolic and mitochondria fractions, respectively. Data are shown as mean ± SEM. Statistical analysis (for figure A-C, n=3) was performed with one-way ANOVA and Sidak's post-hoc test and paired t-test (for figure B). *$p<0.05$, **$p<0.01$.

5.6. Fragmented mitochondria during *S. pneumoniae* challenge do not associate with the autophagy marker LC3B

Autophagy is an evolutionarily conserved selective or non-selective intracellular lysosomal degradation process, which is essential to maintain cellular homeostasis (Klionsky and Codogno, 2013). This autophagosomal process is initiated by forming a double-membrane containing vacuole which is regulated by different sets of autophagy-related core proteins (Atg). Among them, Atg8/MAP1LC3 or microtubule associated protein 1 light-chain 3 (i.e. LC3) – particularly in its form conjugated with phosphatidyl-ethanolamine (a membrane bound LC3 also referred to as LC-II or LC3B) - is essential for autophagosome elongation and maturation, and its level is also correlated with the number of autophagosomes (Lee and Lee, 2016). Moreover, recently it has been demonstrated that Parkin ubiquitin ligase is harnessed to mediate autophagy/xenophagy associated intracellular killing of *Mycobacterium tuberculosis*, *Listeria monocytogenes* and *Salmonella Typhimurium* in macrophages (Manzanillo et al., 2013).

Therefore, I hypothesised that macrophages might also recruit autophagy machinery to fragmented mitochondria generated in response to pneumococci, and subsequently clear them by mitophagy. To assess this hypothesis, mitochondria and LC3B were co-stained in macrophages after challenge with pneumococci. Immunofluorescence images, however, demonstrated that there was no-association of LC3B in fragmented mitochondria in response to bacterial internalisation (Figure 5.6A-B). Whereas, macrophages treated with a known mitochondria fission/fragmentation inducer Carbonyl cyanide 4-(trifluoromethoxy) phenylhydrazone (FCCP) upregulated LC3B and most of the LC3B was recruited to fragmented mitochondria (Figure 5.6C).

Moreover, the topographical images with transmission electron microscopy (TEM) allowed observation of the ultrastructure of mitochondria. The TEM images demonstrated that there was no evidence of double membrane vacuoles around the fragmented mitochondria in macrophages, after challenged with pneumococci (Figure 5.7). In addition, the TEM images also depicted that mock-infected macrophage mitochondria are mostly tubular and maintain the distinctive cristae compartments, compared to pneumococci exposed macrophage mitochondria (figure 5.7A-B). Furthermore, the number of cristae per mitochondrion were significantly decreased in fragmented mitochondria after bacterial internalisation, compared to mock-infected macrophage mitochondria (figure 5.7C).

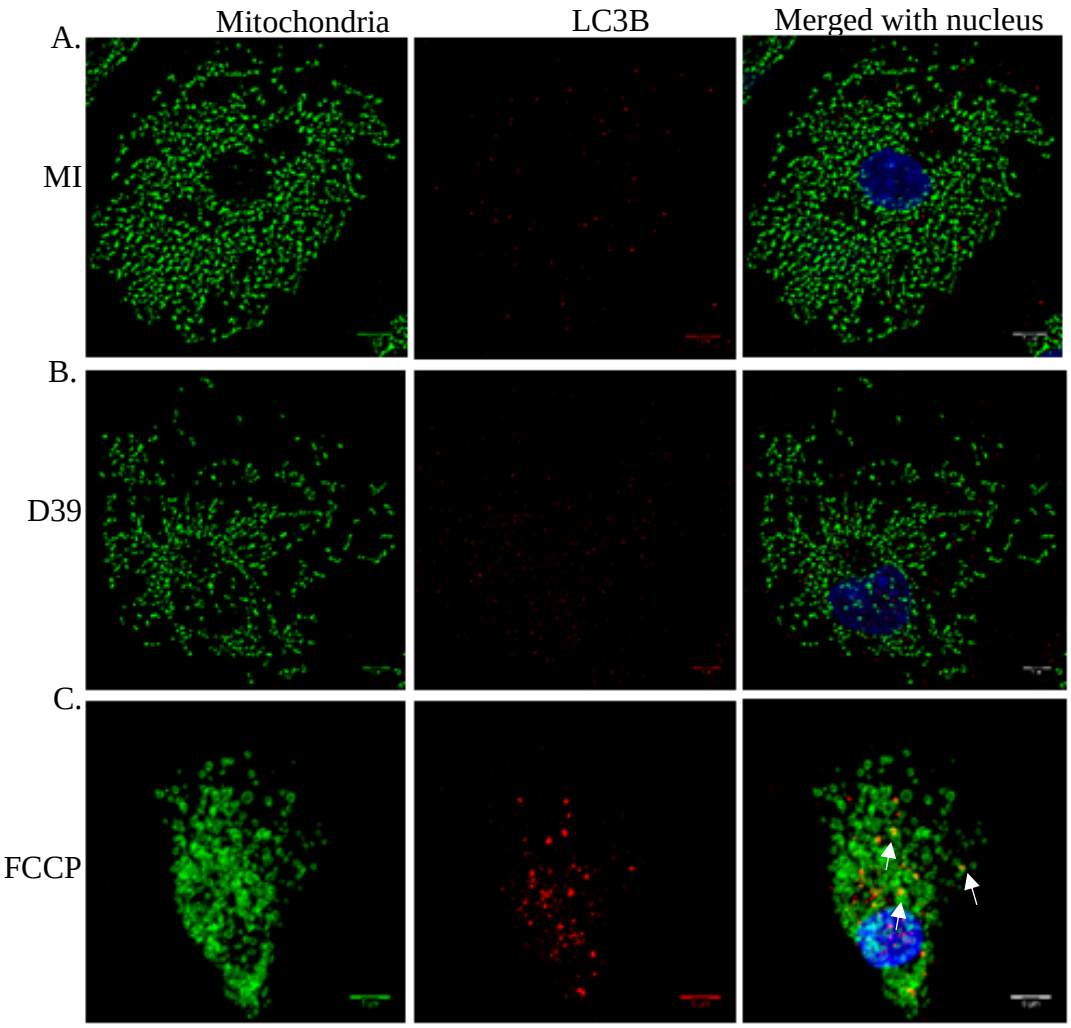

Figure 5.6. ***S. pneumoniae* does not modulate the autophagy marker LC3B.** Human MDM were exposed to *S. pneumoniae* (D39, MOI of 10) for 16 hours. Then the mitochondria specific marker Tom20 and LC3B were labelled by mouse anti-Tom20 and rabbit anti- LC3B primary antibodies, then respective secondary antibodies, goat anti-mouse IgG conjugated with Alexa Fluor 488 and goat anti-rabbit IgG conjugated with Alexa Fluor 568, were added. The figure shows the representative images of mitochondria and LC3B in macrophages after mock-infection (A, top panel) or D39 challenge (B, middle panel). Panel C illustrates the representative images of mitochondria and LC3B in macrophages treated with the mitochondrial OXPHOS uncoupler Carbonyl cyanide 4-(trifluoromethoxy) phenylhydrazone (FCCP, 20µM). Images were captured by Zeiss LSM510 confocal microscopy using 488nm and 543nm excitation with 500-530nm and 565-615nm emission spectrums, respectively. White arrows in panel C merged image show the LC3B and mitochondrial co-localised pixels (yellow). Images shown are representative images from three independent experiments. Scale bars = 5µm.

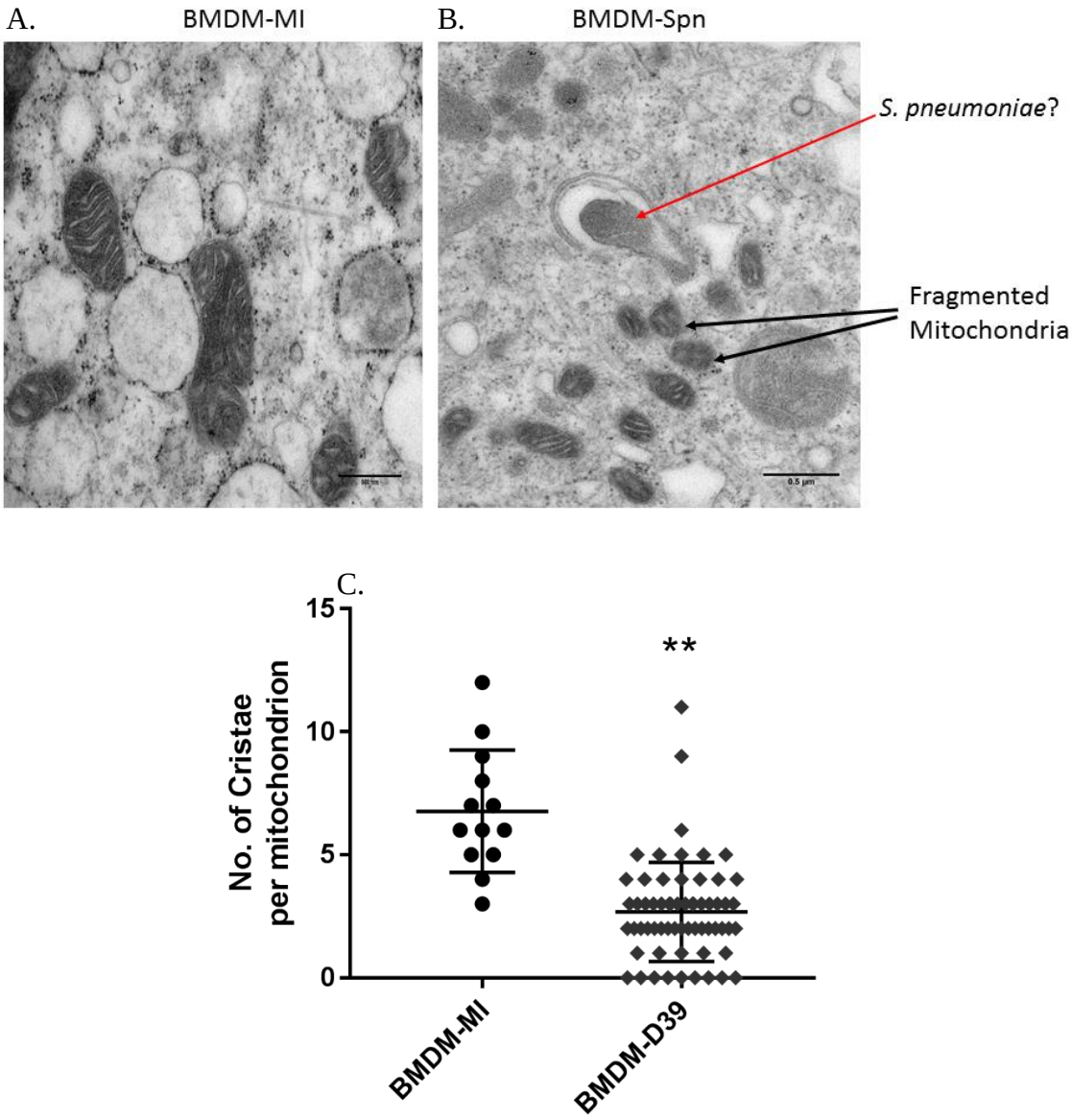

Figure 5.7. **Fragmented mitochondria following *S. pneumoniae* challenge do not engage with mitophagy.** Mouse BMDM were exposed to *S. pneumoniae* for 12 hours. Then, cells were fixed using glutaraldehyde and osmium tetroxide followed by dehydration with 75-100% ethanol. Subsequently, macrophages pellets were embedded in Araldite Resin followed by sectioning into ultra-thin (90nm) sections using a diamond knife in a Ultramicrotome. Next, images of each section were captured following Transmission Electron Microscopy using an attached Gatan digital camera after staining with uranyl acetate and lead acetate. Figure A shows the representative TEM image of mock-infected macrophages. Figure B shows the representative TEM image of macrophages after exposure to pneumococci. Figure C shows the average number of cristae per mitochondrion in mock-infected and pneumococci exposed macrophages. Cristae number was counted from the ultrastructural images of mitochondria, from two independent TEM experiments. Data are shown as mean ± SD and statistical analysis was performed with paired t-test. **p=0.0016. Scale bars = 500nm/0.5µm.

5.7. Fragmented mitochondria stay proximal to the lysosome/phagolysosome

In the previous chapter, I have shown that mitochondrial ROS are generated close to the phagosome/phagolysosome and engage in intracellular bacterial killing. Recently West et al. have demonstrated that mitochondria also translocate to the phagosome and trigger mROS production, participating in intracellular bacterial killing. They have also shown that mROS is generated via TLR-mediated signally involving tumour necrosis factor receptor-associated factor 6 (TRAF6), which in turn activates evolutionarily conserved signalling intermediate in Toll pathways (ECSIT) a protein contributing to mitochondrial respiratory chain assembly to enable intracellular killing in the phagosome/phagolysosome (West et al., 2011a).

To investigate whether the fragmented mitochondria following bacterial challenge were associated with the phagolysosomes, mitochondrial (e.g. Tom20) and lysosomal/phagolysosomal (e.g. LAMP1- lysosome-associated membrane protein 1) markers were co-stained and immunofluorescence carried out. Co-stained fluorescence images of macrophages after bacterial internalisation demonstrated that Tom20 on fragmented mitochondria co-localises or is proximal with LAMP1, whereas in mock-infected macrophages co-localisation was not apparent (Figure 5.8A-B). This observation suggests that fragmented mitochondria in macrophages, following interaction with bacteria, and the associated production of mROS, are associated with phagolysosomes, to maximise mitochondrial-mediated innate immune responses against intracellular bacteria. For example, the orthogonal view of a representative z-stack fluorescence image illustrated that mitochondria, mROS and intracellular pneumococci are proximally associated in macrophages (Figure 5.8C).

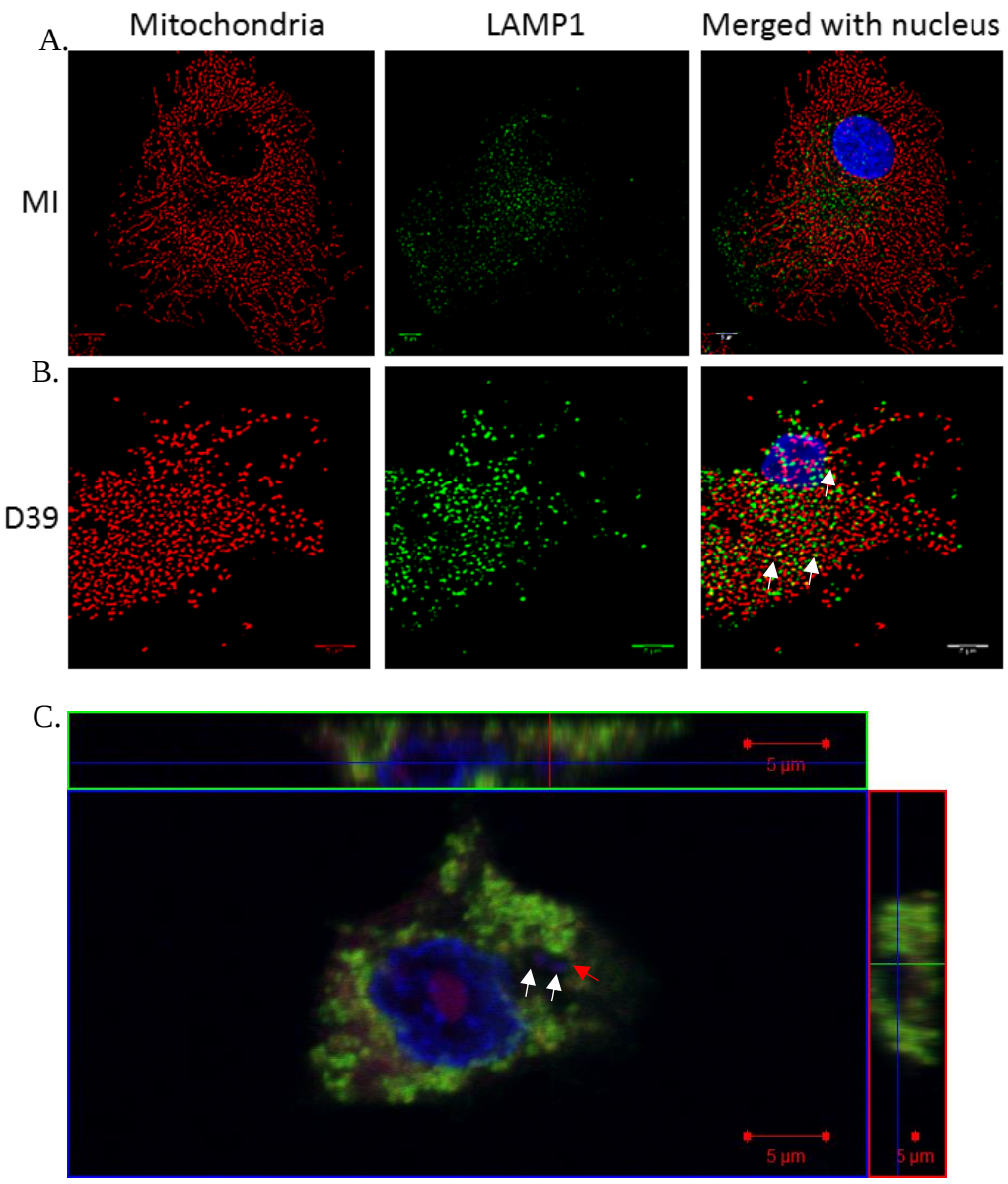

Figure 5.8. **Fragmented-mitochondria in response to pneumococci are associated with lysosomes/phagolysosomes.** Human MDM were exposed to *S. pneumoniae* (D39, MOI of 10) for 16 hours, and mitochondria and lysosomes/phagolysosomes were co-stained using rabbit anti-Tom20 (tagged with Alexa Fluor 568 labelled-red) and mouse anti-LAMP1 antibody (tagged with Alexa Fluor 488-green). Each panel shows the representative images of mitochondria and lysosomes/phagolysosomes in mock-infected (A), or pneumococci exposed macrophages (B). The white arrows in the panel B merged image shows the co-localised pixels (yellow) of Tom20 and LAMP1. Representative images were taken from three independent experiments. Figure C shows the orthogonal view of mitochondrial ROS probe MitoSox red (red), Tom20 (green) and D39 (blue) in the same compartment. The white arrows (in figure C) shows the mROS (red) blobs on D39 (blue) and red arrow shows the mitochondrial area which is overlapped with D39.

5.8. Inhibiting mitochondrial fission by 3-methyladenine decreases mROS production

Balanced mitochondrial dynamics (e.g. fission/fusion) are critical to maintain cellular homeostasis. In contrast, oxidative stress causes excessive mitochondrial fission/fragmentation, which is associated with mROS production and apoptosis in neuronal cells (Qi et al., 2013). In the literature, it has been shown that apart from Drp1/Fis1, mitochondrial protein MTP18 is also an important regulator of mitochondrial fission in mammalian cells (Tondera et al., 2005). Previously, this same group has also shown that MTP18 works as the downstream target of phosphatidyl-inositol-3 kinase (PI-3K) signalling. They have shown that PI-3K inhibition, by the pan-PI-3K inhibitor Ly294002 or anti-sense RNA, not only blocks mitochondrial membrane protein MTP18 expression at mRNA and protein levels, but also prevents fission-associated mitochondrial morphological alteration in HaCat/Cos-7 cells, which causes induction of apoptosis (Tondera et al., 2004). However, the latter observation is controversial because most of the literature suggests that mitochondrial fission rather than fusion occur as an upstream process of apoptosis (Suen et al., 2008). I hypothesised that PI-3K could also play a role in mitochondrial fission/fragmentation; following pneumococcal challenge. Therefore, mouse BMDM were pre-treated with the type I/III PI-3K inhibitor 3-methyladenine and challenged with pneumococci for 12 hours, then mitochondrial outer membrane specific Tom20 was labelled and immunofluorescence measured as before. Pneumococci challenge induced mitochondrial fission, diminishing mitochondrial network complexity/mitochondrial connectivity, however, this effect was reversed with 3-methyladenine treatment (Figure 5.9A-C). Moreover, 3-methyladenine also decreased mROS production from 12 hours onwards after pneumococcal challenge (Figure 5.9D).

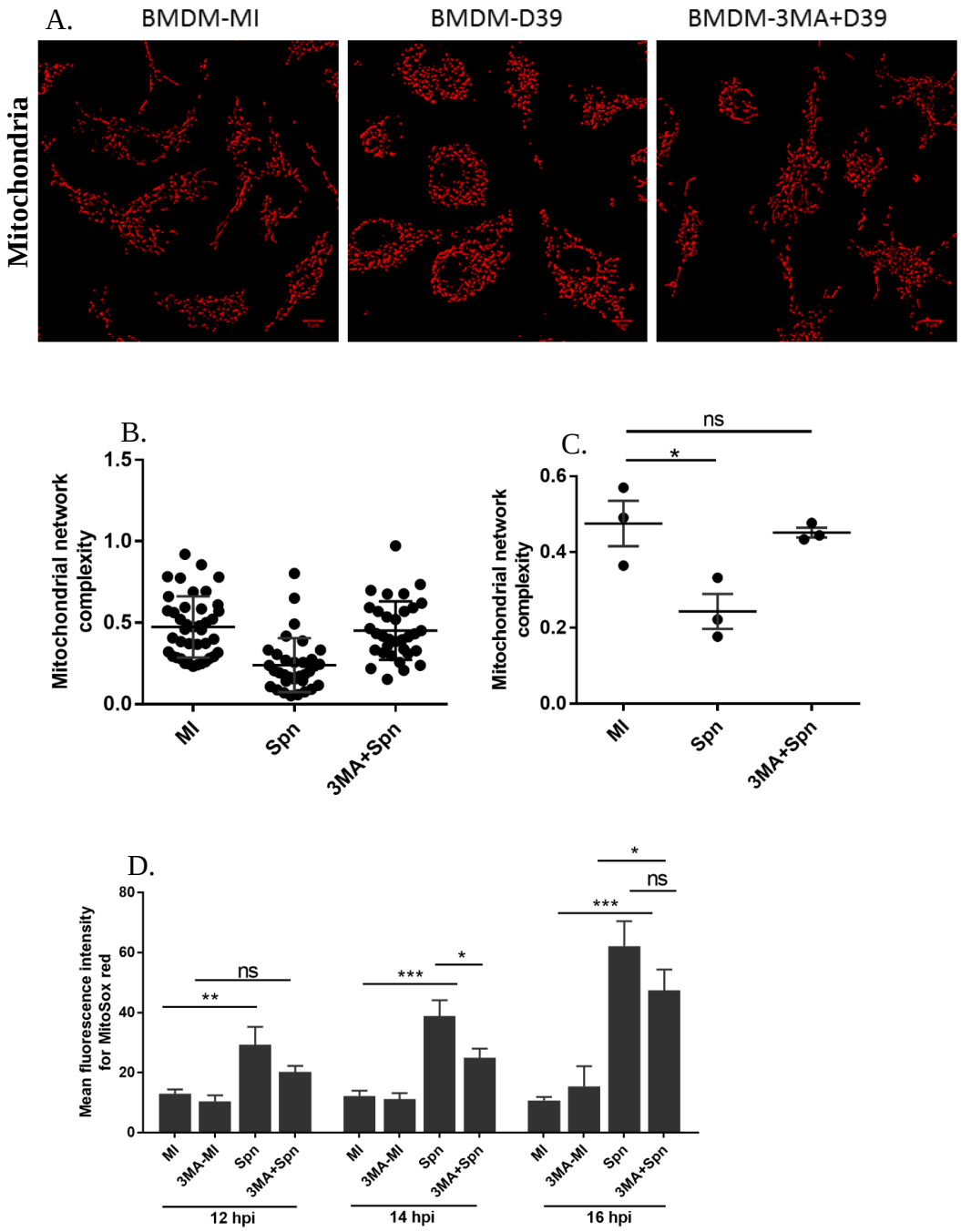

Figure 5.9. **The PI-3K inhibitor 3-methyladenine inhibits mitochondrial fission and mROS production in macrophages**. Mouse BMDM were pre-treated with 3-methyladenine (3MA) or Pan-PI-3K inhibitor (Ly294002) for 1 hour. Next, BMDM were exposed to *S. pneumoniae* (D39, MOI of 10) for 12 hours. The mitochondrial outer membrane specific marker Tom20 was labelled using rabbit anti-Tom20 primary antibody and a secondary goat anti-rabbit IgG conjugated with Alexa Fluor 568. Images were captured by Zeiss LSM510 confocal microscopy using 543nm excitation and 565-615nm emission spectrums. Figure A shows the representative mitochondrial images of BMDM after mock-infection (MI) or challenge with D39 in the untreated or 3MA pre-treated conditions, respectively. Figure B shows the mitochondrial network complexity of individual cell and figure C shows the average network complexity of each donor's macrophages, which was quantified by the ImageJ from the mitochondrial images of BMDM with mock-infected or D39 exposed for 12 hours, with or without 3MA pre-treatment condition (n=3). Figure D shows the mean fluorescence intensity for the mROS staining probe Mitosox red, from mouse

BMDM under the above mentioned conditions at 12, 14 and 16 hours time points. Data are shown as mean ± SD and statistical analysis was performed with one-way ANOVA and Bonferroni post-hoc test. *p<0.05, **p<0.01, ***p<0.001, *ns- non-significant, n=5.

5.9. Inhibition of PI-3K by 3MA restores mitochondrial inner transmembrane potential and decreases caspase activation

Mitochondrial fission/fragmentation downregulates mitochondrial oxidative phosphorylation, ATP production, permeabilises the mitochondrial outer membrane, causing membrane blebbing and induces loss of mitochondrial inner transmembrane potential. Moreover, it has been shown that cytochrome c, an apoptosis initiator is released in to the cytosol from mitochondria, during mitochondrial fission/fragmentation in Hela cells (Suen et al., 2008). Subsequently, cytochrome c activates caspases, to trigger apoptosis or programme cell death.

To assess macrophages mitochondrial inner transmembrane potential and caspase activity after challenge with pneumococci, macrophages were stained with the mitochondrial inner transmembrane potential sensitive and live cell dyes, JC-1 and NucView 530, respectively. JC-1 is aggregated in intact mitochondria with polarised inner transmembrane potential, and loss of JC-1 aggregates implies loss of mitochondrial inner transmembrane potential ($\Delta\psi_m$). NucView 530 carries a caspase 3/7 substrate-tagged with DNA intercalating fluorescence dye, which is detached in the presence of caspases and binds with nuclear DNA. JC-1 stained macrophages were measured by flow cytometry. NucView 530 positive macrophages were counted via fluorescence microscopy. Pneumococci noticeably induced loss of $\Delta\psi_m$ in macrophages 16 hours post-challenge, and the PI-3K inhibitor 3-methyladenine restored the loss of $\Delta\psi_m$ (Figure 5.10 A-B). Moreover, pneumococci also upregulated the activity of intrinsic apoptosis mediators, caspases 3 and 7, in macrophages, particularly after 16 hours bacterial exposure (Figure 5.10C), indicating that macrophage apoptosis occurs after mitochondrial fission. However, to further confirm this speculation, it would be important observe mitochondrial fission and apoptosis in the presence of caspase inhibitors (e.g the pan-caspase inhibitor z-VAD-fmk) and show that this block apoptosis but not fission.

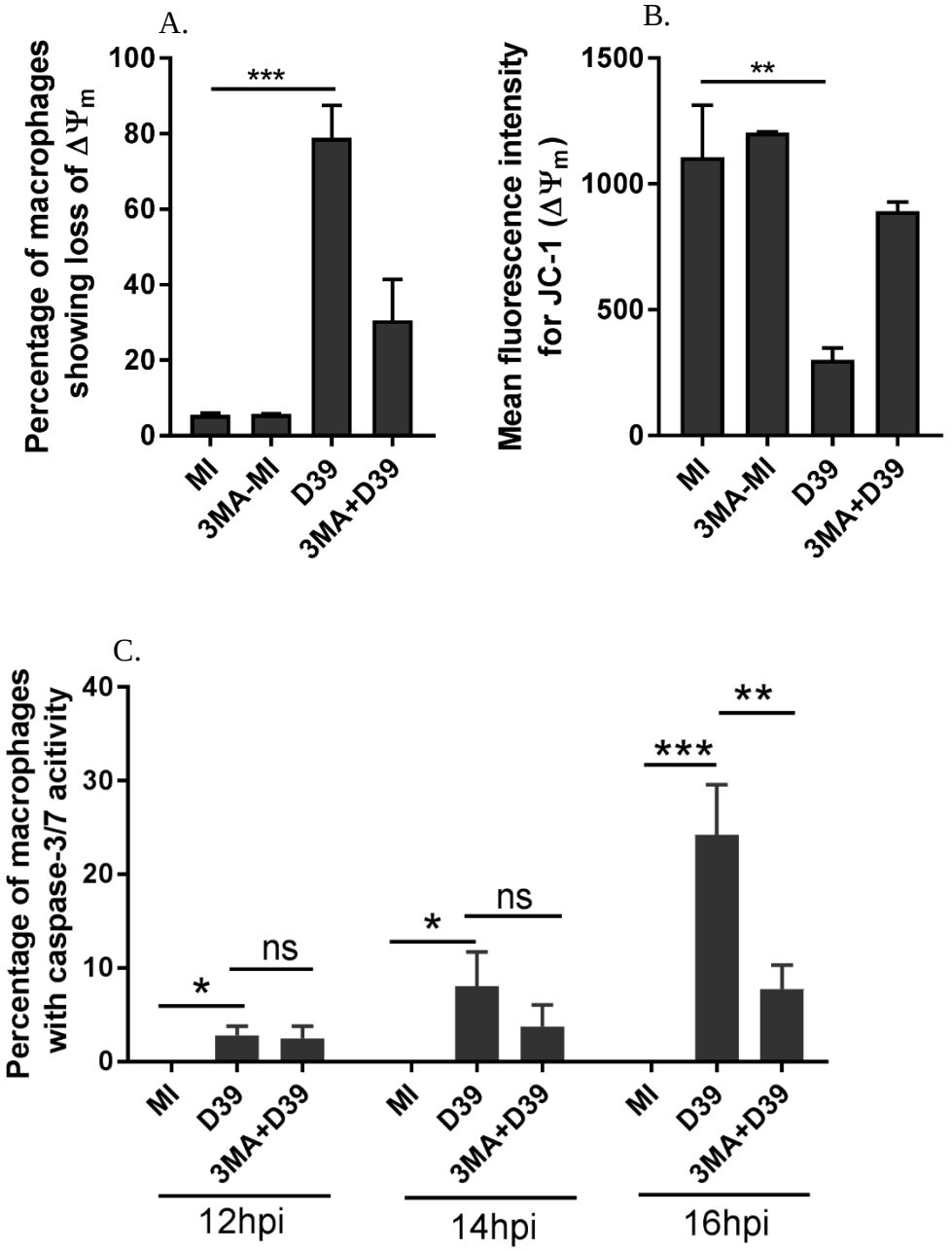

Figure 5.10. **The PI-3K inhibitor 3-methyladenine restores mitochondrial inner transmembrane potential and decreases macrophage apoptosis.** Mouse BMDM were pre-treated with 3-methyladenine (3MA) for 1 hour. Then, BMDM were exposed to *S. pneumoniae* (D39, MOI of 10) for 12, 14 or 16 hours. Figure A shows the percentage of macrophages showing loss of mitochondrial inner transmembrane potential ($\Delta\Psi_m$) or loss of JC-1 (5,5′,6,6′-tetrachloro-1,1′,3,3′-tetraethylbenzimidazolylcarbocyanine iodide) aggregates from the mitochondrial inner transmembrane, after 16 hours of bacterial exposure (n=3). Figure B shows the mean fluorescence intensity of mitochondrial inner membrane, calculated from the data shown in Figure A. Figure C shows the percentage of macrophages with caspase 3/7 activity after 12, 14 and 16 hours of bacterial challenge. Caspase 3/7 activity was numerically counted by fluorescence microscopy after live cell staining with NucView 530, a caspase 3/7 substrate tagged with a fluorogenic DNA-intercalating dye. Data are shown as mean ± SEM and statistical analysis (for figure A and B) was performed with one-way ANOVA and Bonferroni's post-hoc test. Figure C data were analysed with one-way ANOVA and Sidak's post-hoc test. *p<0.05, **p<0.01, ***p<0.001.

9.10. The PI-3K inhibitor, 3-methyladenine decreases intracellular bacterial killing

Previous research suggests that induction of autophagy in lung epithelial cells works as a host-protective mechanism against intracellular bacteria such as *Mycobacterium tuberculosis* (Guo et al., 2013) and *S. pneumoniae* (Li et al., 2015). Moreover, recently it has been shown that virulent *Mycobacterium tuberculosis* (H37Rv) evades autophagy-associated intracellular killing or xenophagy by modulating autophagosomal maturation in macrophages (Pallavi et al., 2015). However, I have not found an association of autophagy or mitophagy in a nutrient-rich cell culture model after pneumococcal challenge (Figure 5.6 and 5.7). Rather, my data (Figure 5.9) indicates that PI-3K signalling is a positive mediator of pneumococci induced mitochondrial fission and mROS production. Therefore, I hypothesised that PI-3K inhibition could also alter mROS-associated intracellular bacterial killing in macrophages.

To assess intracellular *S. pneumoniae* killing in macrophages, mouse BMDM were pre-treated with either the PI-3K inhibitor 3-methyladenine, the Drp1 assembly inhibitor Mdivi-1 or lysosomal fusion (with phagosomes) blocker bafilomycin A1. Macrophages were then challenged with pneumococci for 8, 12 and 16 hours, and a gentamycin protection assay carried out. The intracellular bacterial survival data suggest that 3MA, Mdivi-1 and bafilomycin A1 did not alter intracellular killing at 8 hours post-bacterial killing (Fig 5.11A). But 3-MA significantly decreased intracellular bacterial killing at 12 hours (circa 4-fold decrease) and 16 hours (circa 9-fold decrease) compared to untreated (vehicle) macrophages. Whereas, the Drp1 inhibitor Mdivi-1 did not noticeably alter killing at 8, 12 or 16 hours (Figure 5.11 B and C). Moreover, the lysosomal fusion inhibitor bafilomycin A1 did not alter intracellular killing at 8 or12 hours, but significantly decreased at 16 hours post-bacterial challenge (circa 7.5 fold decrease) (Figure 5.11B and C).

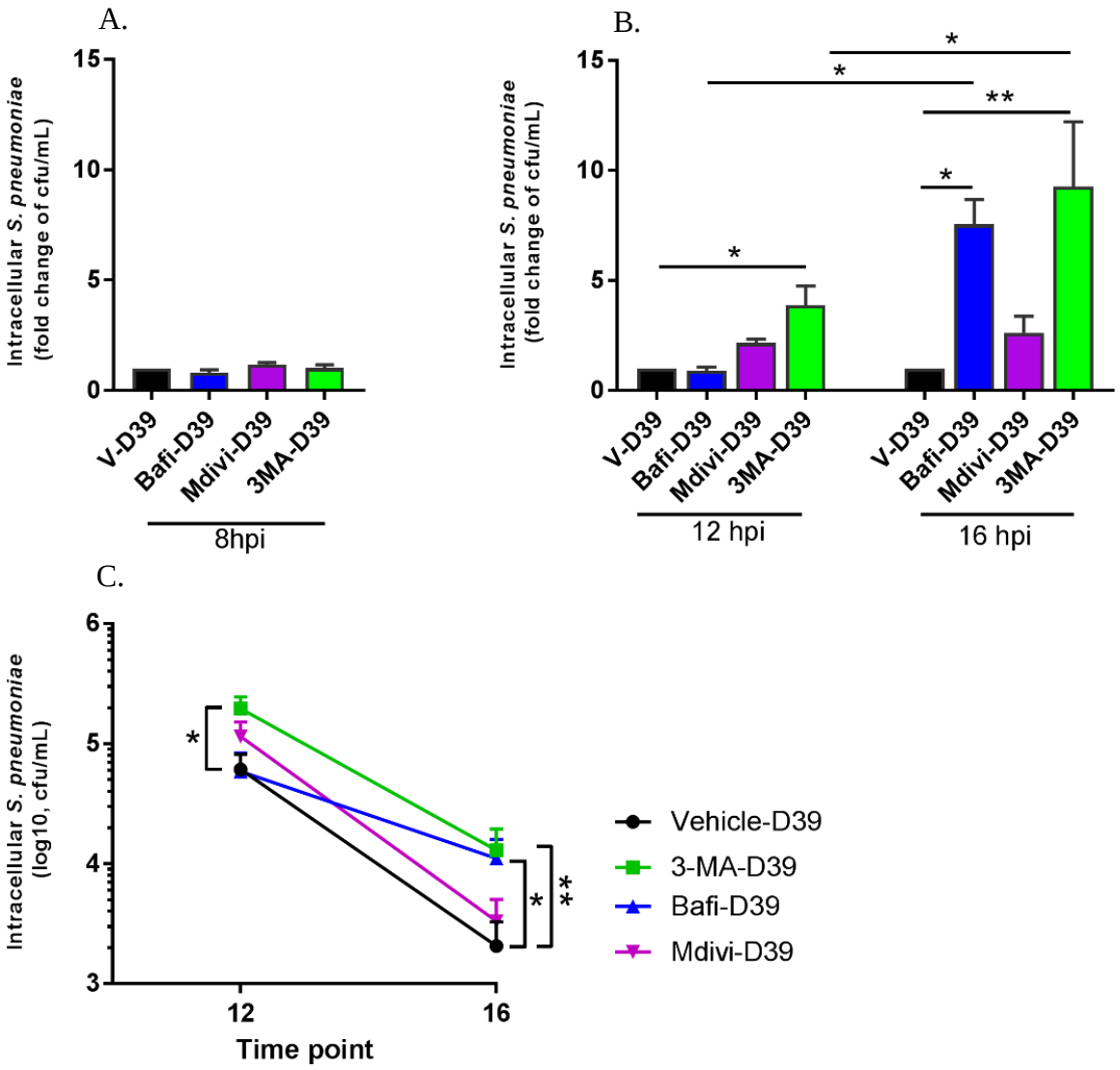

Figure 5.11. **Bafilomycin A1 and PI-3K inhibitor 3-methyladenine decreases intracellular bacterial killing.** Mouse BMDM were exposed to *S. pneumoniae* (D39, MOI of 10) for 8 hours, or 12 and 16 hours and a gentamycin protection assay was carried out. Briefly, for an 8 hour intracellular killing assay, cells were washed 3 times with PBS after 4 hours, then incubated 4 hours more with normal cell culture media, then cells were treated with gentamycin (20µg/mL) and penicillin (40megaU/mL) for 30 minutes to kill extracellular bacteria, before cell lysis (with 0.02% saponin) to assess intracellular pneumococci. In another set of experiment, for 12 hour time point, at 12 hours cells were treated with gentamycin plus penicillin for half an hour before cell lysis and estimation of colony forming units by Miles-Mirsa assay. For the 16 hour time point, after 12-hours incubation, cells were treated with gentamycin plus penicillin for half an hour, then incubated 4 hours more with vancomycin (0.75mg/mL), then lysed with 0.02% saponin and performed Miles-Mirsa serial dilution assay. Figure A shows the fold change in survival of intracellular pneumococci in macrophages after 8 hours and figures B shows 12 to 16 hours of bacterial challenge. Figure C shows the intracellular pneumococci growth curve (cfu/mL in a log10 scale) of 3-MA, bafilomycin A1 and Mdivi-1 pre-treated macrophages, after 12 and 16 hours post-bacterial challenge. Data are shown as mean ± SEM. Statistical analysis was performed with one-way ANOVA and Bonferroni's multiple comparison test, and paired t-test for pair-wise comparison between two-time points. *p<0.05, **p=0.005, n=6.

5.11. Discussion

In this chapter, I have observed that macrophages ingesting *S. pneumoniae* demonstrate altered mitochondrial dynamics, with increased mitochondrial fission or network fragmentation in human MDM and in mouse BMDM. Mitochondrial fission after pneumococcal phagocytosis occurs in a Drp1 independent non-canonical manner, like the fission previously described as triggered by the bacterial pore-forming toxin listeriolysin O in Hela cells (Stavru et al., 2011, Stavru et al., 2013). Moreover, the macrophage response to *S. pneumoniae* also upregulates Parkin (an E3 ubiquitin ligase) and induces Parkin translocation to fragmented mitochondria. In addition, I have also assessed the association of selective autophagy or mitophagy with fragmented mitochondria following bacterial challenge, and both my Immunostaining and Transmission electron microscopy findings demonstrate that fission in response to bacterial ingestion does not trigger mitophagy/autophagy. Moreover, in this chapter I have shown that mitochondrial fission following pneumococcal ingestion has a role in innate immunity, particularly mROS production and intracellular bacterial killing. These observations suggest that the mitochondrial dynamics of macrophages, especially fission, could represent a host-protective mechanism against intracellular bacteria.

In healthy cells, mitochondrial dynamics (e.g. fission/fusion) is a constant process, and is essential to maintain an interconnecting network and cellular homeostasis (Suen et al., 2008). For example, interruption of mitochondrial fusion causes the loss of mitochondrial inner transmembrane potential ($\Delta\psi_m$), as well as hampering of embryonic development (Chen et al., 2003). Whereas, defective mitochondrial fission is associated with increased inflammation in macrophages (Sangjun et al., 2015). In addition, mitochondria fission is universally linked with programmed cell death (i.e. apoptosis) (Suen et al., 2008). However, excessive fission can occur without triggering apoptosis. For example, FCCP-induced mitochondrial fission is reversible upon drug removal and it does not induce apoptosis (Richard and Mariusz, 2005). Rather FCCP-mediated excessive mitochondrial fission triggers autophagy or mitophagy (Narendra et al., 2008). Moreover, viral infection, for instance with cytomegalovirus (CMV), also induces mitochondrial fission/fragmentation which also does not induce apoptosis, as CMV viral proteins interact with pro-apoptotic Bcl-2 family members and blocks mitochondrial-associated apoptosis (Damien et al., 2004, Poncet et al., 2004). However, viral protein R of HIV-1 and hepatitis B virus protein HBx respectively interact with mitochondrial outer membrane protein VDAC and VDAC3, resulting in the opening of mPTP, loss of $\Delta\Psi_m$

and leading to massive mitochondrial fragmentation, and rapid programmed cell death (Jacotot et al., 2000, Rahmani et al., 2000).

On the other hand, the pathogenic bacteria, for example *Listeria monocytogenes,* induces Drp1 independent mitochondrial fragmentation and loss of $\Delta\psi_m$ through its pore-forming toxin listeriolysin O (LLO), which decreases respiration associated ATP production in Hela cells (Stavru et al., 2011, Stavru et al., 2013). I have observed that macrophages generating a host response to pneumococci demonstrate mitochondrial fission or fragmentation in primary macrophages. Moreover, the pharmacological fission inhibitor Mdivi-1, an assembly blocker of Drp1 with Fis1 (Cassidy-Stone et al., 2008), does not inhibit fission during the macrophage response to pneumococci, which implies that fission occurs in a non-canonical fashion. Since pneumolysin deficient pneumococci also trigger mitochondrial fragmentation in macrophages with a high bacterial dose (MOI of >40), my findings suggest pneumolysin related cholesterol dependent cytolysin is not essential for fission. Rather it appears pneumolysin may enhance the frequency of fission, but is dispensable for mitochondrial fission in macrophages after challenge with metabolically active pneumococci (figure 5.2). Previously my laboratory group has demonstrated that pneumolysin's pore-forming activity is not essential for apoptosis induction in macrophages although in this case there was very little apoptosis in the absence of pneumolysin (Bewley et al., 2014),whereas in my model fission still occur in the absence of apoptosis if the inoculum is high enough.

ER-mitochondria tethering is indispensable for mitochondrial fission (Friedman et al., 2011). F-actin filaments are required to regulate mitochondrial network fragmentation in DRP-1 dependent models of fission (De Vos et al., 2005). Inhibition of F-actin polymerisation with cytochalasin D inhibits LLO mediated non-canonical mitochondrial network fragmentation (Stavru et al., 2013). The latter observation implies that F-actin polymerisation could also be essential for pneumococci induced fission. However, I would not able to assess mitochondrial morphological network features in the presence intracellular pneumococci and cytochalasin D, because cytochalasin D inhibits >90% of pneumococcal internalisation (Ribes et al., 2010), as actin polymerisation is essential for phagocytosis and subsequent phagosome formation (Coppolino et al., 2001).

On the other hand, apart from Drp1/Fis1, the mitochondrial protein MTP18 is also an important regulator for mitochondrial fission in mammalian cells (Tondera et al., 2005). Moreover, MTP18 is a downstream target of PI-3K signalling, and genetic or chemical inhibition of PI-3K both downregulates MTP18 expression at transcriptional and

translational levels, but also decreases mitochondrial fission (Tondera et al., 2004). These observations align with my findings, where I have shown that pneumococci challenged macrophages, following pre-treatment with 3-methyladenine (3MA), a type I/III inhibitor of PI-3K, demonstrate decreased mitochondrial fission/fragmentation. Moreover, the macrophage response to pneumococci induces Parkin upregulation and translocation to fragmented mitochondria in macrophages. Admittedly, since 3MA pre-treatment appeared to reverse the increased Parkin recruitment to mitochondria following bacterial challenge, this observation further corroborated the suggestion that PI-3K played a role in fission regulation. It is well established Parkin is recruited to damaged mitochondria, and ubiquitinates the damaged mitochondrial proteins to activate their degradation in the 26S proteasome system (Yoshii et al., 2011).

In addition, Parkin activation and recruitment at extensively damaged mitochondria are essential to trigger selective autophagy or mitophagy and to minimise cellular toxicity (Narendra et al., 2008). I found no evidence of mitophagy or selective autophagy in macrophages after pneumococcal challenge. However, the mitochondrial oxidative phosphorylation uncoupler FCCP induced the autophagy marker LC3B and its recruitment to fragmented mitochondria, allowing FCCP to function as a positive control for mitophagy (Narendra et al., 2008). Apart from these roles, Parkin also has a role in innate immunity. For example, point mutations in Parkin's regulatory regions cause increased susceptibility to infectious diseases such as typhoid and leprosy, infections associated with intracellular pathogens (Ali et al., 2006, Mira et al., 2004). In addition, Parkin interacts with the mitochondrial TSPO-VDAC1 protein complex to aid innate immunity against bacterial infection in Drosophila (Cho et al., 2015). Interestingly, TSPO blocks mitophagy, allowing accumulation of dysfunctional mitochondria, and TSPO interaction with VDAC1 diminishes mitochondrial coupling and triggers ROS production in fibroblasts (Gatliff et al., 2014). I have also observed that the macrophage response to pneumococci induces mROS production along with fragmented mitochondria, instead of recruiting autophagy or mitophagy pro-survival machinery in macrophages. Presumably, mitochondrial fission-associated fragmentation augments mROS production (Yu et al., 2006).

Although I have not found an association between the macrophage host response to pneumococci-associated mitochondrial fission and autophagy/mitophagy in macrophages, I do observe fragmented mitochondria producing mROS are proximal to lysosomes/phagolysosomes, inferring the signature of a mitochondrial innate immune

response to intracellular bacterial cues. Interestingly, the interaction of mitochondria and mROS with bacteria-containing phagolysosomes are considered a new avenue of mitochondria mediated innate immunity against intracellular bacteria (West et al., 2011b). Moreover, recent publications by my host group and others also suggested that mROS is essential for intracellular bacterial killing (Bewley et al., 2017, West et al., 2011a).

In addition, PI-3K inhibition by 3-MA decreases mROS production in macrophages challenged with pneumococci, however, it is not clear how PI-3K decreased mROS production. Perhaps, it could be a direct result of the downregulation of mitochondrial fission/fragmentation by 3-MA. Besides, recently it has been shown that Akt1, a downstream target of PI-3K signalling, increases mROS production in alveolar macrophages during pulmonary fibrosis (Larson-Casey et al., 2016), suggesting that 3-MA inhibition of mROS production may involve PI-3K mediated Akt1 activation. Interpretation of PI-3K inhibition could be confounded by differential effects on phagocytosis since PI-3K signalling is involved in phagocytosis of larger opsonised objects (Daniel et al., 2015) and PI-3K blocks phagocytosis of a broad-spectrum of IgG and complement opsonised particles or of unopsonised zymosan and bacteria (Aderem, 2003).

Recent data, however, suggests PI-3K is dispensable for the ingestion of IgG opsonised particles ≤5 μm which would be the size range of opsonised pneumococci (Daniel et al., 2015) My host group has recently demonstrated that PI-3K-specific inhibitors do not alter uptake of unopsonised *S. pneumoniae* or earlier intracellular killing in macrophages (Martin et al.). Although my bacteria were opsonised I have also observed that 3MA does not alter intracellular bacterial numbers at 8 hours before fission occurred, and in fact I found increased numbers of bacteria from 12 hours onwards, so the reduction in fission does not appear to be a consequence of reduced phagocytosis and intracellular bacterial burden following use of the PI-3K inhibitor. Macrophage responses result in gradual increases in mROS production over time with highest levels being observed after caspase induction when mROS plays its main role in the late phase of apoptosis-associated killing (Bewley et al., 2017). Thus, the 3-MA mediated reduction in killing at 16 hours could reflect a reduction in mROS associated with apoptosis induction and be a consequence of PI-3K inhibition of apoptosis induction or the mitochondrial fission that precedes apoptosis and therefore may be necessary to maximise mROS release during apoptosis (Karbowski, 2010). At earlier times (e.g. 12 hours) the 3-MA mediated decrease in killing

could be linked to a decrease in mROS production from mitochondria undergoing fission before apoptosis induction, although further experiments would be needed to block this phase of killing with an mROS inhibitor such as MitoTEMPO and to increase the number of experiments measuring mROS to determine if the apparent reduction by 3-MA was significant.

Finally, mitochondrial fission is associated with apoptosis. I have also observed that inhibition of fission by 3-MA also decreases activity of caspase 3/7 (apoptosis executioners), especially at a late time point (e.g. 16 hour) when apoptosis occurs in this infection model (Marriott et al., 2005). In addition, 3-MA also reduced loss of $\Delta\psi_m$ in macrophages exposed to pneumococci. My host groups previous publications demonstrated that apoptosis triggers more mROS and re-engages intracellular killing when it has become exhausted via the mechanism of apoptosis-associated intracellular killing (Bewley et al., 2017, Jubrail et al., 2016). These suggest that 3-MA not only down-regulates fission-associated mROS production, but also limits apoptosis-associated intracellular killing. A potential link could be via Parkin which as Carroll *et al.*, have shown can induce ubiquitination and downregulation of Mcl-1, which is a key regulator of apoptosis in this infection model in macrophages (Carroll et al., 2014, Marriott et al., 2005).

Overall, this section shows that macrophages engaging in innate responses to *S. pneumoniae* not only modulate mitochondrial dynamics but also recruits Parkin to mitochondria which are likely to becoming dysfunctional with loss of $\Delta\psi_m$. Conversely, the confocal and electron microscopy data suggest that these fragmented mitochondria in macrophages responding to pneumococci do not activate macroautophagy/mitophagy. Rather the fragmented mitochondria produce mROS and engage with phagolysosomes to kill intracellular bacteria. Ultimately the fragmented mitochondria, which preceded caspase activation appear to facilitate downstream apoptosis activation which results in caspase activation and further increases in mROS to enhance intracellular bacterial killing.

Chapter 6. General Discussion

6.1. Background discussion

S. pneumoniae is one of the major causative agents of community-acquired pneumonia. Macrophages are a critical cellular effector of innate immune responses against *S. pneumoniae*. In this thesis I have focused on host-pathogen interactions at the cellular level, particularly focusing on macrophage compartments involving mitochondria and phagolysosomes and their relationship to critical microbicidals, mROS and NO and internalised pneumococci. I have also focused on the pneumococcal effect on the human monocyte-derived macrophages metabolic phenotype and examined the impact of the HIV-1 glycoprotein gp120 and of COPD on metabolic phenotype. Macrophages sense bacteria rapidly via cell membrane and cytoplasmic pattern recognition receptors and demonstrate plasticity in morphology, functional phenotype and metabolism. Moreover, macrophages adapt these responses to recruit appropriate antimicrobial responses following phagocytosis. These responses include mitochondria-mediated responses such as generation of mROS and apoptosis, to eradicate intracellular bacteria. This thesis has explored novel mitochondrial dynamics relating to anti-microbial strategies against intracellular bacteria. Mitochondria are considered the metabolic hub of eukaryotic cells and the major supplier of cellular energy, which is essential for immune cells physiological functions such as migration and phagocytosis (Buttgereit et al., 2000). Furthermore, mitochondrial immunometabolism and dynamics are essential components for cellular homeostasis.

6.2. Key findings in the study

I have assessed macrophage metabolic phenotypes and carried out functional experiments with mouse bone marrow-derived macrophages and human monocyte-derived macrophages (MDM). I report that *S. pneumoniae* rewires macrophages metabolism from oxidative phosphorylation (OXPHOS) to glycolysis, and that overexpression of the human Mcl-1 protein in mouse BMDMs modulates baseline mitochondrial respiration capacity. Moreover, pneumococci also increase proton and electron leak from the mitochondrial inner membrane during mitochondrial OXPHOS. As a result, *S. pneumoniae* diminishes inner mitochondrial transmembrane potential ($\Delta\Psi_m$), ATP-linked OXPHOS and augments mROS production. Apart from this, this thesis also reported that macrophage mROS and NO are engaged with intracellular pneumococci in phagolysosomes (Bewley et al., 2017).

In addition, I have also reported that macrophage mitochondrial respiration is further decreased in MDMs following pneumococcal challenge in MDM derived from a COPD cohort, when compared to age-matched health volunteers. This thesis reported that the HIV-1 glycoprotein gp120 diminishes both baseline and pneumococcal induced proton leak, which upheld Collini and colleagues recent observation on preservation of intact mitochondrial inner transmembrane potential in gp120 pre-treated MDM in the same infection model. These findings bring a plausible explanation as to why alveolar macrophages from HIV-1 seropositive cohorts cannot enhance mROS generation after challenge with pneumococci (Collini et al., 2018). Although proton uncoupling can limit mROS generation (Jastroch et al., 2010) presumably, excessive proton leak can enhance mROS production due to loss of inner mitochondrial transmembrane potential, activation of caspases and inhibition of Complex I, -a major mROS production site (Ricci et al., 2003).

In addition, this thesis also showed that metabolically active pneumococci induce noncanonical mitochondrial fission which has a positive role in facilitating intracellular bacterial killing. Instead of autophagy or selective mitophagy, fragmented mitochondria recruit the E3 ubiquitin Parkin, a determinant of mitochondrial quality. Moreover, 3-methyladenine a type I/III inhibitor of PI-3K not only inhibits pneumococcal induced mitochondrial fission but also protects $\Delta\Psi_m$ and decreases mROS production, apoptosis and intracellular bacterial killing in macrophages. All the above mentioned key findings are summarised as a table below.

Table 6.1. Summary of key findings of all models

Cell model	Challenge with *S. pneumonaie*/stimuli	Host Responses	
		Metabolic phenotype/response	**Mitochondrial fission/fragmentation**
i.Mouse BMDM	Heat inactivated *S. pneumoniae*	-Increases the maximum glycolytic capacity.	-No effect on mitochondrial fission
	Metabolically active wild type *S. pneumoniae*	-Increases basal and maximum glycolytic metabolism, -Decreases mitochondrial respiration capacity and ATP-linked OCR, -Increases proton leak and mROS production.	-Induces Drp1 independent mitochondrial fragmentation, -Upregulates Parkin expression and recruits them to mitochondria, -Does not recruit mitophagy or double membrane vacuole to fragmented mitochondria. -Mitochondrial fission occurs prior to apoptosis.
	LPS and INFγ	-Increases both basal and maximum glycolytic capacity.	Did not investigate yet.
	IL-4	-No effect on glycolytic metabolism.	Did not investigate yet.
	Pneumolysin mutant or deficient *S. pneumoniae*	Did not investigate yet.	-Insignificant effect with low burden of bacteria (e.g. MOI of 10), -Induces mitochondrial fragmentation with a higher MOI (e.g. MOI ≥40).
	Exogenous pneumolysin	Did not investigate yet.	-Induces mitochondrial fragmentation with a higher titre (e.g. ≥2μg/mL).

ii.Human MDM	Challenge with metabolically active wild type *S. pneumoniae*	-Increases basal and maximum glycolytic metabolism, -Decreases mitochondrial respiration capacity and ATP-linked OCR, -Increases proton leak.	Did not investigate yet.
iii. HIV infection model	Human MDM pre-treated with HIV-1 recombinant gp120 and challenge with *S. pneumoniae*	-Increases basal and maximum glycolytic metabolism, -Decreases mitochondrial respiration capacity and ATP-linked OCR, -Increases proton leak but gp120 decreases the baseline proton leak.	Did not investigate yet.
iv. COPD infection model	COPD MDM Challenge with *S. pneumoniae*	-Decreases both baseline and pneumococci induce mitochondrial respiration capacity and respiration reserve. -Decreases baseline ATP-linked OCR, -Increases baseline proton leak.	Did not investigate yet.

6.3. Macrophages metabolic phenotype and its role in controlling internalised bacteria

Immunometabolism is considered a fast evolving research area which investigates how the metabolic phenotype of immune cells achieves effective function in response to distinct microenvironmental cues (Geeraerts et al., 2017). From the literature it has been shown that M1 macrophages are mostly dependent on glycolysis rather than OXPHOS, whereas M2 macrophages rely on mitochondrial metabolism for their physiological function (Haschemi et al., 2012). Moreover, LPS or IFNγ stimulated M1 macrophages produce pro-inflammatory cytokines and microbicidal reactive nitrogen and oxygen species, whereas IL-4/13 stimulated M2 macrophages produce anti-inflammatory cytokines and anti-parasitic mediators (e.g. polyamines) (Galvan-Pena and O'Neill, 2014). Recently, it has been shown that bacterial endotoxin LPS and IFNγ activated macrophages accumulate TCA cycle intermediates succinate and citrate (reviewed by (Geeraerts et al., 2017). Subsequently the accumulated citrate acts as a precursor of itaconic acid – a macrophage-specific metabolite which has an anti-microbial role against intracellular bacteria (Alessandro et al., 2013). LPS/IFNγ (classical activation) upregulates the immune-responsive gene 1 (irg1) which encodes the itaconic acid producing enzyme cis-aconitate decarboxylase (Jha et al., 2015).

Like classical activation, pneumococci stimulate macrophages to develop M1-like characteristics, such as generation of pro-inflammatory cytokines (Bewley mBIO) and indicible nitric oxide synthase (Marriott FasebJ). Therefore, activation of macrophages towards an M1 metabolic phenotype, is not unexpected and since studies suggest these metabolic function may drive immune effector functions further driving this phenotype could help macrophages handle pneumococci more effectively, particularly in conditions like COPD where activation may not show the required classical polarisation (Shaykhiev et al., 2009a), as a potential way to cope with intracellular bacteria.

6.4. Importance of mitochondrial dynamics in innate responses against ingested extracellular bacteria

Mitochondrial dynamics (fission and fusion) represent a continuous process which maintains cellular homeostasis. Although mitochondrial fission is an upstream process in mitophagy (Narendra et al., 2008), I observed that pneumococcal challenge induced fragmented mitochondria that do not recruit the autophagy or mitophagy marker LC3B, and do not form double membrane vacuoles around fragmented mitochondria. Rather the

fragmented mitochondria produce mROS in close proximity to lysosomes/phagolysosomes, implying that fission might have an anti-microbial role. 3-MA not only inhibits mitochondrial fission and protects mitochondrial inner transmembrane potential, but also decreases mROS production as well as intracellular pneumococcal killing. Thus I have postulated that fission is an upstream process of apoptosis as reviewed in (Suen et al., 2008). Besides I have also observed that Parkin, a ubiquitin E3 ligase, is recruited to fragmented mitochondria following pneumococcal challenge which, as Carroll *et al.*, have shown, can induce ubiquitination and downregulation of the anti-apoptotic protein Mcl-1, a key regulator of apoptosis-associated killing of ingested extracellular bacteria in macrophages (Carroll et al., 2014, Marriott et al., 2005).

Moreover, previous research also demonstrated that mitochondrial fission augments mROS production (Yu et al., 2006). Apart from this, macrophage apoptosis is essential to resolve lung inflammation during chronic diseases (e.g. COPD) (Robb et al., 2016). Therefore, mitochondrial fission and subsequent apoptotic pathways in macrophages might be a potential therapeutic target to eradicate internalised extracellular bacteria as well as control chronic tissue inflammation.

6.5. Limitations

Although I have discussed possible caveats in each results chapter, biological techniques and research with *in vitro* or *ex vivo* cell models always have some limitations. For example, the metabolic phenotype of macrophages was assessed by the Extracellular flux analyser (e.g. XF24), which can only measure the major metabolic outputs such as glycolytic rate and mitochondrial OXPHOS rate in a real time basis. However, individual metabolites or other metabolic pathways, such as fatty acid oxidation (β-oxidation) or the pentose phosphate pathway would not be measurable with the XF24 flux analyser. Whereas NMR or Mass spectrometry could measure total cellular metabolites, which more directly implies the metabolic phenotype of cells. Moreover, this research was conducted with either human circulatory MDM or mouse BMDM which do not represent exact lung tissue macrophages (e.g. alveolar macrophages). Therefore, it is needed to further confirm these findings with alveolar macrophages.

In addition, mitochondrial fission is reported as a non-canonical fission which occurs in a Drp-1 independent manner. However, possible mediators causing the non-canonical

fission, are yet to be identified. However, the mitochondrial co-staining with phosphorylated Drp1 or LC3B could not able to check with mouse cell model because available matching species of mitochondrial Tom20 antibody (mouse anti-Tom20) did not bind with mouse macrophages mitochondrial Tom20. Although I had rabbit anti-Tom20 antibody which binds with mouse macrophages mitochondrial Tom20, the species overlaps with available species raised p-Drp1 or LC3B primary antibodies species (i.e. Rabbit). In addition, the mitochondrial fission-associated intracellular bacterial killing needs further confirmation, using genetic manipulation or with more specific pharmacological inhibitors of PI-3K (e.g. PI-3K γ or δ-inhibitors) rather than the relatively non-specific inhibition provided by 3-methyladenine. All findings in this thesis are based on *in vitro* or *ex vivo* infection cell models, and therefore a relevant *in vivo* mouse or zebrafish model is warranted to elucidate mitochondrial dynamics and its role to internalised bacteria. Besides, all infection related experiments in this thesis are carried out with opsonised type 2 serotype of *S. pneumoniae* (D39), and therefore the *in vivo* infection study should be conducted with more relevant clinical serotypes (e.g. S14) and with other extracellular bacteria.

6.6. Hypothetical model

Some major findings of this thesis are linked with other bacterial infection related mouse models in the literature described by other key papers on this topic (West et al., 2011b, Roca and Ramakrishnan, 2013, Sonoda et al., 2007). The major sites of electron leak and mROS production are Complex I and III in the mitochondrial inner membrane, and mROS are produced adjacent to phagolysosomes to kill internalised pneumococci (Bewley et al., 2017). Similarly West and colleagues demonstrated that TLR1/2 and 4-agonists allow the TLR adaptor protein tumour necrosis factor receptor-associated factor 6 (TRAF6) to translocate to the mitochondria where it interacts with evolutionary conserved signalling intermediate in Toll pathways (ECSIT), allowing its ubiquitination. ECSIT plays a role enabling assembly of Complex I of the electron transport chain, and triggering mROS production in proximity to the phagolysosome (West et al., 2011a).

Moreover, like other classical stimuli, *S. pneumoniae* switches the macrophage metabolic phenotype from OXPHOS to glycolysis. This metabolic reprogramming and modification of Complex I assembly modifies proton and electron leakage, reorientates mitochondrial electron transfer away from ATP generation and instead promotes mROS production in pneumococci challenged macrophages. I hypothesise that intracellular oxidative stress

and mitochondrial protein modification induce irreversible mitochondrial fission that further increases mROS production. Subsequently, *S. pneumoniae* challenged macrophages with fragmented mitochondria lose their inner mitochondrial transmembrane potential and further diminish their ATP-linked OXPHOS. Consequently macrophages rely on glycolysis for energy production as the role of mitochondria shifts away from effective ATP generation and rather mROS production. Parkin is also recruited to these fragmented and depolarised mitochondria. But instead of autophagy marker recruitment - a pro-survival process - fragmented mitochondria develop mitochondrial outer membrane permeabilisation, potentially due to the extent of the mitochondrial changes and release cytochrome c which activates the apoptososme and caspase 9 activation upstream of caspase 3/7 to execute programmed cell death via apoptosis. Previously my host group has demonstrated that mROS production also increases with apoptosis, which kills internalised bacteria as an apoptosis-associated bacterial killing mechanism (Bewley et al., 2017). My model shows how metabolism and mitochondrial dynamics upstream of this also promote mROS and lead to conditions which make the cell susceptible to apoptosis.

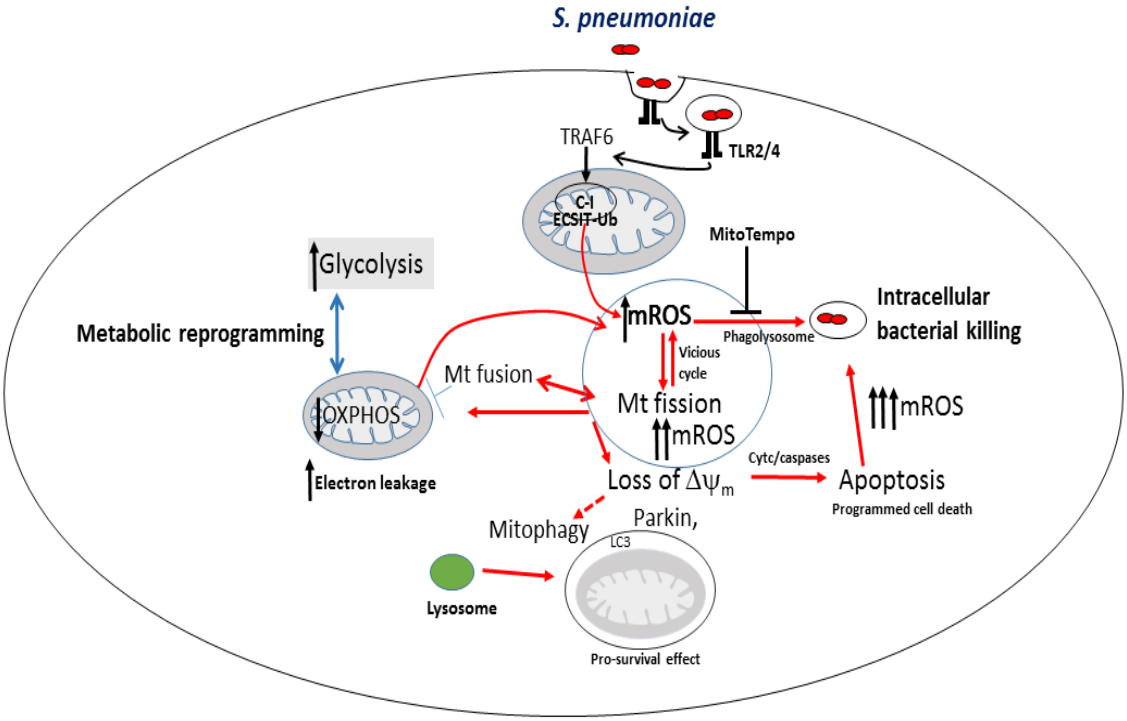

Figure 6.1. **Schematic diagram of my hypothetical model.** Opsonised pneumococci are internalised and like the *Salmonella* infection model could also activate TRAF6 signalling pathway and ubiquitinate ECSIT leading to assembly of complex I of the mitochondrial electron transport chain and induce mROS production, described in (West et al., 2011a). On the other hand, pneumococci stimulate metabolic reprogramming and trigger mitochondrial fission in

macrophages. Fragmented mitochondria develop loss of inner mitochondrial transmembrane potential ($\Delta\Psi_m$) and ultimately accumulate Parkin, but activate the intrinsic programmed cell death pathway rather than engage mitophagy as a pro-survival effect. In addition, mROS or apoptosis-associated mROS are produced adjacent to internalised pneumococci in phagolysosomes. MitoTempo inhibits intracellular bacterial killing by scavenging mROS. ECSIT –Evolutionary conserved signalling intermediate in Toll pathways, C-I –Complex I, TLR –Toll-like receptor, TRAF6 –Tumour necrosis factor receptor-associated factor 6, Mt –Mitochondria, Ub –ubiquitination, mROS –Mitochondrial reactive oxygen species, LC3 –Microtubule associated protein light chain 3.

6.7. Future work directions

i. It is essential to further confirm the link between immuno-metabolism and mitochondrial dynamics in *in vivo* infection models.
ii. It would be important to observe macrophages mitochondrial metabolism after challenge with pneumolysin mutant *S. pneumoniae*.
iii. It would be important to perform live cell imaging with a transfected fluorochrome marker of mitochondria is essential for bone-fide evidence of mitochondrial fission and its downstream consequences in macrophages.
iv. I would like to develop a Parkin knock out or overexpression macrophage cell model, to characterise its relationship to fission and its consequences for apoptosis and intracellular bacterial killing.
v. It would be important to identify the molecular pathway associated with non-canonical fission.
vi. I would need to further confirm that mitochondrial apoptosis acts as a downstream process of fission by applying appropriate caspase inhibitors (e.g. pan-caspase inhibitor z-VAD-fmk) and showing these do not alter fission only apoptosis, in order to confirm fission is not an artefact of apoptosis (even though my time course experiments argue against this since fission precedes apoptosis).

6.8. Conclusions

This thesis demonstrates that *S. pneumoniae* modulates macrophage metabolic phenotype and manipulates mitochondrial morphology. Like classical activation, pneumococci stimulate macrophages into a pro-inflammatory phenotype, which turns on aerobic glycolysis and augments mROS and NO production. The latter are engaged with intracellular pneumococci in the phagolysosome. Moreover, mitochondrial fission allows development of a host-protective mechanism to kill internalised pneumococci in

macrophages and shifts the mitochondrial function away from OXPHOS-linked ATP generation to mROS generation. This provides a potent but time-limited microbicidal response which ultimately ends in programmed cell death.

Chapter 7: Appendices

7.1 XF assay medium for Glycol-stress test (200 mL)

Reagents	Amount
XF assay media	196 mL
L-glutamine (200mM)	2 mL
Penicillin/Streptomycin	2 mL
D-glucose (anhydrous)	0.90 g (4.5 g/L)
Adjust pH 7.4 with 1.0 M NaOH and passed through 0.22 µm filter	

7.2 XF assay medium for Mito-stress test (200 mL)

Reagents	Amount
XF assay media	194 mL
L-glutamine (200mM)	2 mL
Sodium-pyruvate (100mM)	2 mL
Penicillin/Streptomycin	2 mL
D-glucose (anhydrous)	0.90 g (4.5 g/L)
Adjust pH 7.4 with 1.0 M NaOH and passed through 0.22 µm filter	

7.3 Brain hear infusion broth (BHI broth) preparation (200 mL)

Reagents	Amount
BHI powder (Oxoid, CM1135)	7.4 g
Distilled water	200 mL
Autoclaved at 121^{o}C for 15 minutes	

7.4 Quenching solution for Immunofluorescence assay (500 mL)

Reagents	Amount
PBS (1x)	500 mL
Triton-x-100	500 µL (0.1 %)
Ammonium chloride (NH_4Cl)	1.34 g

7.5 Blocking/PGAT solution for Immunofluorescence assay

Reagents	Amount
PBS (1x)	500 mL
Gelatine	1.0 g (0.2 %)
Triton-x-100	50 µL (0.01 %)
Sodium-Azide	0.1 g (0.02 %)

7.6 Reagents used in Western blotting

i. Lysis buffer for cytosolic and mitochondrial fractions (10 mL)

Reagents	Amount
PBS (1x)	7.5 mL
0.1 M NaH_2PO_4	200 µL
0.2 M Na_2HPO_4	800 µL
1.0 M NaCl	1.5 mL
Add 3.75 µL digitonin (5% stock) in 1 mL lysis buffer [or add 9.38 µg digitonin per million cells); Add 1:25 complete protease inhibitor (Roche) [Stock: Add 1 tablet to 2 mL distilled water].	

ii. 2x Sample buffer (for 25 mL)

Reagents	Amount
20% SDS	5 mL
Glycerol	5 mL
Bromophenol Blue	0.5 mL
2-Mercaptoethanol	2.5 mL
Tris HCl pH 6.8	6.25 mL
Water	5.75 mL

iii. Stacking gel preparation (5% for 2 gels)

Reagents	Amount
Distilled water	6 mL
40% Acrylamide	1240 µL
0.5M Tris buffer pH 6.8	2520 µL
20% sodium dodecyl sulphate (SDS)	50 µL
20% Ammonium persulphate (APS)	100 µL
Tetramethyl ethylene diamine (TEMED)	10 µL

iv. Resolving gel preparation (12% for 2 gels)

Reagents	Amount
Distilled water	9.9 mL
40% Acrylamide	6.8 mL
1.5M Tris buffer pH 8	5.8 mL

20% sodium dodecyl sulphate (SDS)	112.5 µL
20% Ammonium persulphate (APS)	225 µL
Tetramethyl ethylene diamine (TEMED)	9 µL

v. 10x Running buffer

Reagents	Amount
Glycine (Fisher Scientific)	190 g
Tris Base (Fisher Scientific)	30.3 g
20% SDS solution	50 mL
Distilled water	Up to 1000 mL

vi. 1x Running buffer

Reagents	Amount
10x Running buffer	100 mL
Distilled water	900 mL

vii. 1x Transfer buffer

Reagents	Amount
Glycine (Fisher Scientific)	2.9 g
Tris Base (Fisher Scientific)	1.45 g
20% SDS solution	925 µL
Methanol	100 mL
Distilled water	500 mL

viii. 10x TBS

Reagents	Amount
Tris-HCl 1.0 M pH 8.0 (Bio-Rad Lab)	100 mL
NaCl (Fisher Scientific)	97.3 g
Distilled water	Up to 1000 mL

iX. 10x TBS-Tween

Reagents	Amount
Tris-HCl 1.0 M pH 8.0 (Bio-Rad Lab)	100 mL
NaCl (Fisher Scientific)	97.3 g
Tween-20 (Fisher Scientific)	5 mL
Distilled water	Up to 1000 mL

X. Blocking solution (5% skimmed milk) (40 mL)

Reagents	Amount
Skim milk powder (Sigma-aldrich)	2 g
1x TBS-tween	40 mL

7.7 Araldite resin preparation (20 mL) (for TEM assay)

Reagents	Amount
CY212 resin	10 mL
DDSA hardener	10 mL
BDMA accelerator	1 drop per 1 mL of resin mixture

7.8 Growth of *S. pneumoniae* in cell culture media with mitochondrial fission inhibitors

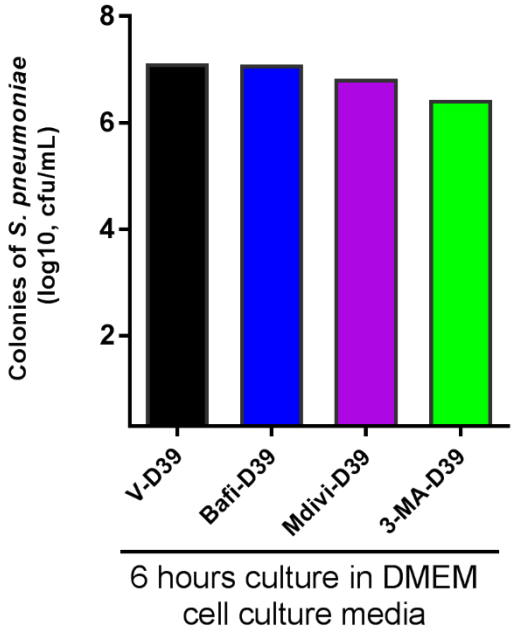

Figure 7.1. ***S. pneumoniae*** **culture in DMEM cell media**. 8-10 colonies of *S. pneumoniae* (D39) inoculated in vehicle (DMSO) or Bafilomycin A1 (100nM) or Mdivi-1 (25µM) or 3-Methyladenine (3MA, 10mM) and incubated at 37^{o}C and 5% CO_2 for 6 hours. Then 1 mL bacterial suspension was serial diluted and plated in the Columbia blood agar plates (Miles-Mirsa method). Bacterial colonies were counted after 16 hours incubation at 37^{o}C and 5% CO_2. (n=1).

Chapter 8: References

ABERDEIN, J. D., COLE, J., BEWLEY, M. A., MARRIOTT, H. M. & DOCKRELL, D. H. 2013. Alveolar macrophages in pulmonary host defence – the unrecognized role of apoptosis as a mechanism of intracellular bacterial killing.

ABEYTA, M., HARDY, G. & YOTHER, J. 2003. Genetic Alteration of Capsule Type but Not PspA Type Affects Accessibility of Surface- Bound Complement and Surface Antigens of Streptococcus pneumoniae. *Infection and Immunity,* 71**,** 218-225.

ADEREM, A. 2003. Phagocytosis and the inflammatory response. *J. Infect. Dis.,* 187**,** S340-S345.

ADEREM, A. & UNDERHILL, D. M. 1999. Mechanisms of phagocytosis in macrophages. *Annual review of immunology,* 17**,** 593.

AKTAN, F. 2004. iNOS- mediated nitric oxide production and its regulation.

ALESSANDRO, M., THEKLA, C., JENNY, G., ARNAUD, P., NORBERT, R., OLIVER, G., TINA, B., ANDRÉ, W., ARAVIND, T., ANTONIO, R., MANUEL, B., CAROLE, L. L., EVA, M., RUDI, B. & KARSTEN, H. 2013. Immune- responsive gene 1 protein links metabolism to immunity by catalyzing itaconic acid production. *Proceedings of the National Academy of Sciences,* 110**,** 7820.

ALI, F., LEE, M. E., READ, R. C., DOCKRELL, D. H., MITCHELL, T. J., IANNELLI, F. & POZZI, G. 2003. Streptococcus pneumoniae- Associated Human Macrophage Apoptosis after Bacterial Internalization via Complement and Fcγ Receptors Correlates with Intracellular Bacterial Load. *Journal of Infectious Diseases,* 188**,** 1119-1131.

ALI, S., VOLLAARD, A. M., WIDJAJA, S., SURJADI, C., VAN DE VOSSE, E. & VAN DISSEL, J. T. 2006. PARK2/ PACRG polymorphisms and susceptibility to typhoid and paratyphoid fever. *Clinical & Experimental Immunology,* 144**,** 425-431.

ARANGO DUQUE, G. & DESCOTEAUX, A. 2014. Macrophage cytokines: involvement in immunity and infectious diseases. *Frontiers in immunology,* 5**,** 491-491.

ARNOLD, K. E., LEGGIADRO, R. J., BREIMAN, R. F., LIPMAN, H. B., SCHWARTZ, B., APPLETON, M. A., CLEVELAND, K. O., SZETO, H. C., HILL, B. C., TENOVER, F. C., ELLIOTT, J. A. & FACKLAM, R. R. 1996. Risk factors for carriage of drug- resistant Streptococcus pneumoniae among children in Memphis, Tennessee. *The Journal of Pediatrics,* 128**,** 757-764.

ARREDOUANI, M., YANG, Z. & IMRICH, A. 2006. The Macrophage Scavenger Receptor SR- AI/ II and Lung Defense against Pneumococci and Particles. *American Journal of Respiratory Cell and Molecular Biology,* 35**,** 474-8.

ARREDOUANI, M., YANG, Z., NING, Y., QIN, G., SOININEN, R., TRYGGVASON, K. & KOBZIK, L. 2004. The scavenger receptor MARCO is required for lung defense against pneumococcal pneumonia and inhaled particles. *The Journal of experimental medicine,* 200**,** 267.

AUSTRIAN, R. 1981. Some observations on the pneumococcus and on the current status of pneumococcal disease and its prevention. *Reviews of Infectious Diseases,* 3**,** S1-S17.

AVDOSHINA, V., FIELDS, J., CASTELLANO, P., DEDONI, S., PALCHIK, G., TREJO, M., ADAME, A., ROCKENSTEIN, E., EUGENIN, E., MASLIAH, E. & MOCCHETTI, I. 2016. The HIV Protein gp120 Alters Mitochondrial Dynamics in Neurons. *Neurodegeneration, Neuroregeneration, Neurotrophic Action, and Neuroprotection,* 29**,** 583-593.

BALABAN, R. S., NEMOTO, S. & FINKEL, T. 2005. Mitochondria, Oxidants, and Aging. *Cell,* 120**,** 483-495.

BALAKRISHNAN, I., CROOK, P., MORRIS, R. & GILLESPIE, S. H. 2000. Early Predictors of Mortality in Pneumococcal Bacteraemia. *Journal of Infection,* 40**,** 256-261.

BAQUERO, F., MARTINEZ-BELTRAN, J. & LOZA, E. 1991. A review of antibiotic resistance patterns of Streptococcus pneumoniae in Europe. *Journal of Antimicrobial Chemotherapy,* 28**,** 31-38.

BAYRHUBER, M., MEINS, T., HABECK, M., BECKER, S., GILLER, K., VILLINGER, S., VONRHEIN, C., GRIESINGER, C., ZWECKSTETTER, M. & ZETH, K. 2008. Structure of the human voltage-dependent anion channel. *Proceedings of the National Academy of Sciences of the United States of America,* 105**,** 15370-15375.

BECKETT, E. L., STEVENS, R. L., JARNICKI, A. G., KIM, R. Y., HANISH, I., HANSBRO, N. G., DEANE, A., KEELY, S., HORVAT, J. C., YANG, M., OLIVER, B. G., VAN ROOIJEN, N., INMAN, M. D., ADACHI, R., SOBERMAN, R. J., HAMADI, S., WARK, P. A., FOSTER, P. S. & HANSBRO, P. M. 2013. A new short- term mouse model of chronic obstructive pulmonary disease identifies a role for mast cell tryptase in pathogenesis. *Journal of Allergy and Clinical Immunology,* 131**,** 752-e7.

BECKMAN, J. S. & KOPPENOL, W. H. 1996. Nitric oxide, superoxide, and peroxynitrite: The good, the bad, and the ugly. *American Journal of Physiology - Cell Physiology,* 271**,** C1424-C1437.

BELÉN, B., ANTHONY, M., MICHAEL, R. D., JORGE, D. E. & SALVADOR, M. 2000. The effect of nitric oxide on cell respiration: A key to understanding its role in cell survival or death. *Proceedings of the National Academy of Sciences of the United States of America,* 97**,** 14602.

BENEDIKT, W. 2010. Mitochondrial fusion and fission in cell life and death. *Nature Reviews Molecular Cell Biology,* 11**,** 872.

BEREITERHAHN, J. & VOTH, M. 1994. DYNAMICS OF MITOCHONDRIA IN LIVING CELLS - SHAPE CHANGES, DISLOCATIONS, FUSION, AND FISSION OF MITOCHONDRIA. *Microscopy Research and Technique,* 27**,** 198-219.

BERG JM, T. J., STRYER L. 2002. *The Respiratory Chain Consists of Four Complexes: Three Proton Pumps and a Physical Link to the Citric Acid Cycle*.

BEWLEY, M. A., BELCHAMBER, K. B. R., CHANA, K. K., BUDD, R. C., DONALDSON, G., WEDZICHA, J. A., BRIGHTLING, C. E., KILTY, I., DONNELLY, L. E., BARNES, P. J., SINGH, D., WHYTE, M. K. B., DOCKRELL, D. H., GAW, A., MAYER, R. J., TAL-SINGER, R., SALMON, M. & ROUBENOFF, R. 2016. Differential effects of p38, MAPK, PI3K or Rho kinase inhibitors on bacterial phagocytosis and efferocytosis by macrophages in COPD. *PLoS ONE,* 11**,** <xocs:firstpage xmlns:xocs=""/>.

BEWLEY, M. A., MARRIOTT, H. M., TULONE, C., FRANCIS, S. E., MITCHELL, T. J., READ, R. C., CHAIN, B., KROEMER, G., WHYTE, M. K. B. & DOCKRELL, D. H. 2011. A Cardinal Role for Cathepsin D in Co- Ordinating the Host- Mediated Apoptosis of Macrophages and Killing of Pneumococci. *PLoS Pathog.,* 7.

BEWLEY, M. A., NAUGHTON, M., PRESTON, J., MARRIOTT, H. M., DOCKRELL, D. H., MITCHELL, A., MITCHELL, T. J., HOLMES, A., READ, R. C. & WHYTE, M. K. B. 2014. Pneumolysin activates macrophage lysosomal membrane permeabilization and executes apoptosis by distinct mechanisms without membrane pore formation. *mBio,* 5.

BEWLEY, M. A., PRESTON, J. A., MOHASIN, M., MARRIOTT, H. M., BUDD, R. C., SWALES, J., COLLINI, P., GREAVES, D. R., CRAIG, R. W., BRIGHTLING, C. E., DONNELLY, L. E., BARNES, P. J., SINGH, D., SHAPIRO, S. D., WHYTE, M. K. B. & DOCKRELL, D. H. 2017. Impaired Mitochondrial Microbicidal Responses in Chronic Obstructive Pulmonary Disease Macrophages.

BRAND, M. D., BRINDLE, K. M., BUCKINGHAM, J. A., HARPER, J. A., ROLFE, D. F. S. & STUART, J. A. 1999. The significance and mechanism of mitochondrial proton conductance. *International Journal of Obesity,* 23**,** S4-S11.

BRAND, M. D., PAKAY, J. L., OCLOO, A., KOKOSZKA, J., WALLACE, D. C., BROOKES, P. S. & CORNWALL, E. J. 2005. The basal proton conductance of mitochondria depends on adenine nucleotide translocase content. *Biochemical Journal,* 392**,** 353-362.

BRAUN, J. S., NOVAK, R., GAO, G., MURRAY, P. J. & SHENEP, J. L. 1999. Pneumolysin, a protein toxin of Streptococcus pneumoniae, induces nitric oxide production from macrophages. *Infection and Immunity,* 67**,** 3750-3756.

BUCK, M. D., O'SULLIVAN, D., GELTINK, R. I. K., CURTIS, J. D., CHANG, C.-H., SANIN, D. E., QIU, J., KRETZ, O., BRAAS, D., VAN DER WINDT, G. J. W., CHEN, Q., HUANG, S. C.-C., O'NEILL, C. M., EDELSON, B. T., PEARCE, E. J., SESAKI, H., HUBER, T. B., RAMBOLD, A. S. & PEARCE, E. L. 2016. Mitochondrial Dynamics Controls T Cell Fate through Metabolic Programming. *Cell,* 166**,** 63-76.

BUSTOS, R. & SOBRINO, F. 1992. Stimulation of glycolysis as an activation signal in rat peritoneal macrophages. Effect of glucocorticoids on this process. *The Biochemical journal,* 282 (Pt 1)**,** 299.

BUTTGEREIT, F., BURMESTER, G.-R. & BRAND, M. D. 2000. Bioenergetics of immune functions: fundamental and therapeutic aspects. *Immunology Today,* 21**,** 194-199.

CAI, Q. & TAMMINENI, P. 2016. Alterations in Mitochondria! Quality Control in Alzheimer's Disease. *Front. Cell. Neurosci.*

CALBO, E. & GARAU, J. 2010. Of mice and men: innate immunity in pneumococcal pneumonia. *International Journal of Antimicrobial Agents,* 35**,** 107-113.

CANNON, B. & NEDERGAARD, J. 2004. Brown adipose tissue: Function and physiological significance. *Physiological Reviews,* 84**,** 277-359.

CAPELLI, A., DI STEFANO, A., GNEMMI, I., BALBO, P., CERUTTI, C. G., BALBI, B., LUSUARDI, M. & DONNER, C. F. 1999. Increased MCP- 1 and MIP- 1 beta in bronchoalveolar lavage fluid of chronic bronchitics. *Eur. Resp. J.,* 14**,** 160-165.

CARDELLI, J. 2001. Phagocytosis and macropinocytosis in Dictyostelium: Phosphoinositide- based processes, biochemically distinct. *Traffic,* 2**,** 311-320.

CARROLL, RICHARD G., HOLLVILLE, E. & MARTIN, SEAMUS J. 2014. Parkin Sensitizes toward Apoptosis Induced by Mitochondrial Depolarization through Promoting Degradation of Mcl-1. *Cell Reports,* 9**,** 1538-1553.

CASSIDY-STONE, A., CHIPUK, J. E., INGERMAN, E., SONG, C., YOO, C., KUWANA, T., KURTH, M. J., SHAW, J. T., HINSHAW, J. E., GREEN, D. R. & NUNNARI, J. 2008. Chemical Inhibition of the Mitochondrial Division Dynamin Reveals Its Role in Bax/ Bak- Dependent Mitochondrial Outer Membrane Permeabilization. *Developmental Cell,* 14**,** 193-204.

CASSOL, E., ALFANO, M., BISWAS, P. & POLI, G. 2006. Monocyte-derived macrophages and myeloid cell lines as targets of HIV-1 replication and persistence. *Journal of Leukocyte Biology,* 80**,** 1018-1030.

CHAN, D. C. 2006. Mitochondria: Dynamic Organelles in Disease, Aging, and Development. *Cell,* 125**,** 1241-1252.
CHAN, D. C. 2012. Fusion and Fission: Interlinked Processes Critical for Mitochondrial Health. *Annu. Rev. Genet.*
CHANG, C.-R. & BLACKSTONE, C. 2007. Cyclic AMP-dependent protein kinase phosphorylation of Drp1 regulates its GTPase activity and mitochondrial morphology. *Journal of Biological Chemistry,* 282**,** 21583-21587.
CHEN, H. & CHAN, D. C. 2010. Physiological functions of mitochondrial fusion. *Mitochondrial Research in Translational Medicine,* 1201**,** 21-25.
CHEN, H., DETMER, S., EWALD, A. & GRIFFIN, E. 2003. Mitofusins Mfn1 and Mfn2 coordinately regulate mitochondrial fusion and are essential for embryonic development. *The Journal of Cell Biology,* 160**,** 189-200.
CHO, J. H., PARK, J. H., CHUNG, C. G., SHIM, H.-J., JEON, K. H., YU, S.-W. & LEE, S. B. 2015. Parkin- mediated responses against infection and wound involve TSPO- VDAC complex in Drosophila. *Biochemical and Biophysical Research Communications,* 463**,** 1-6.
CICALA, C., ARTHOS, J., SELIG, S. M., DENNIS, G., HOSACK, D. A., VAN RYK, D., SPANGLER, M. L., STEENBEKE, T. D., KHAZANIE, P., GUPTA, N., YANG, J., DAUCHER, M., LEMPICKI, R. A. & FAUCI, A. S. 2002. HIV envelope induces a cascade of cell signals in non-proliferating target cells that favor virus replication. *Proceedings of the National Academy of Sciences of the United States of America,* 99**,** 9380-9385.
CIRCU, M. L. & AW, T. Y. 2010. Reactive oxygen species, cellular redox systems, and apoptosis. *Free Radical Biology and Medicine,* 48**,** 749-762.
CLEETER, M. W. J., COOPER, J. M., DARLEY - USMAR, V. M., MONCADA, S. & SCHAPIRA, A. H. V. 1994. Reversible inhibition of cytochrome c oxidase, the terminal enzyme of the mitochondrial respiratory chain, by nitric oxide. *FEBS Letters,* 345**,** 50-54.
COLLINI, P., NOURSADEGHI, M., SABROE, I., MILLER, R. F. & DOCKRELL, D. H. 2010. Monocyte and Macrophage Dysfunction as a Cause of HIV-1 Induced Dysfunction of Innate Immunity. *Current Molecular Medicine,* 10**,** 727-740.
COLLINI, P. J., BEWLEY, M. A., MOHASIN, M., MARRIOTT, H. M., MILLER, R. F., GERETTI, A.-M., BELOUKAS, A., PAPADIMITROPOULOS, A., READ, R. C., NOURSADEGHI, M. & DOCKRELL, D. H. 2018. HIV gp120 in Lungs of ART- treated Individuals Impairs Alveolar Macrophage Responses To Pneumococci. *American journal of respiratory and critical care medicine*.
COLLINS, T. J., BERRIDGE, M. J., LIPP, P. & BOOTMAN, M. D. 2002. Mitochondria are morphologically and functionally heterogeneous within cells. *EMBO Journal,* 21**,** 1616-1627.
CONLEY, K. E., AMARA, C. E., JUBRIAS, S. A. & MARCINEK, D. J. 2007. Mitochondrial function, fibre types and ageing: new insights from human muscle in vivo. *Experimental Physiology,* 92**,** 333-339.
COPPOLINO, M. G., KRAUSE, M., HAGENDORFF, P., MONNER, D. A., TRIMBLE, W., GRINSTEIN, S., WEHLAND, J. & SECHI, A. S. 2001. Evidence for a molecular complex consisting of Fyb/ SLAP, SLP- 76, Nck, VASP and WASP that links the actin cytoskeleton to Fcgamma receptor signalling during phagocytosis. *Journal of cell science,* 114**,** 4307.
CORBETT, J. R., WRIGHT, K. AND BAILLIE, A. C. 1984. *Biochemical Mode of Action of Pesticides,* Academic Press, London.
CORRALIZA, I. M., SOLER, G., EICHMANN, K. & MODOLELL, M. 1995. Arginase induction by suppressors of nitric oxide synthesis (IL-4, IL-10 and

PGE 2) in murine bone- marrow- derived macrophages. *Biochemical and Biophysical Research Communications,* 206**,** 667-673.

CROWE, S. M. & SONZA, S. 2000. HIV-1 can be recovered from a variety of cells including peripheral blood monocytes of patients receiving highly active antiretroviral therapy: a further obstacle to eradication. *Journal of Leukocyte Biology,* 68**,** 345-350.

CUMMINS, N. W., RIZZA, S. A. & BADLEY, A. D. 2010. How much gp120 is there? *The Journal of infectious diseases,* 201**,** 1273.

DAIGNEAULT, M., PRESTON, J. A., MARRIOTT, H. M., WHYTE, M. K. B. & DOCKRELL, D. H. 2010. The identification of markers of macrophage differentiation in PMA- stimulated THP- 1 Cells and monocyte- derived macrophages.

DAMIEN, A., LAURA, M. B., ANNA, S., DELPHINE, P., NAOUFAL, Z., PETER, U. P., JUANITA, S., RICHARD, J. Y. & VICTOR, S. G. 2004. Cytomegalovirus cell death suppressor vMIA blocks Bax- but not Bak- mediated apoptosis by binding and sequestering Bax at mitochondria. *Proceedings of the National Academy of Sciences of the United States of America,* 101**,** 7988.

DANIEL, S., RICHARD, D. B., SPENCER, A. F., RICHARD, F. C., TONY, P., GREGORY, D. F. & SERGIO, G. 2015. Phosphoinositide 3- kinase enables phagocytosis of large particles by terminating actin assembly through Rac/ Cdc42 GTPase- activating proteins. *Nature Communications,* 6.

DAVID, N. & MICHAEL, C. 2008. *Lehninger Principles of Biochemisty,* Palgrave Macmillan.

DE BOER, W. I., SONT, J. K., VAN SCHADEWIJK, A., STOLK, J., VAN KRIEKEN, J. H. & HIEMSTRA, P. S. 2000. Monocyte chemoattractant protein 1, interleukin 8, and chronic airways inflammation in COPD. *J. Pathol.,* 190**,** 619-626.

DE VOS, K. J., ALLAN, V. J., GRIERSON, A. J. & SHEETZ, M. P. 2005. Mitochondrial Function and Actin Regulate Dynamin- Related Protein 1-Dependent Mitochondrial Fission. *Current Biology,* 15**,** 678-683.

DESSING, M. C., FLORQUIN, S., PATON, J. C. & VAN DER POLL, T. 2008. Toll-like receptor 2 contributes to antibacterial defence against pneumolysin-deficient pneumococci. *Cellular Microbiology,* 10**,** 237-246.

DI STEFANO, A., CARAMORI, G., OATES, T., CAPELLI, A., LUSUARDI, M., GNEMMI, I., IOLI, F., CHUNG, K. F., DONNER, C. F., BARNES, P. J. & ADCOCK, I. M. 2002. Increased expression of nuclear factor-κB in bronchial biopsies from smokers and patients with COPD. *European Respiratory Journal,* 20**,** 556-563.

DING, W. X., NI, H. M., LI, M., LIAO, Y., CHEN, X. Y., STOLZ, D. B., DORN, G. W. & YIN, X. M. 2010. Nix Is Critical to Two Distinct Phases of Mitophagy, Reactive Oxygen Species-mediated Autophagy Induction and Parkin-Ubiquitin-p62-mediated Mitochondrial Priming. *Journal of Biological Chemistry,* 285**,** 27879-27890.

DOCKRELL, D. H., LEE, M., LYNCH, D. H. & READ, R. C. 2001. Immune-mediated phagocytosis and killing of Streptococcus pneumoniae are associated with direct and bystander macrophage apoptosis. *Journal of Infectious Diseases,* 184**,** 713-722.

DOCKRELL, D. H., MARRIOTT, H. M., PRINCE, L. R., INCE, P. G., WHYTE, M. K. B., RIDGER, V. C. & HELLEWELL, P. G. 2003. Alveolar Macrophage Apoptosis Contributes to Pneumococcal Clearance in a Resolving Model of Pulmonary Infection. *Journal of Immunology,* 171**,** 5380-5388.

DOCKRELL, D. H., WHYTE, M. K. B. & MITCHELL, T. J. 2012a. Pneumococcal Pneumonia Mechanisms of Infection and Resolution. *Chest,* 142**,** 482-491.
DOCKRELL, D. H., WHYTE, M. K. B. & MITCHELL, T. J. 2012b. Pneumococcal pneumonia: Mechanisms of infection and resolution. *Chest,* 142**,** 482-491.
DRAPIER, J. C. & HIBBS JR, J. B. 1988. Differentiation of murine macrophages to express nonspecific cytotoxicity for tumor cells results in L- arginine- dependent inhibition of mitochrondrial iron- sulfur enzymes in the macrophage effector cells. *Journal of Immunology,* 140**,** 2829-2838.
DUCHIN, S. J., BREIMAN, F. R., DIAMOND, B. A., LIPMAN, L. H., BLOCK, A. S., HEDRICK, A. J., FINGER, A. R. & ELLIOTT, A. J. 1995. High prevalence of multidrug- resistant Streptococcus pneumoniae among children in a rural Kentucky community. *The Pediatric Infectious Disease Journal,* 14**,** 745-750.
EDWARDS, J. P., ZHANG, X., FRAUWIRTH, K. A. & MOSSER, D. M. 2006. Biochemical and functional characterization of three activated macrophage populations. *Journal of Leukocyte Biology,* 80**,** 1298-1307.
EMILIO, C., GUY CHARLES, B., MARTIN, F. & SALVADOR, M. 1998. Persistent inhibition of cell respiration by nitric oxide: Crucial role of S- nitrosylation of mitochondrial complex I and protective action of glutathione. *Proceedings of the National Academy of Sciences of the United States of America,* 95**,** 7631.
EPELMAN, S., LAVINE, KORY J. & RANDOLPH, GWENDALYN J. 2014. Origin and Functions of Tissue Macrophages. *Immunity,* 41.
FANG, F. C. 2004. Antimicrobial reactive oxygen and nitrogen species: Concepts and controversies. *Nature Reviews Microbiology,* 2**,** 820-832.
FANG, R., TSUCHIYA, K., KAWAMURA, I., SHEN, Y., HARA, H., SAKAI, S., YAMAMOTO, T., FERNANDES-ALNEMRI, T., YANG, R., HERNANDEZ-CUELLAR, E., DEWAMITTA, S. R., XU, Y., QU, H., ALNEMRI, E. S. & MITSUYAMA, M. 2011. Critical roles of ASC inflammasomes in caspase- 1 activation and host innate resistance to Streptococcus pneumoniae infection. *Journal of immunology (Baltimore, Md. : 1950),* 187**,** 4890.
FIELDS, J. A., SERGER, E., CAMPOS, S., DIVAKARUNI, A. S., KIM, C., SMITH, K., TREJO, M., ADAME, A., SPENCER, B., ROCKENSTEIN, E., MURPHY, A. N., ELLIS, R. J., LETENDRE, S., GRANT, I. & MASLIAH, E. 2016. HIV alters neuronal mitochondrial fission/ fusion in the brain during HIV- associated neurocognitive disorders. *Neurobiology of Disease,* 86**,** 154-169.
FLANNAGAN, R. S., COSIO, G. & GRINSTEIN, S. 2009. Antimicrobial mechanisms of phagocytes and bacterial evasion strategies. *Nature Reviews Microbiology,* 7**,** 355-366.
FRANK, M., DUVEZIN-CAUBET, S., KOOB, S., OCCHIPINTI, A., JAGASIA, R., PETCHERSKI, A., RUONALA, M. O., PRIAULT, M., SALIN, B. & REICHERT, A. S. 2012. Mitophagy is triggered by mild oxidative stress in a mitochondrial fission dependent manner. *Biochimica Et Biophysica Acta-Molecular Cell Research,* 1823**,** 2297-2310.
FRIEDMAN, J. R., LACKNER, L. L., WEST, M., DIBENEDETTO, J. R., NUNNARI, J. & VOELTZ, G. K. 2011. ER tubules mark sites of mitochondrial division. *Science (New York, N.Y.),* 334**,** 358.
FUKUZUMI, M., SHINOMIYA, H., OHISHI, K., UTSUMI, S. & SHIMIZU, Y. 1996. Endotoxin- induced enhancement of glucose influx into murine peritoneal macrophages via GLUT 1. *Infection and Immunity,* 64**,** 108-112.
GALVAN-PENA, S. & O'NEILL, L. A. J. 2014. Metabolic reprograming in macrophage polarization. *Frontiers in immunology,* 5**,** 420-420.
GARCHA, D. S., THURSTON, S. J., PATEL, A. R. C., MACKAY, A. J., GOLDRING, J. J. P., DONALDSON, G. C., MCHUGH, T. D. & WEDZICHA,

J. A. 2012. Changes in prevalence and load of airway bacteria using quantitative PCR in stable and exacerbated COPD. *Thorax,* 67**,** 1075-1080.
GARCIA-SUAREZ, M. D., FLOREZ, N., ASTUDILLO, A., VAZQUEZ, F., VILLAVERDE, R., FABRIZIO, K., PIROFSKI, L. A. & MENDEZ, F. J. 2007. The role of pneumolysin in mediating lung damage in a lethal pneumococcal pneumonia murine model. *Respiratory Research,* 8.
GATLIFF, J., EAST, D., CROSBY, J., ABETI, R., HARVEY, R., CRAIGEN, W., PARKER, P. & CAMPANELLA, M. 2014. TSPO interacts with VDAC1 and triggers a ROS- mediated inhibition of mitochondrial quality control. *Autophagy,* 10**,** 2279-2296.
GEERAERTS, X., BOLLI, E., FENDT, S. M. & VAN GINDERACHTER, J. 2017. Macrophage Metabolism As Therapeutic Target for Cancer, Atherosclerosis, and Obesity. *Front. Immunol.*
GEOFFREY, C. M. 2000. *Bioenergetics and Metabolism - Mitochondria, Chloroplasts, and Peroxisomes*

The Cell: A molecular approach.
GEOFFROY, C., GAILLARD, J. L., ALOUF, J. E. & BERCHE, P. 1987. Purification, characterization, and toxicity of the sulfhydryl- activated hemolysin listeriolysin O from Listeria monocytogenes. *Infection and immunity,* 55**,** 1641.
GHONEIM, H. E., THOMAS, P. G. & MCCULLERS, J. A. 2013. Depletion of alveolar macrophages during influenza infection facilitates bacterial superinfections. *Journal of immunology (Baltimore, Md. : 1950),* 191**,** 1250.
GLICK, D., BARTH, S. & MACLEOD, K. F. 2010. Autophagy: cellular and molecular mechanisms. *Journal of Pathology,* 221**,** 3-12.
GOLD, V. A. M., IEVA, R., WALTER, A., PFANNER, N., VAN DER LAAN, M. & KUHLBRANDT, W. 2014. Visualizing active membrane protein complexes by electron cryotomography. *Nature Communications,* 5.
GORDIN, F. M., ROEDIGER, M. P., GIRARD, P. M., LUNDGREN, J. D., MIRO, J. M., PALFREEMAN, A., RODRIGUEZ-BARRADAS, M. C., WOLFF, M. J., EASTERBROOK, P. J., CLEZY, K. & SLATER, L. N. 2008. Pneumonia in HIV-infected persons - Increased risk with cigarette smoking and treatment interruption. *American Journal of Respiratory and Critical Care Medicine,* 178**,** 630-636.
GORDON, S. B., MOLYNEUX, M. E., BOEREE, M. J., KANYANDA, S., CHAPONDA, M., SQUIRE, S. B. & READ, R. C. 2001. Opsonic Phagocytosis of Streptococcus pneumoniae by Alveolar Macrophages Is Not Impaired in Human Immunodeficiency Virus- Infected Malawian Adults. *The Journal of Infectious Diseases,* 184**,** 1345-1349.
GRAY, M. W., BURGER, G. & LANG, B. F. 1999. Mitochondrial evolution. *Science,* 283**,** 1476-1481.
GREENBERG, S. & GRINSTEIN, S. 2002. Phagocytosis and innate immunity. *Current Opinion in Immunology,* 14**,** 136-145.
GROSS, A., SPIESSER, S., TERRAZA, A., ROUOT, B., CARON, E. & DORNAND, J. 1998. Expression and bactericidal activity of nitric oxide synthase in Brucella suis- infected murine macrophages. *Infection and Immunity,* 66**,** 1309-1316.
GUILLIAMS, M., DE KLEER, I., HENRI, S., POST, S., VANHOUTTE, L., DE PRIJCK, S., DESWARTE, K., MALISSEN, B., HAMMAD, H. & LAMBRECHT, B. 2013. Alveolar macrophages develop from fetal monocytes that differentiate into long- lived cells in the first week of life via GM- CSF. *JOURNAL OF EXPERIMENTAL MEDICINE*.

GUO, X.-G., JI, T.-X., XIA, Y. & MA, Y.-Y. 2013. Autophagy protects type II alveolar epithelial cells from Mycobacterium tuberculosis infection. *Biochemical and Biophysical Research Communications,* 432**,** 308-313.

HALL, CHRISTOPHER J., BOYLE, RACHEL H., ASTIN, JONATHAN W., FLORES, MARIA V., OEHLERS, STEFAN H., SANDERSON, LESLIE E., ELLETT, F., LIESCHKE, GRAHAM J., CROSIER, KATHRYN E. & CROSIER, PHILIP S. 2013. Immunoresponsive Gene 1Augments Bactericidal Activity of Macrophage-Lineage Cells by Regulating β-Oxidation-Dependent Mitochondrial ROS Production. *Cell Metabolism,* 18**,** 265-278.

HANSFORD, R., HOGUE, B. & MILDAZIENE, V. 1997. Dependence of H2O2 Formation by Rat Heart Mitochondria on Substrate Availability and Donor Age. *Journal of Bioenergetics and Biomembranes,* 29**,** 89-95.

HASCHEMI, A., HAAS, R., JANDL, C., AMIR, S., ESTERBAUER, H., BILBAN, M., WAGNER, O., STARKL, P., KNAPP, B., SCHMID, J. A., LUBEC, G., OTTERBEIN, L. E., KOSMA, P., GILLE, L., EVANS, C. R., BURANT, C. F., PARK, J., BRIZUELA, L. & POSPISILIK, J. A. 2012. The sedoheptulose kinase CARKL directs macrophage polarization through control of glucose metabolism. *Cell Metabolism,* 15**,** 813-826.

HENRICHSEN, J. 1995. Six newly recognized types of Streptococcus pneumoniae. *Journal of Clinical Microbiology,* 33**,** 2759-2762.

HEYTLER, P. G. 1980. Uncouplers of oxidative phosphorylation. *Pharmacology & therapeutics,* 10**,** 461.

HIRST, R. A., KADIOGLU, A., CALLAGHAN, C. & ANDREW, P. W. 2004. The role of pneumolysin in pneumococcal pneumonia and meningitis. Oxford, UK.

HODGE, S., HODGE, G., AHERN, J., JERSMANN, H., HOLMES, M. & REYNOLDS, P. N. 2007. Smoking alters alveolar macrophage recognition and phagocytic ability: Implications in chronic obstructive pulmonary disease. *American Journal of Respiratory Cell and Molecular Biology,* 37**,** 748-755.

HOFMANN, J., CETRON, M. S., FARLEY, M. M., BAUGHMAN, W. S., FACKLAM, R. R., ELLIOTT, J. A., DEAVER, K. A. & BREIMAN, R. F. 1995. The Prevalence of Drug- Resistant Streptococcus pneumoniae In Atlanta. *The New England Journal of Medicine,* 333**,** 481-486.

HONG, S. & PEDERSEN, P. 2008. ATP Synthase and the Actions of Inhibitors Utilized To Study Its Roles in Human Health, Disease, and Other Scientific Areas. *Microbiol. Mol. Biol. Rev.*

HOSHINO, K., TAKEUCHI, O., KAWAI, T., SANJO, H., OGAWA, T., TAKEDA, Y., TAKEDA, K. & AKIRA, S. 1999. Cutting edge: Toll-like receptor 4 (TLR4)-deficient mice are hyporesponsive to lipopolysaccharide: Evidence for TLR4 as the Lps gene product. *Journal of Immunology,* 162**,** 3749-3752.

ICHINOSE, M., SUGIURA, H., YAMAGATA, S., KOARAI, A. & SHIRATO, K. 2000. Increase in reactive nitrogen species production in chronic obstructive pulmonary disease airways. *American Journal of Respiratory and Critical Care Medicine,* 162**,** 701-706.

ILES, K. E., FORMAN, H. J. & ILES, H. J. 2002. Macrophage signaling and respiratory burst. *Immunologic Research,* 26**,** 95-105.

INFANTINO, V., CONVERTINI, P., CUCCI, L., PANARO, M. A., DI NOIA, M. A., CALVELLO, R., PALMIERI, F. & IACOBAZZI, V. 2011. ACCELERATED PUBLICATION The mitochondrial citrate carrier: a new player in inflammation. *Biochem. J.,* 438**,** 433-436.

INGELS, H. A. 2015. Reccurrent invasive pneumococcal disease in children host factors and vaccination response. *Danish medical journal,* 62**,** <xocs:firstpage xmlns:xocs=""/>.

ISHIHARA, N., JOFUKU, A., OKA, T., MIHARA, K. & TAGUCHI, N. 2007. Mitotic Phosphorylation of Dynamin-related GTPase Drp1 Participates in Mitochondrial Fission. *The Journal of biological chemistry.,* 282**,** 11521-11529.

ISHII, K. J. & AKIRA, S. 2006. Innate immune recognition of, and regulation by, DNA. *Trends in Immunology,* 27**,** 525-532.

ITO, K., HANAZAWA, T., TOMITA, K., BARNES, P. J. & ADCOCK, I. M. 2004. Oxidative stress reduces histone deacetylase 2 activity and enhances IL- 8 gene expression: Role of tyrosine nitration. *Biochemical and Biophysical Research Communications,* 315**,** 240-245.

ITO, K., ITO, M., COSIO, B., ONN, M. K., ADCOCK, I. M., BARNES, P. J., ELLIOTT, W. M., HAYASHI, S., HOGG, J. C., CARAMORI, G. & BARCZYK, A. 2005. Decreased histone deacetylase activity in chronic obstructive pulmonary disease. *New England Journal of Medicine,* 352**,** 1967-1976.

JACOBS, S. R., HERMAN, C. E., MACIVER, N. J., WOFFORD, J. A., WIEMAN, H. L., HAMMEN, J. J. & RATHMELL, J. C. 2008. Glucose uptake is limiting in T cell activation and requires CD28-mediated Akt-dependent and independent pathways. *Journal of immunology (Baltimore, Md. : 1950),* 180**,** 4476.

JACOTOT, E., RAVAGNAN, L., LOEFFLER, M., FERRI, K. F., VIEIRA, H. L. A., ZAMZAMI, N., COSTANTINI, P., DRUILLENNEC, S., HOEBEKE, J., BRIAND, J. P., IRINOPOULOU, T., DAUGAS, E., SUSIN, S. A., COINTE, D., XIE, Z. H., REED, J. C., ROQUES, B. P. & KROEMER, G. 2000. The HIV-1 Viral Protein R Induces Apoptosis via a Direct Effect on the Mitochondrial Permeability Transition Pore. *The Journal of Experimental Medicine,* 191**,** 33-46.

JAKUBZICK, C., GAUTIER, EMMANUEL L., GIBBINGS, SOPHIE L., SOJKA, DOROTHY K., SCHLITZER, A., JOHNSON, THEODORE E., IVANOV, S., DUAN, Q., BALA, S., CONDON, T., VAN ROOIJEN, N., GRAINGER, JOHN R., BELKAID, Y., MA'AYAN, A., RICHES, DAVID W. H., YOKOYAMA, WAYNE M., GINHOUX, F., HENSON, PETER M. & RANDOLPH, GWENDALYN J. 2013. Minimal Differentiation of Classical Monocytes as They Survey Steady- State Tissues and Transport Antigen to Lymph Nodes. *Immunity,* 39**,** 599-610.

JAMES, D. I., PARONE, P. A., MATTENBERGER, Y. & MARTINOU, J. C. 2003. hFis1, a novel component of the mammalian mitochondrial fission machinery. *Journal of Biological Chemistry,* 278**,** 36373-36379.

JASTROCH, M., DIVAKARUNI, A. S., MOOKERJEE, S., TREBERG, J. R. & BRAND, M. D. 2010. Mitochondrial proton and electron leaks. *Essays in Biochemistry: Mitochondrial Function,* 47**,** 53-67.

JEDRZEJAS, M. 2001. Pneumococcal virulence factors: Structure and function. *Microbiol. Mol. Biol. Rev.*

JEREMY, S. B., TRACY, H., SARAH, M. G., DAVID, W. H., JAMES, C. P., MICHAEL, R. E., MARK, J. W. & MARINA, B. 2002. The classical pathway is the dominant complement pathway required for innate immunity to Streptococcus pneumoniae infection in mice. *Proceedings of the National Academy of Sciences of the United States of America,* 99**,** 16969.

JHA, ABHISHEK K., HUANG, STANLEY C.-C., SERGUSHICHEV, A., LAMPROPOULOU, V., IVANOVA, Y., LOGINICHEVA, E., CHMIELEWSKI, K., STEWART, KELLY M., ASHALL, J., EVERTS, B., PEARCE, EDWARD J., DRIGGERS, EDWARD M. & ARTYOMOV, MAXIM N. 2015. Network Integration of Parallel Metabolic and Transcriptional

Data Reveals Metabolic Modules that Regulate Macrophage Polarization. *Immunity,* 42**,** 419-430.
JONATHAN, R. F. & JODI, N. 2014. Mitochondrial form and function. *Nature,* 505**,** 335.
JUBRAIL, J., MORRIS, P., BEWLEY, M. A., STONEHAM, S., JOHNSTON, S. A., FOSTER, S. J., PEDEN, A. A., READ, R. C., MARRIOTT, H. M. & DOCKRELL, D. H. 2016. Inability to sustain intraphagolysosomal killing of Staphylococcus aureus predisposes to bacterial persistence in macrophages. *Cellular Microbiology,* 18**,** 80-96.
KADIOGLU, A., COWARD, W., COLSTON, M. J., HEWITT, C. R. A. & ANDREW, P. W. 2004. CD4- T- lymphocyte interactions with pneumolysin and pneumococci suggest a crucial protective role in the host response to pneumococcal infection. *Infection and immunity,* 72**,** 2689.
KADIOGLU, A., WEISER, J. N., PATON, J. C. & ANDREW, P. W. 2008. The role of Streptococcus pneumoniae virulence factors in host respiratory colonization and disease. *Nature Reviews Microbiology,* 6**,** 288-301.
KARBOWSKI, M. 2010. Mitochondria on Guard: Role of Mitochondrial Fusion and Fission in the Regulation of Apoptosis. *Bcl-2 Protein Family: Essential Regulators of Cell Death,* 687**,** 131-142.
KARBOWSKI, M. & YOULE, R. J. 2003. Dynamics of mitochondrial morphology in healthy cells and during apoptosis. *Cell Death and Differentiation,* 10**,** 870.
KATOH, M., WU, B., NGUYEN, H. B., THAI, T. Q., YAMASAKI, R., LU, H., RIETSCH, A. M., ZORLU, M. M., SHINOZAKI, Y., SAITOH, Y., SAITOH, S., SAKOH, T., IKENAKA, K., KOIZUMI, S., RANSOHOFF, R. M. & OHNO, N. 2017. Polymorphic regulation of mitochondrial fission and fusion modifies phenotypes of microglia in neuroinflammation. *Scientific Reports,* 7**,** <xocs:firstpage xmlns:xocs=""/>.
KIRKHAM, P. A. & BARNES, P. J. 2013. Oxidative Stress in COPD. *Chest,* 144**,** 266-273.
KLIONSKY, D. & CODOGNO, P. 2013. The Mechanism and Physiological Function of Macroautophagy. *J. Innate Immun.*
KNAPP, S., LEEMANS, J. C., FLORQUIN, S., BRANGER, J., MARIS, N. A., PATER, J., VAN ROOIJEN, N. & VAN DER POLL, T. 2003. Alveolar macrophages have a protective antiinflammatory role during murine pneumococcal pneumonia. *American Journal of Respiratory and Critical Care Medicine,* 167**,** 171-179.
KOEDEL, U., RUPPRECHT, T., ANGELE, B., HEESEMANN, J., WAGNER, H., PFISTER, H. & KIRSCHNING, C. J. 2004. MyD88 is required for mounting a robust host immune response to Streptococcus pneumoniae in the CNS. *Brain,* 127**,** 1437-1445.
Koga T, Lim JH, Jono H, Ha UH, Xu H, et al. 2008. Tumor suppressor cylindromatosis acts as a negative for Streptococcus pneumoniae-induced NFAT signaling. J Biol Chem 283; 12546-12554.
KOPPE, U., SUTTORP, N. & OPITZ, B. 2012. Recognition of Streptococcus pneumoniae by the innate immune system. Oxford, UK.
KORNMANN, B., CURRIE, E., COLLINS, S. R., SCHULDINER, M., NUNNARI, J., WEISSMAN, J. S. & WALTER, P. 2009. An ER- mitochondria tethering complex revealed by a synthetic biology screen. *Science (New York, N.Y.),* 325**,** 477.
KRAWCZYK, C. M., HOLOWKA, T., SUN, J., BLAGIH, J., AMIEL, E., DEBERARDINIS, R. J., CROSS, J. R., JUNG, E., THOMPSON, C. B., JONES,

R. G. & PEARCE, E. J. 2010. Toll- like receptor- induced changes in glycolytic metabolism regulate dendritic cell activation. *Blood,* 115**,** 4742.
KRIEG, A. M. 2000. The role of CpG motifs in innate immunity. *Current Opinion in Immunology,* 12**,** 35-43.
KUHLBRANDT, W. 2015. Structure and function of mitochondrial membrane protein complexes. *Bmc Biology,* 13.
KURIHARA, Y., KANKI, T., AOKI, Y., HIROTA, Y., SAIGUSA, T., UCHIUMI, T. & KANG, D. C. 2012. Mitophagy Plays an Essential Role in Reducing Mitochondrial Production of Reactive Oxygen Species and Mutation of Mitochondrial DNA by Maintaining Mitochondrial Quantity and Quality in Yeast. *Journal of Biological Chemistry,* 287**,** 3265-3272.
LAEMMLI, U. K. 1970. CLEAVAGE OF STRUCTURAL PROTEINS DURING ASSEMBLY OF HEAD OF BACTERIOPHAGE-T4. *Nature,* 227**,** 680-&.
LAGOUGE, M. & LARSSON, N. G. 2013. The role of mitochondrial DNA mutations and free radicals in disease and ageing. *Journal of Internal Medicine,* 273**,** 529-543.
LAMBERT, A. J. & BRAND, M. D. 2004. Superoxide production by NADH:ubiquinone oxidoreductase (complex I) depends on the pH gradient across the mitochondrial inner membrane. *The Biochemical journal,* 382**,** 511.
LARSON-CASEY, J. L., DESHANE, J. S., RYAN, A. J., THANNICKAL, V. J. & CARTER, A. B. 2016. Macrophage Akt1 Kinase- Mediated Mitophagy Modulates Apoptosis Resistance and Pulmonary Fibrosis. *Immunity,* 44**,** 582-596.
LAZAROU, M. 2015. Keeping the immune system in check: a role for mitophagy. *Immunology and Cell Biology,* 93**,** 3-10.
LEE, K. S., SCANGA, C. A., BACHELDER, E. M., CHEN, Q. & SNAPPER, C. M. 2007. TLR2 synergizes with both TLR4 and TLR9 for induction of the MyD88-dependent splenic cytokine and chemokine response to Streptococcus pneumoniae. *Cellular Immunology,* 245**,** 103-110.
LEE, Y. & LEE, J. 2016. Role of the mammalian ATG8/ LC3 family in autophagy: differential and compensatory roles in the spatiotemporal regulation of autophagy. *BMB Rep.*
LEE, Y. J., JEONG, S. Y., KARBOWSKI, M., SMITH, C. L. & YOULE, R. J. 2004. Roles of the mammalian mitochondrial fission and fusion mediators Fis1, Drp1, and Opa1 in apoptosis. *Molecular Biology of the Cell,* 15**,** 5001-5011.
LEGROS, F., LOMBÈS, A., FRACHON, P. & ROJO, M. 2002. Mitochondrial fusion in human cells is efficient, requires the inner membrane potential, and is mediated by mitofusins. *Molecular biology of the cell,* 13**,** 4343.
LI, P., SHI, J., HE, Q., HU, Q., WANG, Y. Y., ZHANG, L. J., CHAN, W. T. & CHEN, W.-X. 2015. Streptococcus pneumoniae Induces Autophagy through the Inhibition of the PI3K- I/ Akt/ mTOR Pathway and ROS Hypergeneration in A549 Cells (S . pneumoniae Induces Autophagy in A549 Cells). 10**,** e0122753.
LIM, W. S., MACFARLANE, J. T., BOSWELL, T. C. J., HARRISON, T. G., ROSE, D., LEINONEN, M. & SAIKKU, P. 2001. Study of community acquired pneumonia aetiology (SCAPA) in adults admitted to hospital: implications for management guidelines. *Thorax,* 56**,** 296.
LIU, Y., FISKUM, G. & SCHUBERT, D. 2002. Generation of reactive oxygen species by the mitochondrial electron transport chain. *Journal of Neurochemistry,* 80**,** 780-787.
LLOPIS, J., MCCAFFERY, J. M., MIYAWAKI, A., FARQUHAR, M. G. & TSIEN, R. Y. 1998. Measurement of cytosolic, mitochondrial, and Golgi pH in single living

cells with green fluorescent proteins. *Proceedings of the National Academy of Sciences of the United States of America,* 95**,** 6803-6808.
LOFTUS, R. M. & FINLAY, D. 2016. Immunometabolism: Cellular Metabolism Turns Immune Regulator. *J. Biol. Chem.*
LORSBACH, R. B., RUSSELL, S. W., MURPHY, W. J., LOWENSTEIN, C. J. & SNYDER, S. H. 1993. Expression of the nitric oxide synthase gene in mouse macrophages activated for tumor cell killing: Molecular basis for the synergy between interferon-γ and lipopolysaccharide. *Journal of Biological Chemistry,* 268**,** 1908-1913.
LOSON, O. C., SONG, Z., CHEN, H. & CHAN, D. C. 2013. Fis1, Mff, MiD49, and MiD51 mediate Drp1 recruitment in mitochondrial fission. *Molecular Biology of the Cell,* 24**,** 659-667.
LOU, Y., ZHANG, G., GENG, M., ZHANG, W., CUI, J. & LIU, S. 2014. TIPE2 negatively regulates inflammation by switching arginine metabolism from nitric oxide synthase to arginase. *PLoS ONE,* 9.
LUM, J. J. & BADLEY, A. D. 2003. Resistance to apoptosis: Mechanism for the development of HIV reservoirs. *Current Hiv Research,* 1**,** 261-274.
LYNCH, J. P. & ZHANEL, G. G. 2009. Streptococcus pneumoniae: Epidemiology, Risk Factors, and Strategies for Prevention. *Seminars in Respiratory and Critical Care Medicine,* 30**,** 189-209.
MACMICKING, J., XIE, Q. W., NATHAN, C. & MACMICKING, J. 1997. Nitric oxide and macrophage function. *Annual review of immunology,* 15**,** 323.
MACNEE, W. 2001. Oxidative stress and lung inflammation in airways disease. *European Journal of Pharmacology,* 429**,** 195-207.
MAESTRELLI, P., PÁSKA, P., NOWICKI, P., SAETTA, P., TURATO, P., MONTI, P., FORMICHI, P., MINIATI, P. & FABBRI, P. 2003. Decreased haem oxygenase- 1 and increased inducible nitric oxide synthase in the lung of severe COPD patients. *European Respiratory Journal,* 21**,** 971-976.
MALLEY, R., HENNEKE, P., MORSE, S. C., CIESLEWICZ, M. J., LIPSITCH, M., THOMPSON, C. M., KURT-JONES, E., PATON, J. C., WESSELS, M. R. & GOLENBOCK, D. T. 2003. Recognition of pneumolysin by toll-like receptor 4 confers resistance to pneumococcal infection. *Proceedings of the National Academy of Sciences of the United States of America,* 100**,** 1966-1971.
MANAN, M. M., SAMUEL, E. W. & NAVDEEP, S. C. 2017. Mitochondrial control of immunity: beyond ATP. *Nature Reviews Immunology,* 17.
MANTOVANI, A., SICA, A., SOZZANI, S., ALLAVENA, P., VECCHI, A. & LOCATI, M. 2004. The chemokine system in diverse forms of macrophage activation and polarization. *Trends in Immunology,* 25**,** 677-686.
MANZANILLO, P. S., AYRES, J. S., WATSON, R. O., COLLINS, A. C., SOUZA, G., RAE, C. S., SCHNEIDER, D. S., NAKAMURA, K., SHILOH, M. U. & COX, J. S. 2013. The ubiquitin ligase parkin mediates resistance to intracellular pathogens. *Nature,* 501.
MARKS, L. R., PARAMESWARAN, G. I. & HAKANSSON, A. P. 2012. Pneumococcal Interactions with Epithelial Cells Are Crucial for Optimal Biofilm Formation and Colonization In Vitro and In Vivo. *Infection and Immunity,* 80**,** 2744-2760.
MARRIOTT, H. M., ALI, F., READ, R. C., MITCHELL, T. J., WHYTE, M. K. B. & DOCKRELL, D. H. 2004a. Nitric oxide levels regulate macrophage commitment to apoptosis or necrosis during pneumococcal infection. *Faseb Journal,* 18**,** 1126-+.
MARRIOTT, H. M., ALI, F., READ, R. C., MITCHELL, T. J., WHYTE, M. K. B. & DOCKRELL, D. H. 2004b. Nitric oxide levels regulate macrophage

commitment to apoptosis or necrosis during pneumococcal infection. *FASEB journal : official publication of the Federation of American Societies for Experimental Biology,* 18**,** 1126.

MARRIOTT, H. M., BINGLE, C. D., READ, R. C., BRALEY, K. E., KROEMER, G., HELLEWELL, P. G., CRAIG, R. W., WHYTE, M. K. B. & DOCKRELL, D. H. 2005. Dynamic changes in Mcl- 1 expression regulate macrophage viability or commitment to apoptosis during bacterial clearance. *Journal of Clinical Investigation,* 115**,** 359-368.

MARRIOTT, H. M., GASCOYNE, K. A., GEARY, I., NICKLIN, M. J. H., WHYTE, M. K. B., SABROE, I., DOCKRELL, D. H., GOWDA, R., IANNELLI, F., POZZI, G. & MITCHELL, T. J. 2012. Interleukin-1β regulates CXCL8 release and influences disease outcome in response to Streptococcus pneumoniae, defining intercellular cooperation between pulmonary epithelial cells and macrophages. *Infection and Immunity,* 80**,** 1140-1149.

MARRIOTT, H. M., HELLEWELL, P. G., CROSS, S. S., INCE, P. G., WHYTE, M. K. B. & DOCKRELL, D. H. 2006. Decreased alveolar macrophage apoptosis is associated with increased pulmonary inflammation in a murine model of pneumococcal pneumonia. *Journal of Immunology,* 177**,** 6480-6488.

MARRIOTT, H. M., HELLEWELL, P. G., WHYTE, M. K. B. & DOCKRELL, D. H. 2007. Contrasting roles for reactive oxygen species and nitric oxide in the innate response to pulmonary infection with Streptococcus pneumoniae. *Vaccine,* 25**,** 2485-2490.

MARTÍ-LLITERAS, P., REGUEIRO, V., MOREY, P., SAULEDA, J., BENGOECHEA, J. A., GARMENDIA, J., AGUSTÍ, A. G. N., SAUS, C. & HOOD, D. W. 2009. Nontypeable Haemophilus influenzae clearance by alveolar macrophages is impaired by exposure to cigarette smoke. *Infection and Immunity,* 77**,** 4232-4242.

MARTIN, A. B., KYLIE, B. R. B., KIRANDEEP, K. C., RICHARD, C. B., GAVIN, D., JADWIGA, A. W., CHRISTOPHER, E. B., IAIN, K., LOUISE, E. D., PETER, J. B., DAVE, S., MOIRA, K. B. W. & DAVID, H. D. Differential Effects of p38, MAPK, PI3K or Rho Kinase Inhibitors on Bacterial Phagocytosis and Efferocytosis by Macrophages in COPD. *PLoS ONE,* 11**,** e0163139.

MCALLISTER, L. J., OGUNNIYI, A. D., PATON, J. C., TSENG, H.-J., JENNINGS, M. P. & MCEWAN, A. G. 2004. Molecular analysis of the psa permease complex of Streptococcus pneumoniae. *Molecular Microbiology,* 53**,** 889-901.

MCNEELA, E. A., BURKE, Á., NEILL, D. R., BAXTER, C., FERNANDES, V. E., FERREIRA, D., SMEATON, S., EL-RACHKIDY, R., MCLOUGHLIN, R. M., MORI, A., MORAN, B., FITZGERALD, K. A., TSCHOPP, J., PÉTRILLI, V., ANDREW, P. W., KADIOGLU, A. & LAVELLE, E. C. 2010. Pneumolysin Activates the NLRP3 Inflammasome and Promotes Proinflammatory Cytokines Independently of TLR4 (Pneumolysin Promotes NLRP3 Inflammasome Activation). *PLoS Pathogens,* 6**,** e1001191.

MEDZHITOV, R. & JANEWAY, C. J. 2000. Advances in immunology: Innate immunity. *N. Engl. J. Med.*

MEJA, K. K., SPOONER, G., MARWICK, J. A., CHAKRAVARTY, P., FLETCHER, D., WHITTAKER, P., KIRKHAM, P. A., RAJENDRASOZHAN, S., ADENUGA, D., BISWAS, S. K., SUNDAR, I. K., RAHMAN, I. & MEGSON, I. L. 2008. Curcumin restores corticosteroid function in monocytes exposed to oxidants by maintaining HDAC2. *American Journal of Respiratory Cell and Molecular Biology,* 39**,** 312-323.

MERCADO, N., THOMAS, C. M. R., FENWICK, P. S., CHANA, K. K., DONNELLY, L. E., ITO, K., BARNES, P. J., THIMMULAPPA, R. & BISWAL, S. 2011. Decreased histone deacetylase 2 impairs Nrf2 activation by oxidative stress. *Biochemical and Biophysical Research Communications,* 406**,** 292-298.

MEYER, A., ZOLL, J., CHARLES, A. L., CHARLOUX, A., DE BLAY, F., DIEMUNSCH, P., PIQUARD, F., GENY, B. & SIBILIA, J. 2013. Skeletal muscle mitochondrial dysfunction during chronic obstructive pulmonary disease: Central actor and therapeutic target. *Experimental Physiology,* 98**,** 1063-1078.

MILES, A. A., MISRA, S. S. & IRWIN, J. O. 1938. The estimation of the bactericidal power of the blood. *Journal of Hygiene,* 38**,** 732-749.

MILLS, C., KINCAID, K., ALT, J., HEILMAN, M. & HILL, A. 2000. M- 1/ M- 2 Macrophages and the Th1/ Th2 Paradigm. *Journal of Immunology,* 164**,** 6166-6173.

MINEMATSU, N., SHAPIRO, S. D. & BLUMENTAL-PERRY, A. 2011. Cigarette smoke inhibits engulfment of apoptotic cells by macrophages through inhibition of actin rearrangement. *American Journal of Respiratory Cell and Molecular Biology,* 44**,** 474-482.

MIRA, M., ALCAIS, A., VAN THUC, N., MORAES, M., DI FLUMERI, C., THAI, V., PHUONG, M. C., HUONG, N. T., BA, N. N., KHOA, P., SARNO, E., ALTER, A., MONTPETIT, A., MORAES, M. E., MORAES, JR., DORE, C., GALLANT, C. J., LEPAGE, P., VERNER, A., VAN DE VOSSE, E., HUDSON, T., ABEL, L. & SCHURR, E. 2004. Susceptibility to leprosy is associated with PARK2 and PACRG. *Nature,* 427**,** 636-640.

MISHRA, P. & CHAN, D. C. 2016. Metabolic regulation of mitochondrial dynamics. *Journal of Cell Biology,* 212**,** 379-387.

MITCHELL, P. 1961. COUPLING OF PHOSPHORYLATION TO ELECTRON AND HYDROGEN TRANSFER BY A CHEMI-OSMOTIC TYPE OF MECHANISM. *Nature,* 191**,** 144-&.

MONTUSCHI, P., COLLINS, J. V., CIABATTONI, G., LAZZERI, N., CORRADI, M., KHARITONOV, S. A. & BARNES, P. J. 2000. Exhaled 8- isoprostane as an in vivo biomarker of lung oxidative stress in patients with COPD and healthy smokers. *American Journal of Respiratory and Critical Care Medicine,* 162**,** 1175-1177.

MOREIRA, D., RODRIGUES, V., ABENGOZAR, M., RIVAS, L., RIAL, E., LAFORGE, M., LI, X., FORETZ, M., VIOLLET, B., ESTAQUIER, J., CORDEIRO DA SILVA, A. & SILVESTRE, R. 2015. Leishmania infantum Modulates Host Macrophage Mitochondrial Metabolism by Hijacking the SIRT1- AMPK Axis (Mitochondrial Metabolic Modulation by L. infantum). 11**,** e1004684.

MUNDER, M., EICHMANN, K. & MODOLELL, M. 1998. Alternative metabolic states in murine macrophages reflected by the nitric oxide synthase/ arginase balance: Competitive regulation by CD4 + T cells correlates with Th1/ Th2 phenotype. *Journal of Immunology,* 160**,** 5347-5354.

MURATORI, C., SISTIGU, A., RUGGIERO, E., FALCHI, M., BACIGALUPO, I., PALLADINO, C., TOSCHI, E. & FEDERICO, M. 2007. Macrophages transmit human immunodeficiency virus type 1 products to CD4- negative cells: involvement of matrix metalloproteinase 9. *Journal of virology,* 81**,** 9078.

MURPHY, C. & NEWSHOLME, P. 1997. The enemy within. The role played by immuno-stimulated macrophages in the pathogenesis of Insulin Dependant Diabetes Mellitus.

MURPHY, M. P. 2009. How mitochondria produce reactive oxygen species. *Biochemical Journal,* 417**,** 1-13.
MUSHER, D. M. 1992. INFECTIONS CAUSED BY STREPTOCOCCUS-PNEUMONIAE - CLINICAL SPECTRUM, PATHOGENESIS, IMMUNITY, AND TREATMENT. *Clinical Infectious Diseases,* 14**,** 801-809.
MUSHER, D. M., WATSON, D. A., NICKESON, D., GYORKEY, F., LAHART, C. & ROSSEN, R. D. 1990. THE EFFECT OF HIV-INFECTION ON PHAGOCYTOSIS AND KILLING OF STAPHYLOCOCCUS-AUREUS BY HUMAN PULMONARY ALVEOLAR MACROPHAGES. *American Journal of the Medical Sciences,* 299**,** 158-163.
NABEYRAT, E., JONES, G. E., FENWICK, P. S., BARNES, P. J. & DONNELLY, L. E. 2003. Mitogen- activated protein kinases mediate peroxynitrite- induced cell death in human bronchial epithelial cells. *American Journal of Physiology - Lung Cellular and Molecular Physiology,* 284**,** L1112-L1120.
NAKAMURA, S., DAVIS, K. M. & WEISER, J. N. 2011. Synergistic stimulation of type I interferons during influenza virus coinfection promotes Streptococcus pneumoniae colonization in mice. *The Journal of clinical investigation,* 121**,** 3657.
NARENDRA, D., TANAKA, A., SUEN, D.-F. & YOULE, R. J. 2008. Parkin is recruited selectively to impaired mitochondria and promotes their autophagy. *The Journal of cell biology,* 183**,** 795.
NATHAN, C. & SHILOH, M. U. 2000. Reactive oxygen and nitrogen intermediates in the relationship between mammalian hosts and microbial pathogens. *Proceedings of the National Academy of Sciences of the United States of America,* 97**,** 8841-8848.
NELSON, A. L., ROCHE, A. M., GOULD, J. M., CHIM, K., RATNER, A. J. & WEISER, J. N. 2007. Capsule enhances pneumococcal colonization by limiting mucus- mediated clearance. *Infection and Immunity,* 75**,** 83-90.
NOSSAMAN, B. D., DABISCH, P. A., LILES, J. T., BABER, S. R., CHAMPION, H. C., KAYE, A. D., FENG, C. J., ANWAR, M., BIVALACQUA, T. J., SANTIAGO, J. A., DE WITT, B. J. & KADOWITZ, P. J. 2004. Peroxynitrite does not impair pulmonary and systemic vascular responses. *Journal of Applied Physiology,* 96**,** 455-462.
O'NEILL, LUKE A. J. 2015. A Broken Krebs Cycle in Macrophages. *Immunity,* 42**,** 393-394.
OPITZ, B., PÜSCHEL, A., SCHMECK, B., HOCKE, A. C., ROSSEAU, S., HAMMERSCHMIDT, S., SCHUMANN, R. R., SUTTORP, N. & HIPPENSTIEL, S. 2004. Nucleotide- binding oligomerization domain proteins are innate immune receptors for internalized Streptococcus pneumoniae. *The Journal of biological chemistry,* 279**,** 36426.
ORMAN, K. L., SHENEP, J. L. & ENGLISH, B. K. 1998. Pneumococci stimulate the production of the inducible nitric oxide synthase and nitric oxide by murine macrophages. *Journal of Infectious Diseases,* 178**,** 1649-1657.
OTERA, H. & MIHARA, K. 2011. Molecular mechanisms and physiologic functions of mitochondrial dynamics. *Journal of Biochemistry,* 149**,** 241-251.
PALLAVI, C., SWAPNIL, G., SUMIT KUMAR, M., SWATI SETH, Y., MANSI, M., ZAVED, S., AMIT, S. & DHIRAJ, K. 2015. Mycobacterium tuberculosis Inhibits RAB7 Recruitment to Selectively Modulate Autophagy Flux in Macrophages. *Scientific Reports,* 5.
PALSSON-MCDERMOTT, EVA M., CURTIS, ANNE M., GOEL, G., LAUTERBACH, MARIO A. R., SHEEDY, FREDERICK J., GLEESON, LAURA E., VAN DEN BOSCH, MIRJAM W. M., QUINN, SUSAN R.,

DOMINGO-FERNANDEZ, R., JOHNSTON, DANIEL G. W., JIANG, J.-K., ISRAELSEN, WILLIAM J., KEANE, J., THOMAS, C., CLISH, C., VANDER HEIDEN, M., XAVIER, RAMNIK J. & O'NEILL, LUKE A. J. 2015. Pyruvate Kinase M2 Regulates Hif- 1α Activity and IL- 1β Induction and Is a Critical Determinant of the Warburg Effect in LPS- Activated Macrophages.

PANTEL, A., TEIXEIRA, A., HADDAD, E., WOOD, E. G., STEINMAN, R. M. & LONGHI, M. P. 2014. Direct Type I IFN but Not MDA5/ TLR3 Activation of Dendritic Cells Is Required for Maturation and Metabolic Shift to Glycolysis after Poly IC Stimulation (Dendritic Cell Maturation by Type I IFNs). 12**,** e1001759.

PAPA, S. & SKULACHEV, V. P. 1997. Reactive oxygen species, mitochondria, apoptosis and aging. *Molecular and cellular biochemistry.,* 174**,** 305-319.

PAREDI, P., KHARITONOV, S. A., LEAK, D., WARD, S., CRAMER, D. & BARNES, P. J. 2000. Exhaled ethane, a marker of lipid peroxidation, is elevated chronic obstructive pulmonary disease. *American Journal of Respiratory and Critical Care Medicine,* 162**,** 369-373.

PARK, C.-Y., KIM, E.-H., CHOI, S.-Y., TRAN, T. D.-H., KIM, I.-H., KIM, S.-N., PYO, S. & RHEE, D.-K. 2010. Virulence attenuation of Streptococcus pneumoniae clpP mutant by sensitivity to oxidative stress in macrophages via an NO- mediated pathway. *Journal of Microbiology,* 48**,** 229-235.

PARKER, N., CRICHTON, P. G., VIDAL-PUIG, A. J. & BRAND, M. D. 2009. Uncoupling protein-1 (UCP1) contributes to the basal proton conductance of brown adipose tissue mitochondria. *Journal of Bioenergetics and Biomembranes,* 41**,** 335-342.

PARKER, N., VIDAL-PUIG, A. & BRAND, M. D. 2008. Stimulation of mitochondrial proton conductance by hydroxynonenal requires a high membrane potential. *Bioscience Reports,* 28**,** 83-88.

PASTEUR 1881. Note sur la maladie nouvelle provoquee par la salive d'un enfant mort de la rage. Paris: Bull. Acad. Med. (Paris).

PATERSON, G. K. & ORIHUELA, C. J. 2010. Pneumococci: immunology of the innate host response. *Respirology,* 15**,** 1057-1063.

PELLETIER, M., BILLINGHAM, L., RAMASWAMY, M. & SIEGEL, R. M. 2014. Extracellular Flux Analysis to Monitor Glycolytic Rates and Mitochondrial Oxygen Consumption. *Methods Enzymol.*

PEPPOLONI, S., COLOMBARI, B., NEGLIA, R., BLASI, E., QUAGLINO, D., IANNELLI, F., OGGIONI, M. R. & POZZI, G. 2006. The lack of Pneumococcal surface protein C (PspC) increases the susceptibility of Streptococcus pneumoniae to the killing by microglia. *Medical Microbiology and Immunology,* 195**,** 21-28.

PERCIAVALLE, R. 2012. Anti- apoptotic MCL- 1 Localizes to the Mitochondrial Matrix and Couples Mitochondrial Fusion to Respiration. *In:* OPFERMAN, J. T., GREEN, D., SENOGLES, S., SHERR, C. & ZAMBETTI, G. (eds.). ProQuest Dissertations Publishing.

PERICONE, C. D., WEISER, J. N., PARK, S. & IMLAY, J. A. 2003. Factors Contributing to Hydrogen Peroxide Resistance in Streptococcus pneumoniae Include Pyruvate Oxidase (SpxB) and Avoidance of the Toxic Effects of the Fenton Reaction. *Journal of Bacteriology,* 185**,** 6815-6825.

PERKINS, G., RENKEN, C., MARTONE, M. E., YOUNG, S. J. & ELLISMAN, M. 1997. Electron tomography of neuronal mitochondria: Three-dimensional structure and organization of cristae and membrane contacts. *Journal of Structural Biology,* 119**,** 260-272.

POMMIER, C. G., INADA, S., FRIES, L. F., TAKAHASHI, T., FRANK, M. M. & BROWN, E. J. 1983. PLASMA FIBRONECTIN ENHANCES PHAGOCYTOSIS OF OPSONIZED PARTICLES BY HUMAN PERIPHERAL-BLOOD MONOCYTES. *Journal of Experimental Medicine,* 157**,** 1844-1854.

PONCET, D., LAROCHETTE, N., PAULEAU, A.-L., BOYA, P., JALIL, A.-A., CARTRON, P.-F., VALLETTE, F., SCHNEBELEN, C., BARTLE, L. M., SKALETSKAYA, A., BOUTOLLEAU, D., MARTINOU, J.-C., GOLDMACHER, V. S., KROEMER, G. & ZAMZAMI, N. 2004. An anti-apoptotic viral protein that recruits Bax to mitochondria. *The Journal of biological chemistry,* 279**,** 22605.

POTTER, A. J., KIDD, S. P., PATON, J. C. & MCEWAN, A. G. 2010. The MerR/NmlR family transcription factor of Streptococcus pneumoniae responds to carbonyl stress and modulates hydrogen peroxide production. *Journal of Bacteriology,* 192**,** 4063-4066.

PRASHANT, M. & DAVID, C. C. 2014. Mitochondrial dynamics and inheritance during cell division, development and disease. *Nature Reviews Molecular Cell Biology,* 15**,** 634.

QI, X., QVIT, N., SU, Y.-C. & MOCHLY-ROSEN, D. 2013. A novel Drp1 inhibitor diminishes aberrant mitochondrial fission and neurotoxicity. *Journal of cell science,* 126**,** 789.

RAHA, S. & ROBINSON, B. H. 2000. Mitochondria, oxygen free radicals, disease and ageing. *Trends in Biochemical Sciences,* 25**,** 502-508.

RAHMAN, I. 2003. Oxidative Stress, Chromatin Remodeling and Gene Transcription in Inflammation and Chronic Lung Diseases. *Journal of biochemistry and molecular biology,* 36**,** 95-109.

RAHMAN, I., VAN SCHADEWIJK, A. A. M., CROWTHER, A. J. L., HIEMSTRA, P. S., STOLK, J., MACNEE, W. & DE BOER, W. I. 2002. 4- Hydroxy- 2-nonenal, a specific lipid peroxidation product, is elevated in lungs of patients with chronic obstructive pulmonary disease. *American Journal of Respiratory and Critical Care Medicine,* 166**,** 490-495.

RAHMANI, Z., HUH, K. W., LASHER, R. & SIDDIQUI, A. 2000. Hepatitis B virus X protein colocalizes to mitochondria with a human voltage- dependent anion channel, HVDAC3, and alters its transmembrane potential. *Journal of virology,* 74**,** 2840.

RATHMELL, J., ELSTROM, R., CINALLI, R. M. & THOMPSON, C. 2003. Activated Akt promotes increased resting T cell size, CD28-independent T cell growth, and development of autoimmunity and lymphoma. *Eur. J. Immunol.,* 33**,** 2223-2232.

Ratner AJ, Hippe KR, Aguilar JL, Bender MH, Nelson AL, et al. 2006. Epithelial cells are sensitive detectors of bacterial pore-forming toxins. J Biol Chem 281: 12994-12998.

REALES-CALDERÓN, J. A., MOLERO, G., GIL, C., AGUILERA-MONTILLA, N. & CORBÍ, Á. L. 2014. Proteomic characterization of human proinflammatory M1 and anti- inflammatory M2 macrophages and their response to Candida albicans. *Proteomics,* 14**,** 1503-1518.

RETAMALES, I., ELLIOTT, W. M., MESHI, B., COXSON, H. O., PARE, P. D., SCIURBA, F. C., ROGERS, R. M., HAYASHI, S. & HOGG, J. C. 2001. Amplification of inflammation in emphysema and its association with latent adenoviral infection. *Am. J. Respir. Crit. Care Med.,* 164**,** 469-473.

RIBES, S., EBERT, S., REGEN, T., AGARWAL, A., TAUBER, S. C., CZESNIK, D., SPREER, A., BUNKOWSKI, S., EIFFERT, H., HANISCH, U.-K.,

HAMMERSCHMIDT, S. & NAU, R. 2010. Toll- like receptor stimulation enhances phagocytosis and intracellular killing of nonencapsulated and encapsulated Streptococcus pneumoniae by murine microglia. *Infection and immunity,* 78**,** 865.

RICCI, J. E., GOTTLIEB, R. A. & GREEN, D. R. 2003. Caspase-mediated loss of mitochondrial function and generation of reactive oxygen species during apoptosis. *Journal of Cell Biology,* 160**,** 65-75.

RICHARD, J. Y. & MARIUSZ, K. 2005. Mitochondrial fission in apoptosis. *Nature Reviews Molecular Cell Biology,* 6**,** 657.

RICHENS, T. R., LINDERMAN, D. J., HORSTMANN, S. A., LAMBERT, C., XIAO, Y.-Q., BOÉ, D. M., VANDIVIER, R. W., KEITH, R. L., MORIMOTO, K., BOWLER, R. P., DAY, B. J., JANSSEN, W. J. & HENSON, P. M. 2009. Cigarette smoke impairs clearance of apoptotic cells through oxidant- dependent activation of RhoA. *American Journal of Respiratory and Critical Care Medicine,* 179**,** 1011-1021.

ROBB, C., REGAN, K., DORWARD, D. & ROSSI, A. 2016. Key mechanisms governing resolution of lung inflammation. *Seminars in Immunopathology,* 38**,** 425-448.

ROCA, FRANCISCO J. & RAMAKRISHNAN, L. 2013. TNF Dually Mediates Resistance and Susceptibility to Mycobacteria via Mitochondrial Reactive Oxygen Species. *Cell,* 153**,** 521-534.

ROCK, K. L., LATZ, E., ONTIVEROS, F. & KONO, H. 2010. The Sterile Inflammatory Response. *Annual Review of Immunology, Vol 28,* 28**,** 321-342.

RODRÍGUEZ-PRADOS, J.-C., CASCANTE, M., TRAVÉS, P. G., MARTÍN-SANZ, P., BOSCÁ, L., CUENCA, J., RICO, D. & ARAGONE, J. 2010. Substrate fate in activated macrophages: A comparison between innate, classic, and alternative activation. *Journal of Immunology,* 185**,** 605-614.

RUBINS, J. B. & JANOFF, E. N. 1998. Pneumolysin: A multifunctional pneumococcal virulence factor. *Journal of Laboratory and Clinical Medicine,* 131**,** 21-27.

SABROE, I., READ, R. C., WHYTE, M. K. B., DOCKRELL, D. H., VOGEL, S. N. & DOWER, S. K. 2003. Toll-like receptors in health and disease: Complex questions remain. *Journal of Immunology,* 171**,** 1630-1635.

SANDERS, M., NORCROSS, E., MOORE, Q., ONWUBIKO, C., KING, L., FRATKIN, J. & MARQUART, M. 2008. A comparison of pneumolysin activity and concentration in vitro and in vivo in a rabbit endophthalmitis model. *Clinical Ophthalmology,* 2**,** 793-800.

SANGJUN, P., JI-HEE, W., INHWA, H., SUJEONG, H., HEUNG KYU, L. & JE-WOOK, Y. 2015. Defective mitochondrial fission augments NLRP3 inflammasome activation. *Scientific Reports,* 5.

SAPEY, E. & STOCKLEY, R. 2006. COPD exacerbations . 2: Aetiology. *In:* SAPEY, E. (ed.).

SCHLEYER, M. & NEUPERT, W. 1985. TRANSPORT OF PROTEINS INTO MITOCHONDRIA - TRANSLOCATIONAL INTERMEDIATES SPANNING CONTACT SITES BETWEEN OUTER AND INNER MEMBRANES. *Cell,* 43**,** 339-350.

SCOTT, A. D. & DAVID, C. C. 2007. Functions and dysfunctions of mitochondrial dynamics. *Nature Reviews Molecular Cell Biology,* 8**,** 870.

SESAKI, H., ADACHI, Y., KAGEYAMA, Y., ITOH, K. & IIJIMA, M. 2014. In vivo functions of Drp1: Lessons learned from yeast genetics and mouse knockouts. *BBA - Molecular Basis of Disease,* 1842**,** 1179-1185.

SHAO, D., LIU, Y., LIU, X., ZHU, L., CUI, Y., CUI, A., QIAO, A., KONG, X., FANG, F., CHANG, Y., LIU, Y., CHEN, Q. & GUPTA, N. 2010. PGC-1β-

Regulated mitochondrial biogenesis and function in myotubes is mediated by NRF- 1 and ERRα. *Mitochondrion,* 10**,** 516-527.
SHAPIRO, S. D. 1999. The macrophage in chronic obstructive pulmonary disease.
SHAYKHIEV, R., KRAUSE, A., SALIT, J., STRULOVICI-BAREL, Y., HARVEY, B.-G., CONNOR, T. P. & CRYSTAL, R. G. 2009a. Smoking- dependent reprogramming of alveolar macrophage polarization: implication for pathogenesis of chronic obstructive pulmonary disease. *Journal of immunology (Baltimore, Md. : 1950),* 183**,** 2867.
SHAYKHIEV, R., KRAUSE, A., SALIT, J., STRULOVICI-BAREL, Y., HARVEY, B., CONNOR, T. P. & CRYSTAL, R. G. 2009b. Smoking-Dependent Reprogramming of Alveolar Macrophage Polarization: Implication for Pathogenesis of Chronic Obstructive Pulmonary Disease. *J. Immunol.,* 183**,** 2867-2883.
SIMON, S., ANGELA, M. M., JIN, Z., CATHERINE, S. & MARIO, S. 2007. Apoptotic killing of HIV- 1- infected macrophages is subverted by the viral envelope glycoprotein. *PLoS Pathogens,* 3**,** 1281-1290.
SIMONSEN, L., TAYLOR, R., YOUNG-XU, Y., HABER, M., MAY, L. & KLUGMAN, K. 2011. Impact of Pneumococcal Conjugate Vaccination of Infants on Pneumonia and Influenza Hospitalization and Mortality in All Age Groups in the United States. *mBio,* 2**,** e00309-e00309.
SINDRILARU, A., PETERS, T., WIESCHALKA, S., PETER, H., HAINZL, A., SCHATZ, S., QI, Y., SCHLECHT, A., WEISS, J. M., WLASCHEK, M., SCHARFFETTER-KOCHANEK, K., BAICAN, C., BAICAN, A. & SUNDERKÖTTER, C. 2011. An unrestrained proinflammatory M1 macrophage population induced by iron impairs wound healing in humans and mice. *Journal of Clinical Investigation,* 121**,** 985-997.
SONG, J.-H., THAMLIKITKUL, V. & HSUEH, P.-R. 2011. Clinical and economic burden of community- acquired pneumonia amongst adults in the Asia- Pacific region. *International Journal of Antimicrobial Agents,* 38**,** 108-117.
SONG, J. Y., EUN, B. W. & NAHM, M. H. 2013. Diagnosis of Pneumococcal Pneumonia: Current Pitfalls and the Way Forward. *Infection & Chemotherapy,* 45**,** 351-366.
SONODA, J., LAGANIERE, J., MEHL, I. R., BARISH, G., CHONG, L., LI, X. L., SCHEFFLER, I., MOCK, D. C., BATAILLE, A., ROBERT, F., LEE, C., GIGUERE, V. & EVANS, R. M. 2007. Nuclear receptor ERR alpha and coactivator PGC- 1 beta are effectors of IFN- gamma- induced host defense. *Genes Dev.,* 21**,** 1909-1920.
SORENSEN, U. B. S., BLOM, J., BIRCHANDERSEN, A. & HENRICHSEN, J. 1988. ULTRASTRUCTURAL-LOCALIZATION OF CAPSULES, CELL-WALL POLYSACCHARIDE, CELL-WALL PROTEINS, AND F-ANTIGEN IN PNEUMOCOCCI. *Infection and Immunity,* 56**,** 1890-1896.
SØRENSEN, U. B. S., HENRICHSEN, J., CHEN, H.-C. & SZU, S. C. 1990. Covalent linkage between the capsular polysaccharide and the cell wall peptidoglycan of Streptococcus pneumoniae revealed by immunochemical methods. *Microbial Pathogenesis,* 8**,** 325-334.
SPIKA, J. S., FACKLAM, R. R., PLIKAYTIS, B. D. & OXTOBY, M. J. 1991. Antimicrobial Resistance of Streptococcus pneumoniae in the United States, 1979-1987. *The Journal of Infectious Diseases,* 163**,** 1273-1278.
SRISKANDAN, S. & COHEN, J. 1999. Gram-positive sepsis - Mechanisms and differences from gram-negative sepsis. *Infectious Disease Clinics of North America,* 13**,** 397-+.

Srivastava A, Henneke P, Visintin A, Morse SC, Martin V, et al. 2005. The apoptotic response to pneumolysin is Toll-like receptor 4 dependent and protects against pneumococcal disease. Infect Immun 73: 6479-6487.

ST-PIERRE, J., LIN, J., KRAUSS, S., TARR, P. T., YANG, R., NEWGARD, C. B., SPIEGELMAN, B. M. & ST-PIERRE, J. 2003. Bioenergetic analysis of peroxisome proliferator- activated receptor gamma coactivators 1alpha and 1beta (PGC- 1alpha and PGC- 1beta) in muscle cells. *The Journal of biological chemistry,* 278**,** 26597.

STAVRU, F., BOUILLAUD, F., SARTORI, A., RICQUIER, D. & COSSART, P. 2011. Listeria monocytogenes transiently alters mitochondrial dynamics during infection. *Proceedings of the National Academy of Sciences, USA,* 108**,** 3612-3617.

STAVRU, F., PALMER, A., WANG, C., YOULE, R. & COSSART, P. 2013. Atypical mitochondrial fission upon bacterial infection. *Proceedings of the National Academy of Sciences, USA,* 110**,** 16003-16003.

STEIN, M., KESHAV, S., HARRIS, N. & GORDON, S. 1992. INTERLEUKIN-4 POTENTLY ENHANCES MURINE MACROPHAGE MANNOSE RECEPTOR ACTIVITY - A MARKER OF ALTERNATIVE IMMUNOLOGICAL MACROPHAGE ACTIVATION. *Journal of Experimental Medicine,* 176**,** 287-292.

STEPHEN, W. G. T. & DOUGLAS, R. G. 2010. Mitochondria and cell death: outer membrane permeabilization and beyond. *Nature Reviews Molecular Cell Biology,* 11**,** 621.

STERNBERG, G. M. 1881. A fatal form of septicaemia in the rabbit,

produced by subcutaneous injection of human saliva. National Board of Health

Bulletin.

STROEHER, U. H., PATON, J. C., KIDD, S. P., STAFFORD, S. L., JENNINGS, M. P. & MCEWAN, A. G. 2007. A pneumococcal MerR- like regulator and S-nitrosoglutathione reductase are required for systemic virulence. *Journal of Infectious Diseases,* 196**,** 1820-1826.

SUEN, D., NORRIS, K. & YOULE, R. 2008. Mitochondrial dynamics and apoptosis. *Genes Dev.*

SUNYER, J. 2001. Urban air pollution and chronic obstructive pulmonary disease: A review. *European Respiratory Journal,* 17**,** 1024-1033.

TANNAHILL, G. M., CURTIS, A. M., PALSSON-MCDERMOTT, J., MCGETTRICK, E. M., BERNARD, A. F., KELLY, G., FOLEY, C., JANY, N. J., CORR, B., HANEKLAUS, N. H., KELLY, L., NEILL, A., ADAMIK, Z., AURON, S. S., GOEL, S. C., XAVIER, M., FREZZA, B. E., ZHENG, K., GOTTLIEB, S., FREZZA, F. C., XAVIER, E., GARDET, V., PIERCE, M., CLISH, C. T., TONG, H., LIN, S. L., CAFFREY, E., WALMSLEY, V. P., WHYTE, C., BEASLEY, P. E., NIZET, R. J., CUMMINS, L. A. J., TAYLOR, L. A. J. & MASTERS, L. A. J. 2013. Succinate is an inflammatory signal that induces IL-1β through HIF-1α. *Nature,* 496**,** 238-242.

TAYLOR, A. E., FINNEY-HAYWARD, T. K., THOMAS, J. K., TUDHOPE, C. M. R., BARNES, S. J., DONNELLY, J. A., QUINT, P. J. & WEDZICHA, L. E. 2010. Defective macrophage phagocytosis of bacteria in COPD. *European Respiratory Journal,* 35**,** 1039-1047.

TAYLOR, R. W. & TURNBULL, D. M. 2005. Mitochondrial DNA mutations in human disease. *Nature Reviews Genetics,* 6**,** 389-402.

TILLEY, S. J., ORLOVA, E. V., GILBERT, R. J. C., ANDREW, P. W. & SAIBIL, H. R. 2005. Structural Basis of Pore Formation by the Bacterial Toxin Pneumolysin. *Cell,* 121**,** 247-256.

TO, Y., ITO, K., KIZAWA, Y., FAILLA, M., ITO, M., ADCOCK, I. M., BARNES, P. J., KUSAMA, T., ELLIOTT, W. M. & HOGG, J. C. 2010. Targeting phosphoinositide- 3- kinase-δ with theophylline reverses corticosteroid insensitivity in chronic obstructive pulmonary disease. *American Journal of Respiratory and Critical Care Medicine,* 182**,** 897-904.

TOHRU, K., SHUICHI, A., NOBUTAKA, H., HIROTO, M., YASUHIRO, Y., SHINSEI, M., MASAYUKI, Y., YOSHIKUNI, M. & NOBUYOSHI, S. 1998. Mutations in the parkin gene cause autosomal recessive juvenile parkinsonism. *Nature,* 392**,** 605.

TOMITA, K., BARNES, P. J. & ADCOCK, I. M. 2003. The effect of oxidative stress on histone acetylation and IL- 8 release. *Biochemical and Biophysical Research Communications,* 301**,** 572-577.

TOMOKO, O., KOTOYO, I., KAZUTO, N. & JUN-ICHI, H. 2001. Human cells are protected from mitochondrial dysfunction by complementation of DNA products in fused mitochondria. *Nature Genetics,* 28**,** 272.

TONDERA, D., CZAUDERNA, F., PAULICK, K., SCHWARZER, R., KAUFMANN, J. & SANTEL, A. 2005. The mitochondrial protein MTP18 contributes to mitochondrial fission in mammalian cells. *Journal of Cell Science,* 118**,** 3049-3059.

TONDERA, D., SANTEL, A., SCHWARZER, R., DAMES, S., GIESE, K., KLIPPEL, A. & KAUFMANN, J. 2004. Knockdown of MTP18, a Novel Phosphatidylinositol 3- Kinase- dependent Protein, Affects Mitochondrial Morphology and Induces Apoptosis. *Journal of Biological Chemistry,* 279**,** 31544-31555.

TORRES, A., DORCA, J., ZALACAÍN, R., BELLO, S., EL-EBIARY, M., MOLINOS, L., ARÉVALO, M., BLANQUER, J., CELIS, R., IRIBERRI, M., PRATS, E., FERNÁNDEZ, R., IRIGARAY, R. & SERRA, J. 1996. Community- acquired pneumonia in chronic obstructive pulmonary disease: a Spanish multicenter study. *American journal of respiratory and critical care medicine,* 154**,** 1456.

TOWBIN, H., STAEHELIN, T. & GORDON, J. 1992. Electrophoretic transfer of proteins from polyacrylamide gels to nitrocellulose sheets: procedure and some applications. 1979. *Biotechnology (Reading, Mass.),* 24**,** 145-9.

TRAVES, S. L., CULPITT, S. V., RUSSELL, R. E. K., BARNES, P. J. & DONNELLY, L. E. 2002. Increased levels of the chemokines GRO alpha and MCP- 1 in sputum samples from patients with COPD. *Thorax,* 57**,** 590-595.

TREMPE, J.-F., SAUVÉ, V., GRENIER, K., SEIRAFI, M., TANG, M. Y., MÉNADE, M., AL-ABDUL-WAHID, S., KRETT, J., WONG, K., KOZLOV, G., NAGAR, B., FON, E. A. & GEHRING, K. 2013. Structure of parkin reveals mechanisms for ubiquitin ligase activation. *Science (New York, N.Y.),* 340**,** 1451.

TSENG, H.-J., MCEWAN, A. G., PATON, J. C. & JENNINGS, M. P. 2002. Virulence of Streptococcus pneumoniae: PsaA mutants are hypersensitive to oxidative stress. *Infection and Immunity,* 70**,** 1635-1639.

TWIG, G., ELORZA, A., MOLINA, A. J. A., MOHAMED, H., WIKSTROM, J. D., WALZER, G., STILES, L., HAIGH, S. E., KATZ, S., LAS, G., ALROY, J., WU, M., PY, B. F., YUAN, J., DEENEY, J. T., CORKEY, B. E. & SHIRIHAI, O. S. 2008. Fission and selective fusion govern mitochondrial segregation and elimination by autophagy. *EMBO Journal,* 27**,** 433-446.

UDERHARDT, S., HERRMANN, M., OSKOLKOVA, O., ASCHERMANN, S., BICKER, W., SARTER, K., FREY, B., ROTHE, T., VOLL, R.,

NIMMERJAHN, F., BOCHKOV, V., SCHETT, G. & KRONKE, G. 2012. 12/ 15- LIPOXYGENASE ORCHESTRATES THE CLEARANCE OF APOPTOTIC CELLS AND MAINTAINS IMMUNOLOGIC TOLERANCE. *Annals Of The Rheumatic Diseases,* 71**,** 531-531.

UNDERHILL, D. M. & OZINSKY, A. 2002. Phagocytosis of microbes: complexity in action. *Annual review of immunology,* 20**,** 825.

VAN DER WINDT, G. J. W., SULLIVAN, D., EVERTS, B., HUANG, S. C.-C., BUCK, M. D., CURTIS, J. D., CHANG, C.-H., SMITH, A. M., AI, T., PEARCE, E. J., PEARCE, E. L., FAUBERT, B. & JONES, R. G. 2013. CD8 memory T cells have a bioenergetic advantage that underlies their rapid recall ability. *Proceedings of the National Academy of Sciences of the United States of America,* 110**,** 14336-14341.

VAN FURTH, R. & COHN, Z. A. 1968. The origin and kinetics of mononuclear phagocytes. *Journal of Experimental Medicine,* 128**,** 415-435.

VAN FURTH, R., COHN, Z. A., HIRSCH, J. G., HUMPHREY, J. H., SPECTOR, W. G. & LANGEVOORT, H. L. 1972. The mononuclear phagocyte system: a new classification of macrophages, monocytes, and their precursor cells. *Bulletin of the World Health Organization,* 46**,** 845-852.

VAN OUD ALBLAS, A. B. & VAN FURTH, R. 1979. Origin, Kinetics, and characteristics of pulmonary macrophages in the normal steady state. *The Journal of experimental medicine,* 149**,** 1504-18.

VAN ROSSUM, A. M. C., LYSENKO, E. S. & WEISER, J. N. 2005. Host and bacterial factors contributing to the clearance of colonization by Streptococcus pneumoniae in a murine model. *Infection and Immunity,* 73**,** 7718-7726.

VAN STRAATEN, J. F. M., POSTMA, D. S., COERS, W., NOORDHOEK, J. A., KAUFFMAN, H. F. & TIMENS, W. 1998. Macrophages in lung tissue from patients with pulmonary emphysema express both inducible and endothelial nitric oxide synthase. *Modern Pathology,* 11**,** 648-655.

VANCE, R. E., ISBERG, R. R. & PORTNOY, D. A. 2009. Patterns of Pathogenesis: Discrimination of Pathogenic and Nonpathogenic Microbes by the Innate Immune System. *Cell Host & Microbe,* 6**,** 10-21.

VATS, D., MUKUNDAN, L., ODEGAARD, J. I., ZHANG, L., SMITH, K. L., MOREL, C. R., CHAWLA, A., GREAVES, D. R. & MURRAY, P. J. 2006. Oxidative metabolism and PGC-1β attenuate macrophage- mediated inflammation. *Cell Metabolism,* 4**,** 13-24.

VLAHOS, R. & BOZINOVSKI, S. 2014. Role of alveolar macrophages in chronic obstructive pulmonary disease. *Frontiers in immunology,* 5**,** 435.

VOGEL, F., BORNHOVD, C., NEUPERT, W. & REICHERT, A. S. 2006. Dynamic subcompartmentalization of the mitochondrial inner membrane. *Journal of Cell Biology,* 175**,** 237-247.

WATSON, D. A., JACOBSON, J. W. & VERHOEF, J. 1993. A Brief History of the Pneumococcus in Biomedical Research: A Panoply of Scientific Discovery. *Clinical Infectious Diseases,* 17**,** 913-924.

WELTE, T., TORRES, A. & NATHWANI, D. 2012. Clinical and economic burden of community- acquired pneumonia among adults in Europe. *Thorax,* 67**,** 71.

WEST, A. P., BRODSKY, I. E., RAHNER, C., WOO, D. K., ERDJUMENT-BROMAGE, H., TEMPST, P., WALSH, M. C., CHOI, Y., SHADEL, G. S., GHOSH, S. & ERDJUMENT-BROMAGE, H. 2011a. TLR signaling augments macrophage bactericidal activity through mitochondrial ROS. *Nature,* 472**,** 476-480.

WEST, A. P., SHADEL, G. S. & GHOSH, S. 2011b. Mitochondria in innate immune responses. *Nature Reviews Immunology,* 11**,** 389-402.

WIEGMAN, C. H., MICHAELOUDES, C., HAJI, G., NARANG, P., CLARKE, C. J., RUSSELL, K. E., BAO, W., PAVLIDIS, S., BARNES, P. J., KANERVA, J., BITTNER, A., RAO, N., MURPHY, M. P., KIRKHAM, P. A., CHUNG, K. F. & ADCOCK, I. M. 2015. Oxidative stress– induced mitochondrial dysfunction drives inflammation and airway smooth muscle remodeling in patients with chronic obstructive pulmonary disease. *The Journal of Allergy and Clinical Immunology,* 136**,** 769-780.

WINKELSTEIN, J. A. 1981. THE ROLE OF COMPLEMENT IN THE HOSTS DEFENSE AGAINST STREPTOCOCCUS-PNEUMONIAE. *Reviews of Infectious Diseases,* 3**,** 289-299.

WITZENRATH, M., PACHE, F., LORENZ, D., KOPPE, U., GUTBIER, B., TABELING, C., REPPE, K., MEIXENBERGER, K., DORHOI, A., MA, J., HOLMES, A., TRENDELENBURG, G., HEIMESAAT, M. M., BERESWILL, S., VAN DER LINDEN, M., TSCHOPP, J., MITCHELL, T. J., SUTTORP, N. & OPITZ, B. 2011. The NLRP3 inflammasome is differentially activated by pneumolysin variants and contributes to host defense in pneumococcal pneumonia. *Journal of immunology (Baltimore, Md. : 1950),* 187**,** 434.

XIONG, S., MU, T., WANG, G. & JIANG, X. 2014. Mitochondria- mediated apoptosis in mammals. *Protein & Cell,* 5**,** 737-749.

YESILKAYA, H., KADIOGLU, A., GINGLES, N., ALEXANDER, J. E., ANDREW, P. W. & MITCHELL, T. J. 2000. Role of manganese- containing superoxide dismutase in oxidative stress and virulence of Streptococcus pneumoniae. *Infection and Immunity,* 68**,** 2819-2826.

YIN, Z., RICE, B. D., WAIGHT, P., MILLER, E., GEORGE, R., BROWN, A. E., SMITH, R. D., SLACK, M. & DELPECH, V. C. 2012. Invasive pneumococcal disease among HIV-positive individuals, 2000-2009. *Aids,* 26**,** 87-94.

YOSHII, S. R., KISHI, C., ISHIHARA, N. & MIZUSHIMA, N. 2011. Parkin mediates proteasome- dependent protein degradation and rupture of the outer mitochondrial membrane. *The Journal of biological chemistry,* 286**,** 19630.

YU, J., BRYANT, A. P., MARRA, A., LONETTO, M. A., INGRAHAM, K. A., CHALKER, A. F., HOLMES, D. J., HOLDEN, D., ROSENBERG, M. & MCDEVITT, D. 2001. Characterization of the Streptococcus pneumoniae NADH oxidase that is required for infection. *Microbiology,* 147**,** 431-438.

YU, T. Z., ROBOTHAM, J. L. & YOON, Y. 2006. Increased production of reactive oxygen species in hyperglycemic conditions requires dynamic change of mitochondrial morphology. *Proceedings of the National Academy of Sciences of the United States of America,* 103**,** 2653-2658.

ZIVIANI, E., TAO, R. N. & WHITWORTH, A. J. 2010. Drosophila Parkin requires PINK1 for mitochondrial translocation and ubiquitinates Mitofusin. *Proceedings of the National Academy of Sciences of the United States of America,* 107**,** 5018-5023.

ZIZZO, G., HILLIARD, B. A., COHEN, P. L. & MONESTIER, M. 2012. Efficient clearance of early apoptotic cells by human macrophages requires M2c polarization and MerTK induction. *Journal of Immunology,* 189**,** 3508-3520.

ZYCHLINSKY, A. & SANSONETTI, P. 1997. Perspectives series: host/ pathogen interactions. Apoptosis in bacterial pathogenesis. *The Journal of clinical investigation,* 100**,** 493-495.

The End